The Soil Microbiome and Its Response to Permafrost Thaw in Arctic Tundra

by

Karl J. Romanowicz IV

A dissertation submitted in partial fulfillment
of the requirements for the degree of
Doctor of Philosophy
(Ecology and Evolutionary Biology)
in the University of Michigan
2022

Doctoral Committee:

Professor George W. Kling, Chair
Associate Professor Vincent J. Denef
Professor Gregory J. Dick
Professor Thomas M. Schmidt

Karl J. Romanowicz IV

kjromano@umich.edu

ORCID iD: 0000-0001-8732-3272

Dedication

To Genny, KJ, and James.

If I could do it all over again, and relive my vision in the twenty-first century, I would be a microbial ecologist. Ten billion bacteria live in a gram of ordinary soil, a mere pinch held between thumb and forefinger. They represent thousands of species, almost none of which are known to science. Into that world I would go with the aid of modern microscopy and molecular analysis in order to discover new ways of life.

— EDWARD O. WILSON (1929 – 2021)

Acknowledgements

I owe thanks to many people for their role in this dissertation research. First, I would like to thank my advisor, George Kling, for his unwavering support, patience, and insistence on excellence. I am a better scientist for his high standards and practical advice on scientific reasoning and writing. I am also grateful for his assistance in the lab and the field. I would also like to thank my committee, Greg Dick, Tom Schmidt, and Vincent Denef for sharing their lab spaces, equipment, and their thoughtful guidance and contributions to the development of this work over the years. I gratefully acknowledge my funding sources – Department of Ecology and Evolutionary Biology, Rackham Graduate School, and the National Science Foundation.

I thank many current and former members of the Kling Lab including Jason Dobkowski, Chris Cook, Riley Peterson, Johanna Albrigtsen, and Alex Kolenda for their support in the lab and the field. I would also like to thank Rose Cory and her students and technicians including Adrianna Trusiak, Lija Treibergs, Jenny Bowen, Emma Rieb, and Katie Polik. I would especially like to thank Byron Crump who has not only been an invaluable collaborator for my dissertation work, but also a great mentor and advocate for my scientific success beyond my dissertation. I also thank Byron's students Natasha Christman, Natasha Griffin, Ted Bambakidis, and former postdoc Jerome Payet for their valuable assistance in the lab and field. A special thanks to Jacob Evans (Denef Lab), Derek Smith (Dick Lab), and Robert Hein (Schmidt Lab) for their help in establishing my bioinformatic pipelines, without which much of this dissertation would not have been possible.

Thanks also to the many EEB graduate students I have had the privilege to know and work with during my time in the program including Wes Bickford, Buck Castillo, Nikesh Dahal, Morgan Lindback, Rumaan Malhotra, Meagan Simons, and Anthony Wing. I would also like to thank and acknowledge support staff in the EEB Department as well as those at the Advanced Genomics Core, Microbiome Core, and Advanced Research and Computing Technology Services who have provided valuable advice and logistical support that enabled my dissertation research.

Most of all, I want to thank my family. I never could have done what I am doing today without their unwavering love and support. To my parents, Karl and Marie Romanowicz, for inspiring my interest in the natural world, opening doors of opportunity throughout my life, and always supporting my decision to pursue scientific research. To my in-laws, John and Lynn Gierke, who never failed to make a trip to visit or help at home while I spent months away in the Arctic for fieldwork. Thank you to our two boys, Karl and James, especially for their patience with me when fieldwork called me away for the summers. And mostly, thank you to my wife, Genny, for being supportive from the beginning and putting up with the challenges of raising two kids while both pursuing a PhD. You were my constant sounding board and biggest supporter. I couldn't have asked for a better partner in science or in life.

As a member of the University of Michigan, I respectfully acknowledge that the university and surrounding communities occupy Indigenous lands of the Meškwahki·aša·hina (Fox), Peoria, Anishinaabeg, and Bodwéwadmi (Potawatomi) peoples. I deeply appreciate their historic connection to this land and further acknowledge that our university stands, like most property in the United States, on lands obtained, generally in unconscionable ways, from Indigenous peoples. As a member of the Arctic research community, I acknowledge that Toolik Field Station and the surrounding areas are located on the ancestral hunting grounds of the Nunamiut, and occasional hunting grounds and routes of the Gwich'in, Koyukuk, and Iñupiaq peoples. I am grateful for the Indigenous people who inhabit and steward this beautiful land. Knowing where we live and work does not change the past, but understanding and acknowledging the history, culture, and impacts of this past can empower us in our research, teaching, and outreach to create an equitable and sustainable future.

Table of Contents

List of Tables

List of Figures

List of Appendices

Abstract

A majority (~60%) of the global belowground organic carbon (OC) pool is trapped in a perennially frozen state in permafrost soils underlying the Arctic tundra. Climate warming has initiated thaw in large regions of permafrost. Such thaw will likely trigger increased microbial activity leading to faster degradation of previously frozen OC and its release as carbon dioxide (CO_2) and methane (CH_4) to the atmosphere. Yet it remains uncertain how the soil microbiome (community of microorganisms) will respond to permafrost thaw or modulate the relative proportions of CO_2 and CH_4 produced by the decomposition of OC in thawing permafrost soils. This dissertation advances our understanding of the dynamics and functions of the tundra soil microbiome in response to permafrost thaw using field-based and laboratory experiments.

Permafrost soils remain water-saturated during thaw, leading to oxygen (O_2) limitations that promote anaerobic and fermentative microbial processes responsible for OC degradation. Rainfall contributes to soil saturation but can also introduce an influx of O_2, potentially altering anaerobic metabolism and reducing CH_4 production. A rainfall event was simulated in tundra soil mesocosms and the genomic response of the soil microbiome was assessed through a multi-omics sequencing approach. Soil drainage rates had the greatest effect on soil oxygenation following the rainfall event. Specifically, rainfall-induced soil oxidation increased aerobic microbial metabolism and CO_2 respiration in a slow-draining tundra soil. However, the residence time of oxygenated rainwater in a rapidly-draining tundra soil was insufficient to alter anaerobic and fermentative microbial processes that continued to promote CH_4 production. Thus, the microbial response to rainfall in thawing permafrost soils depends on drainage rates that differ by tundra type.

The microbial response to permafrost thaw also depends on how thaw duration (thaw days in summer) affects the composition of the soil microbiome. Field observations revealed that the composition of the soil microbiome was strongly correlated with annual thaw duration by depth. Compositional differences were greatest across transition depths from thawed to permafrost soil. Multi-decadal thaw surveys showed that differences in thaw duration by depth were significantly

positively correlated with dominant taxa in the surface active-layer depths and negatively correlated with dominant taxa in the permafrost. Microbial composition within the transition-zone (recently thawed permafrost) depths was statistically similar to that in the permafrost, indicating that recent decades of intermittent thaw have not yet induced a shift from permafrost to active-layer microbes. These results suggest that thaw duration rather than thaw frequency has a greater impact on the composition of the microbiome within tundra soils. Monitoring thaw duration and microbial composition at depth may help predict the microbial response to future permafrost thaw.

To test the microbial response to thaw duration, a laboratory incubation experiment was conducted to simulate thaw along a tundra soil profile. An extended thaw duration of 30 days induced a microbiome-wide shift in composition and genomic potential dominated by an increase in iron (Fe) cycling bacteria. This shift was greatest within the transition-zone and permafrost microbiomes where the relative abundance of Fe-cycling bacteria accounted for ~80% of the community after 30 days. Microbial gene expression for Fe(III) reduction, Fe(II) oxidation, as well as OC degradation also increased concurrently with thaw duration. The growth of Fe-cycling bacteria and subsequent degradation of OC through Fe(III) reduction could promote greater CO_2 production over CH_4 production with extended thaw duration in permafrost soils.

Chapter 1.
Advancing our Understanding of the Soil Microbiome and its Response to Permafrost Thaw in Arctic Tundra

1.1 Soil Microbial Ecology

Soils represent a globally important ecosystem supporting a vast diversity of organisms and abiotic conditions that play a key role in the global response to climate change (Jansson & Hofmockel 2020). Microorganisms dominate the heterotrophic soil community and are largely responsible for the cycling of organic carbon (OC) and other soil nutrients that contribute to climate feedbacks (Friedlingstein et al. 2006, Wang et al. 2017). For instance, soil microbes directly influence the composition of the atmosphere by governing the turnover and uptake of OC and its release as greenhouse gases (GHGs). Soils contain the greatest portion of OC in the terrestrial biosphere, storing more OC than vegetation and the atmosphere combined (Schlesinger & Bernhardt 2013). Heterotrophic microbes within the soil microbiome – including bacteria, archaea, and fungi – govern the cycling and turnover of the OC pool through ecosystem processes that regulate the uptake and release of OC in different forms. These processes include the mineralization of OC into carbon dioxide (CO_2) performed by a diverse range of microorganisms as well as the production and uptake of methane (CH_4) that can only be performed by certain microbial groups (Crowther et al. 2019). Changes in the rate of OC processing are an important control on biogeochemical cycles and the rate of climate change (Cavicchioli et al. 2019). However, understanding and predicting the dynamics and functions of the soil microbiome that governs these vital ecosystem processes remains a challenge for the field of microbial ecology due to the inherently opaque and heterogeneous nature of soils (Hall et al. 2018, Smercina et al. 2021).

1.2 Arctic Tundra as a Model Soil System

Climate conditions primarily govern the functioning of the soil microbiome by regulating its metabolic activity and the rate of OC turnover (Bradford et al. 2017). Cold and saturated soil

conditions in high latitude ecosystems restrict respiratory carbon losses to a greater extent than primary production, and the greatest accumulation of soil OC stocks occurs in the Arctic (Hengl et al. 2017). As such, the Arctic tundra and its permafrost soils have become a major focus of study for global biogeochemical cycling because these soils contain more than half (~60%) of all terrestrial belowground OC in a perennially frozen state (Hugelius et al. 2014) that is increasingly threatened by anthropogenic climate change (Euskirchen et al. 2006, 2017). Recent warming in the Arctic has already increased soil temperatures and thawed large areas of permafrost (Osterkamp & Romanovsky 1999, Zhang et al. 2006). Warming has also altered the net CO_2 balance of tundra soils with the atmosphere (Oechel et al. 1993, Euskirchen et al. 2017) such that tundra soils no longer serve as a net sink for atmospheric carbon (Miller et al. 1983, McGuire et al. 2009). These warming-induced changes to tundra soils will likely trigger increased microbial activity, leading to faster degradation of previously-frozen OC and the release of CO_2 and CH_4 to the atmosphere (Schuur et al. 2009, Grosse et al. 2011, Xue et al. 2016). Yet it remains uncertain how the soil microbiome will respond to permafrost thaw or modulate the relative proportions of CO_2 and CH_4 produced by the decomposition of OC in thawing permafrost soils.

This dissertation advances our understanding of the dynamics and functions of the soil microbiome in arctic tundra by investigating how the composition of the microbiome, its genomic potential, and its gene expression changes in response to permafrost thaw. In the following chapters, I describe a series of field observations, manipulations, and laboratory incubations that answer the following questions: (1) How does rainfall-induced soil oxidation alter anoxic redox conditions and the soil microbiome in thawing permafrost soils; (2) How does summer thaw duration and frequency correlate with the composition of the soil microbiome by depth; and (3) How does extended thaw duration shift the composition and genomic potential of the soil microbiome within distinct soil layers along the soil profile (Figure 1.1). I approach each research question from a landscape-level perspective and employ multi-omics sequencing techniques coupled with abiotic measurements and a mass balance model. Below, I provide a general background on the abiotic factors known to influence the composition and genomic potential of the soil microbiome in arctic tundra, which supplements introductions in the following chapters. I then briefly describe each research question and summarize the potential implications and conclude by describing the study sites and methodological approaches for my dissertation research.

1.3 Factors Influencing the Soil Microbiome in Arctic Tundra

Climate warming in the Arctic has accelerated permafrost thaw and increased annual thaw depth and duration in tundra soils, while also increasing the availability of previously frozen OC to microbial degradation and release as GHGs (Herndon et al. 2015). However, the relative proportions of CO_2 and CH_4 released from the microbial degradation of OC following permafrost thaw are likely to vary across the landscape due to differences in soil microbiome composition and soil redox conditions (Smith et al. 2005, Sturtevant & Oechel 2013). For example, the composition of the soil microbiome varies by landscape position due to differences in the overlying tundra vegetation that establishes on hillslopes or lowlands based on soil drainage patterns and the duration of soil saturation during the growing season (Walker et al. 1994, Judd et al. 2006, Zak & Kling 2006). Specifically, hillslopes support tussock tundra and are dominated by sedges (*Eriophorum vaginatum*) and dwarf shrubs (*Betula nana*, *Ledum palustre*) that occur on gently rolling topography with mineral soils overlain by 30 to 50 cm of organic soils at the surface (Walker et al. 1994). These soils are typically moist but not saturated and have maximum thaw depths ~50 cm (Hobbie et al. 2002). Lowlands support wet sedge tundra dominated by sedges (*Carex aquatilis, C. chordorrhiza, C. rotunda*) due to the accumulation of soil water and persistent soil saturation (Walker et al. 1994). These organic soils are often covered with 1 to 5 cm of standing water throughout the growing season (Hobbie et al. 2002). Maximum thaw depth is 50 to 70 cm and typically does not reach mineral soils. Together, tussock and wet sedge tundra cover ~80% of the vegetated arctic tundra (Hobbie & Kling 2014). Differences in the composition of the soil microbiome between tussock and wet sedge tundra soils differentially affects the extent and rate of microbial OC degradation and GHG production following permafrost thaw (Chu et al. 2011).

Soil redox conditions also vary across the arctic landscape due to differences in soil drainage patterns. Tussock tundra soils on hillslopes have a relatively lower water table resulting in wet but not constantly saturated soils with better drainage, resulting in more oxidizing conditions that promote aerobic respiration and CO_2 production (Gebauer et al. 1996, Hobbie et al. 2002). Wet sedge tundra soils in lowlands remain saturated due to the lack of drainage through the underlying permafrost (Zona 2016), resulting in anoxic soil conditions that promote anaerobic and fermentative pathways of OC metabolism and CH_4 production (Gebauer et al. 1996, Judd & Kling 2002). Thus, differences in soil redox conditions between tundra types, as regulated by landscape

position and soil drainage, influence the composition of the soil microbiome and its genomic potential to degrade OC by altering the availability of oxygen (O_2) in tundra soils.

The composition of the soil microbiome also varies with depth along the soil profiles of tussock tundra and wet sedge tundra from the annually-thawed surface 'active layer' to the permafrost at deeper soil depths (Yergeau et al. 2010, Mackelprang et al. 2011, Frank-Fahle et al. 2014, Gittel et al. 2014, Deng et al. 2015). Abiotic factors such as annual thaw depth and soil type (organic vs. mineral) as well as climatic variables including temperature and rainfall can influence the composition of the active-layer microbiome (Castro et al. 2010, Nielsen & Ball 2015, Malard et al. 2019). Landscape age influences the composition of the permafrost microbiome in response to increasing age, weathering, and associated stresses of the harsh permafrost environment (Mackelprang et al. 2017, Saidi-Mehrabad et al. 2020). Additional abiotic factors such as ice content (Burkert et al. 2019), dispersal limitations (Bottos et al. 2018), and thermodynamic constraints imposed by prolonged freezing (Bottos et al. 2018) also influence the composition of the permafrost microbiome.

Recent studies have shown an additional, distinct microbiome composition in the transition zone (layer of recently thawed permafrost soil) between the overlying active layer and deeper permafrost (Müller et al. 2018). The transition zone has often been overlooked in past studies because it represents a gradient of active layer and permafrost soils that complicates studies designed specifically to test differences between the active-layer and permafrost microbiomes. Yet the distinct microbial composition in the transition zone has consequences for the interpretation of microbial activity between the upper active layer and deeper permafrost because the transition zone is the soil region where newly thawed permafrost OC first becomes accessible to microbial degradation. It remains unknown if recent decades of soil warming have induced a compositional change in the transition-zone microbiome away from the composition of the deeper permafrost microbiome and towards the composition of the active-layer microbiome.

1.4 Research Questions and Potential Implications

Recent decades of warming have also begun to increase rainfall intensity, frequency, and accumulation in tundra soils (Kumar et al. 2012, Spence & Phillips 2015, Bintanja & Andry 2017). Increased rainfall has led to deeper permafrost thaw (Douglas et al. 2020) and greater CH_4 release to the atmosphere from thawing permafrost soils (Neumann et al. 2019). Rainfall contributes to

soil saturation and O_2 limitations, especially in lowland wet sedge tundra soils that remain saturated due to the lack of drainage through the underlying permafrost (Zona 2016). In Chapter 2, I investigate how rainfall events can rapidly change the oxidation state of tussock tundra and wet sedge tundra soils by flushing O_2-rich water into mesocosms containing saturated tundra soil (Question 1; Figure 1.1). The oxidation state of saturated tundra soils typically supports methanogenic archaea, Fe-reducing bacteria, and other anaerobic microbial competitors such as acetogens whose activity is mediated by the availability of CO_2, hydrogen (H_2), Fe(III) minerals, and acetate, some of which can be further reduced to CH_4 by methanogenic archaea (Stams et al. 2006). However, rainfall events may be capable of inducing a sufficient change to the oxidation state of saturated soils by introducing a large influx of dissolved O_2 (Trusiak et al. 2019). The implications of rainfall-induced soil oxidation could be a substantial increase in the abundance and genomic expression of aerobic heterotrophic microbes such as CH_4-oxidizing bacteria that increase CO_2 production from these typically anoxic soils.

In order to better predict the microbial response to permafrost thaw we also need to understand how an increase in annual thaw frequency (whether a certain depth thaws each summer) and duration (number of thaw days at a certain depth each summer) affects the composition and genomic potential of the soil microbiome in arctic tundra. Recent studies show that warmer soil temperatures, earlier spring thaw, and later fall freeze-up have all contributed to an increase in annual thaw depth and the duration of annual thaw with depth along tundra soil profiles (Serreze et al. 2000, Euskirchen et al. 2006, Barichivich et al. 2012). In Chapter 3, I report on soil surveys from the active layer through the transition zone and deeper permafrost in tussock tundra and wet sedge tundra at three separate sites across the North Slope of Alaska. The changes I observe in microbiome composition and genomic potential between soil layers are then coupled with long-term thaw depth surveys to determine how differences in thaw duration and frequency by depth correlate with dominant taxa along the soil profiles (Question 2; Figure 1.1). Notably, I found that the microbiome composition within the transition-zone depths was indistinguishable from that in the permafrost, which implies that recent decades of intermittent thaw have not yet induced a shift from permafrost to active-layer microbes.

The implications from my soil profile surveys (Chapter 3) suggest that thaw duration rather than thaw frequency (intermittent thaw probability) has a greater impact on microbiome composition and genomic potential within tundra soils. In Chapter 4, I report on a laboratory

incubation experiment designed to test the microbial response to extended thaw duration along the soil profile of wet sedge tundra (Question 3, Figure 1.1). For this experiment, frozen soil samples from the active-layer, transition-zone, and permafrost depths of wet sedge tundra were gradually thawed and incubated under anoxic conditions for 30 days. My results suggest that extended thaw duration induced a microbiome-wide shift in composition and genomic potential. This shift was dominated by Fe(III)-reducing bacteria, especially within the transition-zone and permafrost microbiomes. Fe(III) minerals are known to stabilize OC by sorption/co-precipitation and protect it from degradation by generating Fe-OC associations in tundra soils (Baldock et al. 2000, Lalonde et al. 2012, Kleber et al. 2015). However, it appears likely that Fe(III) minerals are also providing a terminal electron acceptor for anaerobic respiration during extended thaw duration, consistent with recent studies conducted along collapsing permafrost hillslopes (Patzner et al. 2020, 2022). This suggests that Fe(III) minerals are unlikely to preserve OC following extended thaw duration, but rather serve to enhance the growth of Fe(III)-reducing bacteria that is likely coupled with greater OC degradation and CO_2 production. The potential implications of my research are that previously frozen permafrost soils will promote greater growth and subsequent gene expression from Fe(III)-reducing bacteria as permafrost thaw duration increases at depth. This Fe-mediated microbial response during extended thaw will also likely lead to substantial quantities of Fe-bound OC being released to microbial degradation following future permafrost thaw.

1.5 Study Sites

All field research for this dissertation was conducted near the NSF Arctic Long-Term Ecological Research (LTER) site at Toolik Field Station on the North Slope of the Brooks Range in northern Alaska, USA (68°38'N, 149°36'W; Fig. 1.2). The Arctic LTER is a representative landscape of low-arctic tundra consisting of several distinct vegetation types. Upland tussock tundra (Britton 1966) is the most common plant community, covering ~40% of land in the Upper Kuparuk River Basin (Walker et al. 1994). Wet sedge tundra occurs at the base of slopes in low lying areas in the foothills region and across the coastal plains (Walker et al. 1994). This entire region is underlain by continuous permafrost with a mean annual air temperature of -8.5°C (Hobbie & Kling 2014). However, this region and the entire circumpolar Arctic are warming at unprecedented rates (Hinzman et al. 2005), where near-surface temperatures of the North Slope have warmed more than 3°C over the past 60 years (Shulski & Wendler 2007). The indirect effects

of this warming are an increase in the depth of the active layer and greater rates of soil weathering as well as an increase in the height and density of vascular plants that are shifting towards a shrub-dominated landscape (Hobbie & Kling 2014). Climate models predict that this region will be 0.5-3°C warmer by the end of this century with 1.5-3 times the amount of current rainfall (Cherry et al. 2014, Bintanja & Andry 2017). This combination of temperature and rainfall increase, as well as greater quantities of OC becoming accessible from thawing permafrost soils, will likely have direct effects on the dynamics and functions of the soil microbiome in arctic tundra.

1.6 Methodological Approaches

Throughout this dissertation, I use high-throughput 16S rRNA gene sequencing for bacterial and archaeal taxonomic identification (Chapters 2-4). The use of 16S rRNA gene sequences to study bacterial and archaeal taxonomy has been by far the most common housekeeping genetic marker used in microbial studies (Janda & Abbott 2007) for a number of reasons. These reasons include: (1) its presence in all bacteria and archaea, (2) the function of the 16S rRNA gene over time has not changed, and (3) the 16S rRNA gene (1,500 bp) is large enough for informatics purposes (Patel 2001). Primer selection for 16S rRNA gene sequencing follows the Earth Microbiome Project (Thompson et al. 2017), using dual-barcoded primers 515f-806r (Apprill et al. 2015, Parada et al. 2016) to profile the bacterial and archaeal communities.

In Chapters 2 and 4, I also use multi-omics sequencing techniques including metagenomics and metatranscriptomics. Metagenomics, defined as the functional and sequence-based analysis of the collective microbial genomes extracted directly from the environment (Handelsman 2004), enables *in situ* quantification of the genomic potential of the soil microbiome by resolving how functional genes are partitioned in and among species populations (Cowan et al. 2004, Riesenfeld et al. 2004, Streit & Schmitz 2004). Metatranscriptomics provide *in situ* snapshots of transcriptional profiles (i.e., expressed genes) that correspond to discrete species populations within the soil microbiome at the time of sampling (Moran 2009). Here, these multi-omics sequencing techniques reveal the composition and diversity of the tundra soil microbiome, its genomic potential, and its gene expression through a series of experiments that manipulate rainfall, redox conditions, and permafrost thaw in tussock and wet sedge tundra soils.

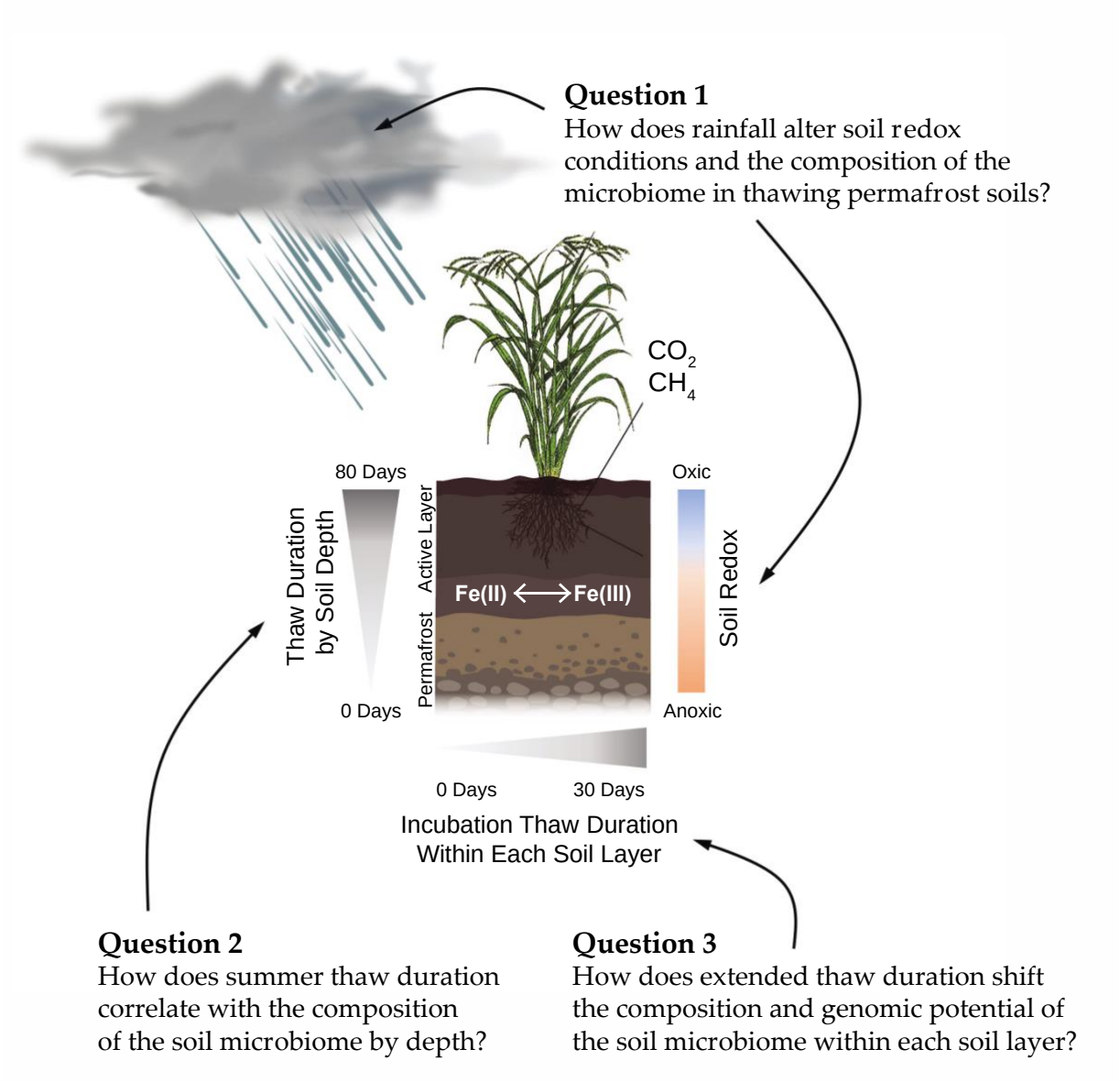

Figure 1.1 Conceptual Diagram of Research Questions. It remains uncertain how the dynamics and functions of the soil microbiome will change in response to permafrost thaw or modulate the relative proportions of CO_2 and CH_4 produced by the decomposition of organic carbon in thawing permafrost soils. My dissertation addresses the following research questions: (1) how rainfall-induced soil oxidation alters anoxic redox conditions and the composition of the soil microbiome in thawing permafrost soils, (2) how summer thaw duration correlates with the composition of the soil microbiome by depth, and (3) how extended thaw duration shifts the composition and genomic potential of the soil microbiome within distinct soil layers.

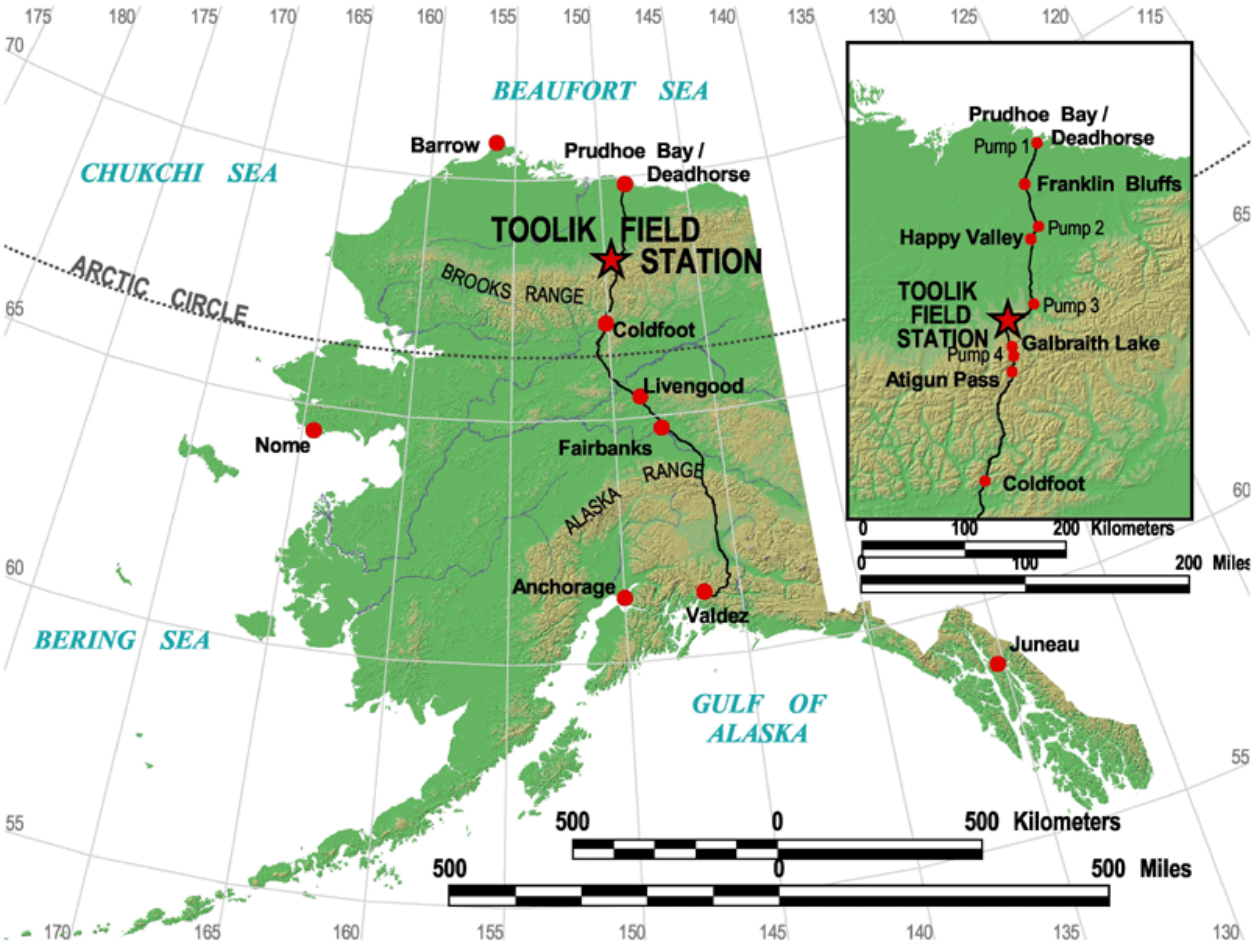

Figure 1.2 Map of the NSF Arctic LTER field site in Alaska. Research in Arctic Alaska was conducted at Toolik Field Station on the North Slope of the Brooks Range (68°38'N, 149°36'W).

1.7 References

Apprill, A., McNally, S., Parsons, R. and Weber, L., 2015. Minor revision to V4 region SSU rRNA 806R gene primer greatly increases detection of SAR11 bacterioplankton. Aquatic Microbial Ecology, 75(2), 129-137.

Baldock, J.A. and Skjemstad, J.O., 2000. Role of the soil matrix and minerals in protecting natural organic materials against biological attack. Organic geochemistry, 31(7-8), 697-710.

Barichivich, J., Briffa, K.R., Osborn, T.J., Melvin, T.M. and Caesar, J., 2012. Thermal growing season and timing of biospheric carbon uptake across the Northern Hemisphere. Global Biogeochemical Cycles, 26(4).

Bintanja, R. and Andry, O., 2017. Towards a rain-dominated Arctic. Nature Climate Change, 7(4), 263-267.

Bottos, E.M., Kennedy, D.W., Romero, E.B., Fansler, S.J., Brown, J.M., Bramer, L.M., Chu, R.K., Tfaily, M.M., Jansson, J.K. and Stegen, J.C., 2018. Dispersal limitation and thermodynamic constraints govern spatial structure of permafrost microbial communities. FEMS microbiology ecology, 94(8), fiy110.

Bradford, M.A., Veen, G.F., Bonis, A., Bradford, E.M., Classen, A.T., Cornelissen, J.H.C., Crowther, T., De Long, J.R., Freschet, G.T., Kardol, P. and Manrubia-Freixa, M., 2017. A test of the hierarchical model of litter decomposition. Nature ecology & evolution, 1(12), 1836-1845.

Britton, M.E., 1966. Vegetation of the arctic tundra. *In* H.P. Hanson, ed. Arctic Biology. Oregon State University Press, Corvallis, OR, 67-130.

Burkert, A., Douglas, T.A., Waldrop, M.P. and Mackelprang, R., 2019. Changes in the active, dead, and dormant microbial community structure across a Pleistocene permafrost chronosequence. Applied and environmental Microbiology, 85(7), e02646-18.

Castro, H.F., Classen, A.T., Austin, E.E., Norby, R.J. and Schadt, C.W., 2010. Soil microbial community responses to multiple experimental climate change drivers. Applied and environmental microbiology, 76(4), 999-1007.

Cavicchioli, R., Ripple, W.J., Timmis, K.N., Azam, F., Bakken, L.R., Baylis, M., Behrenfeld, M.J., Boetius, A., Boyd, P.W., Classen, A.T. and Crowther, T.W., 2019. Scientists' warning to humanity: microorganisms and climate change. Nature Reviews Microbiology, 17(9), 569-586.

Chu, H., Neufeld, J.D., Walker, V.K. and Grogan, P., 2011. The influence of vegetation type on the dominant soil bacteria, archaea, and fungi in a low Arctic tundra landscape. Soil Science Society of America Journal, 75(5), 1756-1765.

Cowan, D.A., Arslanoglu, A., Burton, S.G., Baker, G.C., Cameron, R.A., Smith, J.J. and Meyer, Q., 2004. Metagenomics, gene discovery and the ideal biocatalyst. Biochemical Society Transactions, 32(2), 298-302.

Crowther, T.W., Van den Hoogen, J., Wan, J., Mayes, M.A., Keiser, A.D., Mo, L., Averill, C. and Maynard, D.S., 2019. The global soil community and its influence on biogeochemistry. Science, 365(6455), eaav0550.

Deng, J., Gu, Y., Zhang, J., Xue, K., Qin, Y., Yuan, M., Yin, H., He, Z., Wu, L., Schuur, E.A. and Tiedje, J.M., 2015. Shifts of tundra bacterial and archaeal communities along a permafrost thaw gradient in A laska. Molecular ecology, 24(1), 222-234.

Douglas, T.A., Turetsky, M.R. and Koven, C.D., 2020. Increased rainfall stimulates permafrost thaw across a variety of Interior Alaskan boreal ecosystems. NPJ Climate and Atmospheric Science, 3(1), 1-7.

Euskirchen, E.S., McGUIRE, A.D., Kicklighter, D.W., Zhuang, Q., Clein, J.S., Dargaville, R.J., Dye, D.G., Kimball, J.S., McDonald, K.C., Melillo, J.M. and Romanovsky, V.E., 2006. Importance of recent shifts in soil thermal dynamics on growing season length, productivity, and carbon sequestration in terrestrial high-latitude ecosystems. Global Change Biology, 12(4), 731-750.

Euskirchen, E.S., Bret-Harte, M.S., Shaver, G.R., Edgar, C.W. and Romanovsky, V.E., 2017. Long-term release of carbon dioxide from arctic tundra ecosystems in Alaska. Ecosystems, 20(5), 960-974.

Frank-Fahle, B.A., Yergeau, É., Greer, C.W., Lantuit, H. and Wagner, D., 2014. Microbial functional potential and community composition in permafrost-affected soils of the NW Canadian Arctic. PLoS One, 9(1), e84761.

Friedlingstein, P., Cox, P., Betts, R., Bopp, L., von Bloh, W., Brovkin, V., Cadule, P., Doney, S., Eby, M., Fung, I. and Bala, G., 2006. Climate–carbon cycle feedback analysis: results from the C4MIP model intercomparison. Journal of climate, 19(14), 3337-3353.

Gebauer, R.L., Tenhunen, J.D. and Reynolds, J.F., 1996. Soil aeration in relation to soil physical properties, nitrogen availability, and root characteristics within an arctic watershed. Plant and Soil, 178(1), 37-48.

Gittel, A., Bárta, J., Kohoutová, I., Mikutta, R., Owens, S., Gilbert, J., Schnecker, J., Wild, B., Hannisdal, B., Maerz, J. and Lashchinskiy, N., 2014. Distinct microbial communities associated with buried soils in the Siberian tundra. The ISME journal, 8(4), 841-853.

Grosse, G., Romanovsky, V., Jorgenson, T., Anthony, K.W., Brown, J. and Overduin, P.P., 2011. Vulnerability and feedbacks of permafrost to climate change. Eos, Transactions American Geophysical Union, 92(9), 73-74.

Hall, E.K., Bernhardt, E.S., Bier, R.L., Bradford, M.A., Boot, C.M., Cotner, J.B., Del Giorgio, P.A., Evans, S.E., Graham, E.B., Jones, S.E. and Lennon, J.T., 2018. Understanding how microbiomes influence the systems they inhabit. Nature microbiology, 3(9), 977-982.

Handelsman, J., 2004. Metagenomics: application of genomics to uncultured microorganisms. Microbiology and molecular biology reviews, 68(4), 669-685.

Hengl, T., Mendes de Jesus, J., Heuvelink, G.B., Ruiperez Gonzalez, M., Kilibarda, M., Blagotić, A., Shangguan, W., Wright, M.N., Geng, X., Bauer-Marschallinger, B. and Guevara, M.A., 2017. SoilGrids250m: Global gridded soil information based on machine learning. PLoS one, 12(2), e0169748.

Herndon, E.M., Mann, B.F., Roy Chowdhury, T., Yang, Z., Wullschleger, S.D., Graham, D., Liang, L. and Gu, B., 2015. Pathways of anaerobic organic matter decomposition in tundra soils from Barrow, Alaska. Journal of Geophysical Research: Biogeosciences, 120(11), 2345-2359.

Hinzman, L.D., Bettez, N.D., Bolton, W.R., Chapin, F.S., Dyurgerov, M.B., Fastie, C.L., Griffith, B., Hollister, R.D., Hope, A., Huntington, H.P. and Jensen, A.M., 2005. Evidence and implications of recent climate change in northern Alaska and other arctic regions. Climatic change, 72(3), 251-298.

Hobbie, J.E. and Kling, G.W., 2014. Ecological consequences of present and future changes in Arctic Alaska. Alaska's Changing Arctic: Ecological Consequences for Tundra, Streams, and Lakes, Academic Press.

Hobbie, S.E., Miley, T.A. and Weiss, M.S., 2002. Carbon and nitrogen cycling in soils from acidic and nonacidic tundra with different glacial histories in Northern Alaska. Ecosystems, 5(8), 0761-0774.

Hugelius, G., Strauss, J., Zubrzycki, S., Harden, J.W., Schuur, E.A.G., Ping, C.L., Schirrmeister, L., Grosse, G., Michaelson, G.J., Koven, C.D. and O'Donnell, J.A., 2014. Estimated stocks of circumpolar permafrost carbon with quantified uncertainty ranges and identified data gaps. Biogeosciences, 11(23), 6573-6593.

Janda, J.M. and Abbott, S.L., 2007. 16S rRNA gene sequencing for bacterial identification in the diagnostic laboratory: pluses, perils, and pitfalls. Journal of clinical microbiology, 45(9), 2761-2764.

Jansson, J.K. and Hofmockel, K.S., 2020. Soil microbiomes and climate change. Nature Reviews Microbiology, 18(1), 35-46.

Judd, K.E. and Kling, G.W., 2002. Production and export of dissolved C in arctic tundra mesocosms: the roles of vegetation and water flow. Biogeochemistry, 60(3), 213-234.

Judd, K.E., Crump, B.C. and Kling, G.W., 2006. Environmental drivers control ecosystem function in bacteria through changes in community composition. Ecology, 87(8), 2068-2079.

Kleber, M., Eusterhues, K., Keiluweit, M., Mikutta, C., Mikutta, R. and Nico, P.S., 2015. Mineral–organic associations: formation, properties, and relevance in soil environments. Advances in agronomy, 130, 1-140.

Kumar, M., Wang, R. and Link, T.E., 2012. Effects of more extreme precipitation regimes on maximum seasonal snow water equivalent. Geophysical Research Letters, 39(20).

Lalonde, K., Mucci, A., Ouellet, A. and Gélinas, Y., 2012. Preservation of organic matter in sediments promoted by iron. Nature, 483(7388), 198-200.

Mackelprang, R., Waldrop, M.P., DeAngelis, K.M., David, M.M., Chavarria, K.L., Blazewicz, S.J., Rubin, E.M. and Jansson, J.K., 2011. Metagenomic analysis of a permafrost microbial community reveals a rapid response to thaw. Nature, 480(7377), 368-371.

Mackelprang, R., Burkert, A., Haw, M., Mahendrarajah, T., Conaway, C.H., Douglas, T.A. and Waldrop, M.P., 2017. Microbial survival strategies in ancient permafrost: insights from metagenomics. The ISME journal, 11(10), 2305-2318.

Malard, L.A., Anwar, M.Z., Jacobsen, C.S. and Pearce, D.A., 2019. Biogeographical patterns in soil bacterial communities across the Arctic region. FEMS microbiology ecology, 95(9), fiz128.

McGuire, A.D., Anderson, L.G., Christensen, T.R., Dallimore, S., Guo, L., Hayes, D.J., Heimann, M., Lorenson, T.D., Macdonald, R.W. and Roulet, N., 2009. Sensitivity of the carbon cycle in the Arctic to climate change. Ecological Monographs, 79(4), 523-555.

Miller, P.C., Kendall, R. and Oechel, W.C., 1983. Simulating carbon accumulation in northern ecosystems. Simulation, 40(4), 119-131.

Moran, M.A., 2009. Metatranscriptomics: eavesdropping on complex microbial communities. Microbe, 4(7), p.7.

Müller, O., Bang-Andreasen, T., White III, R.A., Elberling, B., Taş, N., Kneafsey, T., Jansson, J.K. and Øvreås, L., 2018. Disentangling the complexity of permafrost soil by using high resolution profiling of microbial community composition, key functions and respiration rates. Environmental microbiology, 20(12), 4328-4342.

Neumann, R.B., Moorberg, C.J., Lundquist, J.D., Turner, J.C., Waldrop, M.P., McFarland, J.W., Euskirchen, E.S., Edgar, C.W. and Turetsky, M.R., 2019. Warming effects of spring rainfall increase methane emissions from thawing permafrost. Geophysical Research Letters, 46(3), 1393-1401.

Nielsen, U.N. and Ball, B.A., 2015. Impacts of altered precipitation regimes on soil communities and biogeochemistry in arid and semi-arid ecosystems. Global change biology, 21(4), 1407-1421.

Oechel, W.C., Hastings, S.J., Vourlrtis, G., Jenkins, M., Riechers, G. and Grulke, N., 1993. Recent change of Arctic tundra ecosystems from a net carbon dioxide sink to a source. Nature, 361(6412), 520-523.

Osterkamp, T.E. and Romanovsky, V.E., 1999. Evidence for warming and thawing of discontinuous permafrost in Alaska. Permafrost and periglacial Processes, 10(1), 17-37.

Parada, A.E., Needham, D.M. and Fuhrman, J.A., 2016. Every base matters: assessing small subunit rRNA primers for marine microbiomes with mock communities, time series and global field samples. Environmental microbiology, 18(5), 1403-1414.

Patel, J.B., 2001. 16S rRNA gene sequencing for bacterial pathogen identification in the clinical laboratory. Molecular diagnosis, 6(4), 313-321.

Patzner, M.S., Mueller, C.W., Malusova, M., Baur, M., Nikeleit, V., Scholten, T., Hoeschen, C., Byrne, J.M., Borch, T., Kappler, A. and Bryce, C., 2020. Iron mineral dissolution releases iron and associated organic carbon during permafrost thaw. Nature communications, 11(1), 1-11.

Patzner, M.S., Logan, M., McKenna, A.M., Young, R.B., Zhou, Z., Joss, H., Mueller, C.W., Hoeschen, C., Scholten, T., Straub, D. and Kleindienst, S., 2022. Microbial iron cycling during palsa hillslope collapse promotes greenhouse gas emissions before complete permafrost thaw. Communications Earth & Environment, 3(1), 1-14.

Riesenfeld, C.S., Schloss, P.D. and Handelsman, J., 2004. Metagenomics: genomic analysis of microbial communities. Annu. Rev. Genet., 38, 525-552.

Saidi-Mehrabad, A., Neuberger, P., Hajihosseini, M., Froese, D. and Lanoil, B.D., 2020. Permafrost Microbial Community Structure Changes Across the Pleistocene-Holocene Boundary. Frontiers in Environmental Science, 133.

Schlesinger, W.H. and Bernhardt, E.S., 2013. Biogeochemistry: an analysis of global change. Waltham, MA.

Shulski, M. and Wendler, G., 2007. The climate of Alaska. University of Alaska Press.

Schuur, E.A., Vogel, J.G., Crummer, K.G., Lee, H., Sickman, J.O. and Osterkamp, T.E., 2009. The effect of permafrost thaw on old carbon release and net carbon exchange from tundra. Nature, 459(7246), 556-559.

Serreze, M.C., Walsh, J.E., Chapin, F.S., Osterkamp, T., Dyurgerov, M., Romanovsky, V., Oechel, W.C., Morison, J., Zhang, T. and Barry, R.G., 2000. Observational evidence of recent change in the northern high-latitude environment. Climatic change, 46(1), 159-207.

Smercina, D.N., Bailey, V.L. and Hofmockel, K.S., 2021. Micro on a macroscale: relating microbial-scale soil processes to global ecosystem function. FEMS Microbiology Ecology, 97(7), fiab091.

Smith, L.C., Sheng, Y., MacDonald, G.M. and Hinzman, L.D., 2005. Disappearing arctic lakes. Science, 308(5727), 1429-1429.

Spence, C. and Phillips, R.W., 2015. Refining understanding of hydrological connectivity in a boreal catchment. Hydrological Processes, 29(16), 3491-3503.

Stams, A.J., De Bok, F.A., Plugge, C.M., Van Eekert, M.H., Dolfing, J. and Schraa, G., 2006. Exocellular electron transfer in anaerobic microbial communities. Environmental microbiology, 8(3), 371-382.

Streit, W.R. and Schmitz, R.A., 2004. Metagenomics–the key to the uncultured microbes. Current opinion in microbiology, 7(5), 492-498.

Sturtevant, C.S. and Oechel, W.C., 2013. Spatial variation in landscape-level CO2 and CH4 fluxes from arctic coastal tundra: Influence from vegetation, wetness, and the thaw lake cycle. Global Change Biology, 19(9), 2853-2866.

Thompson, L.R., Sanders, J.G., McDonald, D., Amir, A., Ladau, J., Locey, K.J., Prill, R.J., Tripathi, A., Gibbons, S.M., Ackermann, G. and Navas-Molina, J.A., 2017. A communal catalogue reveals Earth's multiscale microbial diversity. Nature, 551(7681), 457-463.

Trusiak, A., Treibergs, L.A., Kling, G.W. and Cory, R.M., 2019. The controls of iron and oxygen on hydroxyl radical (• OH) production in soils. Soil systems, 3(1), p.1.

Walker, M.A., Daniëls, F.J. and van der Maarel, E., 1994. Circumpolar arctic vegetation: Introduction and perspectives. Journal of vegetation science, 5(6), 757-764.

Wang, K., Peng, C., Zhu, Q., Zhou, X., Wang, M., Zhang, K. and Wang, G., 2017. Modeling global soil carbon and soil microbial carbon by integrating microbial processes into the ecosystem process model TRIPLEX-GHG. Journal of Advances in Modeling Earth Systems, 9(6), 2368-2384.

Xue, K., M Yuan, M., J Shi, Z., Qin, Y., Deng, Y.E., Cheng, L., Wu, L., He, Z., Van Nostrand, J.D., Bracho, R. and Natali, S., 2016. Tundra soil carbon is vulnerable to rapid microbial decomposition under climate warming. Nature Climate Change, 6(6), 595-600.

Yergeau, E., Hogues, H., Whyte, L.G. and Greer, C.W., 2010. The functional potential of high Arctic permafrost revealed by metagenomic sequencing, qPCR and microarray analyses. The ISME journal, 4(9), 1206-1214.

Zak, D.R. and Kling, G.W., 2006. Microbial community composition and function across an arctic tundra landscape. Ecology, 87(7), 1659-1670.

Zhang, Y., Chen, W. and Riseborough, D.W., 2006. Temporal and spatial changes of permafrost in Canada since the end of the Little Ice Age. Journal of Geophysical Research: Atmospheres, 111(D22).

Zona, D., 2016. Long-term effects of permafrost thaw. Nature, 537(7622), 625-626.

Chapter 2.

Rainfall Alters Permafrost Soil Redox Conditions, but Meta-Omics Show Divergent Microbial Community Responses by Tundra Type in the Arctic [1]

2.1 Abstract

Soil anoxia is common in the annually thawed surface ('active') layer of permafrost soils, particularly when soils are saturated, and supports anaerobic microbial metabolism and methane (CH_4) production. Rainfall contributes to soil saturation, but can also introduce oxygen (O_2), causing soil oxidation and altering anoxic conditions. We simulated a rainfall event in soil mesocosms from two dominant tundra types, tussock tundra and wet sedge tundra, to test the impacts of rainfall-induced soil oxidation on microbial communities and their metabolic capacity for anaerobic CH_4 production and aerobic respiration following soil oxidation. In both types, rainfall increased total soil O_2 concentration, but in tussock tundra there was a 2.5-fold greater increase in soil O_2 compared to wet sedge tundra due to differences in soil drainage rates and the residence time of oxygenated rainwater. Metagenomic and metatranscriptomic analyses found divergent microbial responses to rainfall between tundra types. Active microbial taxa in the tussock tundra community, including bacteria and fungi, responded to rainfall with a decline in gene expression for anaerobic metabolism and a concurrent increase in gene expression for cellular growth. In contrast, the wet sedge tundra community showed no significant changes in microbial gene expression from anaerobic metabolism, fermentation, or methanogenesis following rainfall, despite an initial increase in soil O_2 concentration. These results suggest that rainfall induces soil oxidation and enhances aerobic microbial respiration in tussock tundra communities but may not accumulate or remain in wet sedge tundra soils long enough to induce a community-wide shift from anaerobic metabolism, mainly due to differences in soil drainage rates between tundra types.

[1] Published as: Karl J. Romanowicz, Byron C. Crump, George W. Kling. Rainfall alters permafrost soil redox conditions, but meta-omics show divergent microbial community responses by tundra type in the Arctic. Soil Systems. 2021. 5(17), 1-29.

2.2 Introduction

Permafrost soils consist of permanently frozen ground (permafrost) overlain by a shallow, seasonally-thawed active soil layer (the 'active layer'). These soils store nearly half of all global belowground organic carbon (OC; ~1,300 Pg) (Hugelius et al. 2014). The decomposition and net storage of OC is controlled in large part by redox conditions in the active layer that are regulated by the availability of oxygen (O_2) (Gorham 1991). Permafrost affects redox conditions by confining soil water to the active layer, resulting in soil saturation and thus periodic or persistent soil anoxia (Margesin 2009, Zona 2016). Anoxic conditions develop when O_2 is consumed through biochemical processes (e.g., aerobic respiration) or geochemical reactions (e.g., iron oxidation) faster than it is introduced to the soil by diffusion, plant roots, or infiltrating rainwater (Trusiak et al. 2019, Herndon et al. 2020). Permafrost soils support anaerobic microbial metabolism and serve as a major source of methane (CH_4) when OC is decomposed under anoxic conditions (Bubier et al. 1995, Turetsky et al. 2008, Olefeldt et al. 2013).

In the Arctic, permafrost soils serve as a net sink for atmospheric carbon (Miller et al. 1983, McGuire et al. 2009), but the net carbon dioxide (CO_2) balance of these soils with the atmosphere is changing with recent warming (Oechel et al. 1993, Euskirchen et al. 2017) that has thawed large regions of permafrost and deepened the active layer (Osterkamp & Romanovsky 1999, Brown et al. 2000, Jorgenson et al. 2006). Warming has also increased rainfall intensity, frequency, and accumulation in active layer soils (Kumar et al. 2012, Spence & Phillips 2015, Bintanja & Andry 2017) that has led to deeper permafrost thaw (Douglas et al. 2020) and greater CH_4 release from thawing permafrost soils (Neumann et al. 2019). Thus, permafrost thaw and changes in drainage and precipitation will likely lead to greater fluctuations in water levels and redox conditions in the active layer (Herndon et al. 2020). These warming-induced changes will likely trigger increased microbial activity that leads to faster rates of OC decomposition and the release of CO_2 and CH_4 to the atmosphere (Schuur et al. 2009, Grosse et al. 2011, Mackelprang et al. 2011, Xue et al. 2016). Research has shown that soil draining and water-level variation leads to rapid aerobic decomposition of soil OC to CO_2 (Wickland et al. 2006, Merbold et al. 2009, Huemmrich et al. 2010, Zona et al. 2012, Elberling et al. 2013, Lawrence et al. 2015). Previous research has also found that adding O_2-rich rainwater to saturated active layer soils rapidly changed redox conditions, which increased the abiotic degradation of OC to CO_2 (Trusiak et al. 2019). What remains unknown is the impact of rainfall and altered redox conditions on the microbial

communities in these active layer soils, and specifically their metabolic capacity for anaerobic CH_4 production and aerobic respiration following soil oxidation.

Redox conditions regulate the microbial decomposition of soil OC into CH_4 or CO_2 by controlling microbial gene expression in response to O_2 availability (Lawrence et al. 2015). Under anoxic conditions, OC is degraded stepwise through anaerobic pathways of fermentation and acetogenesis that supply alcohols and organic acids as substrates for methanogenesis (Lipson et al. 2013). In oxidized soils, aerobic heterotrophic microbes decompose biopolymers into simple sugars (Ivanova et al. 2016) or oxidize CH_4 to CO_2 as an energy source (Kolb 2009). Thus, the microbial response to rainfall within anoxic active layer soils will likely be controlled by changes in soil redox conditions via an increase in dissolved O_2 concentration. However, the extent to which microbial communities can respond to rainfall-induced changes in soil redox conditions, or the duration of their response following rainfall, has yet to be determined.

Rainfall and soil oxidation may also stimulate microbial community responses that differ between distinct tundra types. The low arctic landscape is dominated by two tundra types, tussock tundra and wet sedge tundra, that differ in landscape position, dominant vegetation, soil properties, redox conditions, and microbial community composition (Walker et al. 1994, Judd & Kling 2006, Judd et al. 2006, Zak & Kling 2006, Hobbie & Kling 2014, Ward & Cory 2015). Previous studies in the low arctic that use next-generation sequencing techniques to characterize the microbial taxa inhabiting permafrost soils have focused on polygonal tundra of the coastal plains (Lipson et al. 2013, Tas et al. 2018) or boreal forests and shrub-dominated tundra in the discontinuous permafrost zone (Deng et al. 2015, Hultman et al. 2015, Tripathi et al. 2018). Current characterizations of the microbial communities within tussock tundra and wet sedge tundra are limited to phospholipid fatty acid (PLFA) analyses (Zak & Kling 2006) and terminal restriction fragment length polymorphism (T-RFLP) analyses (McMahon et al. 2011), which limits our ability to predict how these distinct microbial communities may respond metabolically to rainfall-induced changes in soil redox conditions. It is likely that the extent of the microbial response to rainfall and soil oxidation among these tundra types will be constrained by the microbial species composition and their functional genes, as well as the expression of their genes under changing soil redox conditions; we test that idea in this paper.

Here, we provide mechanistic explanations for the microbial community response to rainfall-induced soil oxidation using an integrated meta-omics approach coupled with soil O_2 modeling. Meta-omics studies reveal the composition and diversity of soil microbial communities, their functional potential, and *in situ* gene expression during environmental disturbances without the need for cultivation (Jansson & Hofmockel 2018). As such, we determined the taxonomic composition and genomic potential of the soil microbial communities within tussock tundra and wet sedge tundra using 16S rRNA amplicons and metagenomics. Using metatranscriptomics we determined microbial gene expression within the communities of both tundra types under initial anoxic conditions and again following a simulated rainfall event to oxidize the soil. To determine the magnitude and temporal extent of rainfall-induced soil oxidation, we modeled both the accumulation of dissolved O_2 added to the soil in rainfall and the consumption of dissolved O_2 following rainfall as the saturated soils re-acclimated. Our modeled concentrations of dissolved O_2 after rainfall were then coupled with the observed patterns in microbial gene expression in response to rainfall at 4-hours and 24-hours following the rainfall event. We also conducted a separate soil incubation experiment to measure rates of microbial respiration and CH_4 production under anoxic and oxic conditions that mimic pre- and post-rainfall soil redox conditions. We hypothesized that an increase in soil oxygenation by rainfall would (1) decrease the microbial expression for anaerobic metabolism genes as well as the rates of CH_4 production, while (2) increasing growth expression for aerobic microbial taxa and subsequent CO_2 emissions in response to the rapid shift in soil redox conditions. We also hypothesized that the extent of rainfall-induced changes in microbial gene expression patterns depends on the genomic potential of tussock tundra or wet sedge tundra microbial communities to respond to changing soil redox conditions, as well as on the amount of dissolved O_2 supplied to the soil.

2.3 Materials and Methods

2.3.1 Mesocosm Design

A total of 12 intact soil-plant cores (diameter 28 cm; length 31 ± 4 cm) were collected from two dominant tundra types, tussock tundra and wet sedge tundra, near Toolik Lake, Alaska (68°38’ N, 149°43’ W) between July and August 2017 and transferred to 20 L plastic buckets to establish the mesocosm experiment. Triplicate mesocosms from each tundra type were separated into two distinct study groups: (1) biotic response cores (N = 6) and (2) abiotic response cores (N = 6),

where results from the abiotic response cores are previously described (Trusiak et al. 2019). The full mesocosm experiment was split into two study groups to avoid the effects of destructive soil sampling necessary for the biotic response cores. The mesocosm experimental procedures for biotic and abiotic cores were identical and consisted of an acclimation period under static waterlogged conditions (i.e., no flowing water) for 4-7 days to generate reducing conditions observed in intact soils in the field (Page et al. 2014, Trusiak et al. 2018), followed by a flushing period over 1-4 hours to mimic the effects of brief and rapid changes in redox conditions induced by rainfall (see Figure SI 2.7). The flushing period consisted of ten individual flushes of 2 L of DI water per flush for each replicate mesocosm. The total volume of water flushed was chosen to represent rainfall events up to and in excess of the natural rainfall pattern near Toolik Field Station, which received ~270 mm of rainfall between 1 June and 30 September 2017 (Environmental Data Center). Additional details of the mesocosm design are provided in Appendix A.

2.3.2 Soil Properties

Soil properties for pH, conductivity (μS cm-1), temperature (°C), dissolved soil O_2 (mg O_2 L^{-1}), and soil moisture (% water), the latter of which was calculated as the volumetric water content (VWC) of the soil, were measured directly at 10-20 cm depth in the biotic response cores at the end of the anoxic acclimation period prior to rainfall treatments. Soil properties for bulk density (g soil dry cm^{-3}), porosity (% soil volume), organic matter content (%), and organic carbon content (% C) were determined from subsamples of the biotic response cores taken at the end of the experiment. All tussock tundra soil cores were composed of an upper organic soil layer (0-20 cm) and a lower mineral soil layer (20-30 cm) whereas all wet sedge tundra soil cores were composed entirely of organic soil (0-30 cm). Additional details are provided in Appendix A.

2.3.3 Soil Sample Collection

For all biotic response cores, an initial soil sampling event was conducted at the end of the anoxic acclimation period, representing sampling time point "T0". Mesocosm replicates were then flushed to simulate rainfall as described above (Figure SI 2.7). Additional soil sampling events were conducted at 4-hours ("T4") and 24-hours ("T24") following simulated rainfall. At each sampling time point, duplicate soil cores (diameter 2.54 cm, length 30 cm) were extracted from each mesocosm replicate and homogenized by depth in 10-cm increments. The 10-20 cm soil increment, composed of organic soil in all mesocosms, was chosen for all downstream microbial

analyses and preserved in RNA*later* Stabilization Reagent (Qiagen, Hilden, Germany) in sterile tubes at 4°C for 18 hours and then stored at -80°C until thawed for extraction (N=18).

2.3.4 Modeling Soil O_2 Accumulation and Consumption Rates

A mass balance model was developed to estimate the rates of soil O_2 accumulation introduced through rainfall and soil O_2 consumption following rainfall, as well as the final concentrations of soil O_2 at each sampling time point in the mesocosm experiment (Figure SI 2.8). Measurements derived from both the abiotic response cores (Trusiak et al. 2019) and the biotic response cores (this study) in the mesocosm experiment were incorporated into the mass balance model to estimate the rates of rainfall O_2 (F_{rain}) and soil O_2 consumption (S_{all}) (Figure SI 2.8). The rates of soil O_2 diffusion (F_{atm}) were considered to be zero during this relatively short experiment, and there was no groundwater O_2 (F_{ground}) or soil O_2 leaching (F_{leach}) (Figure SI 2.8). The initial concentration of soil O_2 (M_t; mg O_2 L^{-1}) in the biotic response cores was measured at the end of the anoxic acclimation period (T0) prior to simulated rainfall (details in Appendix A). No additional measurements for soil O_2 concentration were taken in the biotic response cores, and soil measurements for tussock tundra and wet sedge tundra reported for the abiotic response cores (Trusiak et al. 2019) were used to model rates of soil O_2 accumulation during the DI water flush (F_{rain}; mg O_2 L^{-1} hr^{-1}) and calculate the final soil O_2 concentration at the end of the DI water flush (M_f; mg O_2 L^{-1}) in the biotic response cores (details in Appendix A). Likewise, additional soil measurements for tussock tundra and wet sedge tundra reported for the abiotic response cores (Trusiak et al. 2019) were used to model the rates of soil O_2 consumption during the re-acclimation phase following simulated rainfall (S_{all}; mg O_2 L^{-1} hr^{-1}) and calculate the final soil O_2 concentration at 4-hour (M_{f+4}; T4) and 24-hour (M_{f+24}; T24) following DI water flush (details in Appendix A).

2.3.5 Nucleic Acid Extraction and Sequencing

Microbial RNA and DNA were extracted from soil samples collected at the 10-20 cm depth in each tundra mesocosm at each sampling time point (N=18) in the biotic response cores using the RNeasy PowerSoil Total RNA Isolation kit (Qiagen) and RNeasy PowerSoil DNA Elution Accessory kit (Qiagen), respectively, following the manufacturer protocol. PCR amplicon sequencing of the 16S ribosomal RNA genes was conducted on the extracted DNA following the Earth Microbiome Project protocol (N=18; details in Appendix A). Samples for 16S amplicons were sequenced at the University of Michigan Microbiome Core with Illumina MiSeq 2 x 150 bp

paired-end reads. Metagenome sequences were generated from extracted DNA (N=15; details in Appendix A) and sequenced at the University of Michigan Advanced Genomics Core with Illumina HiSeq (4000) 150 bp paired-end reads. Metatranscriptome reads were generated from total RNA extractions (N=12; details in Appendix A) and sequenced at the University of Michigan Advanced Genomics Core with Illumina HiSeq (4000) 150 bp paired-end reads.

2.3.6 16S rRNA Gene Analysis

The 16S amplicon sequences were paired, quality filtered, dereplicated, and aligned to the SILVA reference database (Quast et al. 2013) (v.132) with chimeras removed using the VSEARCH algorithm (Rognes et al. 2016), all using MOTHUR (Schloss et al. 2009). The remaining quality-controlled (QC) reads were classified using a Bayesian classifier with the RDP training set (Wang et al. 2007). Reads were then clustered at 97% similarity to form operational taxonomic units (OTUs) and rarefied to 9,565 sequences per sample (average 14,562 QC sequences per sample prior to rarefying; Table SI 2.6) with raw counts transformed into relative abundance (average 95% community coverage for rarefied samples; Table SI 2.6). The consensus taxonomy for each OTU was assigned using the RDP classifier trained to the SILVA database (v.132). OTUs classified as Eukaryote, Chloroplast, Mitochondria, and Unknown were removed, with raw counts for remaining OTUs and their taxonomic classification provided in an OTU table.

2.3.7 Metagenome Assembly

DNA sequences were trimmed and quality-filtered with the BBDuk algorithm from BBMap (Bushnell 2015) with dereplication. Quality-controlled metagenome reads from each sample (average 36.8 x 10^6 QC reads per sample; Table SI 2.7) were normalized to 20x kmer coverage with kmers below 5x coverage removed using BBNorm from BBmap (Bushnell 2015) prior to co-assembling using MEGAHIT (Li et al. 2015). The co-assembled contigs were indexed using Bowtie2 (Langmead & Salzberg 2012) and short reads from each sample were individually mapped to the indexed contigs using BBMap (Bushnell 2015). A contigs database was created from the co-assembly using Anvi'o (Eren et al. 2015) with the abundance information for all contigs merged into an Anvi'o profile. Coding sequences (CDS) within the contigs database were predicted with PRODIGAL (Hyatt et al. 2010) while HMMER (Eddy 2011) was used to search for and tabulate the occurrence of single-copy housekeeping genes for bacteria and archaea from two collections (Campbell et al. 2013, Rinke et al. 2013). CDS were also annotated to the Kyoto

Encyclopedia of Genes and Genomes database (KEGG) (Kanehisa et al. 2008) as well as taxonomically annotated using the online GhostKOALA program (Kanehisa et al. 2016) and imported into the contigs database. Counts per annotation were normalized to genes per million (GPM) (Wagner et al. 2012) to reduce biases associated with library size and CDS length, and to express all counts as a portion of one million. The mapping information for each sample mapped to the contigs database was merged into a single Anvi'o profile prior to binning contigs into metagenome assembled genomes (MAGs) using CONCOCT (Alneberg et al. 2014) and MetaBAT (Kang et al. 2015). Redundant MAGs derived from the independent binning algorithms were dereplicated using DASTools (Sieber et al. 2018) to generate the final MAGs dataset, where MAGs with > 70% completeness and < 10% redundancy were retained. Retained MAGs were queried against the Genome Taxonomy Database (GTDB) (Parks et al. 2020) using the contigs and profile databases within Anvi'o to generate a consensus taxonomy for each MAG and its relative abundance across all samples.

2.3.8 Metatranscriptome Assembly

RNA sequences were trimmed and quality-filtered with the BBDuk algorithm from BBMap (Bushnell 2015) without dereplication to determine the abundance of transcribed genes. Quality-controlled metatranscriptome reads (average 26.3 x 10^6 QC reads per sample; Table SI 2.8) were mapped to KEGG-annotated coding sequences (CDS) indexed from the metagenome assembly using BBMap to generate pile-up files (average read depth per gene), while SAMtools was used to extract counts and CDS lengths from the BBMap output (Bushnell 2015). On average, 65% of the metatranscriptome CDS were expressed (> 1 count per read) with 40% of expressed CDS assigned KEGG functional annotations, of which 99% were also assigned taxonomic annotations. Counts per annotation were normalized to transcripts per million (TPM) (Wagner et al. 2012) to reduce biases associated with library size and CDS length, and to express all counts as a portion of one million. This workflow assembled metatranscriptomic reads into functionally and taxonomically annotated KEGG orthologs (KOs) by mapping reads to whole genome sequences derived from the co-extracted DNA-based metagenomes.

2.3.9 Taxonomic Composition and Diversity

The taxonomic composition and diversity of the total microbial communities within tussock tundra and wet sedge tundra soils were determined from the 16S rRNA amplicons and metagenomes. Within the 16S rRNA amplicons, taxonomic composition was based on the classification of OTUs clustered at 97% similarity. Within the metagenomes, the taxonomic composition and diversity metrics were based on the relative abundance of GPM-normalized genes annotated as KEGG tier III "Ribosomes" (03010 Ribosome PATH: ko03010) further separated at the KEGG tier IV level into annotations for "small subunit ribosomal protein" (ssu) analogous to bacterial and archaeal 16S ssu rRNA and fungal 18S ssu rRNA. Similarly, the taxonomic composition and diversity of the active microbial communities within tussock tundra and wet sedge tundra soils were determined from the TPM-normalized metatranscriptomes annotated as the KEGG tier IV ribosomal category "ssu". Pairwise comparisons between microbial taxa within total or active tundra communities were calculated using paired t-tests or between sampling time points within tundra communities using two-way ANOVA based on differences in relative abundance. Shannon-Wiener diversity index was calculated with raw taxonomic gene counts and assessed via two-way ANOVA to determine the effects of tundra type on total and active taxonomic alpha diversity. Beta diversity treatment effects were estimated using permutational multivariate analysis of variance (PERMANOVA) based on Bray-Curtis dissimilarity distance between taxonomic gene counts using the vegan package (Oksanen & Blanchet 2019) in the R software environment (R Core Development Team 2017), and PCoA plots were generated using the ggplot2 package (Wickham 2016). Throughout this paper, all statistical analyses were considered significant at $p < 0.05$.

2.3.10 Genomic Potential and Functional Gene Expression

The genomic potential and functional gene expression within the total and active communities in tussock tundra and wet sedge tundra soils were determined from the GPM-normalized metagenomes and TPM-normalized metatranscriptomes, respectively, based on the relative abundance of genes annotated to KEGG tiers II-IV. Pairwise comparisons among functional genes between tundra communities were calculated using paired t-tests or between sampling time points within tundra communities using two-way ANOVA based on differences in relative abundance and visualized with Z-score transformations using pheatmap (Kolde 2015) in

R. Diversity analyses of the functional genes were performed using the vegan package (Oksanen & Blanchet 2019) in R. Shannon-Wiener diversity index was calculated with raw functional gene counts and assessed via two-way ANOVA with post hoc Tukey honest significant differences (HSD) tests to determine the effect of tundra type on functional alpha diversity. Beta diversity treatment effects were estimated using PERMANOVA based on Bray-Curtis dissimilarity distance between GPM- or TPM-normalized functional gene counts with the R-vegan function adonis.

2.3.11 Differential Gene Expression

Differential gene expression (DGE) analysis was applied to the TPM-normalized metatranscriptomes, where DGE between sampling time points within each tundra type was determined using the glmFit function within edgeR (Robinson & Oshlack 2010) based on KO values, after setting calcnormfactors to "none" to avoid default TMM normalization by edgeR. The generalized linear models were fit to a design matrix based on the experimental design to test for differential expression between sampling time points while adjusting for differences between mesocosm replicates at each sampling time point. This was considered an additive linear model with mesocosm replicates at each sampling time point as the blocking factor. DGE for TPM-normalized KOs were considered differentially expressed if the false discovery rate (FDR) (Benjamini & Hochberg 1995) value of p was < 0.05.

2.3.12 Oxygen-Regulated Gene Expression

Results from the DGE analysis (log fold-change) were evaluated for the differential expression of oxygen (O_2)-regulated functional KOs (i.e., genes) between sampling time points within each tundra type. Genes identified as O_2-regulated infers that their expression can be either positively or negatively affected by O_2 availability and the differential expression of these genes is an indication that simulated rainfall changed soil redox conditions through an increase in dissolved O_2 concentration. Select marker genes that are considered to be O_2-regulated were chosen from previous studies (Kieft et al. 2018) and includes genes from obligate anaerobic pathways of carbon fixation, fermentation, denitrification, and methanogenesis, as well as genes from obligate aerobic pathways of carbon fixation and methane oxidation. Additional O_2-regulated genes from KEGG Metabolism categories were chosen from the reference database in Wu and Moore (2010), which identified KO groups of which gene distributions were statistically different for aerobic vs. anaerobic environmental conditions. In the reference study, complete prokaryotic

genomes in NCBI's Microbial Genome Project Database were used to statistically predict correlations between functional KO groups and O_2 requirements (see Wu & Moore 2010).

2.3.13 Iron Redox Cycling Gene Expression

The microbial pathways for iron (Fe) oxidation and dissimilatory Fe reduction were quantified as additional proxies for obligate aerobic or anaerobic gene expression, respectively. Established gene annotation pipelines such as GhostKOALA (Kanehisa et al. 2016), used in this study, generally do not incorporate hidden Markov models (HMMs) capable of annotated Fe redox cycling genes (Garber et al. 2020). We re-annotated the metatranscriptome contigs using FeGenie (Garber et al. 2020), which provides a comprehensive database of HMMs based on genes related to Fe oxidation or reduction in bacteria and archaea. Counts within each Fe gene category were summarized as their relative abundance against the sum of all identified Fe genes with only those genes identified for Fe oxidation or reduction presented in this study. Pairwise comparisons with two-way ANOVA were conducted across sampling time points within the Fe oxidation or reduction gene categories to determine if rainfall-induced soil oxidation changed obligate redox-dependent gene expression.

2.3.14 Microbial Respiration and Methane Production

The rates of microbial respiration (CO_2) and net methane (CH_4) production were measured from a separate soil incubation experiment using a subset of each homogenized soil sample originally collected from the 10-20 cm sampling depth in each tussock tundra and wet sedge tundra mesocosm in the biotic response cores at each sampling time point (N=18). Each soil sample (average of 15 ± 5 g per sample) was placed in an individual 250 mL glass jar sealed with an airtight lid containing a septum for gas sampling. Jars containing soil collected from the T0 sampling time point were purged with N_2 to reproduce anoxic field conditions. Jars containing soil from the T4 and T24 sampling time points were purged with compressed air to reproduce oxic field conditions. Jars were incubated for 48 hours in the dark at field temperature (5°C). Following the 48-hour incubation, 20 mL of headspace gas was collected using an evacuated syringe and immediately analyzed for CO_2 and CH_4 concentrations via gas chromatography on a Shimadzu GC-14A with TCD and FID detectors (Shimadzu, Kyoto, Japan). Gas concentrations were converted to rates of gas production per hour relative to the dry mass of soil.

2.4 Results

2.4.1 Soil Properties

We measured soil properties within tussock tundra and wet sedge tundra mesocosms in the biotic response cores at the end of the anoxic acclimation period (T0) prior to simulated rainfall. Soil pH and conductivity were lower in tussock tundra soil compared to wet sedge tundra soil (paired t-test; $p = 0.03$, 0.05, respectively; Table 2.1), with measured values consistent with previous studies conducted in younger landscape tundra soils in the Toolik Lake region (Page et al. 2014, Trusiak et al. 2018, 2019). Soil temperature, moisture, and dissolved O_2 concentrations were similar between both tundra soils prior to simulated rainfall (paired t-test; $p > 0.1$ for all; Table 2.1). Organic matter content and its corresponding organic carbon content were lower in tussock tundra soil compared to the wet sedge tundra soil (paired t-test; $p = 0.04$, 0.04; Table 2.1). Bulk density was greater in tussock tundra soil compared to wet sedge tundra soil (paired t-test; $p = 0.02$; Table 2.1), with lower porosity than in wet sedge tundra soil ($p = 0.02$; Table 2.1).

2.4.2 Soil O_2 Accumulation and Consumption Rates and Final Concentrations

We added 20 L of DI water to all tundra mesocosms in the biotic response cores during the simulated rainfall event (Table 2.2). However, the duration of the DI water flush differed between tundra type due to differences in soil drainage rates, with the DI water flush taking an average of 3.77 hours to completely drain through the tussock tundra soil and 1.13 hours to completely drain through the higher-porosity wet sedge tundra soil (paired t-test; $p = 0.02$; Table 2.2). Our modeled rates of soil O_2 accumulation (F_{rain}; mg O_2 L^{-1} hr^{-1}) at the 15-cm sampling depth during the DI water flush were similar between the tussock tundra and wet sedge tundra soils (paired t-test; $p = 0.7$; Table 2.2). Yet, due to differences in the duration of the DI water flush and the residence time of the oxygenated DI water among tundra soils, the soil O_2 concentration (M_f; mg O_2 L^{-1}) at the 15-cm sampling depth at the end of the DI water flush for tussock tundra increased 8.5-fold while increasing only 4-fold in wet sedge tundra (Table 2.2). Overall, the soil O_2 concentration at the end of the DI water flush was 2.5-fold greater in the tussock tundra soil than in wet sedge tundra soil (paired t-test; $p = 0.02$; Table 2.2). Our modeled rates of soil O_2 consumption (S_{all}; mg O_2 L^{-1} hr^{-1}) during the re-acclimation phase following the DI water flush were greater in the tussock tundra soil compared to the wet sedge tundra soil (paired t-test; $p = 0.03$; Table 2.2).

2.4.3 Taxonomic Composition and Diversity of the Microbial Communities

Using 16S rRNA amplicons and metagenomes annotated as KEGG tier III "Ribosomes", we found that the total microbial communities from both tundra types were dominated by Bacteria (> 98% relative abundance; Figure 2.1A; 2.1B), but there were significant differences in the relative abundance of bacterial phyla between tundra communities (paired t-test; $p < 0.05$ for all; Table 2.3). Specifically, bacterial taxa in the tussock tundra total community were dominated by Acidobacteria, Actinobacteria, Alphaproteobacteria, Gammaproteobacteria, Planctomycetes, and Verrucomicrobia (> 85% of total community; Figure 2.1A; Table 2.3). Bacterial taxa in the wet sedge tundra total community were dominated by the same phyla as the tussock tundra community, but with elevated contributions of Betaproteobacteria, Deltaproteobacteria, Bacteriodetes, Chloroflexi, and Firmicutes (Figure 2.1B; Table 2.3). Archaeal taxa were composed primarily of methanogenic Euryarchaeota (Table 2.3), which were present only in the wet sedge tundra total community and included dominant taxa such as *Methanobacterium*, *Methanocella*, *Methanomicrobia*, *Methanoregula*, *Methanosarcina*, and *Methanothrix*. Fungal taxa were composed primarily of Ascomycetes (Table 2.3), which were present almost exclusive to the tussock tundra community and included dominant taxa *Aspergillus*, *Coccidioides*, *Glarea*, *Histoplasma*, *Marssonina*, *Phialocephala*, and *Sclerotinia*.

As expected, the taxonomic composition of the total microbial communities did not differ between sampling time points (24 hr) within tussock tundra or wet sedge tundra soils in any dataset (ANOVA; $p > 0.05$ for all). The total community from wet sedge tundra had significantly higher taxonomic alpha diversity of ribosome genes than the tussock tundra community (paired t-test; $p < 0.01$; Table SI 2.9). Beta diversity results indicated significant differences in taxonomic composition between tundra communities ($p < 0.01$), but no difference between sampling time points ($p = 0.7$) or the interaction of tundra community by sampling time points (PERMANOVA; $p = 0.6$; Table SI 2.10). The majority of our high-quality metagenome-assembled genomes (MAGs; > 70% complete, < 10% redundancy) were classified to the dominant bacterial phyla Acidobacteria, Actinobacteria, Chloroflexi, and multiple classes of Proteobacteria (Table SI 2.11). The majority of MAGs recovered were found predominantly in the wet sedge tundra community compared to the tussock tundra community based on their relative abundance (Table SI 2.11). However, MAGs with greater relative abundance in the tussock tundra community also had larger genomes (Table SI 2.11).

We also determined differences in the relative abundance of active microbial taxa between tussock tundra and wet sedge tundra communities using the TPM-normalized metatranscriptomes annotated as KEGG tier III "Ribosomes." Active taxa within each tundra community were an expressed subset of the total community identified in the metagenome (Figure 2.1A; 2.1B) with no significant differences in the relative abundance of active microbial taxa between sampling time points for tussock tundra or wet sedge tundra soils (ANOVA; $p > 0.05$). Within tussock tundra, Actinobacteria and Acidobacteria accounted for 83% of the active community (Table 2.3). Methanogenic Euryarchaeota were also detected in the tussock tundra active community, including taxa from *Methanosarcina* and *Methanothrix*, although at significantly lower abundance than in the wet sedge tundra active community (paired t-test; $p < 0.05$ for all; Table SI 2.12). Within wet sedge tundra, Actinobacteria and Acidobacteria accounted for only 48% of the active community with high relative abundance of Deltaproteobacteria (13%), Firmicutes (10%), Chloroflexi (8%), and archaeal Euryarchaeota (7%) (Table 2.3). Deltaproteobacteria were dominated by *Geobacter* spp., representing 3% of the active community relative abundance (Table SI 2.12). The high relative abundance of active Euryarchaeota is due mainly to an increase in *Methanosarcina* and *Methanothrix* spp. (4%, 1%, respectively; Table SI 2.12).

2.4.4 Genomic Potential and Functional Gene Diversity of the Microbial Communities

The genomic potential of tussock tundra and wet sedge tundra microbial communities indicated that the KEGG tier II category "Metabolism" had the greatest relative abundance of annotated functional genes in both tundra communities, followed by genes annotated as "Genetic Information Processing", "Environmental Information Processing", and "Cellular Processes", with significant differences in relative abundance between tussock tundra and wet sedge tundra communities for all categories except Genetic Information Processing (Figure SI 2.9). At the KEGG tier III level (sub-categories within tier II), we found significant differences in the relative abundance of most functional gene categories (15 of 22 categories) between tundra communities (ANOVA; $p < 0.05$ for all; Figure 2.2A; 2.2B). Specifically, there was significantly greater abundance for Metabolism functional genes associated with amino acids, carbohydrates, nucleotides, biosynthesis of secondary metabolites, and xenobiotics degradation in the tussock tundra community relative to the wet sedge tundra community (Figure 2.2B). There was also greater relative abundance of functional genes associated with folding, sorting and degradation,

signal transduction, as well as cellular communities, cell motility, and transport and catabolism in the tussock tundra community. In contrast, there was greater relative abundance of functional genes associated with energy metabolism, translation, and membrane transport in the wet sedge tundra community (Figure 2.2B). The wet sedge tundra microbial community had significantly higher alpha diversity of functional genes than the tussock tundra community (paired t-test; $p < 0.001$; Figure SI 2.9; Table SI 2.9). Beta diversity results indicated significant differences in the relative abundance of functional genes between tundra communities ($p < 0.001$), but no difference in relative abundance between sampling time points ($p = 0.8$) or the interaction of tundra communities by sampling time points (PERMANOVA; $p = 0.6$; Figure SI 2.9; Table SI 2.10).

2.4.5 Microbial Community Expression in Response to Rainfall

The change in microbial gene expression in response to rainfall was determined using the relative abundance of TPM-normalized metatranscriptomes annotated at KEGG tiers II-IV. Within the tussock tundra community, the relative abundance of expressed functional genes annotated to the KEGG tier II category of Metabolism was significantly greater at T0 relative to the abundance of expressed genes at T4 and T24 (ANOVA; $p < 0.01$ for both; Figure 2.3A). Following simulated rainfall, the relative abundance of expressed genes at T4 and T24 was significantly greater for the KEGG tier II category of Genetic Information Processing relative to T0 (ANOVA; $p < 0.01$ for both; Figure 2.3A). The relative abundance of expressed genes for the KEGG tier II category of Cellular Processes was also significantly greater at T4 relative to T0 (ANOVA; $p < 0.01$; Figure 2.3A) but was not significantly different at T24 relative to T0 (ANOVA; $p = 0.1$; Figure 2.3A).

In contrast to the tussock tundra community, broad patterns of microbial gene expression in the wet sedge tundra community for the KEGG tier II categories of Metabolism, Genetic Information Processing, Environmental Information Processing, or Cellular Processes showed no significant change in relative abundance between any sampling time points (ANOVA; $p > 0.05$ for all; Figure 2.3B). Expressed gene abundance was greatest in the Metabolism category and included numerous anaerobic pathways with oxygen-regulated KOs for carbohydrate metabolism (K00128, K00161, K00656, K00975), amino acid metabolism (K00146), lipid metabolism (K00763), and energy metabolism, the latter of which included KOs from multiple pathways of methanogenesis (hydrogenotrophic: K00200, K00204, K00319, K00672, K01499, K13942; acetoclastic: K00193, K00625, K00925, K01895; and methylotrophic: K04480, K14080, K14081) as well as

methanotrophy (K10944, K14028, K16157, K16160, K23995) (Table SI 2.13). Additional pathways with oxygen-regulated KOs included anaerobic carbon fixation (K00174, K00194, K00244, K00855, K01648), fermentation (K00169, K00016), and denitrification (K00368, K00370, K00376, K02305, K02567, K15864) (Table SI 2.13). Using DGE analysis, we found no significant differences in the expression of any oxygen-regulated KO between sampling timepoints, but there were significant increases in the expression of obligate anaerobic denitrification KOs including nitrite reductases (K00368, K00370, K15864), nitric oxide reductases (K02305, K04561), and nitrous-oxide reductase (K00376) following rainfall at T4 relative to T0 (DGE; FDR < 0.05 for all). Overall, the alpha diversity of expressed functional genes was similar between sampling time points throughout the experiment (ANOVA; $p > 0.5$; Figure SI 2.10; Table SI 2.9). Beta diversity results indicated no significant difference in the relative abundance of expressed functional genes between sampling time points within the wet sedge tundra community (PERMANOVA; $p = 0.2$; Figure SI 2.10; Table SI 2.10).

Within the tussock tundra community, the relative abundance of expressed transcripts in the Metabolism KEGG tier IV pathways of glycolysis / gluconeogenesis and butanoate metabolism (tier III carbohydrates), nicotinate and nicotinamide metabolism (tier III cofactors and vitamins), and carbon metabolism, fatty acid metabolism, and degradation of aromatic compounds (tier III overview), were significantly greater at T0 relative to their abundance at T4 and T24 (ANOVA; $p < 0.05$ for all; Figure 2.4). For Genetic Information Processing, the KEGG tier IV pathway of ribosome (tier III translation) had significantly greater abundance of expressed transcripts at T24 relative to T0, but not initially following rainfall at T4 relative to T0 (ANOVA; $p = 0.02$, $p = 0.07$, respectively; Figure 2.4). The KEGG tier IV pathway of RNA degradation (tier III folding, sorting and degradation) had significantly greater abundance of expressed transcripts at T4 relative to T0 (ANOVA; $p < 0.01$; Figure 2.4). For Cellular Processes, the KEGG tier IV pathway of Caulobacter cell cycling (tier III cell growth and death) had significantly greater abundance of expressed transcripts at T4 relative to T0 (ANOVA; $p < 0.01$; Figure 2.4). Likewise, the relative abundance of expressed transcripts in the tier IV pathway of ferroptosis was significantly greater at T4 relative to T0 (ANOVA; $p = 0.02$, not shown).

Within significant KEGG-Metabolism categories (ANOVA; Figure 2.4), we found several KOs explicitly identified as O_2-regulated (Wu & Moore 2010) that were significantly differentially expressed to a lower extent at T4 relative to T0 in the tussock tundra community using DGE

analysis (DGE; FDR < 0.05 for all; Table 2.4). This included O_2-regulated KOs that are negatively affected by O_2 availability expressed in carbohydrate metabolism (K00975, K00656), cofactor and vitamins metabolism (K00763), amino acid metabolism (K01915), and carbon metabolism (K00873, K01623, K00626) (Table 2.4). Only aldehyde dehydrogenase (K00128), an O_2-regulated KO positively affected by O_2 availability expressed in carbohydrate metabolism, was expressed at a significantly higher rate at T4 relative to T0 (Table 2.4). We also found that O_2-regulated KOs negatively affected by O_2 availability expressed in anaerobic carbon fixation (K00174, K00855), fermentation (K00169), and acetoclastic methanogenesis (K00625, K00925, K01895), were all expressed to a significantly lower extent at T4 relative to T0 in the tussock tundra community (DGE; FDR < 0.05; Table 2.4).

From our DGE analysis, we also found that KOs related to ribosome translation (KEGG tier II Genetic Information Processing), including DNA repair proteins (K03584), RNA polymerase (K03040, K03043, K03046), pre-mRNA-processing factors (K12856, K12821), RNA-binding proteins (K12876), and more than 150 differentially expressed ribosomal protein genes (small subunit, large subunit; ko03010 path) from multiple bacterial phyla and even several species of fungi within the Ascomycetes, were all expressed to a significantly higher extent at T4 relative to T0 in the tussock tundra community (DGE; FDR < 0.05). KOs related to Caulobacter cell cycling (KEGG tier II Cellular Processes), including ATP-dependent Lon protease (K01338), ATP-dependent Clp protease (K01358), and cell division proteins (K03531) also had significantly higher expression at T4 relative to T0 (DGE; FDR < 0.05). KOs related to ferroptosis (KEGG tier II Cellular Processes), including an Fe-regulated transporter for solute carrier family 40 (K14685), which regulates Fe ion transmembrane transporter activity, also had significantly higher expression at T4 relative to T0 (DGE; FDR < 0.05).

Overall, the DGE analysis indicated that the greatest differential expression of KOs was between tussock tundra and wet sedge tundra communities at each sampling time point. Specifically, 24% of KOs (out of 166,754 total KOs) were differentially expressed between tundra communities at T0 (DGE; FDR < 0.05; Table 2.5). Similarly, 28% and 10% of KOs were differentially expressed between tundra communities at T4 and T24, respectively (DGE; FDR < 0.05; Table 2.5). Within the tussock tundra community, DGE results indicated that 1.3% of KOs were differentially expressed between sampling time points T4 and T0 (out of 100,055 total KOs; FDR < 0.05; Table 2.5), which included the oxygen-regulated KOs (Table 2.4) as well as all KOs

in the KEGG tier II categories of Genetic Information Processes and Cellular Processes. The DGE analysis for all remaining timepoint comparisons in both tundra communities indicated that < 0.1% of total KOs were differentially expressed (DGE; FDR < 0.05; Table 2.5).

2.4.6 Iron Redox Cycling Gene Expression

Within the tussock tundra community, the relative abundance of expressed obligate aerobic genes associated with Fe oxidation was significantly greater at T4 relative to their abundance at T0 (ANOVA; $p = 0.04$; Figure 2.5A). The relative abundance of expressed obligate anaerobic genes associated with dissimilatory Fe reduction was negligible (< 1% of expressed Fe gene relative abundance; Figure 2.5A). Furthermore, the relative abundance of dissimilatory Fe reducing genes in the tussock tundra metagenome dataset was negligible (< 1% of total Fe gene relative abundance; Figure 2.5A), indicating a complete lack of dissimilatory Fe reducing genes in the genomic potential of the microbial community. The mean relative abundance of expressed Fe oxidation genes in the tussock tundra community was 43-fold greater than the mean relative abundance of expressed Fe reduction genes when averaged across all sampling time points (paired t-test; $p < 0.01$; Figure 2.5A). In contrast, there were no significant differences in the relative abundance of expressed Fe oxidation genes or Fe reduction genes between sampling time points in the wet sedge tundra community (ANOVA; $p = 0.2$; Figure 2.5B). The mean relative abundance of expressed Fe reduction genes in the wet sedge tundra community was 4-fold greater than the mean relative abundance of expressed Fe oxidation genes when averaged across time points (paired t-test; $p < 0.01$; Figure 2.5B).

2.4.7 Soil Incubations

The rates of microbial respiration (CO_2 as ng C g^{-1} soil hr^{-1}) did not differ significantly between sampling time points in the tussock tundra or wet sedge tundra communities (ANOVA; $p = 0.9, 0.3$, respectively; Figure 2.6A). However, the mean rate of microbial respiration was 4.5-fold higher in tussock tundra compared to wet sedge tundra when averaged across sampling time points (paired t-test; $p < 0.001$; Figure 2.6A). In both tundra soils, the rates for CH_4 production (CH_4 as pg C g^{-1} soil hr^{-1}) measured at T0, which was incubated under anoxic conditions, were significantly higher than rates measured at T4 and T24, where soils were incubated under oxic conditions (ANOVA; $p < 0.001$ for all; Figure 2.6B). Negative values for CH_4 production at T4 and T24 indicate aerobic CH_4 consumption under the oxic incubation conditions (Figure 2.6B).

2.5 Discussion

We used rainfall to add oxygen (O_2) and change redox conditions in the active layer of saturated tundra soils, and measured gene expression of the microbial community. We determined that the microbial response to rainfall was not consistent between tussock and wet sedge tundra types, and the patterns of gene expression differed due to inherent differences in microbial composition and their genomic potential. We also determined that differences in soil drainage rates during the rainfall event led to a greater increase in soil O_2 concentration in the tussock tundra soil. We measured microbial gene expression at broad metabolic levels as well as from select oxygen-regulated marker genes and coupled our observed changes in microbial gene expression to the modeled changes in soil O_2 concentrations following rainfall to determine the mechanistic response of the microbial communities between tundra types.

2.5.1 Microbial Composition Differs among Tundra Communities

Previous research conducted in the Toolik Lake region showed that microbial community composition is distinct among tundra types due to landscape-dependent differences in plant community composition and litter biochemistry (Judd et al. 2006, Zak & Kling 2006), as well as physical gradients of soil drainage (Giblin et al. 1991, Nadelhoffer et al. 1991). Tussock tundra is dominated by sedges (*Eriophorum vaginatum*) and dwarf shrubs (*Betula nana, Ledum palustre*) that occupy hillslopes with greater soil drainage than wet sedge tundra, which is dominated entirely by sedges (*Carex aquatilis, C. chordorrhize, C. rotundata)* at the base of hillslopes and valley bottoms where soil water accumulates (Gebauer et al. 1996). These ecological and physical differences lead to compositionally distinct microbial communities between tussock tundra and wet sedge tundra soils, but previous studies of these communities were limited to PLFA and T-RFLP analyses (Zak & Kling 2006, McMahon et al. 2011), which provided limited information about the phylogenetic composition of these communities.

Here, higher resolution meta-omics analyses showed significant differences in the relative abundance of nearly all bacterial phyla between tussock tundra and wet sedge tundra communities (Table 2.3). Specifically, we found greater relative abundance of Acidobacteria in the tussock tundra community, likely related to the lower pH of the tussock tundra soil compared to wet sedge tundra soil (Table 2.1). This is consistent with previous studies showing strong negative correlations between Acidobacteria abundance and soil pH (Lauber et al. 2009, Rousk et al. 2010,

Tveit et al. 2013). We also found a greater relative abundance of Alpha- and Gammaproteobacteria in tussock tundra soil that could be related to their copiotrophic life strategies because nutrient levels are normally greater in tussock tundra soils relative to the downslope wet sedge tundra soils (Chapin et al. 1988), albeit with seasonal soil nitrogen limitations on microbial growth (Sistla et al. 2012). In addition, our MAGs annotated as Acidobacteria, Alpha- and Gammaproteobacteria had relatively large genomes (Table SI 2.11), which is a feature of copiotrophs that prefer nutrient-rich environments (Lauro et al. 2009). The high relative abundance of Actinobacteria in both tundra communities is likely due to the periodic (tussock tundra) or persistent (wet sedge tundra) saturation of the active layer and subsequent anoxia because Actinobacteria play an important role in the anaerobic degradation of soil organic carbon (OC) (Tveit et al. 2013). Firmicutes are also known to contribute to anaerobic soil OC degradation (Tveit et al. 2013) and their greater relative abundance in the wet sedge tundra community likely emphasizes the fact that wet sedge tundra soils experience more persistent soil anoxia due to longer periods of soil water ponding than in tussock tundra soils. Furthermore, we found that wet sedge tundra soils also harbored greater relative abundance of Deltaproteobacteria (Table 2.3), which included known anaerobic iron (Fe)-reducing *Geobacter* spp. (Table SI 2.12) that have previously been found in high abundance in the Toolik Lake region (Emerson et al. 2015).

The dominant archaeal taxa were primarily methanogenic Euryarchaeota, almost exclusive to the wet sedge tundra community (Table 2.3; Figure 2.1A; 2.1B). Specifically, we found that *Methanobacteria*, *Methanosarcina*, and *Methanothrix* were the dominant archaeal taxa in the wet sedge tundra community (Table SI 2.12), which is consistent with previous findings in organic soils across circumpolar arctic sites (Lipson et al. 2013, Deng et al. 2015, Hultman et al. 2015, Tripathi et al. 2018, Kim et al. 2016). Members of the *Methanobacteria* are hydrogenotrophic methanogens most commonly found in upper, saturated soils (Deng et al. 2015, Conrad et al. 1987) while members of *Methanosarcina* and *Methanothrix* are acetoclastic methanogens that are typically the dominant archaeal taxa in organic peat soils (Metje & Frenzel 2007, Tveit et al. 2015). The high relative abundance of both groups of methanogens in the wet sedge tundra community suggests an even greater genomic potential for CH_4 production because multiple pathways of methanogenesis can be carried out depending on substrate availability in the soil. In contrast, we were only able to detect a very low abundance of archaeal taxa in the tussock tundra community, mainly *Methanosarcina* and *Methanothrix* spp. This may be due to the greater extent of soil

drainage in the active layer that prevents substantial colonization by anaerobic archaeal taxa, or it may be an artifact of our soil samples being collected at the 10-20 cm depth in the organic active layer, which may have under-sampled the bulk of methanogenic taxa reportedly found in deeper mineral soil layers in arctic soils (Deng et al. 2015). However, even the low abundance of these active acetoclastic methanogens in the tussock tundra community led to significant declines in the expression of phosphate acetyltransferase, acetate kinase, and acetyl-CoA synthetase genes (Table 4), which are essential genes in the production pathway of CH_4 from acetate, following rainfall-induced soil oxidation.

Soil fungi were more abundant in the tussock tundra community than the wet sedge tundra community (Table 2.3; Figure 2.1A; 2.1B), confirming previous findings using PLFA ratios (Zak & Kling 2006). Historically, soil fungi have been under-sampled in arctic tundra (Malard & Pearce 2018), and we provide some of the first evidence that numerous filamentous taxa within the Ascomycetes are common in tussock tundra and absent from wet sedge tundra (Table SI 2.12). The lack of fungi in the wet sedge tundra community may be due to environmental limitations on filamentous fungi, which with few exceptions are obligate aerobes (Alexander 1976), and to their inability to disperse into and colonize the persistently anaerobic conditions of the wet sedge tundra soil (Zak & Kling 2006). Also, sedge species (*Carex* spp.) that dominate wet sedge tundra vegetation do not typically associate with mycorrhizal fungi whereas most dwarf shrubs in the tussock tundra plant community (*Betula* and *Salix*) form mycorrhizal associations (Hobbie et al. 2009). In addition, taxa within the *Leotiomycetes* class (Helotiales order) such as *Glarea* spp. and *Sclerotinia* spp. found here are known to express a broad suite of functional genes that degrade cellulolytic plant litter (Boberg et al. 2011). The presence of fungi, even though their abundance in the microbial community is relatively small, likely increases the genomic potential of the tussock tundra community to degrade soil organic carbon under aerobic conditions because of their unique suite of functional genes.

Differences in the relative abundance and diversity of microbial taxa between tussock tundra and wet sedge tundra communities likely reflect landscape-dependent patterns of community composition and lifestyle strategies. For example, the composition of the tussock tundra community suggests a copiotrophic soil community dominated by relatively few bacterial phyla and filamentous fungi that prefer more frequently-aerated, nutrient-rich soils. In contrast, the higher diversity and composition of the microbial community within the persistently saturated

wet sedge tundra soils appear more similar to oligotrophic sediment communities measured from lakes and streams in the Toolik Lake region (Judd et al. 2006, Crump et al. 2012). This comparison is reasonable given that the greater nutrient availability in tussock tundra soils (Chapin et al. 1988) likely supports more copiotrophic life strategies prevalent among the dominant taxa found in the tussock tundra community. Likewise, wet sedge tundra borders stream and lake margins (Hobbie & Kling 2014), where groundwater flows through the active layer of wet sedge tundra and into adjacent waterways, likely transporting the soil microbial taxa (Judd et al. 2006) that constitute the bulk of the diversity in river or sediment communities (Crump et al. 2012).

2.5.2 Genomic Potential Differs between Tundra Communities

Consistent with the differences in microbial composition between tundra communities, we found that the genomic potential of these distinct tundra communities differed from each other at the broad KEGG tier II categories (Figure SI 2.9). The wet sedge tundra community had a greater relative abundance of genes belonging to the Energy Metabolism pathway, suggesting a greater genomic potential for carbon metabolism, especially methanogenesis under anoxic soil conditions. In contrast, the tussock tundra community had a greater relative abundance of most other Metabolism categories at all sampling time points during our rainfall experiment (Figure 2.2A; 2.2B), possibly due to the fact that the tussock tundra community had lower alpha diversity of functional genes relative to the wet sedge tundra community (Table SI 2.9; SI 2.10). Yet, stark differences in the relative abundance of functional genes between tundra communities are seen in the beta diversity PCoA plot (Figure SI 2.9) where functional genes separate most strongly by tundra type independent of differences in soil redox conditions between soil sampling time points. Taken together, our results suggest that community composition and the associated functional genes (i.e., genomic potential) are distinct between tundra communities, which in turn may constrain or predict the microbial gene expression patterns following rainfall-induced redox changes in tussock tundra and wet sedge tundra soils.

2.5.3 Soil O_2 Accumulation during Rainfall Differs among Tundra Soils

A novel aspect of our mesocosm experimental design was our ability to model (Figure SI 2.8) the rates of soil O_2 accumulation introduced during the simulated rainfall event (F_{rain}) and soil O_2 consumption (S_{all}) during the stagnant re-acclimation phase following rainfall. Using the soil O_2 accumulation rates, we estimated the final soil O_2 concentration immediately following rainfall

(M_f). Then, by incorporating the soil O_2 consumption rates, we further estimated the final concentrations of soil O_2 at the 10-20 cm sampling depth within tussock tundra and wet sedge tundra at the 4-hour (M_{f+4}) and 24-hour (M_{f+24}) sampling time points following the rainfall event. In our mass balance model (Figure SI 2.8), we assumed that the contribution of O_2 from atmospheric diffusion into saturated soils (F_{atm}) to a depth of 10-20 cm was negligible following the rainfall event given that gas diffusion in water is slower than in air by a factor of 10^4 (Moldrup et al. 2000, Thorbjorn et al. 2008). We also assumed that the extent of any atmospheric O_2 introduced deep into saturated soils via diffusion through the aerenchyma tissues of dominant sedge species (Armstrong 1964, King et al. 1998) would be limited to the immediate vicinity surrounding plant roots because of the slow diffusion rate of gas in water, thus limiting the role of plant-mediated increases in soil O_2 concentrations. Likewise, we assumed that the contribution of soil O_2 introduced through groundwater flow (F_{ground}) or removed through soil leaching (F_{leach}) would be zero given that our mesocosm chambers were only open at the top and sealed at the bottom, except during the rainfall event.

Our mass balance model found that the accumulation of soil O_2 introduced through rainfall differed among tundra soils, with tussock tundra soils accumulating 2.5-fold more soil O_2 than wet sedge tundra soils (Table 2.2). This greater accumulation of soil O_2 in tussock tundra occurred even though both tundra soils experienced similar rates of soil O_2 accumulation and were flushed with identical volumes of DI water during the simulated rainfall event. We found that the duration of the DI water flush, which took nearly 3.5 times longer to complete in the tussock tundra soil, was the primary mechanism responsible for the longer residence time of oxygenated rainwater that lead to a greater accumulation of soil O_2. Soil drainage through the active layer of tussock tundra is strongly inhibited by the dense mineral layer located below the surface organic layer. Typically, the mineral layer in tussock tundra strictly limits deeper soil drainage under field conditions and the surface organic layer remains saturated periodically following rain events due to its high water-holding capacity (Steiglitz et al. 2003, O'Connor et al. 2020) until the soil water drains downslope through the organic layer into wet sedge tundra soils located at the base of hills (Neilson et al. 2018). Thus, the longer residence time of oxygenated rainwater added to the surface organic layer of tussock tundra led to greater O_2 concentrations at the 10-20 cm sampling depth at the end of the rainfall event compared with the wet sedge tundra soil, which drained the oxygenated rainwater quickly through its porous organic soil. This rapid flushing of the oxygenated rainwater through

the saturated wet sedge tundra mesocosm chamber is likely similar to field conditions where rainwater rapidly flushes through the saturated active layer and into an adjacent stream or lake, thus limiting O_2 accumulation in the soil.

The greater accumulation of soil O_2 in the tussock tundra soil compared to the wet sedge tundra soil at the end of the rainfall event was based solely on the accumulation rate of soil O_2 introduced during the DI water flush. However, after applying the soil O_2 consumption rates that were modeled from the re-acclimation phase following rainfall, we still found that the final soil O_2 concentrations at 4-hours and 24-hours following rainfall were 2.5-fold greater in tussock tundra soil compared with wet sedge tundra soil (Table 2.2). This difference in soil O_2 concentration between tundra soils was consistent among time points even though the rate of soil O_2 consumption was greater in the tussock tundra soil than in the wet sedge tundra soil (Table 2.2). An important note is that the soil O_2 consumptions rates are likely minimum estimates of O_2 consumption from abiotic reactions and biotic processes because the rates do not account for O_2 consumed during the slow diffusion of O_2 into the stagnant boundary layer of the soil cores (Trusiak et al. 2019).

2.5.4 Tussock Tundra Community Responds to Rainfall-Induced Soil Oxidation

For the tussock tundra community, we identified short-term (T4) and longer-term (T24) changes in microbial gene expression (Figure 2.3A; 2.4) following an 8.5-fold increase in total soil O_2 concentration introduced during rainfall (Table 2.2). These changes suggest that the increase in soil O_2 stimulated microbial taxa to invest more energy towards growth by transcribing ribosomal protein genes, and to invest less in resource acquisition via membrane transport and associated metabolic pathways. These changes also suggest a shift in expression from lower-energy anaerobic metabolic pathways to higher energy aerobic pathways (Figure 2.4; Table 2.4). DGE analysis identified elevated expression of more than 150 ribosomal protein genes across multiple bacterial and fungal taxa, and of genes for DNA repair proteins, RNA polymerase, pre-mRNA-processing factors, and RNA-binding proteins. This functional gene response to rainfall was similar to the response observed in a previous study investigating the effects of sunlight photo-alteration of dissolved organic matter (DOM) leached from tussock tundra soils on microbial gene expression (Nalven et al. 2020). This study concluded that photo-chemical changes in DOM made available easily metabolized compounds that cause microbes to enter lag phase or log phase growth. This idea that rainfall and soil oxygenation releases compounds that boost microbial growth in tussock

tundra is further supported by results from the abiotic response cores (Trusiak et al. 2019) showing that the composition of dissolved organic carbon (DOC) changed during flushing. In these cores there was a significant decrease in the fluorescence index of the DOC as the volume of water flushed through the soil increased, indicating that the DOC exported was likely more aromatic (McKnight et al. 2001), which could stimulate an increase in microbial metabolism that leads to rapid growth.

The increase in expression of genes for microbial growth following rainfall was coupled with a subsequent decrease in the expression of genes for anaerobic methane metabolism associated with acetoclastic methanogenesis such as phosphate acetyltransferase, acetate kinase, and acetyl-CoA synthetase (Table 2.4). There were also significant declines in the expression of genes for anaerobic carbon fixation and fermentation (Table 2.4). We found lower expression for glucose-1-phosphate adenylyltransferase (Table 2.4), which has been considered the rate-limiting step of bacterial glycogen biosynthesis (Shen & Preiss 1965) or the first step of glycogen hydrolysis (Sekar et al. 2020). Glycogen can serve as an alternative carbon source for bacterial survival in carbon-depleted anaerobic environments (Sekar et al. 2020) or to prolong the lifespan of microorganisms while dormant (Lennon 2020). Thus, the lower expression of glucose-1-phosphate adenylyltransferase, an O_2-regulated gene negatively affected by O_2 availability, following rainfall provides further evidence that the increase in soil oxygenation made available more easily metabolized carbon substrates (e.g., aromatic DOC) (Nalven et al. 2020) such that microbes no longer needed to synthesize and degrade glycogen, or possibly that microbial cells may have started to leave their dormant state. We found lower expression for formate C-acetyltransferase (Table 2.4) in multiple Actinobacterial taxa, which is another O_2-regulated gene negatively affect by O_2 availability that helps regulate anaerobic glucose metabolism (Jia et al. 2017). Furthermore, we found lower expression for pyruvate kinase (Table 2.4), a negatively affected O_2-regulated gene involved in glycolysis that helps regulate anaerobic cell metabolism (Veith et al. 2013). In contrast, we found higher expression for aldehyde dehydrogenase (NAD+) (Table 2.4), an O_2-regulated gene positively affected by O_2 availability that catalyzes the oxidation of aldehydes into carboxylic acids (Marchitti et al. 2008) or promotes the production of acetate from acetaldehyde under aerobic conditions (Nosova et al. 1996). The change in expression (higher or lower) of each of these marker genes that are positively or negatively regulated by O_2

availability following rainfall is consistent with our expectations given the rapid increase in soil O_2 introduced during the rainfall event.

We also investigated the microbial expression of aerobic Fe(II) oxidation by Fe-oxidizing bacteria as further support that our rainfall event stimulated gene expression by aerobic bacteria in the tussock tundra community. Previous studies showed that Fe-oxidizing Betaproteobacteria such as *Leptothrix* and *Gallionella* spp. are found in abundance in the Toolik Lake region (Emerson et al. 2015). Here, we found evidence of their ribosomal genes in our metagenomic and metatranscriptomic datasets. These Fe-oxidizing bacteria use Fe(II) as their primary energy source to fix CO_2 into cellular biomass by reducing dissolved O_2 to water (Weber et al. 2006). Thus, the greater expression of aerobic Fe-oxidizing genes following our simulated rainfall event in tussock tundra (T4; Figure 2.5A) is also consistent with our expectations for aerobic gene expression following the rapid increase in soil O_2 availability introduced during our rainfall event.

Our metatranscriptomic analysis also revealed an increase in ferroptosis gene expression following rainfall in tussock tundra (Figure 2.4). Ferroptosis is a form of regulated cell death that results from the Fe-dependent accumulation of lipid peroxides associated with reactive oxygen species (Stockwell et al. 2017). Previous research has found that the overproduction of hydroxyl radical is significantly associated with lipid peroxidation in ferroptosis (Li et al. 2019). Here, it is likely that gene expression for ferroptosis is directly linked with the overproduction of hydroxyl radical given that hydroxyl radical production associated with the geochemical oxidation of Fe(II) can increase in tussock tundra following rainfall (Trusiak et al. 2019). However, little is known about the regulation of ferroptosis in soil environments or even how it is regulated within microbial cells regardless of environment (Conrad et al. 2018). While we find this potential association between hydroxyl radical generation and ferroptosis expression after rainfall interesting, more studies need to be done to determine any direct link between these two processes.

2.5.5 Wet Sedge Community Maintains Anaerobic Gene Expression During Rainfall

Results previously reported from the abiotic response cores (Trusiak et al. 2019) indicate that the amount of soil O_2 introduced during rainfall was sufficient to increase geochemical (abiotic) oxidation reactions in wet sedge tundra soils, although these geochemical reactions occurred at a lower rate than in tussock tundra soils. Here, we were unable to detect a significant increase in the relative abundance of expressed genes involved in aerobic respiration or bacterial

Fe oxidation (Figure 2.5B) following rainfall in wet sedge tundra regardless of the 4-fold increase in total soil O_2 concentration introduced during the rainfall event (Table 2.2). Furthermore, we were unable to detect a significant change in the relative abundance of any expressed gene pathways (Figure 2.3B), O_2-regulated genes (Table SI 2.13), or Fe-cycling genes (Figure 2.5B) following rainfall. Active microbial taxa continued to express genes that degrade organic compounds and inorganic nutrients through anaerobic respiration or fermentation pathways, and actually increased their expression of numerous anaerobic denitrification genes following rainfall. This suggests that the redox conditions in the soil environment were comparatively poor for microbial growth because they promoted anaerobic microbial taxa to allocate more energy towards resource acquisition, which microbes only do when resources are scarce (Ratledge 1994).

The lack of microbial response to rainfall in our wet sedge cores may be due to an insufficient accumulation of oxygenated rainwater during the rainfall event because it drained through the porous organic soil too quickly. In addition, rainwater O_2 may have been consumed too rapidly by abiotic reactions before microbes could respond and shift their expression to promote aerobic respiration pathways. For example, the higher pH in wet sedge tundra (6.12 ± 0.06; Table 2.1) likely promotes the abiotic oxidation of Fe(II) over biotic processes (Weber et al. 2006), which could account for the observed rates of Fe(II) oxidation in the abiotic response cores (Trusiak et al. 2019). However, we observed gene expression for the aerobic oxidation of Fe(II) in the wet sedge tundra community (Figure 2.5B), which suggests that some soil O_2 was available and consumed through biotic processes throughout the experiment. It is also plausible that energetic constraints caused by the low availability of dissolved O_2 and alternative electron acceptors maintained anaerobic metabolism and fermentation pathways throughout the rainfall event (cf. Brune et al. 2000). The high abundance and diversity of oligotrophic, and mainly anaerobic microbial taxa in the wet sedge tundra community may also have constrained a community-wide shift from anaerobic metabolism following soil oxidation. This argument applies well to the short timeframe of the rainfall-induced oxidation event, where our soil model implies that the bulk of the O_2 in rainwater was consumed back to pre-rainfall anoxic concentrations within several days. As such, the oligotrophic community in wet sedge tundra soils may be poorly adapted to respond rapidly to periodic bursts of soil oxygenation introduced during rainfall.

We also observed that the relative expression of genes for Fe(III) reduction by Fe-reducing bacteria did not decline following our rainfall event, with expression for Fe(III) reduction occurring at 4-fold greater abundance relative to the expression for Fe(II) oxidation averaged across sampling time points (Figure 2.5B). Emerson et al. (2015) found Fe(III)-reducing *Geobacter* spp. (Deltaproteobacteria) in high abundance in the Toolik Lake region. We also found evidence of *Geobacter* spp. ribosomal genes in our metagenomic and metatranscriptomic datasets, but only in the wet sedge tundra community (Table SI 2.12). These Fe(III)-reducing bacteria use Fe(III) as a terminal electron acceptor to carry out anaerobic respiration coupled to the mineralization of OC under anoxic conditions (Emerson & Revsbech 1994). The consistent expression of anaerobic Fe-reducing genes before and after rainfall, and in greater abundance relative to the aerobic Fe-oxidizing genes in the wet sedge tundra community further implies that rainfall does not appear to alter community-wide anaerobic gene expression regardless of the rapid increase in soil O_2 availability introduced during the rainfall event.

Taken together, rainfall events in wet sedge tundra may serve only to maintain persistently saturated soil conditions that promote anaerobic metabolism and CH_4 production. The unaltered expression of anaerobic and fermentative pathways following an increase in soil O_2 concentration introduced during rainfall, coupled with the high diversity and abundance of methanogenic archaea active within these soils provides support for this interpretation. Also, the combination of warmer soil temperatures driven by an increase in rainfall and the concurrent increase in active layer depth with persistently saturated conditions throughout the active layer profile has led to an increase in CH_4 emissions by ~30% (Neumann et al. 2019). Here, we add further evidence that rainfall will likely enhance CH_4 production from low-lying permafrost regions such as wet sedge tundra by maintaining saturated soil conditions rather than altering the highly reduced soil redox conditions through an increase in dissolved O_2 availability.

2.5.6 Relating Microbial Expression to Rates of Respiration and CH_4 Production

Our results showed no correlation between aerobic microbial gene expression and rates of microbial respiration (CO_2 production) following rainfall in tussock tundra soils. Specifically, the consistent rates of microbial respiration before and after rainfall (Figure 2.6A) did not reflect the increase we observed in aerobic microbial gene expression in the tussock tundra community following rainfall (Figure 2.4). This result is not unexpected because previous studies have also

been unable to directly link microbial dynamics and carbon emissions (Doherty et al. 2020), likely because respiration is the product of many processes in microbial communities. Here, the artificial conditions of the respiration rate incubations (i.e., N_2 gas for anoxic conditions, compressed air for oxic conditions) were intended to replicate field conditions, similar to previous incubation studies (Zak & Kling 2006), but it is possible that other conditions in these incubations such as total O_2 availability and soil moisture differed from conditions in the soil mesocosms where microbial gene expression was sampled. It should be noted that our measured rates of CO_2 production (Figure 2.6A) were similar to rates previously measured from soil waters at our study sites (19.6 ± 3.0 ng C g^{-1} soil hr^{-1}) (Judd & Kling 2002). Also, the greater rate of CO_2 production in the tussock tundra soil compared with the wet sedge tundra soil was consistent with the ~3.4-fold greater release of carbon from aerobic soils compared with anaerobic soils across circumpolar arctic sites (Schadel et al. 2016).

Our measured rates of CH_4 production under anoxic incubation conditions (Figure 2.6B) were also comparable with previous rates (37.2 ± 51.8 pg C g^{-1} soil hr^{-1}) (Judd & Kling 2002). These results support a common interpretation that CH_4 was produced by methanogenic archaea in the anoxic environment but likely consumed by CH_4-oxidizing bacteria in the oxidized environment. We have evidence of gene expression from multiple pathways of methanogenesis associated with methanogenic archaea as well as evidence of gene expression from methanotrophic pathways associated with Actinobacteria and multiple classes of Proteobacteria in both tundra communities (Table SI 2.13). However, the greater production of CH_4 under anoxic conditions at T0 from the tussock tundra soil compared to the wet sedge tundra soil (Figure 2.6B) is inconsistent with the lower relative abundance of methanogenic archaea in the tussock tundra community compared to the wet sedge tundra community (Table 2.3) or with the broader suite of methanogenic pathways available to the diverse composition of methanogenic archaea within the wet sedge tundra. It is possible that the rates of CH_4 production measured from our tussock tundra soil incubations (and to some extent measured in our wet sedge tundra soils) represent the natural release of trapped CH_4 following disturbance to the soil (Margesin 2009), rather than just biological production under the saturated, anoxic soil conditions in this study.

2.6 Conclusion

We conclude that differences in the extent of soil oxygenation introduced during rainfall and their impact on soil redox conditions clearly control whether microbial communities will shift gene expression from anaerobic metabolism to aerobic microbial growth, or simply continue to express anaerobic genes typical of anoxic soil conditions. Here, the microbial response in the tussock tundra community was consistent with our hypothesis that rainfall-induced soil oxidation would alter anaerobic gene expression and promote aerobic microbial activity, in large part due to the longer residence time of oxygenated rainwater in the soil as well as the greater abundance of aerobic bacterial and fungal taxa and their suite of aerobic functional genes. In contrast, an influx of O_2 from rainfall does not appear to accumulate long enough, or to a sufficient concentration, in wet sedge tundra soils to induce a community-wide shift from anaerobic metabolism; rainfall may serve only in maintaining persistently saturated conditions that could potentially enhance CH_4 production due to the high diversity of methanogenic archaea inhabiting these low-lying permafrost soils across the arctic landscape.

2.7 Acknowledgements

We thank Rose Cory, Adrianna Trusiak, Lija Triebergs, Jason Dobkowski, Chris Cook, Jacob Evans, Derek Smith, Jerome Payet, and researchers, technicians, and support staff of the Arctic LTER project and Toolik Field Station for assistance with fieldwork. Additional thanks to the University of Michigan Advanced Genomics Core, Microbiome Core, and Advanced Research Computing Technology Services.

Table 2.1 Abiotic Soil Properties. The chemical and physical soil properties in tussock tundra and wet sedge tundra mesocosm in the biotic response cores were measured at the end of the anoxic acclimation period (T0). Bulk soil properties were measured at the end of the experiment (mean ± SD; N = 3 per tundra type). Asterisks indicate significant differences in mean pairwise similarity between tussock and wet sedge tundra soils (paired t-test; * $p < 0.05$).

Soil Properties	Tundra Soil		Mean Difference between Tundra
	Tussock	Wet Sedge	
Chemical Properties			
pH	4.58 ± 0.39	6.12 ± 0.06	1.54 *
Conductivity (µS cm^{-1})	65.9 ± 18.6	123.6 ± 14.4	57.7 *
Physical Properties			
Temperature (ºC)	7.8 ± 0.3	8.5 ± 0.3	0.7
Moisture (% water)	63.1 ± 7.6	70.1 ± 4.2	7.0
Dissolved [O_2] (mg O_2 L^{-1})	1.21 ± 0.23	1.04 ± 0.05	0.17
Bulk Soil Properties			
Organic Matter Content (%)	67.6 ± 8.6	80.7 ± 4.5	13.1 *
Organic Carbon Content (%)	33.8 ± 4.3	40.3 ± 2.3	6.5 *
Bulk density (g soil dry cm^{-3})	0.53 ± 0.10	0.27 ± 0.04	0.26 *
Porosity (% soil volume)	63.3 ± 6.7	81.2 ± 2.6	17.9 *

Table 2.2 Mass Balance Model. Soil modeling flush variables, rates of soil O_2 accumulation, and concentrations of soil O_2 after simulated rainfall are for the biotic response cores. The soil O_2 consumption rates are modeled from soil properties reported for the abiotic response cores (Trusiak et al. 2019) and are representative rates within tussock tundra and wet sedge tundra soils under static, waterlogged field conditions. Asterisks indicate significant differences in mean pairwise similarity among tundra soils (paired t-test; * $p < 0.05$).

Soil Modeling Parameters	Tundra Soil		Mean difference between Tundra
	Tussock	Wet Sedge	
Flush Variables			
DI Water Flushed (L)	20 ± 0	20 ± 0	0
Duration of Flush (hr)	3.77 ± 0.42	1.13 ± 0.19	2.64 *
Soil O_2 Accumulation and Consumption Rates			
Net Soil O_2 Accumulation Rate (mg O_2 L^{-1} hr^{-1})	2.31 ± 0.95	2.61 ± 0.99	0.30
Net Soil O_2 Consumption Rate (mg O_2 L^{-1} hr^{-1})	0.055 ± 0.010	0.032 ± 0.004	0.023 *
Soil O_2 Concentrations after Simulated Rainfall			
Soil O_2 Concentration after DI Water Flush (mg O_2 L^{-1})	10.26 ± 1.11	4.10 ± 0.53	6.16 *
Soil O_2 Concentration at T4 Sampling (mg O_2 L^{-1})	10.04 ± 1.14	3.86 ± 0.50	6.18 *
Soil O_2 Concentration at T24 Sampling (mg O_2 L^{-1})	8.93 ± 1.27	3.23 ± 0.47	5.70 *

Table 2.3 Relative Abundance of Dominant Microbial Phyla. Relative abundance calculated for tussock tundra and wet sedge tundra communities averaged across all sampling time points based on KEGG tier III "Ribosome" category from the GPM-normalized metagenome (MG) and TPM-normalized metatranscriptome (MT) datasets (mean ± SD). Asterisks indicate the significance of differences in mean pairwise similarity among tundra communities (paired t-test; * $p < 0.05$, ** $p < 0.01$, *** $p < 0.001$).

Taxonomy	MG Relative Abundance (%)		MG Mean Difference	MT Relative Abundance (%)		MT Mean Difference
	Tussock	Wet Sedge		Tussock	Wet Sedge	
Bacteria						
Acidobacteria	34 ± 5	10 ± 1	24% *	41 ± 12	8 ± 1	33% **
Actinobacteria	24 ± 6	27 ± 4	3%	42 ± 12	40 ± 3	2%
Alphaproteobacteria	15 ± 4	8 ± 4	7%	4 ± 2	3 ± 2	1% **
Betaproteobacteria	2 ± 1	6 ± 3	1% **	1 ± 1	4 ± 2	3% **
Deltaproteobacteria	4 ± 1	13 ± 2	9% **	3 ± 1	13 ± 1	10% ***
Gammaproteobacteria	11 ± 1	2 ± 1	9% ***	3 ± 1	1 ± 0	2% **
Proteobacteria Other	0 ± 0	0 ± 0	0%	0 ± 0	0 ± 0	0%
Bacteroidetes	0 ± 0	2 ± 1	2%	1 ± 0	2 ± 1	1% *
Chloroflexi	0 ± 0	8 ± 1	8% ***	0 ± 0	8 ± 2	8% ***
Firmicutes	4 ± 1	15 ± 3	11% **	2 ± 0	10 ± 2	9% ***
Planctomycetes	1 ± 0	0 ± 0	1%	0 ± 0	0 ± 0	0%
Verrucomicrobia	2 ± 0	2 ± 1	0%	0 ± 0	1 ± 0	0%
Archaea						
Euryarchaeota	0 ± 0	2 ± 1	2% *	0 ± 0	7 ± 6	6% *
Fungi						
Ascomycetes	1 ± 1	0 ± 0	1% *	1 ± 1	0 ± 0	1% *

Table 2.4 Differential gene expression (DGE) for O_2-regulated KEGG orthologs (KOs). Each KO represents an O_2-regulated gene and was included based on DGE significance within Tussock T4 vs. T0 sampling period (FDR M 0.05), where a positive log-fold change (logFC) value indicates higher expression at T4 relative to T0.

KEGG Tier Category	logFC
Carbohydrate Metabolism	
Glycolysis / Gluconeogenesis	
K00128 aldehyde dehydrogenase (NAD+)	3.7 ± 0
Pyruvate Metabolism	
K00656 formate C-acetyltransferase	-4.4 ± 1.8
Starch and Sucrose Metabolism	
K00975 glucose-1-phosphate adenylyltransferase	-2.5 ± 0
Cofactors and Vitamins Metabolism	
Nicotinate and Nicotinamide Metabolism	
K00763 nicotinate phosphoribosyltransferase	-3.5 ± 0
Overview Metabolism	
Biosynthesis of Amino Acids	
K01915 glutamine synthetase	-3.2 ± 0.6
Carbon Metabolism	
K00873 pyruvate kinase	-3.6 ± 0
K01623 fructose-bisphosphate aldolase	-4.0 ± 0
K00626 acetyl-CoA C-acetyltransferase	-2.6 ± 0.2
Energy Metabolism	
Anaerobic Carbon Fixation	
K00174 2-oxoglutarate/2-oxoacid ferredoxin oxidoreductase	-3.9 ± 0.4
K00855 phosphoribulokinase	-3.8 ± 0
Methane Metabolism	
K00625 phosphate acetyltransferase	-5.3 ± 0.6
K00925 acetate kinase	-3.0 ± 0.2
K01895 acetyl-CoA synthetase	-3.7 ± 1.3
Fermentation	
K00169 pyruvate ferredoxin oxidoreductase	-3.1 ± 0

Table 2.5 Summary of differential gene expression (DGE) analysis. Values represent counts of KEGG orthologs (KOs; i.e., genes) considered to be differentially expressed if the False Discovery Rate (FDR) was < 0.05. "Higher" or "Lower" differential expression is relative to the first variable in the comparison (e.g., T4 vs T0 summarizes higher or lower expression at T4 relative to T0).

DGE Analysis	Unique KEGG Orthologs (KOs) Expressed			Overall Difference
	Higher	Lower	Not Significant	
Tussock vs Wet Sedge				
T0	27,239	12,732	126,783	24%
T4	32,366	13,512	120,876	28%
T24	12,123	4,774	149,857	10%
Tussock Tundra				
T4 vs T0	667	588	100,055	1%
T24 vs T0	75	67	101,168	< 1%
T24 vs T4	2	5	101,303	< 1%
Wet Sedge Tundra				
T4 vs T0	78	13	139,939	< 1%
T24 vs T0	9	2	140,019	< 1%
T24 vs T4	0	0	140,030	0%

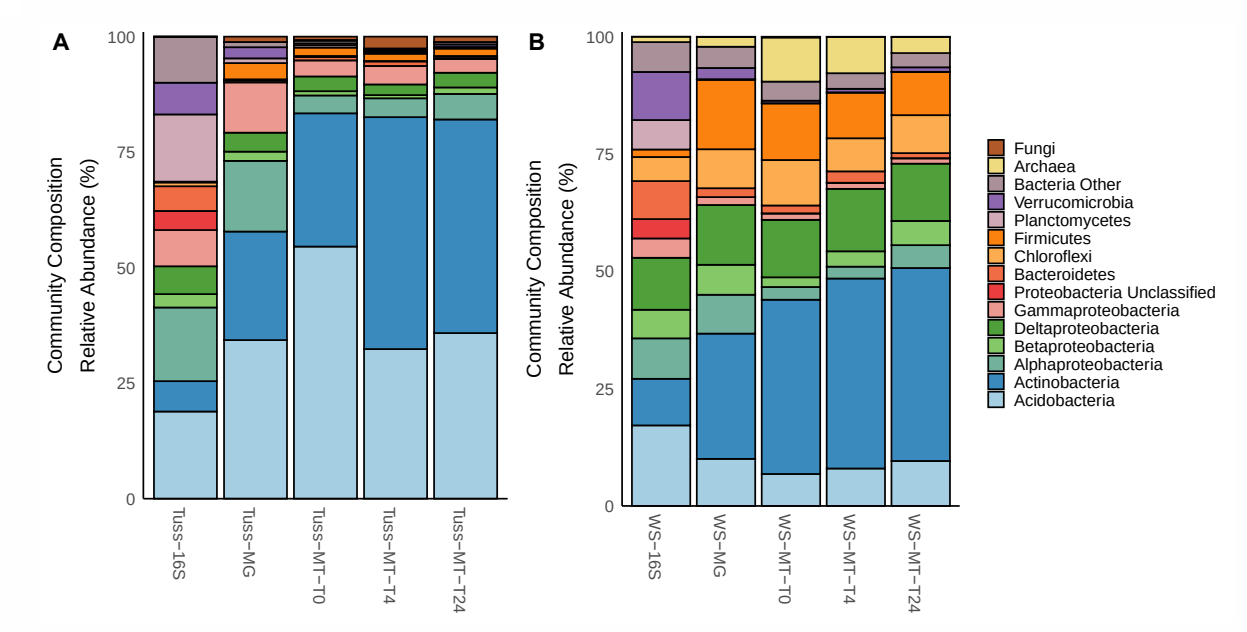

Figure 2.1 Microbial Community Composition. Relative abundance of dominant microbial phyla within (A) tussock tundra and (B) wet sedge tundra soils based on the 16S rRNA amplicons, GPM-normalized metagenome (MG), and TPM-normalized metatranscriptome (MT) genes belonging to Ribosome KEGG tier III pathway.

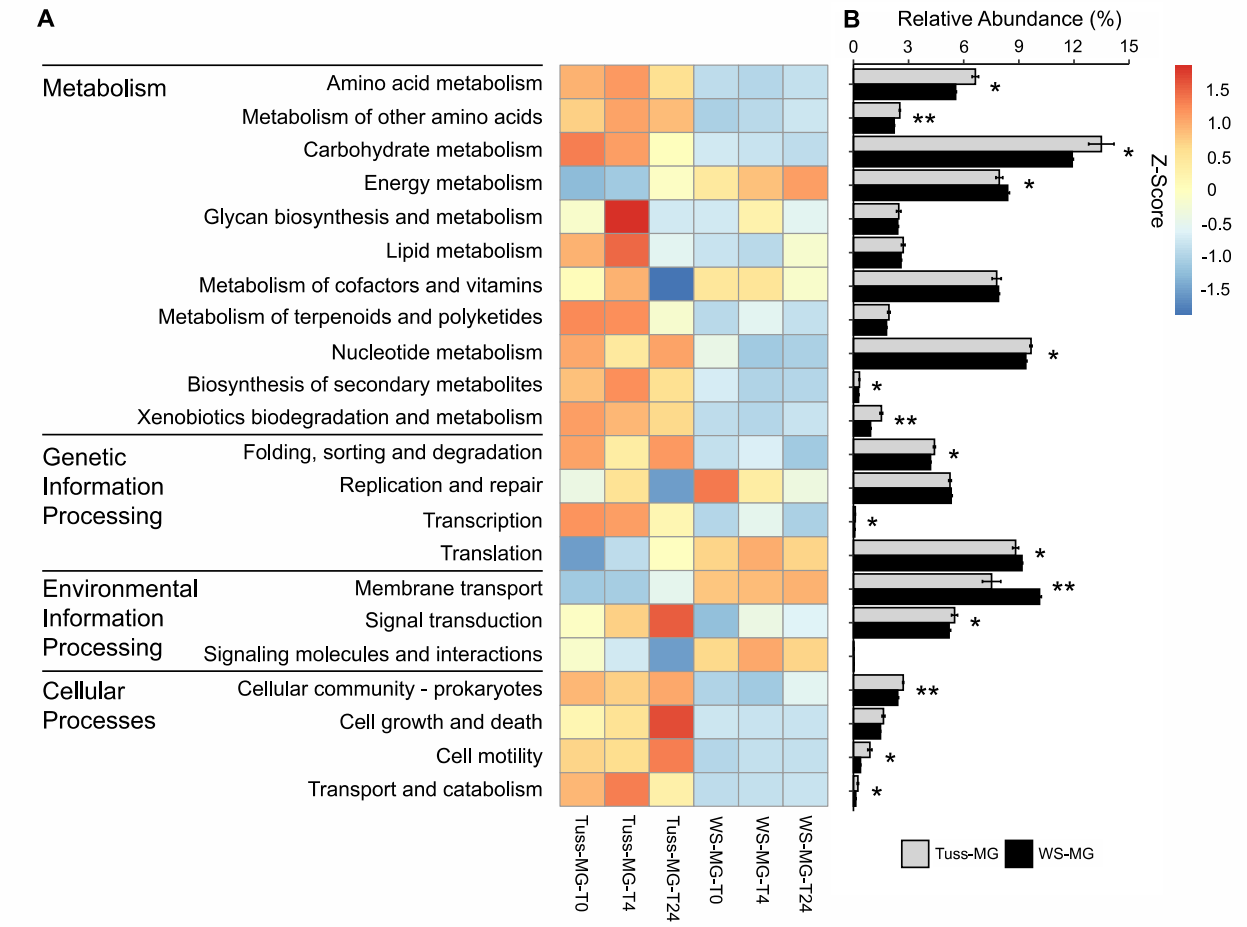

Figure 2.2 Metagenome Genomic Potential. Heatmap (A) and barplot (B) of genomic potential based on the mean relative abundance of GPM-normalized metagenome (MG) genes belonging to KEGG tier III functional pathways by sampling time point in mesocosm replicates of tussock tundra and wet sedge tundra communities. Z-score transformations based on the mean relative abundance of genes between sampling time points for each KEGG pathway. Error bars for each barplot represent standard deviation from the mean. Asterisks mark the significance of differences in mean relative gene abundance between tundra communities for each KEGG tier III pathway (paired t-test; * $p < 0.05$, ** $p < 0.01$).

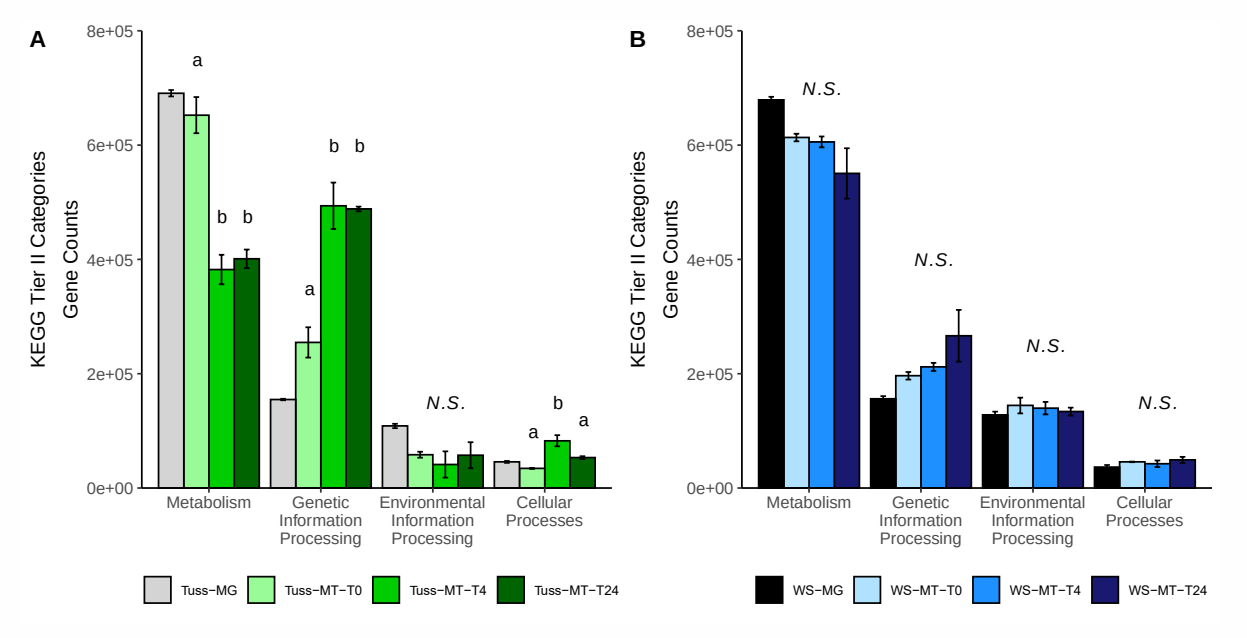

Figure 2.3 Metatranscriptome Gene Expression. Barplot of microbial gene expression based on the mean relative abundance of TPM-normalized metatranscriptome (MT) genes annotated as KEGG tier II functional pathways by sampling time point in (A) tussock tundra and (B) wet sedge tundra communities (error bars represent standard deviation of the mean). Letters indicate significant differences in mean pairwise similarity between sampling time points for each KEGG functional pathway (ANOVA; $p < 0.05$), with non-significant differences among sampling time points indicated as *N.S.* The relative abundance of GPM-normalized metagenome (MG) functional genes is provided for reference only and their abundance was not incorporated in the pairwise statistical analysis.

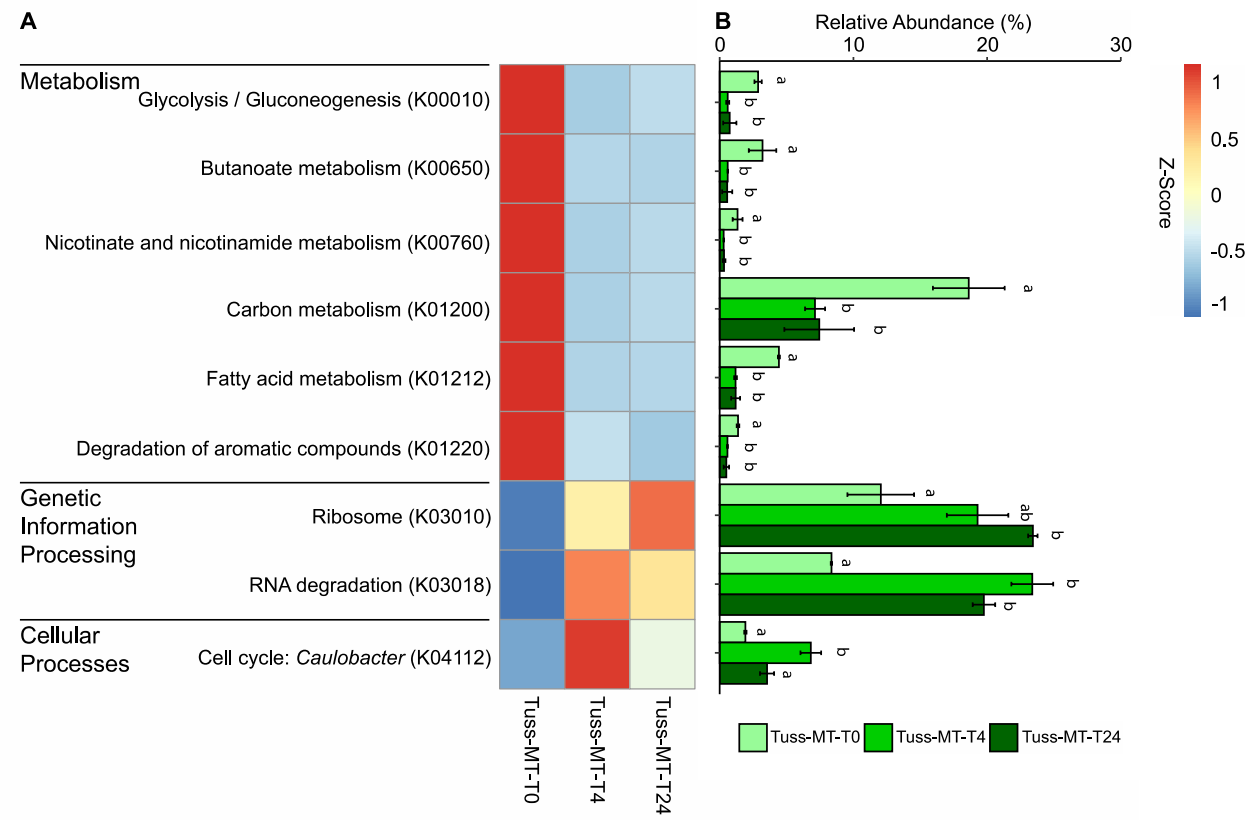

Figure 2.4 Gene Expression in Tussock Tundra. Heatmap (A) and barplot (B) of microbial gene expression between sampling time points within tussock tundra based on the mean relative abundance of TPM-normalized metatranscriptome (MT) gene transcripts belonging to KEGG tier IV functional pathways. Z-score transformations based on the mean relative abundance of transcripts between sampling time points. Error bars for each barplot represent standard deviation from the mean. Letters indicate significant differences in mean pairwise similarity between sampling time points in each KEGG tier IV category (ANOVA; $p < 0.05$).

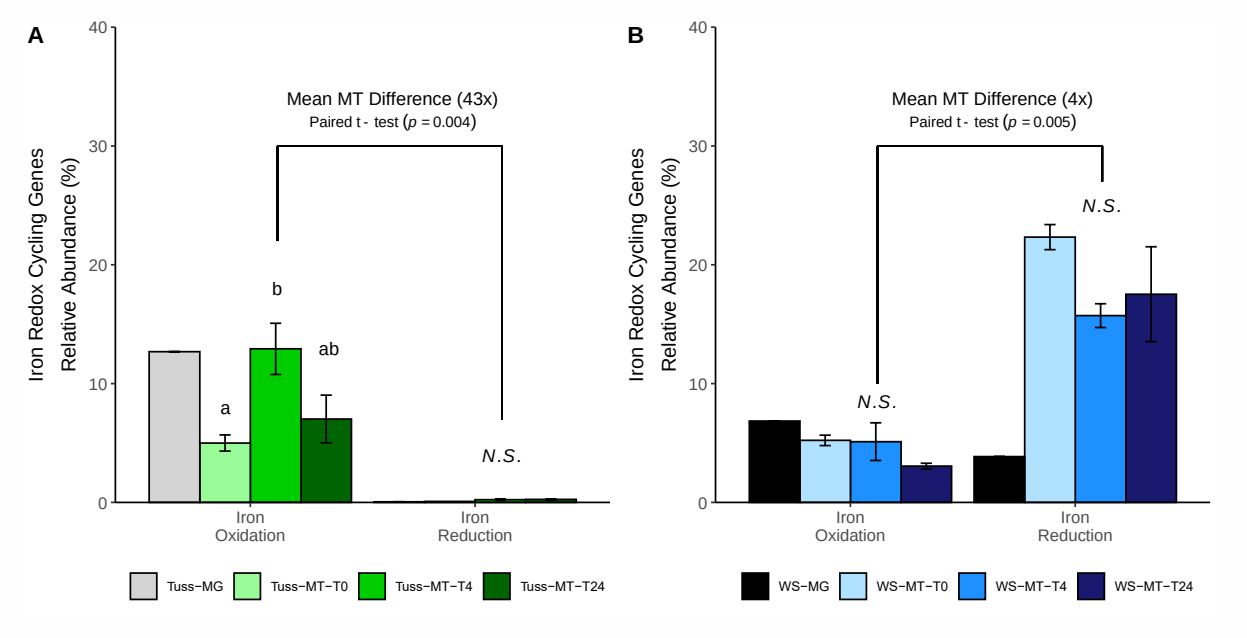

Figure 2.5 Iron Redox Cycling Gene Expression. Barplot of iron redox cycling gene expression based on the mean relative abundance of iron oxidation and iron reduction genes at each sampling time point in (A) tussock tundra and (B) wet sedge tundra communities (error bars represent standard deviation from the mean). Letters indicate significant differences in mean pairwise similarity between sampling time points in each iron redox cycling functional category (ANOVA; $p < 0.05$), with non-significant differences between sampling time points indicated by *N.S.* The relative abundance of each metagenome (MG) iron redox cycling functional category is provided for reference only and was not incorporated in the pairwise analysis.

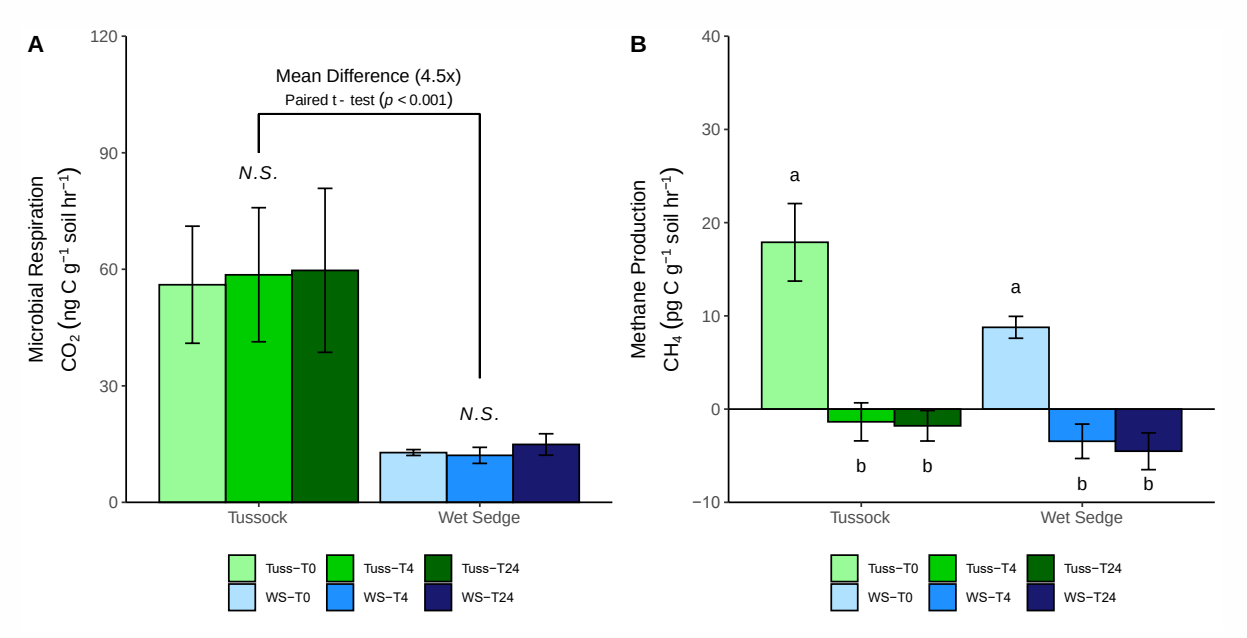

Figure 2.6 Microbial Respiration and CH_4 Production. Barplot of production rates for (A) microbial respiration and (B) methane (CH_4) production for tussock tundra and wet sedge tundra communities (error bars represent standard deviation from the mean). Letters indicate significant differences in mean pairwise similarity between sampling time points (ANOVA; $p < 0.05$), with non-significant differences between sampling time points indicated as *N.S.* Negative values for CH_4 production indicate CH_4 consumption.

Table SI 2.6 Supplemental 16S rRNA Amplicon Sequence Summary. Values for 16S rRNA amplicon (16S) samples (N=18).

Group	Tundra Type	Time Point	Mesocosm Replicate	Total Sequences	Rarified Sequences	Coverage (%)	Unique OTUs	Inverse Simpson
TussT0Rep1	Tussock	T0	1	13,990	9,565	96.2	987	75
TussT0Rep2	Tussock	T0	2	15,111	9,565	96.2	962	87
TussT0Rep3	Tussock	T0	3	15,274	9,565	95.7	1160	100
TussT4Rep1	Tussock	T4	1	26,096	9,565	95.2	1042	45
TussT4Rep2	Tussock	T4	2	13,731	9,565	96.4	908	67
TussT4Rep3	Tussock	T4	3	14,592	9,565	96.5	988	109
TussT24Rep1	Tussock	T24	1	13,583	9,565	95.9	1075	71
TussT24Rep2	Tussock	T24	2	15,715	9,565	96.3	960	70
TussT24Rep3	Tussock	T24	3	12,633	9,565	96.2	1057	107
WST0Rep1	Wet Sedge	T0	1	23,220	9,565	93.9	1292	104
WST0Rep2	Wet Sedge	T0	2	14,261	9,565	95.1	1222	94
WST0Rep3	Wet Sedge	T0	3	13,899	9,565	93	1808	213
WST4Rep1	Wet Sedge	T4	1	10,059	9,565	95.5	1279	123
WST4Rep2	Wet Sedge	T4	2	9,565	9,565	95.7	1172	78
WST4Rep3	Wet Sedge	T4	3	13,071	9,565	93.5	1692	188
WST24Rep1	Wet Sedge	T24	1	13,121	9,565	94.6	1346	135
WST24Rep2	Wet Sedge	T24	2	13,044	9,565	95.3	1183	88
WST24Rep3	Wet Sedge	T24	3	11,152	9,565	94	1678	198

Table SI 2.7 Supplemental Metagenome Sequence Summary. Values for metagenome (MG) samples (N=18).

Sequencing ID	Tundra Type	Time Point	Mesocosm Replicate	Total Reads	QC Reads	Mapped Reads	Mean Length (bp)
S107107	Tussock	T0	1	74,380,412	65,667,254	19,628,380	141
S107108	Tussock	T0	2	49,340,036	43,020,594	12,528,861	141
S107116	Tussock	T4	1	13,990,860	12,312,448	3,372,508	141
S107117	Tussock	T4	2	41,987,432	36,565,234	10,628,986	141
S107119	Tussock	T24	1	54,477,894	47,853,114	11,451,168	141
S107121	Tussock	T24	3	31,692,004	27,632,452	4,767,927	141
S107104	Wet Sedge	T0	1	39,830,500	34,568,010	15,458,362	139
S107105	Wet Sedge	T0	2	27,196,554	24,408,724	12,419,993	140
S107106	Wet Sedge	T0	3	29,570,304	25,734,316	7,180,169	141
S107110	Wet Sedge	T4	1	32,719,864	29,338,238	13,910,613	140
S107111	Wet Sedge	T4	2	46,925,390	41,991,856	17,433,511	141
S107112	Wet Sedge	T4	3	40,126,628	35,302,148	8,871,426	141
S107113	Wet Sedge	T24	1	41,583,302	36,956,594	14,967,853	141
S107114	Wet Sedge	T24	2	37,805,352	33,190,654	15,997,334	140
S107115	Wet Sedge	T24	3	65,564,980	57,805,778	12,782,304	141

Table SI 2.8 Supplemental Metatranscriptome Sequence Summary. Values provided for the metatranscriptome (MT) samples (N=12).

Sequencing ID	Tundra Type	Time Point	Mesocosm Replicate	Total Reads	QC Reads	Mapped Reads	Mean Length (bp)
S108382	Tussock	T0	1	29,660,937	29,147,700	9,229,059	127
S108383	Tussock	T0	2	25,501,797	25,059,233	6,982,871	127
S108391	Tussock	T4	1	27,488,794	26,776,604	8,338,151	125
S108392	Tussock	T4	2	25,901,800	25,445,057	7,387,851	128
S108394	Tussock	T24	1	29,118,959	28,554,557	7,271,424	127
S108396	Tussock	T24	3	21,097,400	20,779,435	5,280,460	129
S108379	Wet Sedge	T0	1	32,968,474	32,334,951	15,825,372	118
S108381	Wet Sedge	T0	3	29,503,233	28,917,592	10,696,764	129
S108385	Wet Sedge	T4	1	27,020,176	26,584,848	11,952,373	129
S108386	Wet Sedge	T4	2	27,182,337	26,756,117	12,152,652	130
S108388	Wet Sedge	T24	1	24,191,597	23,791,693	8,193,077	130
S108390	Wet Sedge	T24	3	21,900,736	21,531,564	6,787,536	129

Table SI 2.9 Supplemental Alpha Diversity Summary. Values for metagenome (MG) and metatranscriptome (MT) taxonomic and functional genes based on richness, relative abundance, and Shannon-Wiener (H') diversity.

Tundra	Alpha Diversity - Taxonomy Genes			Alpha Diversity - Functional Genes		
	Taxa Richness	Taxa Abundance	Taxa Diversity	KO Richness	KO Abundance	KO Diversity
Metagenome						
Tussock						
T0	5,110 ± 539	18,211 ± 121	8.1 ± 0.12	328,633 ± 35,220	4,718,088 ± 1,526,605	11.9 ± 0.16
T4	3,773 ± 960	18,620 ± 179	7.8 ± 0.26	246,883 ± 55,642	2,053,838 ± 1,546,093	11.8 ± 0.14
T24	4,808 ± 444	19,597 ± 1,110	8.0 ± 0.13	293,760 ± 38,415	2,766,130 ± 1,088,053	11.8 ± 0.24
Wet Sedge						
T0	7,100 ± 559	17,382 ± 502	8.5 ± 0.14	464,711 ± 29,557	3,711,650 ± 1,093,558	12.4 ± 0.11
T4	7,255 ± 220	17,798 ± 843	8.5 ± 0.05	468,797 ± 17,157	4,204,979 ± 1,099,636	12.4 ± 0.07
T24	7,524 ± 292	17,738 ± 794	8.5 ± 0.11	480,404 ± 11,735	4,756,021 ± 253,557	12.4 ± 0.07
Metatranscriptome						
Tussock						
T0	3,681 ± 97	61,848 ± 11,204	6.9 ± 0.05	140,873 ± 12,345	1,893,668 ± 445,393	9.5 ± 0.09
T4	4,414 ± 383	104,844 ± 15,618	6.9 ± 0.19	136,376 ± 15,094	2,491,776 ± 38,245	9.5 ± 0.27
T24	4,592 ± 59	114,917 ± 4,557	7.0 ± 0.08	117,577 ± 10,024	1,538,291 ± 451,094	9.5 ± 0.14
Wet Sedge						
T0	6,369 ± 393	45,116 ± 646	7.7 ± 0.01	254,545 ± 19,262	3,348,759 ± 504,519	10.9 ± 0.09
T4	6,499 ± 98	55,095 ± 1,186	7.5 ± 0.14	246,102 ± 9,777	3,552,061 ± 356,986	10.7 ± 0.20
T24	5,824 ± 138	75,461 ± 22,116	7.7 ± 0.07	172,983 ± 25,964	1,467,913 ± 512,711	10.8 ± 0.01

Table SI 2.10 Supplemental Beta Diversity Summary. Values for metagenome (MG) and metatranscriptome (MT) taxonomic and functional genes based on Bray-Curtis dissimilarity values. Asterisks indicate the significance of differences in mean pairwise similarity between tundra types (PERMANOVA; *$p < 0.05$, **$p < 0.01$, ***$p < 0.001$).

Variables	Df	Sums Sqs	Mean Sqs	F Model	R^2	Pr(>F)
Taxonomic Genes						
Metagenome						
Tundra	1	2.35	2.35	18.8	0.62	0.001 ***
Time Point	2	0.17	0.08	0.7	0.04	0.732
Tundra:Time	2	0.17	0.09	0.7	0.05	0.593
Residuals	9	1.13	0.13		0.30	
Total	14	3.82			1	
Metatranscriptome						
Tundra	1	2.12	2.12	21.9	0.63	0.001 ***
Time Point	2	0.34	0.17	1.8	0.10	0.148
Tundra:Time	2	0.31	0.15	1.6	0.09	0.207
Residuals	6	0.58	0.10		0.17	
Total	11	3.35			1	
Functional Genes						
Metagenome						
Tundra	1	2.41	2.41	19.3	0.62	0.001 ***
Time Point	2	0.16	0.08	0.7	0.04	0.755
Tundra:Time	2	0.18	0.09	0.7	0.05	0.622
Residuals	9	1.13	0.13		0.29	
Total	14	3.88			1	
Metatranscriptome						
Tundra	1	1.99	1.99	15.5	0.57	0.001 ***
Time Point	2	0.39	0.20	1.5	0.11	0.171
Tundra:Time	2	0.37	0.19	1.5	0.11	0.226
Residuals	6	0.77	0.13		0.22	
Total	11	3.53			1	

Table SI 2.11 Supplemental Metagenome Assembled Genomes (MAGs) Summary. High-quality (>70% completeness, <10% redundancy), annotated MAGs and their relative abundance in the biotic response group based on metagenome samples.

Binning Result	Completion (%)	Redundancy (%)	Length (nucleotides)	Domain	Phylum	Class	Tussock Tundra	Wet Sedge Tundra
Bin_046	88.9	9.3	1,536,975	Archaea	Halobacteria	Bog-38	0	2.6 ± 2.0
Bin_132	85.6	5.0	6,046,501	Bacteria	Acidobacteria	Acidobacteriae	1.6 ± 3.8	0
Bin_165	84.2	9.4	5,587,269	Bacteria	Acidobacteria	Acidobacteriae	2.1 ± 1.4	0
Bin_142	80.6	3.6	3,918,295	Bacteria	Acidobacteria	Acidobacteriae	0.6 ± 1.0	0
Bin_073	77.0	5.0	2,246,106	Bacteria	Acidobacteria	Aminicenantia	0	0.1 ± 0.3
Bin_080	71.9	3.6	2,414,552	Bacteria	Acidobacteria	Aminicenantia	0	0.5 ± 0.5
Bin_137	78.4	5.0	2,870,570	Bacteria	Acidobacteria	Thermoanaerobaculia	0	0.8 ± 0.9
Bin_051	83.5	7.9	1,789,108	Bacteria	Actinobacteria	Coriobacteriia	0	1.1 ± 1.4
Bin_071	97.1	0.7	2,723,137	Bacteria	Actinobacteria	RBG-13-55-18	0	0.8 ± 1.0
Bin_011	93.5	3.6	3,138,665	Bacteria	Actinobacteria	RBG-13-55-18	0	1.5 ± 1.4
Bin_056	90.7	3.6	2,133,681	Bacteria	Actinobacteria	Thermoleophilia	0.9 ± 1.7	0
Bin_027	88.5	3.6	2,641,710	Bacteria	Actinobacteria	Thermoleophilia	0	1.0 ± 0.9
Bin_089	96.7	2.9	4,758,373	Bacteria	Chloroflexi	Anaerolineae	0	1.5 ± 2.1
Bin_023	82.0	4.3	2,614,541	Bacteria	Chloroflexi	Ellin6529	0	1.2 ± 0.9
Bin_078	84.9	5.8	3,046,540	Bacteria	Chloroflexi	Ellin6529	0	0.8 ± 1.4
Bin_083	82.0	6.5	2,095,666	Bacteria	Chloroflexi	Ellin6529	0	0.7 ± 0.6
Bin_110	74.8	7.9	1,408,896	Bacteria	Chloroflexi	Ellin6529	0	1.5 ± 1.3
Bin_161	74.8	7.2	2,580,286	Bacteria	Chloroflexi	Ellin6529	0	1.9 ± 3.1
Bin_029	72.7	5.0	2,187,888	Bacteria	Chloroflexi	Ellin6529	0	0.8 ± 1.3
Bin_090	98.6	6.5	6,681,655	Bacteria	Methylomirabilota	Methylomirabilia	0	1.4 ± 1.3
Bin_044	74.1	5.0	4,823,662	Bacteria	Myxococcota	Polyangia	0	0.7 ± 0.4
Bin_062	82.0	0.7	1,468,490	Bacteria	Patescibacteria	Saccharimonadia	0	0.9 ± 0.9
Bin_159	90.7	9.4	5,724,953	Bacteria	Proteobacteria	Alphaproteobacteria	0.8 ± 0.8	0
Bin_106	87.8	2.2	2,639,223	Bacteria	Proteobacteria	Alphaproteobacteria	0	0.5 ± 0.4
Bin_031	92.8	9.4	2,714,627	Bacteria	Proteobacteria	Deltaproteobacteria	0	0.8 ± 0.6
Bin_163	89.9	6.5	5,731,451	Bacteria	Proteobacteria	Gammaproteobacteria	0	0.8 ± 0.6

Table SI 2.12 Supplemental Relative Abundance of Dominant Active Microbial Taxa. Values within tussock tundra and wet sedge tundra based on the TPM-normalized metatranscriptome (MT) dataset (mean ± SD). Only those taxa with ≥ 0.5% mean relative abundance shown. Asterisks indicate the significance of differences in mean pairwise similarity between tundra types (paired t-test; ***$p < 0.001$, **$p < 0.01$, *$p < 0.05$, with *NS* for non-significant differences).

Taxonomy	MT Rel. Abund. (%)		MT Difference between Tundra	Taxonomy	MT Rel. Abund. (%)		MT Difference between Tundra
	Tussock	Wet Sedge			Tussock	Wet Sedge	
Archaea				**Bacteria**			
Euryarchaeota				*Alphaproteobacteria*			
Methanobacteria	0 ± 0	0.4 ± 0.1	0.4% *	Rhodoplanes	0.1 ± 0.0	0.6 ± 0.3	0.5% **
Methanosarcina	0.01 ± 0.01	1.2 ± 0.9	1.2% *	Rhodopseudomonas	0.4 ± 0.3	0.1 ± 0.1	0.3% *
Methanothrix	0.04 ± 0.03	3.6 ± 3.5	3.6% *NS*	*Betaproteobacteria*			
Bacteria				Nitrosospira	0 ± 0	0.5 ± 0.2	0.5% **
Acidobacteria				Rhizobacter	0.3 ± 0.3	0.5 ± 0.2	0.2% *NS*
Acidobacteriaceae	9.7 ± 4.4	0.4 ± 0.0	9.3% **	*Deltaproteobacteria*			
Acidobacterium	11.9 ± 6.7	0.3 ± 0.1	11.6% **	Anaeromyxobacter	0.1 ± 0.3	0.3 ± 0.1	0.2% *NS*
Candidatus Koribacter	6.1 ± 0.7	0.8 ± 0.1	5.3% ***	Desulfobacca	0.1 ± 0.1	1.2 ± 0.3	1.1% ***
Candidatus Solibacter	5.5 ± 7.8	2.8 ± 0.7	2.7% *NS*	Desulfobacula	0.7 ± 0.4	0.2 ± 0.0	0.5% **
Granulicella	4.1 ± 1.6	0.1 ± 0.0	4.0% **	Geobacter	0.1 ± 0.0	2.4 ± 0.9	2.3% **
Luteitalea	0.9 ± 0.6	2.6 ± 0.9	1.7% **	Labilithrix	0.6 ± 0.2	0.4 ± 0.2	0.2% *NS*
Terriglobus	2.3 ± 1.2	0.1 ± 0.0	2.2% **	Syntrophus	0 ± 0	0.8 ± 0.4	0.8% **
Actinobacteria				Vulgatibacter	0 ± 0	0.8 ± 0.1	0.8% ***
Acidothermus	1.4 ± 0.4	0.7 ± 0.2	0.7% *	*Gammaproteobacteria*			
Actinobacterium	0.9 ± 0.2	1.3 ± 0.7	0.4% *NS*	Steroidobacter	2.5 ± 0.7	0.1 ± 0.1	2.4% ***
Blastococcus	0 ± 0	1.4 ± 0.7	1.4% **	*Chloroflexi*			
Conexibacter	1.6 ± 1.0	3.3 ± 0.9	1.7% ***	Anaerolinea	0 ± 0	3.3 ± 0.8	3.3% ***
Frankia	0.4 ± 0.2	1.3 ± 0.4	0.9% **	Herpetosiphon	0 ± 0	0.9 ± 0.2	0.9% ***
Geodermatophilus	0.1 ± 0.1	1.6 ± 0.5	1.5% **	Roseiflexus	0 ± 0	0.7 ± 0.4	0.7% **
Kineococcus	0.1 ± 0.0	3.5 ± 0.6	3.4% ***	Sphaerobacter	0 ± 0	0.8 ± 0.2	0.8% ***
Kribbella	4.1 ± 2.3	1.8 ± 0.4	2.3% *	*Firmicutes*			
Microlunatus	1.8 ± 1.0	0.5 ± 0.2	1.3% *	Anoxybacter	0 ± 0	0.6 ± 0.1	0.6% ***
Nakamurella	0.1 ± 0.0	1.9 ± 0.9	1.8% **	Carboxydocella	0 ± 0	0.7 ± 0.1	0.7% ***
Nonomuraea	4.7 ± 1.1	0.3 ± 0.1	4.4% ***	Pelotomaculum	0 ± 0	0.8 ± 0.1	0.8% ***
Plantactinospora	1.7 ± 1.1	0 ± 0	1.7% *	**Fungi**			
Sanguibacter	0 ± 0	1.3 ± 0.4	1.3% ***	*Ascomycetes*			
Streptacidiphilus	0.2 ± 0.1	1.4 ± 0.1	1.2% ***	Glarea	0.2 ± 0.2	0 ± 0	0.2% *
Streptosporangium	6.3 ± 2.0	0.1 ± 0.0	6.2% ***	Marssonina	0.3 ± 0.2	0 ± 0	0.3% *
Thermobifida	4.2 ± 1.3	0.1 ± 0.1	4.1% ***	Paracoccidioides	0.1 ± 0.1	0 ± 0	0.1% *
Thermobispora	1.2 ± 0.3	0.1 ± 0.0	1.1% ***	Phialocephala	0.6 ± 0.5	0 ± 0	0.6% *
Thermomonospora	7.1 ± 2.8	0.8 ± 0.1	6.3% **	Sclerotinia	0.1 ± 0.1	0 ± 0	0.1% *

Table SI 2.13 Supplemental O_2-Regulated Functional KEGG Orthologs (KOs). O_2-regulated genes from carbohydrate metabolism, amino acid metabolism, cofactors and vitamins metabolism, lipid metabolism, and overview metabolism KEGG categories were chosen from the reference database in Wu and Moore (2010), which identified KO groups that were statistically different for aerobic vs. anaerobic environmental conditions. Select marker genes from obligate anaerobic pathways of anaerobic carbon fixation, fermentation, denitrification, and methanogenesis, as well as genes from obligate aerobic pathways of aerobic carbon fixation and methane oxidation were chosen from Kieft et al. (2018).

Carbohydrate Metabolism	**Energy Metabolism**
Glycolysis / Gluconeogenesis	*Denitrification*
K00128 aldehyde dehydrogenase (NAD+)	K00368 nitrite reductase (NO-forming)
K00161 pyruvate dehydrogenase	K00370 nitrate reductase / nitrite oxidoreductase
Pyruvate Metabolism	K00376 nitrous-oxide reductase
K00656 formate C-acetyltransferase	K02305 nitric oxide reductase
Starch and Sucrose Metabolism	K02567 nitrate reductase (cytochrome)
K00975 glucose-1-phosphate adenylyltransferase	K15864 nitrite reductase (NO-forming) / hydroxylamine reductase
Amino Acid Metabolism	*Methane Metabolism - Methanogenesis*
Phenylalanine Metabolism	K00200 formylmethanofuran dehydrogenase subunit
K00146 phenylacetaldehyde dehydrogenase	K00204 4Fe-4S ferredoxin
Cofactors and Vitamins Metabolism	K00319 methylenetetrahydromethanopterin dehydrogenase
Nicotinate and Nicotinamide Metabolism	K00672 formylmethanofuran--tetrahydromethanopterin N-formyltransferase
K00763 nicotinate phosphoribosyltransferase	K11261 formylmethanofuran dehydrogenase subunit
Lipid Metabolism	K13942 5,10-methenyltetrahydromethanopterin hydrogenase
Glycerophospholipid Metabolism	K00193 acetyl-CoA decarbonylase/synthase, CODH/ACS complex
K00006 glycerol-3-phosphate dehydrogenase (NAD+)	K00625 phosphate acetyltransferase
Overview Metabolism	K00925 acetate kinase
Biosynthesis of Amino Acids	K01895 acetyl-CoA synthetase
K01915 glutamine synthetase	K04480 methanol-5-hydroxybenzimidazolylcobamide Co-methyltransferase
Carbon Metabolism	K14080 coenzyme M methyltransferase
K00873 pyruvate kinase	K14081 methanol corrinoid protein
K01623 fructose-bisphosphate aldolase, class I	*Methane Metabolism - Methanotrophy*
K00626 acetyl-CoA C-acetyltransferase	K10944 methane/ammonia monooxygenase subunit
Energy Metabolism	K14028 methanol dehydrogenase (cytochrome c) subunit
Anaerobic Carbon Fixation	K16157 methane monooxygenase component
K00174 2-oxoglutarate/2-oxoacid ferredoxin oxidoreductase	K16160 methane monooxygenase regulatory protein
K00194 acetyl-CoA decarbonylase/synthase complex	K23995 lanthanide-dependent methanol dehydrogenase
K00244 fumarate reductase flavoprotein	*Fermentation*
K00855 phosphoribulokinase	K00016 L-lactate dehydrogenase
K01648 ATP citrate (pro-S)-lyase	K00169 pyruvate ferredoxin oxidoreductase

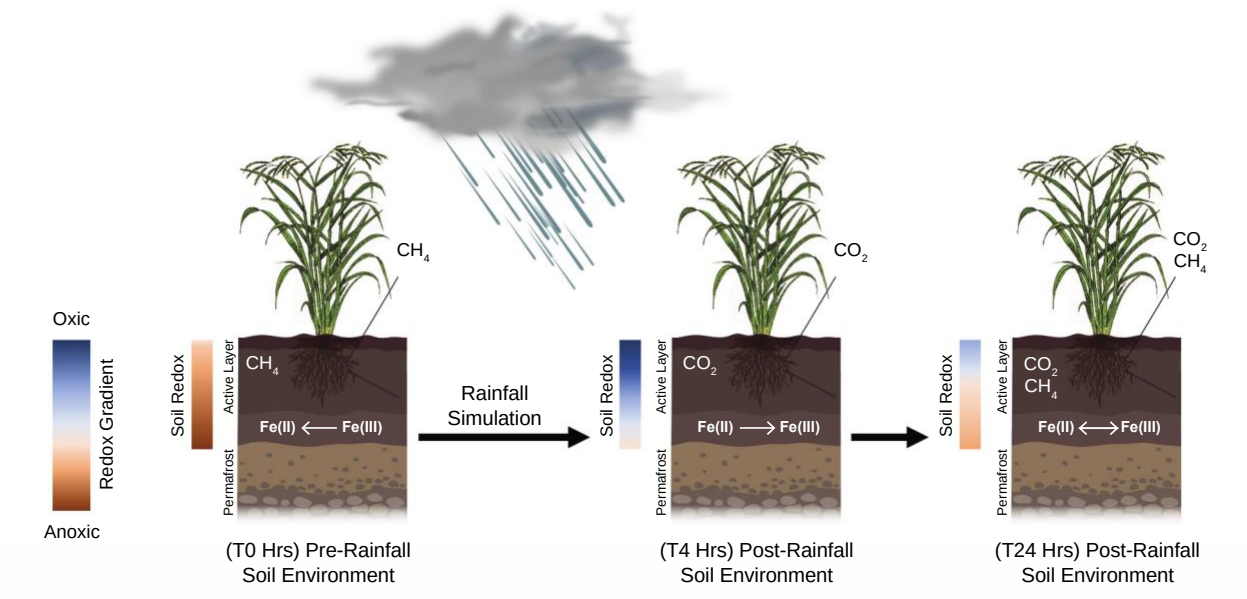

Figure SI 2.7 Supplemental Conceptual Figure. A total of 12 tundra mesocosms (3 replicates x 2 tundra types x 2 response groups) were acclimated initially under static, waterlogged conditions (i.e., no flowing water) for 4-7 days to generate reducing conditions observed in intact soils in the field. Mesocosm chambers were open at the top to allow oxygen diffusion and gas exchange with the atmosphere and sealed at the bottom to prevent drainage and soil oxygen leaching. Under field conditions (i.e., anoxia) at sampling time point T0, microorganisms likely degrade organic carbon through anaerobic and fermentation pathways, producing CH_4. The reduction of Fe(III) to Fe(II) also likely occurs through both abiotic and biotic processes. At sampling time point T4, simulated rainfall and subsequent soil oxygenation should stimulate heterotrophic microorganisms to degrade organic carbon and CH_4 through aerobic metabolic pathways, releasing CO_2. Soil oxygenation should also stimulate aerobic iron oxidizing bacteria that oxidize Fe(II) to Fe(III) and convert CO_2 into microbial biomass. The long-term response at sampling time point T24 will likely be a combination of aerobic and anaerobic metabolism as well as a combination of iron oxidation and reduction reactions as dissolved oxygen is consumed through abiotic and biotic processes.

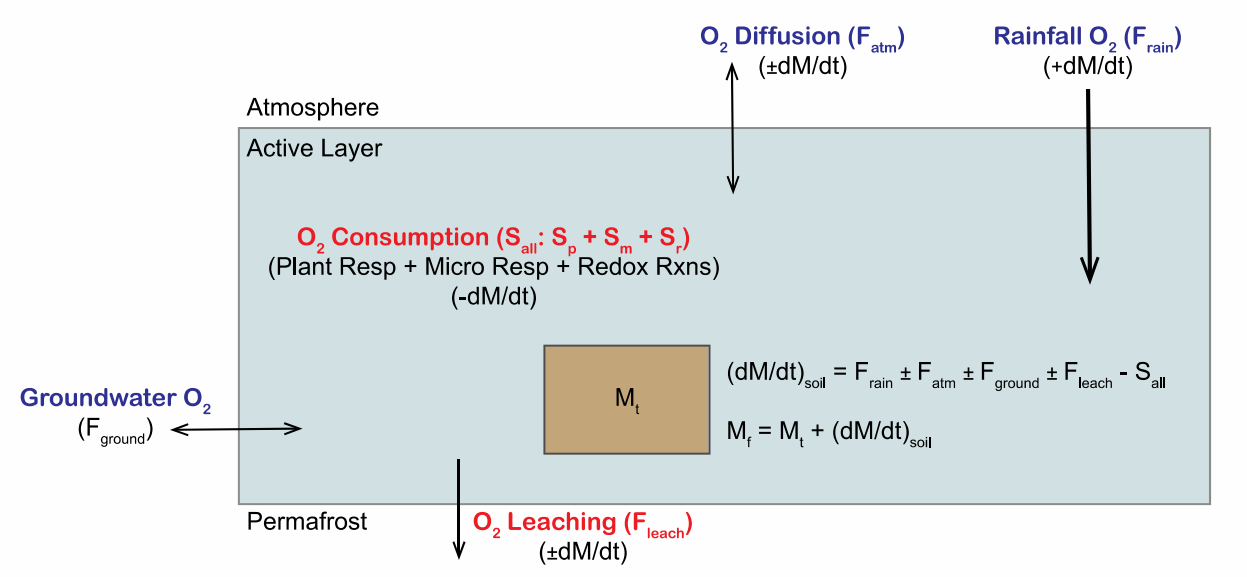

Figure SI 2.8 Supplemental Mass Balance Model. The concentration of dissolved oxygen (O_2) in the active layer of tundra soils (M_t) is regulated by numerous inputs and outputs that can be modeled to determine the rate at which the concentration changes during rainfall and what the final concentration will be following rainfall (M_f). Inputs of dissolved O_2 into the active layer include oxygenated rainwater (F_{rain}), atmospheric diffusion (F_{atm}), and oxygenated groundwater (F_{ground}). Outputs of dissolved O_2 from the active layer include O_2 consumption (S_{all}) through plant respiration (S_p), microbial respiration (S_m) and abiotic redox reactions (S_r), as well as O_2 leaching (F_{leach}) from soil water drainage. Note that there was no groundwater flux in the mesocosms, and O_2 diffusion across the surface boundary layer of the cores in these short-duration experiments (hours) is negligible.

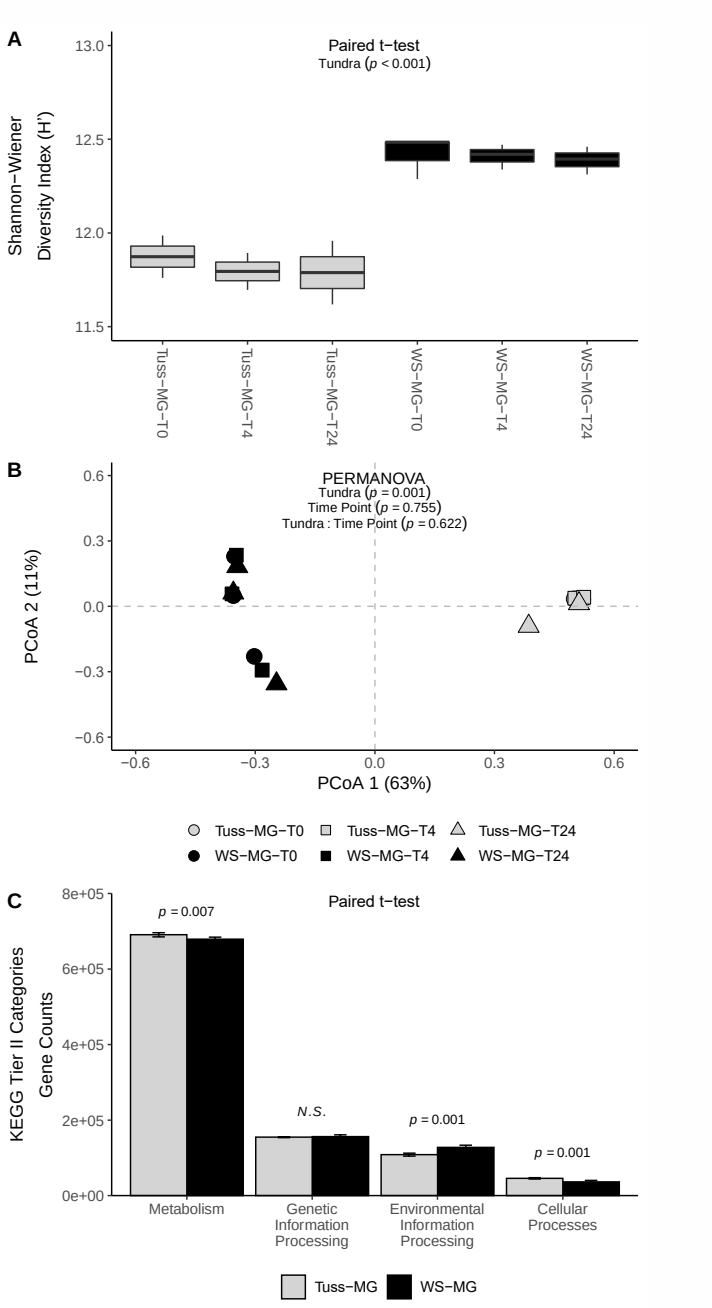

Figure SI 2.9 Supplemental Metagenomic Functional Diversity. Boxplot of (A) Shannon-Wiener alpha diversity (H') by sampling time point within tussock tundra and wet sedge tundra based on functional genes within the metagenomic (MG) dataset. Principle coordinates analysis (PCoA) of (B) beta diversity by sampling time point within tussock tundra and wet sedge tundra based on functional genes within the metagenomic (MG) dataset. Barplot of (C) KEGG tier II categories between tussock tundra and wet sedge tundra based on functional genes within the metagenomic (MG) dataset (error bars represent standard deviation of the mean).

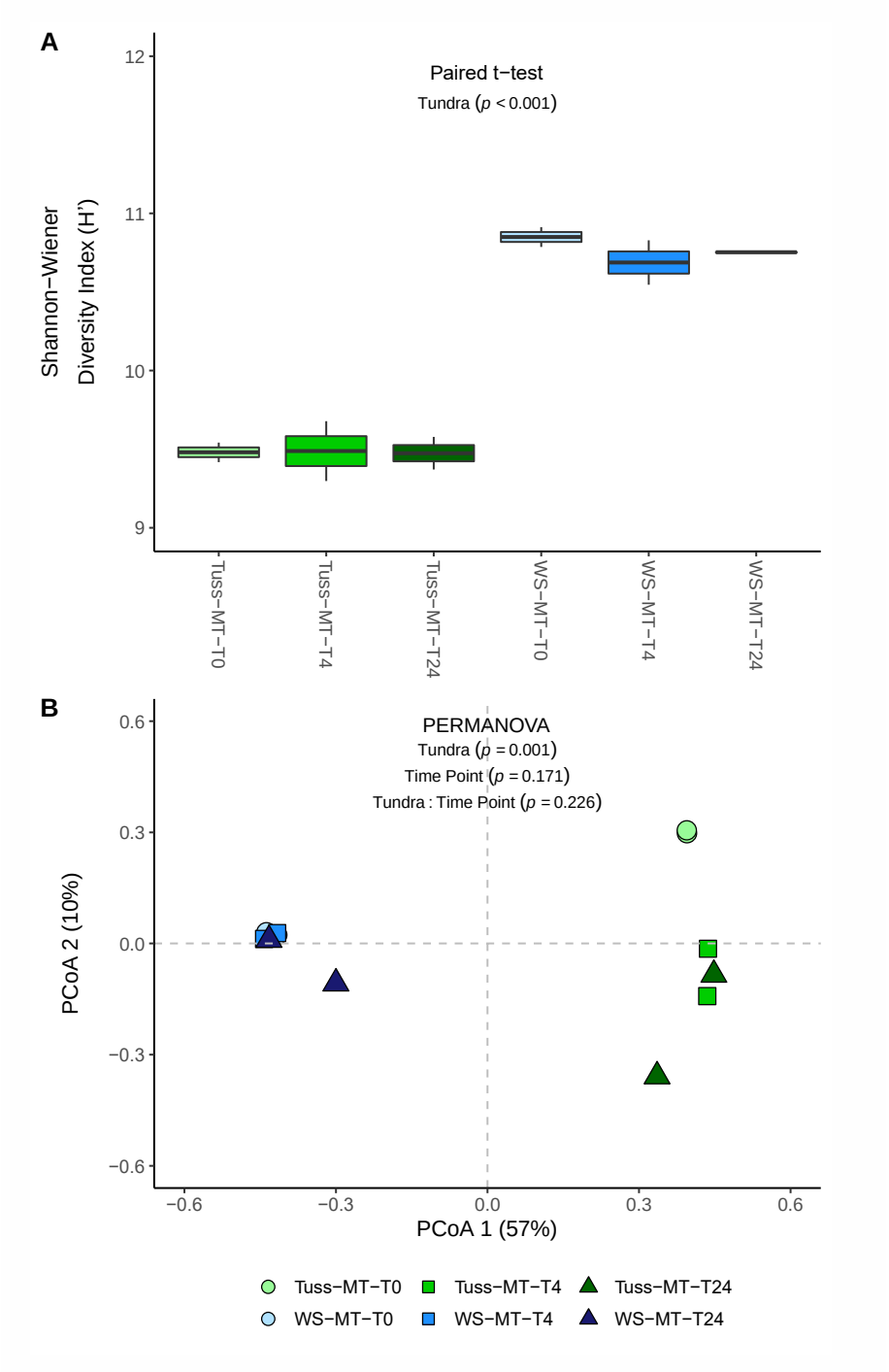

Figure SI 2.10 Supplemental Metatranscriptome Functional Diversity. Boxplot of (A) Shannon-Wiener alpha diversity (H') by sampling time point within tussock tundra and wet sedge tundra based on functional genes within the metatranscriptomic (MT) dataset. Principle coordinates analysis (PCoA) of (B) beta diversity by sampling time point within tussock tundra and wet sedge tundra based on functional genes within the metatranscriptomic (MT) dataset.

2.8 References

Alexander, M. Introduction to Soil Microbiology. 2nd ed.; John Wiley and Sons: New York, NY, USA, 1976.

Alneberg, J.; Bjarnason, B.S.; de Bruijn, I.; Schirmer, M.; Quick, J.; et al. Binning metagenomic contigs by coverage and composition. Nat. Methods 2014, 11, 1144-1146.

Armstrong, W. Oxygen diffusion from the roots of some British bog plants. Nature 1964, 204, 801-802.

Benjamini, Y.; Hochberg, Y. Controlling the false discovery rate: a practical and powerful approach to multiple testing. J. R. Stat. Soc. Ser. B. Methodol. 1995, 57, 289-300.

Bintanja, R.; Andry, O. Towards a rain-dominated Arctic. Nat. Clim. Change 2017, 7, 263-268.

Boberg, J.B.; Ihrmark, K.; Lindahl, B.D. Decomposing capacity of fungi commonly detected in Pinus sylvestris needle litter. Fungal Ecol. 2011, 4, 110-114.

Brown, J.G.; Hinkel, K.M.; Nelson, F.E. The circumpolar active layer monitoring (CALM) program: research designs and initial results. Polar Geogr. 2000, 24, 165-258.

Brune, A.; Frenzel, P.; Cypionka, H. Life at the oxic-anoxic interface: microbial activities and adaptations. FEMS Microbiol. Rev. 2000, 24, 691-710.

Bubier, J.L; Moore, T.R.; Bellisario, L.; Comer, N.T.; Crill, P.M. Ecological controls on methane emissions from a northern peatland complex in the zone of discontinuous permafrost, Manitoba, Canada. Glob. Biogeochem. Cycles 1995, 9(4), 455-470.

Bushnell, B. BBMap Short-Read Aligner and Other Bioinformatics Tools. 2015. [Software].

Campbell, J.H.; O'Donoghue, P.; Campbell, A.G.; Schwientek, P.; Sczyrba, A.; Woyke, T.; et al. UGA is an additional glycine codon in uncultured SR1 bacteria from the human microbiota. Proc. Natl. Acad. Sci. USA 2013, 110, 5540-5545.

Chapin III, F.S.; Fetcher, N.; Kielland, K.; Everett, K.R.; Linkins, A.E. Productivity and nutrient cycling of Alaskan tundra: enhancement with flowing soil water. Ecology 1988, 69(3), 693-702.

Conrad, M.; Kagan, V.E.; Bayir, H.; et al. Regulation of lipid peroxidation and ferroptosis in diverse species. Genes Dev. 2018, 32, 602-619.

Conrad, R.; Schutz, H.; Babbel, M. Temperature limitation on hydrogen turnover and methanogenesis in anoxic paddy soil. FEMS Microbiol. Ecol. 1987, 3, 281-289.

Crump, B.C.; Amaral-Zettler, L.A.; Kling, G.W. Microbial diversity in arctic freshwaters is structured by inoculation of microbes from soils. ISME J. 2012, 6, 1629-1639.

Deng, J.; Gu, Y.; Zhang, J.; Xue, K.; Qin, Y.; Yuan, M.; Yin, H.; et al. Shifts of tundra bacterial and archaeal communities along a permafrost thaw gradient in Alaska. Mol. Ecol. 2015, 24, 222-234.

Doherty, S.J.; Barbato, R.A.; Grandy, A.S.; Thomas, W.K.; Monteux, S.; Dorrepaal, E.; Johansson, M.; Ernakovich, J.G. The transition from stochastic to deterministic bacterial community assembly during permafrost thaw succession. Front. Microbiol. 2020, 11, 596589.

Douglas, T.A.; Turetsky, M.R.; Koven, C.D. Increased rainfall stimulates permafrost thaw across a variety of interior Alaskan boreal ecosystems. NPJ Clim. Atmos. Sci. 2020, 28, 1-7.

Eddy, S.R. Accelerated profile HMM searches. PLoS Comput. Biol. 2011, 7, e1002195.

Elberling, B.; Michelsen, A.; Schadel, C.; Schuur, E.A.G.; Christiansen, H.H.; Berg, L.; Ellipsis-Sigsgaard, C. Long-term CO2 production following permafrost thaw. Nat. Clim. Change 2013, 3, 890–894.

Emerson, D.; Revsbech, N.; Investigation of an iron-oxidizing microbial mat community located near Aarhus, Denmark: laboratory studies. Appl. Environ. Microbiol. 1994, 60, 4032–4038.

Emerson, D.; Scott, J.J.; Benes, J.; Bowden, W.B. Microbial iron oxidation in the Arctic tundra and its implications for biogeochemical cycling. Appl. Environ. Microbiol. 2015, 81, 8066–8075.

Eren, A.M.; Esen, O.C.; Quince, C.; Vineis, J.H.; Morrison, H.G.; Sogin, M.L.; Delmont, T.O. Anvi'o: an advanced analysis and visualization platform for 'omics data. Peer J. 2015, 3, e1319.

Euskirchen, E.S.; Bret-Harte, M.S.; Shaver, G.R.; Edgar, C.W.; Romanovsky, V.E. Long-term release of carbon dioxide from arctic tundra ecosystems in Alaska. Ecosystems 2017, 20(5), 960-974.

Garber, A.I.; Nealson, K.H.; Okamoto, A.; McAllister, S.M.; Chan, C.S.; Barco, R.A.; Merino, N. FeGenie: A Comprehensive Tool for the Identification of Iron Genes and Iron Gene Neighborhoods in Genome and Metagenome Assemblies. Front. Microbiol. 2020, 11(37), 1-23.

Gebauer, R.L.E.; Tenhunen, J.D.; Reynolds, J.F. Soil aeration in relation to soil physical properties, nitrogen availability and root characteristics within an arctic watershed. Plant Soil 1996, 178, 37-48.

Giblin, A.E.; Nadelhoffer, K.J.; Shaver, G.R.; Laundre, J.A.; McKerrow, A.J. Biogeochemical diversity along a river toposequence in arctic Alaska. Ecol. Monogr. 1991, 61, 415-435.

Gorham E. Northern peatlands: role in the carbon cycle and probable responses to climatic warming. Ecol. Appl. 1991, 1(2), 182-195.

Grosse, G.; Romanovsky, V.; Jorgenson, T.; Anthony, K.W.; Brown, J.; Overduin, P.P. Vulnerability and feedbacks of permafrost to climate change. EOS 2011, 92, 73.

Herndon, E.M.; Kinsman-Costello, L.; Godsey, S. Biogeochemical cycling of redox-sensitive elements in permafrost-affected ecosystems. In Biogeochemical Cycles: Ecological Drivers and Environmental Impact, Geophysical Monograph, Dontsova K, Balogh-Brunstad Z, Le Roux G (Eds.) John Wiley & Sons, 2020.

Hobbie, J.E.; Hobbie, E.A.; Drossman, H.; Conte, M.; Weber, J.C.; Shamhart, J.; Weinrobe, M. Mycorrhizal fungi supply nitrogen to host plants in Arctic tundra and boreal forests: 15N is the key signal. Can. J. Microbiol. 2009, 55, 84-94.

Hobbie, J.E.; Kling, G.W. (Eds.) A Changing Arctic: Ecological Consequences for Tundra, Streams, and Lakes; Oxford University Press: Oxford, UK, 2014.

Huemmrich, K.F.; Kinoshita, G.; Gamon, J.A.; Houston, S.; Kwon, H.; Oechel, W.C. Tundra carbon balance under varying temperature and moisture regimes. J. Geophys. Res. 2010, 115, 1–8.

Hugelius, G.; Strauss, J.; Zubrzycki, S.; Harden, J.W.; Schuur, E.A.G.; Ping, C.L.; Schirrmeister, L.; Grosse, G.; Michaelson, G.J.; Koven, C.D.; O'Donnell, J.A.; Elberling, B.; Mishra, U.; Camill, P.; Yu, Z.; Palmtag, J.; Kuhry, P. Estimated stocks of circumpolar permafrost carbon with quantified uncertainty ranges and identified data gaps. Biogeosciences 2014, 11(23), 6573–6593.

Hultman, J.; Waldrop, M.P.; Mackelprang, R.; David, M.M.; McFarland, J.; Blazewicz, S.J.; Harden, J.; Turetsky, M.R.; McGuire, A.D.; Shah, M.B.; VerBerkmoes, N.C.; Lee, L.H.; Mavrommatis, K.; Jansson, J.K. Multi-omics of permafrost, active layer and thermokarst bog soil microbiomes. Nature 2015, 521, 208-212.

Hyatt, D.; Chen, G.L.; LoCascio, P.F.; Land, M.L.; Larimer, F.W.; Hauser, L.J. Prodigal: prokaryotic gene recognition and translation initiation site identification. BMC Bioinformatics 2010, 11, 119.

Ivanova, A.A.; Wegner, C.-E.; Kim, Y.; Liesack, W.; Dedysh, S.N. Identification of microbial populations driving biopolymer degradation in acidic peatlands by metatranscriptomic analysis. Mol. Ecol. 2016, 25, 4818-4835.

Jansson, J.K.; Hofmockel, K.S. The soil microbiome – from metagenomics to metaphenomics. Curr. Opin. Microbiol. 2018, 43, 162-168.

Jia, X.; Xi, B.; Li, M.; Liu, D.; Hou, J.; Hao, Y.; Meng, F. Metaproteomic analysis of the relationship between microbial community phylogeny, function and metabolic activity during biohydrogen-methane coproduction under short-term hydrothermal pretreatment from food waste. Bioresource Technol. 2017, 245, 1030-1039.

Jorgenson, M.T.; Shur, Y.L.; Pullman, E.R. Abrupt increase in permafrost degradation in Arctic Alaska. Geophys. Res. Lett. 2006, 33(2), D22103.

Judd, K.E.; Kling, G.W. Production and export of dissolved C in arctic tundra mesocosms: the roles of vegetation and water flow. Biogeochemistry 2002, 60, 213–234.

Judd, K.E.; Crump, B.C.; Kling, G.W. Environmental drivers control eco- system function in bacteria through changes in community composition. Ecology 2006, 87, 2068–2079.

Kanehisa, M.; Araki, M.; Goto, S.; Hattori, M.; Hirakawa, M.; Itoh, M.; et al. KEGG for linking genomes to life and the environment. Nucleic Acids Res. 2008, 36, D480-D484.

Kanehisa, M.; Sato, Y.; Morishima, K. BlastKOALA and GhostKOALA: KEGG Tools for functional characterization of genome and metagenome sequences. J. Mol. Biol. 2016, 428, 726–731.

Kang, D.D.; Froula, J.; Egan, R.; Wang, Z. MetaBAT, an efficient tool for accurately reconstructing single genomes from complex microbial communities. Peer J. 2015, 3, e1165.

Kieft, B.; Li, Z.; Bryson, S.; Crump, B.C.; Hettich, R.; Pan, C.; Mayali, X.; Mueller, R.S. Microbial community structure-function relationships in Yaquina Bay estuary reveal spatially distinct carbon and nitrogen cycling capacities. Front. Microbiol. 2018, 9, 1282.

Kim, H.M.; Lee, M.J.; Jung, J.Y.; Hwang, C.Y.; Kim, M.; Ro, H.M.; Chun, J.; Lee, Y.K. Vertical distribution of bacterial community is associated with the degree of soil organic matter decomposition in the active layer of moist acidic tundra. J. Microbiol. 2016, 54(11), 713-723.

King, J.Y.; Reeburgh, W.S.; Regli, S.K. Methane emission and transport by arctic sedges in Alaska: results of a vegetation removal experiment. J. Geophys. Res. Atmos. 1998, 103, 29083-29092.

Kolb, S. Aerobic methanol-oxidizing bacteria in soil. FEMS Microbiol. Lett. 2009, 300(1), 1-10.

Kolde, R. pheatmap: Pretty heatmaps. 2015. [Software].

Kumar, M.; Want, R.; Link, T.E. Effects of more extreme precipitation regimes on maximum seasonal snow water equivalent. Geophys. Res. Lett. 2012, 39(20), 1-6.

Langmead, B.; Salzberg, S.L. Fast gapped-read alignment with bowtie 2. Nat. Methods 2012, 9, 357-359.

Lauber, C.L.; Hamady, M.; Knight, R.; Fierer, N. Pyrosequencing-based assessment of soil pH as a predictor of soil bacterial community structure at the continental scale. Appl. Environ. Microbiol. 2009, 75, 5111-5120.

Lauro, F.M.; McDougald, D.; Thomas, T.; Williams, T.J.; Egan, S.; Rice, S.; DeMaere, M.Z.; Ting, L.; Ertan, H.; Johnson, J. The genomic basis of trophic strategy in marine bacteria. Proc. Natl. Acad. Sci. USA 2009, 106, 15527-15533.

Lawrence, D.M.; Koven, C.D.; Swenson, S.C.; Riley, W.J.; Slater, A.G. Permafrost thaw and resulting soil moisture changes regulate projected high-latitude CO2 and CH4 emissions. Environ. Res. Lett. 2015, 10, 094011.

Lennon, J. Microbial life deep underfoot. mBio 2020, 11, e03201-19.

Li, D.; Liu, C.M.; Luo, R.; Sadakane, K.; Lam, T.W. MEGAHIT: an ultra-fast single-node solution for large and complex metagenomics assembly via succinct de Bruijn graph. Bioinformatics 2015, 31, 1674-1676.

Li, H.; Shi, W.; Li, X.; Hu, Y.; Yu, F.; Ma, H. Ferroptosis accompanied by OH generation and cytoplasmic viscosity increase revealed via dual-functioning fluorescence probe. J. Am. Chem. Soc. 2019, 141, 18301-18307.

Lipson, D.A.; Haggerty, J.M.; Srinivas, A.; Raab, T.K.; Sathe, S.; Dinsdale, E.A. Metagenomic insights into anaerobic metabolism along an arctic peat soil profile. PLoS One 2013, 8(5), e64659.

Mackelprang, R.; Waldrop, M.P.; DeAngelis, K.M.; David, M.M.; Chavarria, K.L.; Blazewicz, S.J.; Rubin, E.M.; Jansson, J.K. Metagenomic analysis of a permafrost microbial community reveals a rapid response to thaw. Nature 2011, 480, 368-371.

Malard, L.A.; Pearce, D.A. Microbial diversity and biogeography in Arctic soils. Env. Microbiol. Rep. 2018, 10(6), 611-625.

Marchitti, S.A.; Brocker, C.; Stagos, D.; Vasiliou, V. Non-P450 aldehyde oxidizing enzymes: the aldehyde dehydrogenase superfamily. Expert Opin. Drug Met. 2008, 4(6), 697-720.

Margesin, R. Permafrost Soils, R. Margesin (Ed.), Soil Biology, 2009, vol. 16, Springer Verlag, Berlin Heidelberg.

McGuire, A.D.; Anderson, L.G.; Christensen, T.R.; Dallimore, S.; Guo, L.; et al. Sensitivity of the carbon cycle in the arctic to climate change. Ecol. Monogr. 2009, 79(4), 523-555.

McKnight, D.M.; Boyer, E.W.; Westerhoff, P.K.; Doran, P.T.; Kulbe, T.; Andersen, D.T. Spectrofluorometric characterization of dissolved organic matter for indication of precursor organic material and aromaticity. Limnol. Oceanogr. 2001, 46, 38-48.

McMahon, S.K.; Wallenstein, M.D.; Schimel, J.P. A cross-seasonal comparison of active and total bacterial community composition in arctic tundra soil using bromodeoxyuridine labeling. Soil. Biol. Biochem. 2011, 43, 287-295.

Merbold, L.; Kutsch, W.L.; Corradi, C.; Kolle, O.; Rebmann, C.; Stoy, P.C.; Schulze, E.-D. Artificial drainage and associated carbon fluxes (CO2/CH4) in a tundra ecosystem. Glob. Change Biol. 2009, 15, 2599–2614.

Metje, M.; Frenzel, P. Methanogenesis and methanogenic pathways in a peat from subarctic permafrost. Environ. Microbiol. 2007, 9, 954-964.

Miller, P.C.; Kendall, R.; Oechel, W.C. Simulating carbon accumulation in northern ecosystems. Simulation 1983, 40, 119-131.

Moldrup, P.; Olesen, T.; Gamst, J.; Schjonning, P.; Yamaguchi, T.; Rolston, D. Predicting the gas diffusion coefficient in repacked soil: water-induced linear reduction model. Soil Sci. Soc. Am. J. 2000, 64, 1588-1594.

Nadelhoffer, K.J.; Giblin, A.E.; Shaver, G.R.; Laundre, J. Effects of temperature and organic matter quality on element mineralization in six arctic soils. Ecology 1991, 72, 242-253.

Nalven, S.G.; Ward, C.P.; Payet, J.P.; Cory, R.M.; Kling, G.W.; Sharpton, T.J.; Sullivan, C.M.; Crump, B.C. Experimental metatranscriptomics reveals the costs and benefits of dissolved organic matter photo-alteration for freshwater microbes. Environ. Microbiol. 2020, 22(8), 3505-3521.

Neilson, B.T.; Cardenas, M.B.; O'Connor, M.T.; Rasmussen, M.T.; King, T.V.; Kling, G.W. Groundwater flow and exchange across the land surface explain carbon export patterns in continuous permafrost watersheds. Geophys. Res. Lett. 2018, 45(15), 7596-7605.

Neumann, R.B.; Moorber, C.J.; Lundquist, J.D.; Turner, J.C.; Waldrop, M.P.; McFarland, J.W.; Euskirchen, E.S.; Edgar, C.W.; Turetsky, M.R. Warming effects of spring rainfall increase methane emissions from thawing permafrost. Geophys. Res. Lett. 2019, 46, 1393-1401.

Nosova, T.; Jokelainen, K.; Kaihovaara, P.; Jousimies-Somer, H.; Siitonen, A.; Heine, R.; Salaspuro, M. Aldehyde dehydrogenase activity and acetate production by aerobic bacteria representing the normal flora of human large intestine. Alcohol Alcoholism, 1996, 31(6), 555-564.

O'Connor, M.T.; Cardenas, M.B.; Ferencz, S.B.; Wu, Y.; Neilson, B.T.; Chen, J.; Kling, G.W. Empirical models for predicting water and heat flow properties of permafrost soils. Geophys. Res. Lett. 2020, 47, 1-10.

Oechel, W.C.; Hastings, S.J.; Vourlitis, G.; Jenkins, M.; Riechers, G.; Grulke, N. Recent change of Arctic tundra ecosystems from a net carbon dioxide sink to a source. Nature 1993, 361, 520-523.

Oksanen, J.; Blanchet, F.G.; Friendly, M.; Kindt, R.; Legendre, P.; McGlinn, D.; et al. vegan: Community Ecology Package. R Package version 2.5-5. 2019. [Software].

Olefeldt, D.; Turetsky, M.R.; Crill, P.M.; McGuire, A.D. Environmental and physical controls on northern terrestrial methane emissions across permafrost zones. Glob. Change Biol. 2013, 19(2), 589-603.

Osterkamp, T.E.; Romanovsky, V.E. Evidence for warming and thawing of discontinuous permafrost in Alaska. Permafrost Periglac. 1999, 10; 17-37.

Page, S.E.; Logan, J.R.; Cory, R.M.; McNeill, K. Evidence for dissolved organic matter as the primary source and sink of photochemically produced hydroxyl radical in arctic surface waters. Environ. Sci.-Proc. Imp. 2014, 16(4), 807–822.

Parks, D.H.; Chuvochina, M.; Chaumeil, P.A.; et al. A complete domain-to-species taxonomy for Bacteria and Archaea. Nat. Biotechnol. 2020, 38(9), 1079-1086.

Quast, C.; Pruesse, E.; Yilmaz, P.; Gerken, J.; Schweer, T; et al. The SILVA ribosomal RNA gene database project: improved data processing and web-based tools. Nucleic Acids Res. 2013, 41, D590-D596.

R Core Development Team. R: a language and environment for statistical computing. Vienna, Austria. 2017. [Software].

Ratledge, C. Biochemistry of microbial degradation. Kluwer Academic Publishers, Dordrecht, the Netherlands, 1994.

Rinke, C.; Schwientek, P.; Sczyrba, A.; Ivanova, N.N.; Anderson, I.J.; Cheng, J.-F.; et al. Insights into phylogeny and coding potential of microbial dark matter. Nature 2013, 499, 431-437.

Robinson, M.D.; Oshlack, A. A scaling normalization method for differential expression analysis of RNA-seq data. Genome Biol. 2010, 11, R25.

Rognes, T.; Flouri, T.; Nichols, B.; Quince, C.; Mahe, F. VSEARCH: a versatile open-source tool for metagenomics. Peer J. 2016, 4, e2584.

Rousk, J.; Baath, E.; Brookes, P.C.; Lauber, C.L.; Lozupone, C.; Caporaso, J.G.; Knight, R.; Fierer, N. Soil bacterial and fungal communities across a pH gradient in an arable soil. ISME J. 2010, 4, 1340-1351.

Schadel, C.; Bader, M.K.F.; Schuur, E.A.; Biasi, C.; Bracho, R.; Capek, P.; De Baets, S.; Diakova, K.; Ernakovich, J.; Estop-Aragones, C.; Graham, D.E.; Hartley, I.P.; Iversen, C.M.; Kane, E.; Knoblauch, C.; Lupascu, M.; Martikainen, P.J.; Natali, S.; Norby, R.J.; O'Donnell, J.; Chowdhury, T.R.; Santruckova, H.; Shaver, G.; Sloan, V.L.; Treat, C.C.; Turetsky, M.R.; Waldrop, M.P.; Wickland, K.P. Potential carbon emissions dominated by carbon dioxide from thawed permafrost soils. Nat. Clim. Change 2016, 6, 950–953.

Schloss, P.D.; Westcott, S.L.; Ryabin, T.; Hall, J.R.; Hartmann, M.; et al. Introducing mothur: open-source, platform-independent, community-supported software for describing and comparing microbial communities. Appl. Environ. Microb. 2009, 75(23), 7537-7541.

Schuur, E.A.G.; Vogel, J.G.; Crummer, K.G.; Lee, H.; Sickman, J.O.; Osterkamp, T.E. The effect of permafrost thaw on old carbon release and net carbon exchange from tundra. Nature 2009, 459, 556-559.

Sekar, K.; Linker, S.M.; Nguyen, J.; Grunhagen, A.; Stocker, R.; Sauer, U. Bacterial glycogen provides short-term benefits in changing environments. Appl. Environ. Microb. 2020, 86(9), e00049-20.

Shen, L.; Preiss, J. Biosynthesis of bacterial glycogen. I. Purification and properties of the adenosine diphosphoglucose pyrophosphorylase of Arthrobacter species NRRL B1973. J. Biol. Chem. 1965, 240, 2334-2340.

Sieber, C.M.K.; Probst, A.J.; Sharrar, A.; Thomas, B.C.; Hess, M.; Tringe, S.G.; Banfield, J.F. Recovery of genomes from metagenomes via a dereplication, aggregation and scoring strategy. Nat. Microbiol. 2018, 3, 836–843.

Sistla, S.A.; Asao, S.; Schimel, J.P. Detecting microbial N-limitation in tussock tundra soil: implications for Arctic soil organic carbon cycling. Soil Biol. Biochem. 2012, 55, 78-84.

Spence, C.; Phillips, R.W. Refining understanding of hydrological connectivity in a boreal catchment. Hydrol. Process. 2015, 29(16), 3491-3505.

Stieglitz, M.; Shaman, J.; McNamara, J.; Engel, V.; Shanley, J.; Kling, G.W. An approach to understanding hydrologic connectivity on the hillslope and the implications for nutrient transport. Global Biogeochem. Cycles 2003, 17(4), 1105.

Stockwell, B.R.; Friedmann Angeli, J.P.; Bayir, H.; Bush, A.I.; Conrad, M.; Dixon, S.J.; Fulda, S.; Gascon, S.; Hatzios, S.K.; Kagan, V.E.; Noel, K.; Jiang, X.; Linkermann, A.; Murphy, M.E.; Overholtzer, M.; Oyagi, A.; Pagnussat, G.C.; Park, J.; Ran, Q.; Rosenfeld, C.S.; Salnikow, K.; Tang, D.; Torti, F.M.; Torti, S.V.; Toyokuni, S.; Woerpel, K.A.; Zhang, D.D. Ferroptosis: a regulated cell death nexus linking metabolism, redox biology, and disease. Cell 2017, 171, 273−285.

Tas, N.; Prestat, E.; Wang, S.; Wu, Y.; Ulrich, C.; Kneafsey, T.; Tringe, S.G.; Torn, M.S.; Hubbard, S.S.; Jansson, J.K. Landscape topography structures the soil microbiome in arctic polygonal tundra. Nat. Commun. 2018, 9, 777.

Thorbjorn, A.; Moldrup, P.; Blendstrup, H.; Komatsu, T.; Rolston, D. A gas diffusivity model based on air-, solid-, and water-phase resistance in variably saturated soil. Vadose Zone J. 2008, 7, 1276.

Tripathi, B.M.; Kim, M.; Kim, Y.; Byun, E.; Yang, J.-W.; Ahn, J.; Lee, Y.K. Variations in bacterial and archaeal communities along depth profiles of Alaskan soil cores. Sci. Rep.-U.K. 2018, 8, 504.

Trusiak, A.; Treibergs, L.A.; Kling, G.W.; Cory, R.M. The role of iron and reactive oxygen species in the production of CO2 in arctic soil water. Geochim. Cosmochim. Acta 2018, 224, 80-95.

Trusiak, A.; Treibergs, L.A.; Kling, G.W.; Cory, R.M. The controls of iron and oxygen on hydroxyl radical (OH) production in soils. Soil Syst. 2019, 3(1), 1-23.

Turetsky, M.R.; Treat, C.C.; Waldrop, M.P.; Waddington, J.M.; Harden, J.W.; McGuire, A.D. Short-term response of methane fluxes and methanogen activity to water table and soil warming manipulations in an Alaskan peatland. J. Geophys. Res.-Biogeo. 2008, 113, G00A10.

Tveit, A.T.; Schwacke, R.; Svenning, M.M.; Urich, T. Organic carbon transformations in high-Arctic peat soils: key functions and microorganisms. ISME J. 2013, 7, 299-311.

Tveit, A.T.; Urich, T.; Frenzei, P.; Svenning, M.M. Metabolic and trophic interactions modulate methane production by arctic peat microbiota in response to warming. P. Natl. Acad. Sci. U.S.A. 2015, 112(19), E2507-E2516.

Veith, N.; Feldman-Salit, A.; Cojocaru, V.; Henrich, S.; Kummer, U.; Wade, R.C. Organism-adapted specificity of the allosteric regulation of pyruvate kinase in lactic acid bacteria. PLoS Comput. Biol. 2013, 9(7), e1003159.

Wagner, G.P.; Kin, K.; Lynch, V.J. Measurement of mRNA abundance using RNA-seq data: RPKM measure is inconsistent among samples. Theory Biosci. 2012, 131, 281-285.

Walker, M.D.; Walker, D.A.; Auerback, N.A. Plant communities of a tussock tundra landscape in the Brooks Range foothills, Alaska. J. Veg. Sci. 1994, 5, 843-866.

Wang, Q.; Garrity, G.M.; Tiedje, J.M.; Cole, J.R. Naïve Bayesian classifier for rapid assignment of rRNA sequences into the new bacterial taxonomy. Appl. Environ. Microbiol. 2007, 73(16), 5261-5267.

Ward, C.P.; Cory, R.M. Chemical composition of dissolved organic matter draining permafrost soils. Geochim. Cosmochim. Acta 2015, 167, 63–79.

Weber, K.A.; Achenbach, L.A.; Coates, J.D. Microorganisms pumping iron: anaerobic microbial iron oxidation and reduction. Nat. Rev. Microbiol. 2006, 4, 752-763.

Wickham, H. ggplot2: elegant graphics for data analysis. New York: Springer-Verlag. 2016. [Software].

Wickland, K.P.; Striegl, R.G.; Neff, J.C.; Sachs, T. Effects of permafrost melting on CO2 and CH4 exchange of a poorly drained black spruce lowland. J. Geophys. Res.-Biogeo. 2006, 111, G2.

Wu, H.; Moore, E. Association analysis of the general environmental conditions and prokaryotes' gene distributions in various functional groups. Genomics 2010, 96, 27-38.

Xue, K.; Yuan, M.M.; Shi, Z.J.; Qin, Y.; Deng, Y.; Cheng, L.; Wu, L.; He, Z.; Van Nostrand, J.D.; et al. Tundra soil carbon is vulnerable to rapid microbial decomposition under climate change. Nat. Clim. Change 2016, 6, 595-600.

Zak, D.R.; Kling, G.W. Microbial community composition and function across an arctic tundra landscape. Ecology 2006, 87, 1659–1670.

Zona, D.; Lipson, D.A.; Paw, U.K.T.; Oberbauer, S.F.; Olivas, P.; Gioli, B.; Oechel, W.C. Increased CO2 loss from vegetated drained lake tundra ecosystems due to flooding. Global Biogeochem. Cy. 2012, 26(2), 1–16.

Zona, D. Long-term effects of permafrost thaw. Nature 2016, 537(7622), 625-626.

Chapter 3.
Summer Thaw Duration is a Strong Predictor of the Soil Microbiome and its Response to Permafrost Thaw in Arctic Tundra [2]

3.1 Abstract

Climate warming has increased permafrost thaw in arctic tundra and extended the duration of annual thaw (number of thaw days in summer) along soil profiles. Predicting the microbial response to permafrost thaw depends largely on knowing how increased thaw duration affects the composition of the soil microbiome. Here we determined soil microbiome composition from the annually-thawed surface active layer down through permafrost from two tundra types at each of three sites on the North Slope of Alaska, USA. Variations in soil microbial taxa were found between sites up to ~90 km apart, between tundra types, and between soil depths. Microbiome differences at a site were greatest across transitions from thawed to permafrost depths. Multi-decadal thaw surveys show that differences in thaw duration by depth were significantly positively correlated with abundance of dominant taxa in the active layer and negatively correlated with dominant taxa in the permafrost. Microbiome composition within the transition zone was statistically similar to that in the permafrost, indicating that recent decades of intermittent thaw have not yet induced a shift from permafrost to active-layer microbes. We suggest that thaw duration rather than thaw frequency has a greater impact on the composition of microbial taxa within arctic tundra soils.

3.2 Introduction

Arctic tundra is underlain by permafrost, an ice-hardened soil layer defined by its subzero temperatures for two or more consecutive years (Williams and Smith 1989). The layer of soil that lies above the permafrost undergoes annual freeze-thaw cycles and is known as the active layer.

[2] Submitted as: Karl J. Romanowicz, George W. Kling. Summer thaw duration is a strong predictor of the soil microbiome and its response to permafrost thaw in arctic tundra. Environmental Microbiology. In Review.

Collectively, these soils represent an important microbial ecosystem (Jansson and Tas 2014) and a globally significant pool of sequestered carbon (Schuur et al. 2008, Tarnocai et al. 2009, Hugelius et al. 2014) that is being thawed and mobilized as climate warms (Osterkamp & Romanovsky 1999, Hinzman et al. 2005, Jorgenson et al. 2006). Warmer soil temperatures, earlier spring thaw, and later fall freeze-up have all contributed to an increase in annual thaw depth and an extended duration of annual thaw at specific depths in tundra soil profiles (Serreze et al. 2000, Euskirchen et al. 2006, Barichivich et al. 2012). Yet few studies have explicitly investigated how increased thaw frequency versus average thaw duration over time has affected the soil microbiome. The genomic potential of soil microbiomes determines the biotic decomposition of soil carbon and its release to the atmosphere as carbon dioxide (CO_2) and methane (CH_4) (Chen et al. 2021). Therefore, it is important to determine how increases in frequency and duration of thaw affect the composition of the soil microbiome in order to predict the microbial response to future permafrost thaw and the fate of permafrost soil carbon.

It is well established that microbiome composition varies across tundra soils (Yergeau et al. 2010, Mackelprang et al. 2011, Frank-Fahle et al. 2014, Gittel et al. 2014, Deng et al. 2015, Müller et al. 2018). In the active layer, the composition of the soil microbiome is influenced by geographic distance between sites (Malard et al. 2019) and variations in landscape topography that control dominant plant species and soil physicochemical properties (Judd & Kling 2002, Judd et al. 2006, Zak & Kling 2006, Tas et al. 2018). For example, geographic distance and plant species can change the regional composition of the active-layer microbiome given its direct connection with aboveground environmental conditions (Wallenstein et al. 2007, Chu et al. 2011, Malard & Pearce 2018, Tas et al. 2018, Tripathi et al. 2018, Romanowicz et al. 2021). Additional environmental factors such as active-layer depth or soil type (Malard et al. 2019) as well as climatic variables such as temperature and precipitation (Castro et al. 2010, Nielsen & Ball 2015) can also influence the composition of the active-layer microbiome. In permafrost, the composition of the soil microbiome is influenced by landscape age, with substantial changes in composition found along permafrost chronosequences in response to increasing age and associated stresses of the harsh permafrost environment (Mackelprang et al. 2017, Saidi-Mehrabad et al. 2020). Additional environmental factors such as ice content (Burkert et al. 2019), dispersal limitations (Bottos et al. 2018), and thermodynamic constraints imposed by prolonged freezing (Bottos et al. 2018) can influence the composition of the permafrost microbiome. What remains unclear is whether and

how an increase in the frequency of thaw at depth over time, and the duration of that thaw, will affect the microbial composition of soils in the transition zone between the upper active layer and deeper permafrost.

Recent studies that attempt to predict the microbial response to permafrost thaw often focus on the microbiome composition as it exists at the time of sampling (Waldrop et al. 2010, Mackelprang et al. 2011, Coolen & Orsi 2015, Hultman et al. 2015). Yet, over time the harsh permafrost environment can alter the composition of the microbiome by selecting for a subset of taxa originally present when the permafrost formed (Willerslev et al. 2004, Kraft et al. 2015, Liang et al. 2019). In laboratory-based incubations, these relic permafrost microbiomes have shown rapid, substantial shifts in composition within a few days of thaw (Mackelprang et al. 2011, Coolen & Orsi 2015). The abundance of certain taxa within the relic permafrost microbiome has also been used to predict post-thaw biogeochemical rates such as methanogenesis (Waldrop et al. 2010), iron reduction (Hultman et al. 2015), and soil carbon transformations (Mackelprang et al. 2011, Coolen & Orsi 2015). However, the results of these studies correspond weakly or not at all with multi-year *in situ* soil warming experiments that show little or no change in permafrost microbiome composition (e.g., Rinnan et al. 2007, Biasi et al. 2008, Lamb et al. 2011). Different outcomes between field and lab-based experiments are likely due to differences in the rates that temperature is manipulated. That is, field-based studies involve moderate heating of the active layer to mimic its natural extension into the permafrost, whereas lab-based experiments induce rapid permafrost thaw that can lead to substantial changes in the physicochemical properties of the soil and the composition of the permafrost microbiome and its associated biogeochemical functions (Mackelprang et al. 2011, Schostag et al. 2019, Ricketts et al. 2020). Here, we analyze the natural depth transition between thawed and permafrost soil microbiomes, coupled with estimates of intermittent thaw frequency and duration in this transition zone, to determine if recent decades of intermittent freeze-thaw cycles have induced a compositional change in the relic permafrost microbiome.

Predicting microbial responses to thawing permafrost depends on how thaw frequency and thaw duration affect the depth-dependent composition of the soil microbiome. We approached these questions by assessing how the relic permafrost microbiome responds to intermittent freeze-thaw cycles in the soil transition zone between annually thawed active layer and permafrost. We combine results of thaw frequency and duration from multi-decadal thaw surveys with the genomic

composition of the active layer, transition zone, and permafrost microbiomes measured at 10-cm increments along soil profiles of arctic tundra. The results demonstrate (1) how soil microbiomes differ regionally between sites located on distinct landscape ages and between distinct tundra types; (2) how active layer and permafrost microbiomes differ from each other between sites and tundra types; (3) that the transition zone microbiome remains indistinguishable from the permafrost microbiome even after decades of intermittent thaw, and (4) how thaw duration rather than intermittent thaw frequency has a greater impact on the composition of soil microbiomes at these arctic tundra sites. We propose that changes in microbiome composition across the transition from long-to-short duration thaw may be used to predict shifts in microbiome composition in response to future permafrost thaw.

3.3 Results and Discussion

We sampled the depth-dependent composition of the soil microbiome at 10-cm increments down soil profiles under two distinct tundra types at each of three sites separated by ~90 km on the North Slope of Alaska, USA (Figure 3.1). Tundra types included moist acidic tussock (MAT) tundra found on hillslopes and wet sedge (WS) tundra found in valley bottoms (see Appendix B for full description). The depth-dependent distribution of microbial taxa in tundra soils has previously been investigated (Kim et al. 2016, Müller et al. 2018, Tripathi et al. 2018, 2019) and is known to be highly influenced by geographic separation between sites (biogeography) and distinct tundra types that are associated with the taxonomic composition of the active-layer and permafrost microbiomes (Wilhelm et al. 2011, Deng et al. 2015, Singh et al. 2017, Varsadiya et al. 2021). Our results from high-throughput DNA sequencing analysis of bacteria and archaea are generally consistent with these previous studies by showing geographic and depth-dependent variation in microbiome composition. However, we analyze this variation in detail and relate changes in microbiome composition from the active layer through a transition zone into permafrost to the frequency and duration of intermittent thaw as determined by multi-decadal thaw surveys.

3.3.1 Soil Microbiome Diversity

Our soil microbiome analysis of 16S rRNA gene amplicons resolved into amplicon sequence variants (ASVs) showed no statistical difference in taxonomic alpha diversity between sites, tundra type, or site × tundra type interactions using Chao1 and Shannon diversity metrics (ANOVA; $p > 0.05$ for all; Figure SI 3.6) when all depths were included. However, beta diversity

results based on Bray-Curtis dissimilarity of ASV abundance indicated significant differences in taxonomic composition between sites, tundra type, and site × tundra interactions (PERMANOVA; $p < 0.001$ for all; Figure SI 3.6). Venn diagrams indicated that the greatest relative abundance of ASVs were shared between all three sites (52.8%; Figure 3.2A), with an additional 25.4% of ASV abundance shared between at least two sites (Figure 3.2A). Notably, these ASVs represented 76.5% of the relative abundance of all ASVs shared between sites but consisted of only 4,249 ASVs out of 23,908 total ASVs (Figure 3.2A). Likewise, the dominant ASVs shared between tundra types (69.7%; Figure 3.2B) consisted of only 3,327 ASVs out of 23,908 total ASVs (Fig. 3.2B). The remaining extent of ASVs were unique to each site (19,361 ASVs; Figure 3.2A) or each tundra type (20,581 ASVs; Figure 3.2B). Sagwon had the greatest abundance of unique ASVs (13.4%) compared to Toolik (4%) and Imnavait (4.4%; Figure 3.2A), while WS tundra had more unique ASVs (19.3%) compared to MAT tundra (11%; Figure 3.2B). Collectively, the abundance of unique ASVs by site (21.8%) or by tundra type (30.3%) suggests the potential for regional endemism consistent with previous biogeographical microbiome surveys across the Arctic (Malard et al. 2019).

Differences in ASV abundance by individual soil depths across all sites and tundra types were visualized through unconstrained non-metric multidimensional scaling (NMDS) ordination based on Bray-Curtis dissimilarity (Figure 3.2C). To validate the ecological interpretations of beta diversity based on the Bray-Curtis dissimilarity of ASVs, we compared the ASV-based NMDS (Figure 3.2C) to an NMDS using instead the Bray-Curtis dissimilarity of operational taxonomic units (OTUs) clustered at 97% similarity (Figure SI 3.7). Both NMDS ordinations reveal the same patterns of regional variation by site and between tundra types, and ASVs were retained for all downstream analyses based on recent benchmark studies comparing both sequence inference methods (Callahan et al. 2017, Chiarello et al. 2022). At Toolik and Imnavait sites it appears that the relative abundance of ASVs by soil depth are strongly influenced by tundra types shared between sites rather than between tundra types within each site (Figure 3.2C). Notably, we found that the soil depths corresponding to MAT tundra or WS tundra overlapped between Toolik and Imnavait sites in ordination space based on their shared abundance of ASVs (Figure 3.2C). These results are likely due to differences in the dominant plant species known to affect soil physicochemical properties that regulate microbiome composition (Judd & Kling 2002, Judd et al. 2006, Zak & Kling 2006 Tas et al. 2018). For example, MAT tundra is dominated by sedges

(*Eriophorum vaginatum*) and dwarf shrubs (*Betula nana*, *Ledum palustre*) on hillslopes with greater soil water drainage than WS tundra, which is dominated entirely by sedges (*Carex aquatilis*, *C. chordorrhize*, *C. rotundata*) in valley bottoms where soil water accumulates (Walker et al. 1994). The ecological differences in dominant plant species between MAT and WS tundra affect soil physicochemical properties such as soil pH, water content, and the accumulation of organic C (Table SI 3.3) and likely account for the overlapping ordination of soil depths by tundra type between Toolik and Imnavait sampling locations (Figure 3.2C). Our results are also consistent with numerous studies showing regional variations in taxonomic abundance linked to tundra type (Judd et al. 2006, Zak & Kling 2006, Wallenstein et al. 2007, Chu et al. 2011, Tripathi et al. 2018).

In contrast, we found overlapping ordinations for soil depths corresponding to MAT and WS tundra at Sagwon based on shared ASV abundance within the site, which was the oldest landscape and located farthest geographically from the other two sites (Figure 3.2C). The Sagwon landscape is ~2,500 kyr BP in age compared to the youngest landscape at Toolik (~14 kyr BP) and the intermediate-aged Imnavait (~250 kyr BP), and our sites represent a natural Pleistocene chronosequence across the sampling region. The greater proportion of ASVs unique to the considerably older Sagwon landscape (13.4%; Figure 3.2A) compared to the younger aged landscapes at Toolik and Imnavait (4%, 4.4%, respectively; Figure 3.2A) is also consistent with previous arctic studies showing substantial variations in taxonomic abundance by landscape age due to differences in soil physicochemical properties that develop over geologic time (Mackelprang et al. 2017, Saidi-Mehrabad et al. 2020). Here, we found that soil pH and conductivity were significantly greater at Sagwon compared to the other sites (ANOVA; $p < 0.05$; Table SI 3.3), which may account for the higher proportion of unique ASVs at Sagwon (Figure 3.2A) and the overlapping soil depths by tundra types within Sagwon that ordinated separately from the same tundra types shared between Toolik and Imnavait (Figure 3.2C). Soil pH has previously been identified as a key factor influencing the abundance of microbial taxa over both small and large geographic scales in the Arctic (Chu et al. 2010, Ganzert et al. 2014, Siciliano et al. 2014), and pH can vary by landscape age (Hultman et al. 2015, Mackelprang et al. 2017, Saidi-Mehrabad et al. 2020). Alternatively, the greater geographic distance between Sagwon and Toolik or Imnavait (~90 km; Figure 3.1) may have influenced microbial distribution (e.g., via dispersal limitations) across the region such that the effects of tundra type on ASV abundance by soil depths at Sagwon was minimized in our NMDS ordination (Figure 3.2C).

All of these overlapping ordination patterns of soil depths based on ASV abundance in the unconstrained NMDS plot were consistent with the relative abundance of shared and unique ASVs shown in the Venn diagrams (Figure 3.2A, 3.2B). Furthermore, the surface depth (0-10 cm) from five of six sampling locations (Sagwon MAT tundra as the exception) ordinated separately from all other depths within their respective soil profiles and coalesced near each other in ordination space (gray ellipse; Figure 3.2C). This also included the 10-20 cm surface depth for MAT tundra at Toolik and Imnavait (Figure 3.2C), which together indicate a unique taxonomic composition within the surface depths that is consistent across sampling locations. This strong pattern of shared taxa in surface depths across the tundra region regardless of tundra type or landscape age has not been shown before and could imply that a common dispersal mechanism such as wind is homogenizing the microbiome composition at the soil surface, and that this mechanism is strong enough to overcome the effect of differences in dominant plant species by tundra type.

3.3.2 Soil Microbiome Composition

Using the taxonomic annotations of ASVs, we found that the soil microbiome at all sampling locations with all depths combined was dominated by bacteria (>98% relative abundance), but there were significant differences in the relative abundance of bacterial taxa among sites, tundra type, and site × tundra type interactions (ANOVA; $p < 0.05$ for all). Specifically, site differences in bacterial taxa included Acidobacteria ($p = 0.04$), Alphaproteobacteria ($p < 0.001$), Actinobacteria ($p = 0.006$), Bacteroidetes ($p = 0.002$), and Betaproteobacteria ($p = 0.002$). Tundra type differences in bacterial taxa included Bacteroidetes ($p = 0.02$), Betaproteobacteria ($p < 0.001$), and Deltaproteobacteria ($p < 0.001$). Site × tundra type interactions for differences in bacterial taxa included Alphaproteobacteria ($p = 0.004$) and Deltaproteobacteria ($p = 0.004$). Note that all p values for the main effects of site and tundra type are biased when the interaction term of site × tundra type is statistically significant.

At nearly all sampling locations, the relative abundance of dominant bacterial taxa changed with depth (Figure 3.3). Using hierarchical clustering analysis on depth-dependent differences in bacterial abundance, we found that nearly all soil profiles clustered into two distinct soil layers that we consider equivalent to the active layer (~0-40 cm) and permafrost (~40+ cm) (Figure 3.4). Figure 3.3 delineates distinct soil layers within each soil profile with black horizontal lines between soil depths as determined from hierarchical clustering analysis (Figure 3.4) to visualize the depth-

dependent differences in bacterial abundance along the soil profiles. Within Toolik and Imnavait MAT tundra there was an additional cluster of soil depths within the active layer, where the abundance of bacterial taxa clustered by different soil types with the surface organic soil depths (0-20 cm) clustering distinct from the mineral soil depths (20-40 cm) (Figure 3.4A, 3.4B). Similar results were also found in previous tundra studies where bacterial abundance was strongly related to a shift in substrate availability between the organic and mineral soil horizons (Koyama et al. 2014, Deng et al. 2015). The change from organic to mineral soil type could also account for the distinct ordination patterns of surface depth MAT tundra samples in our NMDS plot (0-10 cm, 10-20 cm; Figure 3.2C). The distinct cluster of bacterial taxa after 40-cm depth in Toolik and Imnavait MAT tundra (Figure 3.4A, 3.4B) was not associated with a change in soil type because all soil depths below 20-cm were composed of mineral soil (Figure 3.3A, 3.3B). The distinct cluster after 40-cm depth likely indicates the average permafrost boundary (described below). In contrast, the WS tundra soil profiles were composed entirely of organic soil (Figure 3.3D-3.3F); thus, the clustering patterns of shared bacterial taxa into two distinct soil layers (Figure 3.4D-3.4F) are not due to major changes in soil type with depth, but rather due to the permafrost boundary and the limitations imposed on the microbiome associated with prolonged freezing (see also Willerslev et al. 2004, Kraft et al. 2015, Liang et al. 2019). Imnavait WS tundra was the only soil profile with several non-significant clusters of bacterial taxa by distinct depths, with only the 40-70 cm depths forming a significantly distinct cluster based on the relative abundance of shared bacterial taxa within these soil depths (95% similarity; Figure 3.4E).

The observed shift in composition between the active-layer and permafrost microbiomes at all sites was largely due to variations in the abundance of Acidobacteria, Bacteroidetes, and Actinobacteria (Figure 3.3), generally consistent with previous studies in arctic soils (Wilhelm et al. 2011, Frank-Fahle et al. 2014, Deng et al. 2015, Kim et al. 2016, Singh et al. 2017, Tripathi et al. 2018, 2019, Müller et al. 2018, Varsadiya et al. 2021). For example, we found that *Acidobacteriales*, *Chloracidobacteria*, and *Solibacteriales* (Acidobacteria) abundance was greater in the active-layer microbiome compared to the permafrost microbiome, especially within MAT tundra, while *Actinomycetales* and *Gaiellales* (Actinobacteria), and *Bacteroidales* (Bacteroidetes) abundance was greater in the permafrost microbiome of both tundra types (ANOVA; $p < 0.05$ where indicated; Table SI 3.4). However, we did find that dominant Acidobacteria taxa in the active-layer soil depths differed between Toolik and Imnavait MAT tundra compared to Sagwon

MAT tundra (Table SI 3.4). Specifically, Acidobacteria within the active-layer microbiome of Toolik and Imnavait MAT tundra consisted of *Acidobacteriales* (~7.5 to 10.5%) and *Solibacteriales* (~3.2 to 3.4%), with less than 2% relative abundance of *Chloracidobacteria* (Table SI 3.4). The Sagwon MAT tundra active-layer microbiome contained no measurable abundance of *Acidobacteriales*, < 0.3% *Solibacteriales*, and > 23% of *Chloracidobacteria* (Table SI 3.4). The active-layer microbiome within Sagwon WS tundra was similar and contained > 18% relative abundance of *Chloracidobacteria* (Table SI 3.4). *Chloracidobacteria* was reported previously from arctic soils and lake sediments (Wang et al. 2016) but represents a thermophilic photoheterotroph isolated from hot spring microbial mats (Tank & Bryant 2015) and might be a misleading annotation from the GreenGenes 16S rRNA database (DeSantis et al. 2006) used in this study. The similarly high relative abundance of *Chloracidobacteria* within Sagwon MAT and WS tundra may also account for their shared ordination patterns in our NMDS plot that clustered distinctly from either tundra type at Toolik and Imnavait (Figure 3.2C).

In addition to the Acidobacteria, the relative abundance of Proteobacteria such as *Rhizobiales* and *Rhodospirillales* (Alphaproteobacteria), *Desulfuromonadales* and *Myxococcales* (Deltaproteobacteria), and *Xanthaomonadales* (Gammaproteobacteria), as well as Verrucomicrobia such as *Pedosphaerales*, *Chthoniobacterales*, and *Opitutales*, were greater in the active-layer microbiome across the region (Table SI 3.4), consistent with studies conducted at numerous sites across the Arctic (reviewed in Malard & Pearce 2018). The higher abundance of Proteobacteria in the active layer could be related to their preference for higher concentrations of nutrients (Kim et al. 2016), especially given that the relative abundance of Alpha- and Gammaproteobacteria taxa were shown to increase after fertilization compared to control plots at Toolik (Campbell et al. 2010, Koyama et al. 2014). Also, the greater abundance of bacterial taxa such as *Desulfuromonadales* (Deltaproteobacteria) in the active-layer microbiome of WS tundra (Table SI 3.4) is likely because they thrive under saturated conditions common in the active layer of WS tundra (Emerson et al. 2015), as has been previously reported from the Toolik Lake region (Romanowicz et al. 2021). This suggests that the depth-dependent variations in the soil microbiome could be related to the different resource needs of each bacterial taxon.

In contrast, the permafrost microbiome was similar across sites due to an increase in the relative abundance of Actinobacteria and Bacteroidetes (Figure 3.3), as mentioned above. In addition, the relative abundance of Firmicutes and Caldiserica also increased in the permafrost

microbiome (Figure 3.3) and clustered together consistently with the greater relative abundance of Actinobacteria and Bacteroidetes with depth (Figure 3.4). We note that Caldiserica (WCHB1-03) in the permafrost microbiome (Figure 3.3; Table SI 3.4), also reported in numerous arctic studies (Monteux et al. 2018, Tas et al. 2018, Tripathi et al. 2018, 2019, Varsadiya et al. 2021), was recently proposed as Candidatus *Cryosericota* phylum (Martinez et al. 2019), although we retain the taxonomic annotation as Caldiserica throughout this study (see Appendix B for full details). The high relative abundance of Actinobacteria such as *Actinomycetales* and *Gaiellales* in the permafrost microbiome (Table SI 3.4) is likely due to their ability to form dormant and spore-like structures (Wunderlin et al. 2014) that can survive radiation, starvation, and extreme desiccation (Johnson et al. 2007, De Vos et al. 2009). Likewise, *Clostridiales* (Firmicutes) and *Bacteroidales* (Bacteroidetes) are known to form endospores under the stressful conditions associated with permafrost, and they persist at higher relative abundance than non-endospore forming taxa common in the active-layer microbiome that perish in the harsh conditions (Burkert et al. 2019). This loss of non-endospore forming taxa is compounded with time causing further convergence in the composition of the permafrost microbiome across the region as the permafrost ages (Mackelprang et al. 2017, Liang et al. 2019).

Total cell counts by depth along each soil profile showed that the absolute abundance of bacterial cells was similar between the active-layer and permafrost depths (~10^6 to 10^8 cells per gram of soil; Table SI 3.5), and only the relative abundance of bacterial taxa changed with depth (Figure 3.3). Likewise, bacterial cell viability assays (% live cells) showed similar numbers of live cells with increasing soil depth across all sampling locations (Table SI 3.5). Thus, the permafrost microbiome maintains a similar abundance of bacterial cells with similar proportions of live cells compared to the active-layer microbiome. However, the permafrost microbiome has developed into a relic composition consisting of only a subset of bacterial taxa originally present at the time of permafrost formation, such as has been shown previously (Burkert et al. 2019, Liang et al. 2019). Our results strongly suggest that the permafrost microbiome has converged towards a shared subset of bacterial taxa capable of withstanding the harsh permafrost environment, and these taxa are no longer regulated by the same environmental factors affecting the overlying active-layer microbiomes across the region.

The relative abundance of archaeal taxa was < 3% at any given site or depth (Figure 3.3, Figure SI 3.8) but still differed statistically between tundra types (ANOVA; $p < 0.001$). Archaeal

taxa consisted primarily of methanogenic Euryarchaeota, including *Methanobacteriales* and *Methanosarcinales* consistent with similar observations across the tundra region (Lipson et al. 2013, Deng et al. 2015, Hultman et al. 2015, Tripathi et al. 2018, Romanowicz et al. 2021). *Methanobacteriales* are hydrogenotrophic methanogens and *Methanosarcinales* are acetoclastic methanogens; both of which are commonly found in saturated organic peat soils (Conrad et al. 1987, Metje & Frenzel 2007, Deng et al. 2015, Tveit et al. 2015). Here, these methanogenic archaeal taxa were found predominantly in the surface depths (0-50 cm) of WS tundra at Toolik and Imnavait, while archaeal taxa in general were negligible in MAT tundra across all sites (Figure SI 3.8). The greater relative abundance of both groups of methanogenic archaea in the WS tundra microbiome is likely due to relatively flat topography and the lack of soil drainage imposed by the permafrost boundary, both of which facilitate persistent saturation of the active layer and subsequent anoxia, providing substrates to carry out multiple fermentative pathways of methanogenesis.

3.3.3 Thaw Frequency and the Transition Zone Microbiome

Thaw depth measurements collected at three of our sampling sites annually in July and August since 1990 (Toolik MAT tundra) or 2003 (Imnavait MAT and WS tundra; see Appendix B for details) show the annual and seasonal extent of thawed versus frozen soil (Table 3.1). The mean August thaw depth (± SD) over the survey duration was 40.5 cm (± 5.3 cm) for Toolik MAT tundra, 43.9 cm (± 6.2 cm) for Imnavait MAT tundra, and 56.3 cm (± 5.7 cm) for Imnavait WS tundra. Thaw depth increased at a mean rate of 0.34 cm yr^{-1} for Toolik MAT tundra, 0.85 cm yr^{-1} for Imnavait MAT tundra, and 0.84 cm yr^{-1} for Imnavait WS tundra. The thaw survey data over time show the frequency of summer thaw to any depth, and we converted thaw depth measurements (cm) into thaw probabilities (% of thaw occurrence in any one year) for each 10-cm increment of the soil profile over the survey duration (Table 3.1). Depths that thawed intermittently in August (i.e., not every year) were considered to be in the "transition zone" between high probability of thaw in a year for the active layer and low probability of thaw in a year for the permafrost. Within MAT tundra, thaw probabilities for July and August in the soil profiles were similar between Toolik and Imnavait, with the active layer extending from 0-40 cm, the transition zone from 40-60 cm, and permafrost from 60+ cm depth (Table 3.1). For Imnavait WS tundra, we found the active layer extended from 0-50 cm, the transition zone from 50-70 cm,

and permafrost from 70+ cm depth (Table 3.1). None of the transition-zone depths at any sampling location experienced thaw at the July sampling point for the entire duration of thaw surveys (July thaw probability = 0%; Table 3.1). By comparing soil depths within each soil layer as determined from thaw surveys, with results from the hierarchical clustering analysis of microbial taxa (Figure 3.4A, 3.4B, 3.4E), we demonstrate statistically that microbial composition in the transition-zone depths always clusters with the composition of the permafrost depths for the three sampling locations having thaw survey data. This indicates that the microbiome composition of the transition zone was statistically indistinguishable from the composition in the permafrost.

Results from the transition-zone microbiome confirm our prediction that the permafrost microbiome has not been substantially altered in composition when exposed to intermittent freeze-thaw cycles. This differs from previous lab-based experiments of the permafrost microbiome that show rapid shifts in the composition and associated biogeochemical functions of microbial taxa within a few days of simulated thaw (Waldrop et al. 2010, Mackelprang et al. 2011, Coolen & Orsi 2015, Hultman et al. 2015). Our results are more consistent with previous field-based warming experiments that show little or no change in permafrost microbiome composition following moderate heating of the active layer that mimics its natural extension into the permafrost (Rinnan et al. 2007, Biasi et al. 2008, Lamb et al. 2011). As such, this study demonstrates that in natural settings it takes more than just intermittent thaw, for example ~ 10% to 80% probability that the soil will thaw in any one year (Table 3.1), to induce compositional change in the transition-zone microbiome.

Our transition-zone microbiome results also contrast with a previous soil profile survey from high Arctic heath at Svalbard, Norway (Müller et al. 2018), where microbial taxa in the thaw transition zone differed in their relative abundance by >60% from the permafrost microbiome. This difference could be because their transition zone is narrower than ours, or they had finer resolution of the soil profile sampling at 3-cm intervals rather than the 10-cm interval we used. Homogenization of microbial taxa within a 10-cm soil increment that spans the depths of the transition zone and permafrost soil layers may have hidden subtle changes in taxonomic abundance between these soil layers. However, our thaw surveys showed that depths with intermittent thaw ranged from a minimum of 15 cm (Imnavait WS tundra) up to 23 cm (Toolik MAT tundra) through the soil profiles; these depths exceed any single 10-cm soil increment, and thus potential homogenization of the transition-zone depths with the permafrost depths should be minimized.

These results are the first to show that composition of the transition-zone microbiome has not significantly shifted from the permafrost microbiome even though these soil depths have experienced intermittent thaw for on average 61% of the past 28 years at Toolik or 65-82% of the past 15 years at Imnavait (Table 3.1).

3.3.4 Thaw Duration

In addition to the frequency of thaw, we determined the thaw duration (i.e., minimum number of thaw days in a summer) that each 10-cm increment along the soil profile experienced in 2018 (Table 3.1); the year 2018 corresponds to the field season when soil profiles were sampled for their microbiome composition. These are "minimum" estimates because a depth may have thawed in between successive thaw survey dates or after the final survey (see Appendix B for details). The transition-zone depths had less than half the number of thaw days than the average thaw days of the active layer. Specifically, the Toolik MAT tundra transition zone (40-60 cm) on average thawed only a quarter of the time (24.7%) that the active layer (0-40 cm) thawed (Table 3.1). In Imnavait MAT tundra the transition zone (40-60 cm) had only 25.5% of mean active layer (0-40 cm) thaw days, and Imnavait WS tundra transition zone (50-70 cm) had 43.9% of mean active layer (0-50 cm) thaw days (Table 3.1). This decline of thaw duration in the transition zone depths compared to the active-layer depths, as well as the complete lack of thaw in the transition zone depths in July over all survey years, may account for the similar composition of the transition zone microbiome with the permafrost microbiome in hierarchical clustering analysis (Figure 3.4).

Spearman's non-parametric rank correlations between thaw duration and the relative abundance of microbial taxa by depth along the soil profiles showed consistent, significant patterns between the three sampling locations associated with thaw survey data. In MAT tundra, Acidobacteria, Alphaproteobacteria, and Verrucomicrobia were significantly positively correlated with thaw duration at Toolik (Figure 3.5A) and Imnavait (Figure 3.5B), Gammaproteobacteria and Planctomycetes also significantly positively correlated with thaw duration at Toolik (Figure 3.5A). This indicates that their relative abundance was greatest in soil depths experiencing the greatest duration of thaw (i.e., active-layer depths). In WS tundra at Imnavait, Acidobacteria was also significantly positively correlated with thaw duration as well as with Deltaproteobacteria and Nitrospirae (Figure 3.5C). This correlation distinguishes the dominant WS tundra microbial taxa from the dominant MAT tundra microbial taxa in the active layer by hierarchical clustering

analysis (Figure 3.4A, 3.4B, 3.4E). In contrast, Actinobacteria, Bacteroidetes, Caldiserica, and Firmicutes were significantly negatively correlated with thaw duration at all three sampling locations (Figure 3.5A-3.5C). This indicates that their relative abundance was greatest in soil depths experiencing the shortest duration of thaw each year (i.e., permafrost depths).

The significant positive and negative correlations between thaw duration and the relative abundance of microbial taxa at each soil depth are consistent with the significant clusters of microbial taxa in the active layer and the permafrost from hierarchical clustering analysis, respectively (Figure 3.4A, 3.4B, 3.4E). Previous studies that focused on changes in soil physicochemical properties such as pH, conductivity, water content, and organic C to explain depth-dependent variations in the soil microbiome concluded that the majority of the variation remained unexplained by these environmental factors (reviewed by Malard & Pearce 2018). We also found weak correlations between soil physicochemical properties and microbial taxa (Table 3.2). For the three sampling locations associated with multi-decadal thaw surveys, we found a significant correlation between a physicochemical property and a certain taxon at only one or two locations instead of significant correlations at all three locations. For example, differences in soil pH by depth were significantly negatively correlated with active layer-dominant Acidobacteria, Alphaproteobacteria, and Gammaproteobacteria at both MAT tundra sites (Toolik and Imnavait), but not significantly correlated (positively or negatively) by soil depth at Imnavait WS tundra (Table 3.2). Likewise, differences in soil pH by depth were significantly positively correlated with the permafrost-dominant taxa Actinobacteria, Bacteroidetes, Caldiserica, and Firmicutes at both MAT tundra sites, but not at Imnavait WS tundra (Table 3.2). Previous studies showed that the relative abundance of Acidobacteria had a strong positive correlation with soil pH and these taxa dominated the more acidic surface depths of the active layer before declining in abundance with depth towards the permafrost (Neufeld & Mohn 2005, Wallenstein et al. 2007, Kim et al. 2016).

In our results, we found a similar correlation between soil pH and Acidobacteria with soil depth at all of our MAT tundra sites. In addition, there were significant correlations with other environmental factors and microbial taxa by soil depth at some sites (Table 3.2); however, there were no general patterns of correlation across sites. For example, those taxa that were significantly correlated with soil conductivity, water content, or organic C content with soil depth in Toolik MAT tundra were not the same taxa that were significantly correlated by soil depth in Imnavait MAT tundra (Table 3.2). Inconsistent patterns occur between many taxa and the physicochemical

properties measured at each sampling location (Table 3.2), making it difficult to draw conclusions about how these particular environmental factors regulate soil microbial abundance in MAT or WS tundra across the region. This analysis indicates that the measured soil physicochemical properties explain a relatively small amount of the among and within site variance in microbiome composition.

In contrast to soil physicochemical properties, the measured thaw frequency and especially thaw duration by depth (Table 3.2) showed consistent correlations with the composition of the active-layer and permafrost microbiomes. The transition zone experienced less than half the number of thaw days than the average for the active layer (Table 3.2). This considerable difference in thaw duration between the active layer and transition zone may explain why the transition zone microbiome was statistically indistinguishable from the permafrost microbiome (Figure 3.5). However, as the thaw duration in the transition zone increases with future warming, we suggest that the abundance of active layer-dominant taxa will increase, including Acidobacteria (*Acidobacteriales*, *Solibacteriales*), Alphaproteobacteria in MAT tundra (*Rhizobiales*, *Rhodospirillales*), Deltaproteobacteria in the WS tundra (*Desulfuromonadales*, *Myxococcales*), as well as Gammaproteobacteria (*Xanthomonadales*), and Verrucomicrobia (*Pedosphaerales*, *Chthoniobacterales*) (Table SI 3.4). We also predict that an increase in thaw duration will likely decrease the relative abundance of Actinobacteria (*Actinomycetales*, *Gaiellales*), Bacteroidetes (*Bacteroidales*), Caldiserica (WCHB1-03), and Firmicutes (*Clostridiales*) in the transition zone of both MAT and WS tundra (Table 3.1). These predicted increases and decreases in particular taxa will shift the transition-zone microbiome away from the current, relic permafrost microbiome and toward the active-layer composition.

3.4 Conclusion

Results from our study are the first to show that thaw duration is a strong environmental factor that operates over time and space to regulate the microbial composition of the active layer, transition zone, and permafrost in soils of arctic tundra. The duration of thaw that soils experience each summer correlates better than does soil physicochemistry with the dominant microbial taxa among regional sites, tundra types, and soil depth. Furthermore, long-term thaw surveys indicate that while thaw depth is increasing over time, the transition-zone microbiome is still very similar to the permafrost microbiome. This suggests that thaw frequency and duration in the transition

zone are still too low to shift the transition-zone microbiome composition away from that in the permafrost and toward that in the active layer. As climate warming increases and thaw frequency and especially thaw duration increases at depth, we predict that for any tundra soil the microbiome composition (and thus function) will shift from the relic permafrost taxa toward current active-layer taxa. These shifts should follow the current thaw duration and microbial composition at each depth (e.g., Table 3.1, Figure 3.3). Monitoring thaw duration and microbiome composition at depth may help predict the microbial response to future permafrost thaw.

3.5 Study Design and Methods

Three sites were selected for this study on the North Slope of the Brooks Range in northern Alaska, USA (Figure 3.1). Sites were (1) Toolik Lake (68°37'16.18"N 149°36'54.17"W); (2) Imnavait Creek (68°36'35.36"N 149°18'29.80"W); and (3) Sagwon Hills (69°20'36.81"N 148°45'31.75"W). Landscape age and glaciation surface differed by site. Soils in the Toolik Lake area formed on an Itkillik II-age landscape (~14 kyr BP), soils in the Imnavait Creek area formed on a Sagavanirktok-age landscape (~250 kyr BP), and soils in the Sagwon Hills area formed on a Gunsight Mountain-age landscape (~2,500 kyr BP). Topography controlled the dominant plant species at each site such that hillslopes supported moist acidic tussock (MAT) tundra and valley bottoms supported wet sedge (WS) tundra. See Appendix B for additional details.

At each site, the vertical soil profile of MAT and WS tundra was sampled in 10-cm increments down to 1 m depth. Within MAT tundra, soil pits (~1 m^2 and 1 m deep) were excavated using a jack hammer, shovels, and pickaxe to expose the soil profile. Soil samples (~25 g) were collected in duplicate from each 10-cm increment along the soil profile using a chisel rinsed with 70% ethanol between depths. Samples were placed in 50 mL Falcon tubes in a cooler with ice, and immediately frozen at -80°C upon return from the field. Within WS tundra, soil cores were collected using a SIPRE (Snow, Ice, and Permafrost Research Establishment, Tarnocai 1993) corer with carbide bits (Jon's Machine Shop, Fairbanks, AK). Soil cores were extruded then scraped parallel to soil layers using aseptic techniques in the field to remove outer layers of soil, and then separated into 10-cm increments. Soil samples (~25 g) were collected in duplicate from each 10-cm increment along the soil core using a chisel rinsed with 70% ethanol between depths. Samples were placed in 50 mL Falcon tubes in a cooler with ice, and immediately frozen at -80°C upon

return from the field. Soil sampling at each site took place over the course of one day between 10-20 July 2018 for a total of 51 samples for analysis.

Soil physicochemical properties including soil pH, electrical conductivity ($\mu S\ cm^{-1}$), water content (%), and organic carbon content (%) were measured from each 10-cm soil profile increment. Bacterial cell viability assays were performed on select soil profile increments using three depths at each sampling location to represent a surface active-layer depth (~10-20 cm), a transition zone depth (~40-50 cm), and a permafrost depth (~70-80 cm). The viability assays were performed with a Live/Dead BacLight Bacterial Viability kit (Invitrogen) following methods from Burkert et al. (2019). Cell counts were corrected to calculate the average number of cells per gram of soil (dry weight). See Appendix B for additional details.

Genomic DNA was extracted from each 10-cm soil profile increment and amplified through polymerase chain reaction (PCR) using dual-barcoded 16S rRNA gene primers 515f-806r (Apprill et al. 2015, Parada et al. 2016) to profile the bacterial and archaeal communities. PCR amplicons were pooled into a single library and submitted to the University of Michigan Microbiome Core for high-throughput sequencing on the Illumina MiSeq platform. Sequencing data were downloaded from Illumina BaseSpace and analyzed using QIIME2 (v. 2020.11) (Bolyen et al. 2019) on the Great Lakes high performance computing cluster (University of Michigan, USA). Raw forward and reverse sequencing reads were quality filtered with DADA2 (Callahan et al. 2016). Taxonomy was assigned to amplicon sequence variants (ASVs) using scikit-learn naïve Bayes taxonomy classifier (Pedregosa et al. 2011) against the GreenGenes 99% database (v. 13.8) (DeSantis et al. 2006). ASVs were chosen over operational taxonomic units (OTUs) following recent benchmark studies (Callahan et al. 2017, Chiarello et al. 2022). See Appendix B for additional details and for a summary of sequencing read statistics (Table SI 3.6). Raw forward and reverse sequencing reads are deposited in the NCBI Sequence Read Archive (SRA) and are publicly available through BioProject accession PRJNA794857.

All statistical analyses were conducted in R (v. 4.0.5) (R Core Team 2018) and considered significant at $p < 0.05$. One-way analysis of variance (ANOVA) was used to assess differences in soil physicochemical properties and microbiome alpha diversity between sites, tundra type, and their interactions across the sampling region. Multivariate statistical analysis of the microbiome data was conducted using the "microeco" package (Liu et al. 2021) and the "vegan" package

(Oksanen et al. 2019). Bray-Curtis dissimilarity was calculated for ASV abundance and analyzed via permutational multivariate analysis of variance (PERMANOVA) using the "adonis()" function (999 permutations) in the "vegan" package to determine the effects of site, tundra type, and their interactions on the composition of the soil microbiome across the sampling region. Venn diagrams were generated to visualize the unique and shared ASV counts and their relative abundance between sampling sites or between tundra types. Differences in ASV abundance by individual soil depths across all sites and tundra types were visualized through unconstrained non-metric multidimensional scaling (NMDS) ordination using the "metaMDS()" function in the "vegan" package.

Hierarchical clustering analysis was used to determine which soil depths were statistically similar to each other based on the vertical distribution of dominant microbial taxa, where an agglomerative clustering algorithm calculated similarity of mean z-scaled relative abundance values by soil depth and determined the optimal number of clusters from 10,000 bootstrap iterations using the "pvclust()" function in the "stats" package (R Core Team 2018). Hierarchical clustering analysis was also used to determine which microbial taxa were statistically similar to each other across soil depths based on the mean z-scaled relative abundance values of each taxon at each depth, with the optimal number of clusters determined from 10,000 bootstrap iterations using the "pvclust()" function. The hierarchical clustering results for soil depth and taxon clusters were visualized together with the "pheatmap" package (Kolde & Kolde 2019). Spearman's non-parametric rank correlations (rho) were used to determine the similarity of the dominant microbial taxa (via relative abundance) with soil physicochemical properties and thaw duration measurements across all depths of the soil profile using the "cor.test()" function. Thaw duration measurements were non-normally distributed along soil profiles and a non-parametric correlations test such as Spearman's rho was most appropriate for the data. See Appendix B for additional details regarding thaw frequency and duration measurements.

3.6 Acknowledgements

We thank Byron Crump, Rose Cory, Nic Jelinski, Jason Dobkowski, Chris Cook, Lija Treibergs, Johanna Albrigtsen, and colleagues of the NSF Arctic LTER and Toolik Lake Field Station for assistance. Additional thanks to Genevieve Romanowicz and Greg Sobocinski for support with fluorescence microscopy.

Table 3.1 Thaw Probability and Thaw Duration. Average thaw probability (%) within each 10-cm increment along the soil profile for moist acidic tussock (MAT) tundra at Toolik and Imnavait and wet sedge (WS) tundra at Imnavait measured annually on 2 July and 11 August (± 1 day) since 1990 (Toolik) or 2003 (Imnavait). Thaw duration (minimum number of thaw days per year) within each 10-cm increment along the soil profile for all three sites was determined from seven measurements taken from 2 June to 20 August 2018 (Toolik) or 21 June to 21 August 2018 (Imnavait). Highlighted rows represent the transition zone (0% < August thaw probability < 100%; light gray) and permafrost (0% August thaw probability; dark gray) soil layers.

	Toolik Lake Moist Acidic Tussock Tundra			Imnavait Creek Moist Acidic Tussock Tundra			Imnavait Creek Wet Sedge Tundra		
Soil Profile Depth (cm)	July Thaw Prob. (%) 1990-2018	August Thaw Prob. (%) 1990-2018	Annual Thaw Dur. (days) 2018	July Thaw Prob. (%) 2003-2018	August Thaw Prob. (%) 2003-2018	Annual Thaw Dur. (days) 2018	July Thaw Prob. (%) 2003-2018	August Thaw Prob. (%) 2003-2018	Annual Thaw Dur. (days) 2018
0-10	100	100	80	100	100	62	100	100	62
10-20	100	100	80	100	100	62	100	100	62
20-30	45.2	100	69	76.5	100	53	100	100	53
30-40	3.2	96.8	46	5.9	100	35	52.9	100	44
40-50	0	61.3	34	0	64.7	27	5.9	100	35
50-60	0	3.2	0	0	11.8	0	0	82.4	27
60-70	0	0	0	0	0	0	0	35.3	18
70-80	0	0	0	0	0	0	0	0	0
80-90	0	0	0	0	0	0	0	0	0
90-100	0	0	0	0	0	0	0	0	0

Table 3.2 Correlations between Abiotic Properties and Microbial Taxa. Spearman non-parametric rank correlations between soil physicochemical properties and microbial taxa at the three sampling locations associated with multi-decadal thaw measurements. When the correlation coefficient (rho) equals 1, it is considered a completely positive correlation; when it equals -1, it is considered a completely negative correlation. Asterisks indicate the significance of the correlation, positive or negative (Spearman; * $p < 0.05$; ** $p < 0.01$; *** $p < 0.001$).

	Soil pH			Soil Conductivity			Soil Water Content			Organic Carbon Content		
Taxonomy	**Toolik MAT**	**Imnavait MAT**	**Imnavait WS**	**Toolik MAT**	**Imnavait MAT**	**Imnavait WS**	**Toolik MAT**	**Imnavait MAT**	**Imnavait WS**	**Toolik MAT**	**Imnavait MAT**	**Imnavait WS**
Acidobacteria	**-0.67***	**-0.92****	0.10	0.05	-0.04	-0.29	-0.18	**0.79***	0.08	-0.12	**0.82***	**0.65***
Actinobacteria	**0.79***	0.74	0.09	-0.02	0.32	0.43	-0.23	-0.71	0.14	-0.17	-0.75	-0.56
Bacteroidetes	**0.81****	**0.96*****	-0.08	-0.03	0.07	0.32	-0.10	**-0.82***	0.01	-0.13	**-0.89***	-0.59
Caldiserica	**0.75***	**0.95****	-0.21	0.24	-0.05	0.24	-0.02	**-0.81***	0.03	0.07	**-0.85***	**-0.70***
Chlorobi	0.33	0.41	-0.30	**-0.80****	-0.32	**-0.69***	**-0.91*****	-0.43	-0.49	**-0.96*****	-0.46	0.18
Chloroflexi	0.45	0.41	0.13	**-0.80****	-0.25	-0.60	-0.33	-0.29	-0.35	-0.53	-0.32	0.39
Firmicutes	**0.69***	**0.99*****	0.02	0.13	-0.11	0.35	0.03	**-0.86***	0.07	0.07	**-0.93****	-0.52
Nitrospirae	0.30	-0.28	0.06	**-0.78***	-0.60	-0.29	**-0.90*****	0.09	0.21	**-0.94*****	0.16	**0.69***
Planctomycetes	**-0.71***	-0.38	-0.49	0.02	0.41	0.31	0.18	0.34	0.16	0.10	0.34	0.12
Alphaproteobacteria	**-0.71***	**-0.87***	0.52	0.17	0.46	0.01	0.08	0.75	0.29	0.10	0.79*	0.51
Betaproteobacteria	0.10	0.34	0.02	**-0.70***	-0.39	0.29	-0.48	-0.36	0.25	-0.58	-0.32	0.25
Deltaproteobacteria	0.39	-0.23	0.42	0.17	0.11	0.13	0.43	0.21	0.21	0.25	0.25	**0.74***
Gammaproteobacteria	**-0.68***	**-0.75***	-0.20	0.18	0.25	-0.81	0.07	0.57	-0.53	0.08	0.61	0.18
Verrucomicrobia	-0.66	**-0.90****	-0.60	-0.02	0.11	**-0.76***	-0.17	0.75	**-0.72***	-0.12	**0.79***	-0.38
Archaea	**0.72***	0.59	-0.24	0.12	-0.04	-0.48	0.27	-0.64	-0.32	0.17	-0.68	0.19

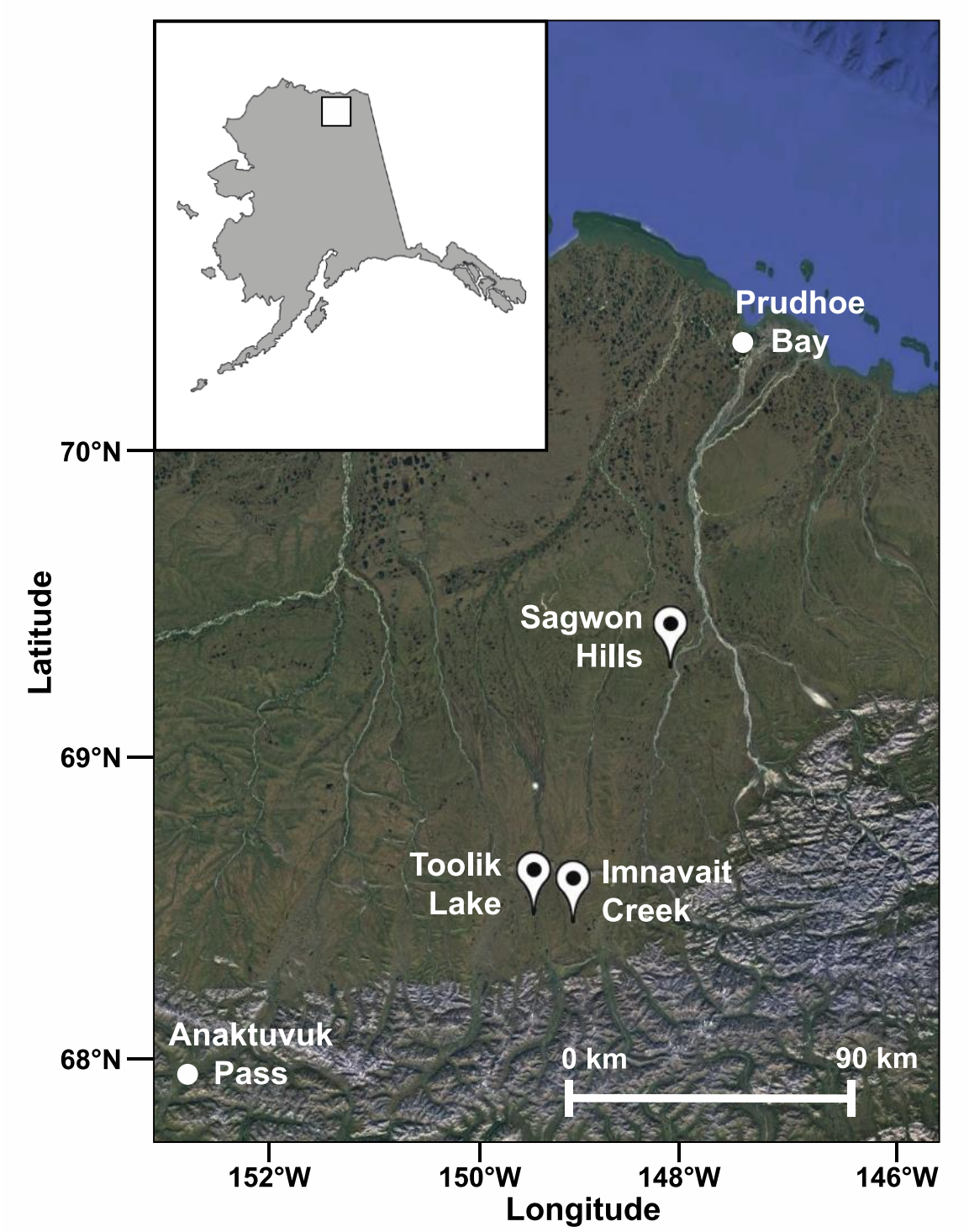

Figure 3.1 Map of Arctic Sampling Sites. Sampling sites located on the North Slope of the Brooks Range in northern Alaska, USA. Three study sites are (1) Toolik Lake; (2) Imnavait Creek; and (3) Sagwon Hills.

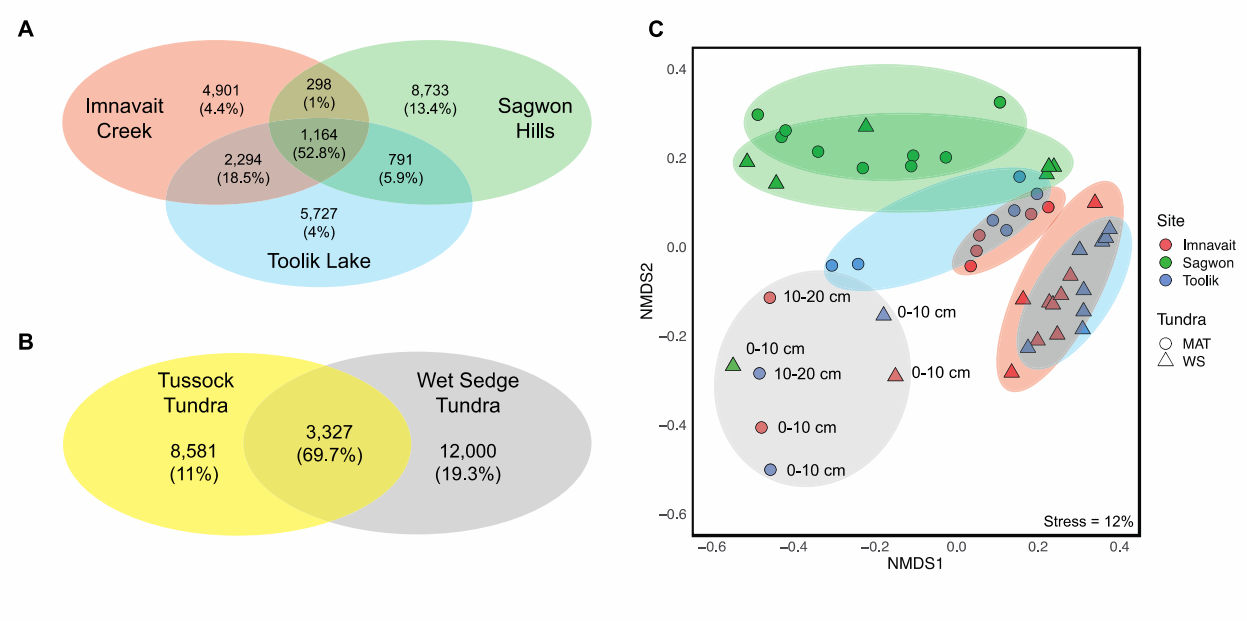

Figure 3.2 Venn Diagram and NMDS Plot of Unique and Shared ASVs. Venn diagram for (A) each site and (B) both tundra types. The total ASVs of each site or tundra type and those ASVs shared between sites or between tundra types are shown as counts. The relative abundance that each ASV count represents is shown as a percentage in parentheses. NMDS ordination (C) based on the Bray-Curtis dissimilarity of ASV abundance within the soil microbiome reveals regional variation by site and between tundra types. The surface depth (0-10 cm) for most sampling locations ordinated separately from all other soil profile depths (gray ellipse). Each marker represents an individual depth sampled along the soil profile of a given site by tundra type in the NMDS plot.

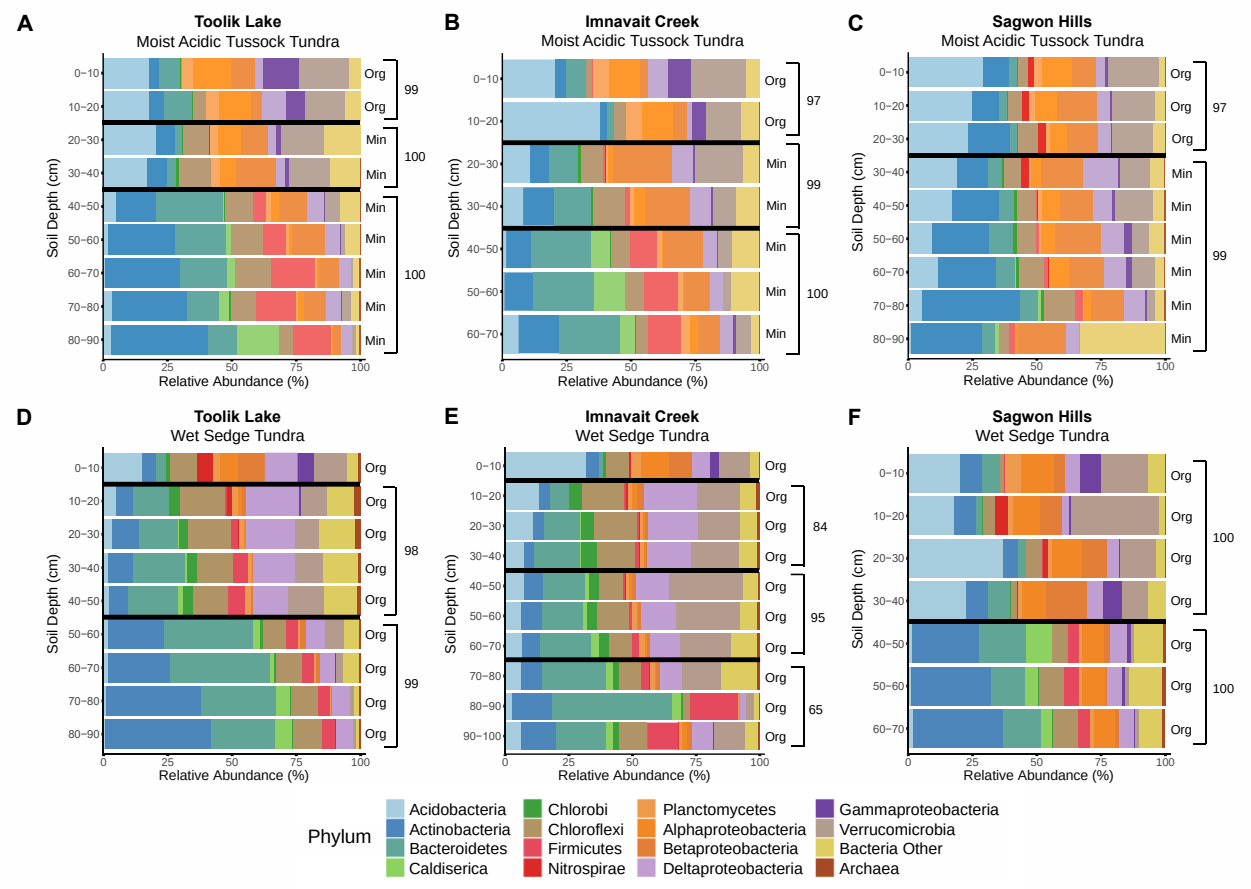

Figure 3.3 Soil Microbiome Composition along Soil Profiles. Microbiome composition within moist acidic tussock (MAT) tundra (A-C) and wet sedge (WS) tundra (D-F) for Toolik (A, D), Imnavait (B, E), and Sagwon (C, F) sampling sites. Soil pits were dug for all MAT tundra sites and soil cores were extracted from all WS tundra sites. Soil type for each sampling depth along the soil profile is indicated as "Org" (organic) or "Min" (mineral). Black horizontal bars delineate distinct soil layers within each soil profile as determined from the hierarchical clustering analysis, with percent similarity values (out of 100) displayed for each cluster.

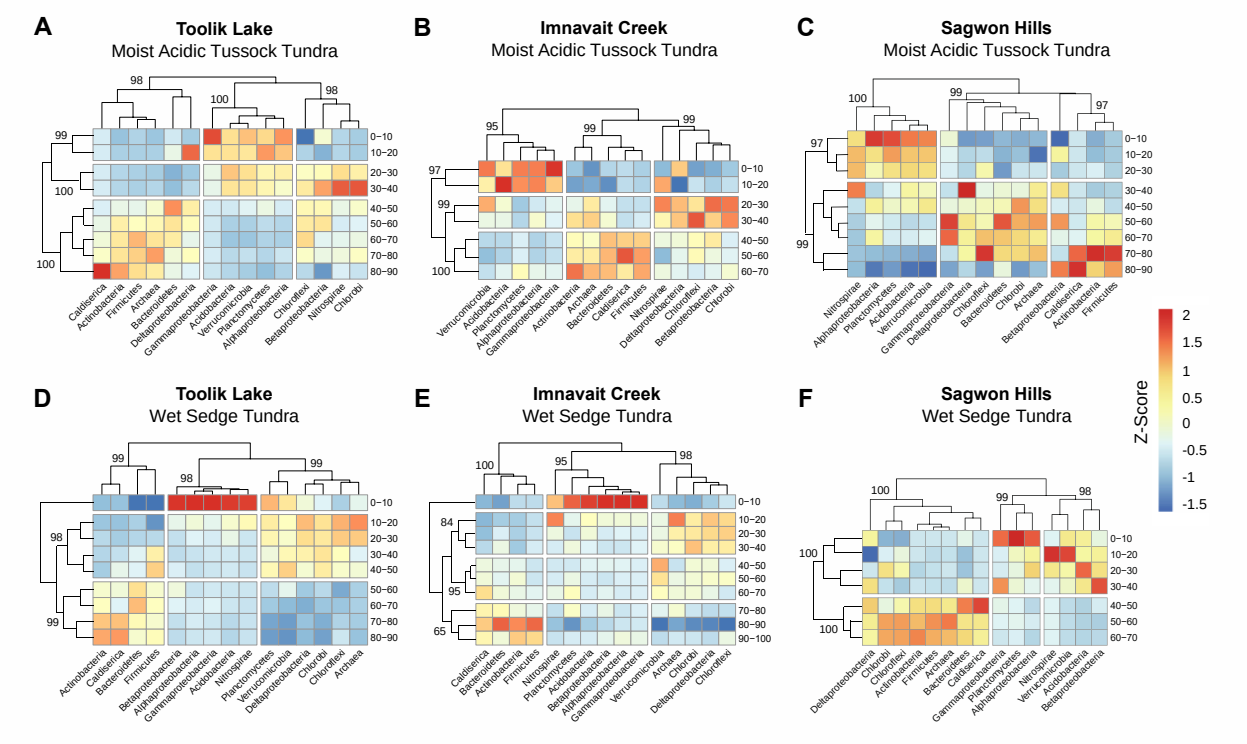

Figure 3.4 Hierarchical Cluster Analysis by Soil Depth and Taxonomy. Heatmap illustrating the significant clustering of distinct soil depths (rows) and microbial taxa (columns) for moist acidic tussock (MAT) tundra (A-C) and wet sedge (WS) tundra (D-F) at Toolik (A, D), Imnavait (B, E), and Sagwon (C, F) based on hierarchical clustering analysis. The optimal number of clusters for soil depths and microbial taxa was determined using gap statistics based on the similarity of mean z-scaled relative abundance values of microbial taxa by soil depth. The percent similarity value (out of 100) is displayed for each cluster with values greater than 95% similarity considered significant.

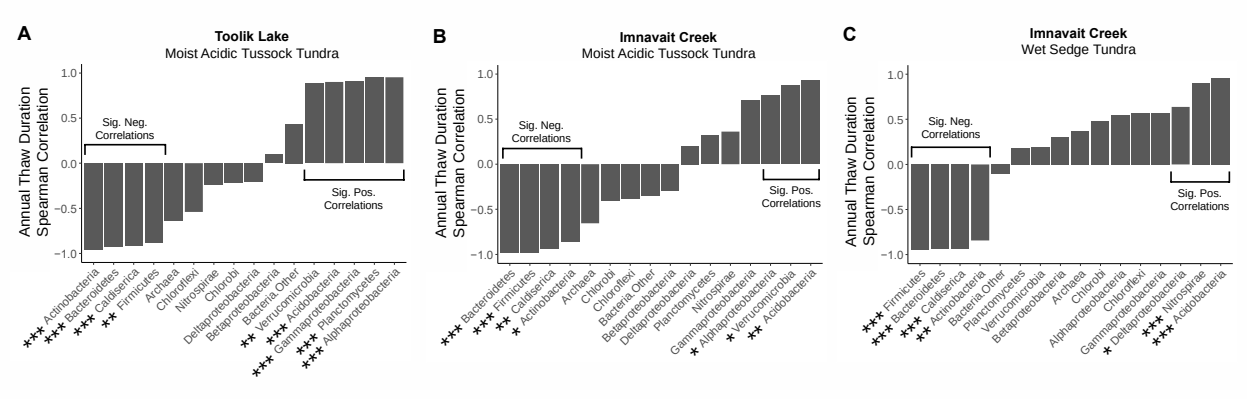

Figure 3.5 Correlation between Thaw Duration and Microbial Taxa. Spearman non-parametric rank correlation plots between thaw duration and microbial taxa along the soil profile of moist acidic tussock (MAT) tundra at Toolik (A) and Imnavait (B) and wet sedge (WS) tundra at Imnavait (C). Correlations are arranged from Spearman's rho values of -1 to 1 among microbial taxa within each plot to emphasize those microbial taxa significantly negatively or positively correlated to thaw duration, respectively. Asterisks indicate the significance of the negative or positive correlation between thaw duration and mean relative abundance of each microbial taxon along the soil profile (Spearman rho; * $p < 0.05$; ** $p < 0.01$; *** $p < 0.001$).

Table SI 3.3 Supplemental Abiotic Soil Properties. Physicochemical properties of soils from Toolik (youngest landscape age), Imnavait (intermediate landscape age), and Sagwon (oldest landscape age) sampling sites (mean ± SD) measured from soil profile samples. Letters indicate significant differences between each site × tundra type interaction (ANOVA; $p < 0.05$).

	Toolik Lake		Imnavait Creek		Sagwon Hills	
Soil Property	**MAT Tundra**	**WS Tundra**	**MAT Tundra**	**WS Tundra**	**MAT Tundra**	**WS Tundra**
Soil pH	5.0 ± 0.5 [a]	5.3 ± 0.3 [a]	5.3 ± 0.4 [a]	4.6 ± 0.3 [b]	6.2 ± 0.4 [c]	5.7 ± 0.2 [a,c]
Conductivity (µS/cm)	30.7 ± 26.9 [a]	18.6 ± 10.0 [a]	22.1 ± 23.5 [a]	22.9 ± 13.7 [a]	84.5 ± 73.4 [b]	52.7 ± 28.5 [a,b]
Water Content (%)	58.7 ± 22.8 [a]	81.2 ± 4.1 [b]	42.4 ± 27.5 [a]	76.7 ± 5.5 [b]	49.7 ± 14.1 [a]	81.8 ± 6.9 [b]
Organic C (%)	7.4 ± 11.7 [a]	24.0 ± 1.4 [b]	7.6 ± 12.9 [a]	21.7 ± 2.9 [b]	4.8 ± 7.1 [a]	30.1 ± 2.2 [b]

Table SI 3.4 Supplemental Dominant Microbial Taxa. Relative abundance (mean ± SD) of dominant microbial taxa (order-level within phylum) separated between active layer (AL) and permafrost (PF) soil layers based on significant soil depth clusters obtained from hierarchical clustering analysis. Letters indicate significant differences between soil layers specifically within each tundra type at each site (ANOVA; $p < 0.05$).

		Toolik Lake				Imnavait Creek				Sagwon Hills			
		MAT Tundra		WS Tundra		MAT Tundra		WS Tundra [1]		MAT Tundra		WS Tundra	
	Taxonomy	AL (0-40 cm)	PF (40-90 cm)	AL (0-50 cm)	PF (50-90 cm)	AL (0-40 cm)	PF (40-70 cm)	AL (0-50 cm)	PF (50-100 cm)	AL (0-30 cm)	PF (30-90 cm)	AL (0-40 cm)	PF (40-70 cm)
Active Layer Dominant Taxa	Acidobacteria												
	Acidobacteriales	**7.6 ± 2.9** [a]	**0.3 ± 0.2** [b]	1.1 ± 1.8	0.1 ± 0.1	**10.5 ± 5.5** [a]	**0.9 ± 1.1** [b]	7.9 ± 7.5	2.5 ± 1.1	0	0	2.0 ± 3.9	0
	Chloracidobacteria	1.8 ± 1.7	0.9 ± 0.7	1.2 ± 1.5	0.7 ± 0.2	1.4 ± 0.9	0.8 ± 0.4	0.4 ± 0.3	0.4 ± 0.2	**23.4 ± 3.9** [a]	**8.4 ± 5.3** [b]	**18.4 ± 13.5** [a]	**1.5 ± 0.2** [b]
	Solibacterales	**3.4 ± 0.9** [a]	**1.3 ± 0.6** [b]	1.3 ± 0.9	0.3 ± 0.1	3.2 ± 1.9	0.6 ± 0.8	**3.4 ± 1.7** [a]	**1.5 ± 0.4** [b]	0.3 ± 0.1	0.4 ± 0.2	1.1 ± 1.0	0.1 ± 0.1
	Alphaproteobacteria												
	Rhizobiales	**4.8 ± 0.8** [a]	**1.2 ± 0.8** [b]	1.2 ± 1.9	0.1 ± 0.1	**4.4 ± 2.3** [a]	**0.7 ± 0.7** [b]	2.1 ± 2.8	0.6 ± 0.5	7.5 ± 2.5	4.1 ± 2.1	7.7 ± 2.3	8.4 ± 0.3
	Rhodospirillales	**3.0 ± 2.3** [a]	**0.2 ± 0.1** [b]	0.3 ± 0.5	0	2.0 ± 2.1	0.4 ± 0.6	0.6 ± 1.0	0.1 ± 0.1	**0.3 ± 0.1** [a]	**0.1 ± 0.1** [b]	1.0 ± 0.8	0
	Betaproteobacteria												
	Burkholderiales	7.4 ± 3.3	7.0 ± 3.3	1.5 ± 2.3	0.5 ± 0.5	8.5 ± 7.1	10.3 ± 3.6	1.8 ± 2.2	0.8 ± 0.4	**6.6 ± 1.5** [a]	**12.4 ± 3.6** [b]	**6.1 ± 3.2** [a]	**1.3 ± 0.9** [b]
	Deltaproteobacteria												
	Desulfuromonadales	0.5 ± 0.6	1.2 ± 0.5	2.2 ± 1.8	0.5 ± 0.6	1.1 ± 1.3	1.6 ± 0.3	**3.0 ± 1.5** [a]	**1.0 ± 0.5** [b]	0.5 ± 0.2	2.8 ± 3.5	0.1 ± 0.1	0.3 ± 0.1
	Myxococcales	3.0 ± 3.1	0.1 ± 0.0	1.4 ± 1.2	0.4 ± 0.1	1.9 ± 2.9	0.5 ± 0.6	1.5 ± 0.9	0.5 ± 0.3	**1.4 ± 0.5** [a]	**0.6 ± 0.4** [b]	**3.1 ± 1.5** [a]	**0.3 ± 0.1** [b]
	Syntrophobacterales	**0.1 ± 0.1** [a]	**3.5 ± 0.6** [b]	9.1 ± 3.1	5.4 ± 0.6	2.3 ± 2.3	2.7 ± 0.6	9.0 ± 4.5	6.9 ± 3.8	2.1 ± 0.3	2.1 ± 0.9	**0.6 ± 0.5** [a]	**4.5 ± 0.5** [b]
	Gammaproteobacteria												
	Xanthomonadales	**5.6 ± 2.4** [a]	**0.1 ± 0.1** [b]	0.2 ± 0.4	0	**3.7 ± 2.0** [a]	**0.5 ± 0.5** [b]	0.7 ± 1.4	0.1 ± 0.1	**0.4 ± 0.1** [a]	**0.1 ± 0.0** [b]	3.3 ± 3.4	0.1 ± 0.0
	Nitrospirae												
	Nitrospirales	0.1 ± 0.1	0	1.7 ± 2.6	0	0.1 ± 0.1	0.1 ± 0.0	0.4 ± 0.3	0.1 ± 0.1	**2.7 ± 0.2** [a]	**0.8 ± 1.2** [b]	1.7 ± 2.2	0
	Verrucomicrobia												
	Pedosphaerales	3.8 ± 1.1	2.0 ± 1.7	**7.7 ± 2.6** [a]	**2.6 ± 2.5** [b]	**9.3 ± 6.2** [a]	**2.1 ± 0.9** [b]	13.4 ± 6.9	13.0 ± 7.2	2.5 ± 0.2	2.6 ± 1.7	**3.6 ± 1.6** [a]	**0.8 ± 0.1** [b]
	Chthoniobacterales	**8.1 ± 4.2** [a]	**0.3 ± 0.2** [b]	2.1 ± 2.2	0.1 ± 0.1	4.0 ± 4.8	0.6 ± 0.9	**2.4 ± 0.9** [a]	**0.7 ± 0.5** [b]	**13.6 ± 2.4** [a]	**3.5 ± 3.3** [b]	12.2 ± 12.7	0.3 ± 0.1
	Opitutales	**2.1 ± 1.4** [a]	**0.2 ± 0.1** [b]	0.7 ± 0.3	0.3 ± 0.2	1.2 ± 1.3	0.2 ± 0.1	1.4 ± 0.6	0.7 ± 0.4	0.3 ± 0.1	0.9 ± 0.6	1.5 ± 1.2	0.2 ± 0.1
Permafrost Dominant Taxa	Actinobacteria												
	Actinomycetales	**4.0 ± 1.8** [a]	**14.7 ± 3.9** [b]	**5.0 ± 1.9** [a]	**13.4 ± 3.3** [b]	3.9 ± 2.9	7.2 ± 0.5	2.4 ± 0.8	5.2 ± 3.3	1.3 ± 0.1	9.6 ± 6.6	**2.7 ± 1.8** [a]	**21.4 ± 2.0** [b]
	Gaiellales	**0.3 ± 0.2** [a]	**11.4 ± 4.8** [b]	**2.2 ± 0.9** [a]	**17.4 ± 6.4** [b]	**0.7 ± 0.8** [a]	**3.4 ± 1.7** [b]	**1.6 ± 1.0** [a]	**4.3 ± 0.8** [b]	4.2 ± 2.3	7.0 ± 2.6	**1.2 ± 0.8** [a]	**7.5 ± 2.6** [b]
	Bacteroidetes												
	Bacteroidales	**0.2 ± 0.2** [a]	**16.1 ± 5.5** [b]	**12.2 ± 5.9** [a]	**31.2 ± 5.7** [b]	**4.5 ± 5.4** [a]	**22.2 ± 1.1** [b]	**9.9 ± 6.5** [a]	**23.6 ± 6.1** [b]	**0** [a]	**3.9 ± 2.2** [b]	**0.2 ± 0.2** [a]	**14.9 ± 2.2** [b]
	Caldiserica												
	WCHB1-03	0	5.0 ± 6.6	**0.7 ± 0.8** [a]	**4.1 ± 2.4** [b]	**0.1 ± 0.1** [a]	**8.5 ± 3.0** [b]	**0.5 ± 0.7** [a]	**2.8 ± 0.7** [b]	0	0.4 ± 0.5	**0** [a]	**6.4 ± 3.0** [b]
	Firmicutes												
	Clostridiales	**0.1 ± 0.1 a**	**12.2 ± 5.0** [b]	3.2 ± 2.9	4.6 ± 0.3	**0.7 ± 0.9** [a]	**12.0 ± 1.2** [b]	**0.7 ± 0.5** [a]	**7.1 ± 4.0** [b]	**0** [a]	**1.3 ± 1.1** [b]	**0.1 ± 0.1** [a]	**4.4 ± 0.8** [b]

Table SI 3.5 Supplemental Bacterial Cell Viability Assay Results. Viable cells (green fluorescence) and dead cells (red fluorescence) were counted from a consistent field of view (~62×212 μm area). The average number of cells per field of view was multiplied by the area of the filter (25 μm diameter) and the dilution factor was then corrected for dry weight to calculate the average number of cells per gram of soil (g dw^{-1}).

Site	Soil Type	Live Cells (g dw^{-1})	Dead Cells (g dw^{-1})	Total Cells (g dw^{-1})	% Live	% Dead
Toolik Lake						
MAT Tundra						
10-20 cm	Organic	1.7E+07	8.8E+06	2.6E+07	66	34
40-50 cm	Mineral	1.0E+07	1.5E+07	2.5E+07	41	59
70-80 cm	Mineral	2.6E+07	1.4E+07	4.0E+07	64	36
WS Tundra						
10-20 cm	Organic	1.8E+08	6.6E+07	2.5E+08	73	27
40-50 cm	Organic	1.1E+08	7.5E+07	1.8E+08	59	41
70-80 cm	Organic	5.8E+07	1.0E+08	1.6E+08	36	64
Imnavait Creek						
MAT Tundra						
10-20 cm	Organic	2.8E+06	4.7E+06	7.5E+06	37	63
40-50 cm	Mineral	1.3E+07	1.4E+07	2.6E+07	48	52
60-70 cm	Mineral	1.8E+06	2.7E+06	4.5E+06	40	60
WS Tundra						
10-20 cm	Organic	7.0E+07	7.2E+07	1.4E+08	49	51
50-60 cm	Organic	3.6E+07	2.8E+07	6.4E+07	56	44
80-90 cm	Organic	5.8E+07	2.5E+07	8.3E+07	70	30
Sagwon Hills						
MAT Tundra						
10-20 cm	Organic	6.7E+06	4.0E+06	1.1E+07	63	37
40-50 cm	Mineral	2.8E+07	3.4E+07	6.2E+07	45	55
70-80 cm	Mineral	3.3E+07	6.4E+06	3.9E+07	84	16
WS Tundra						
10-20 cm	Organic	6.2E+07	2.3E+07	8.5E+07	73	27
50-60 cm	Organic	1.1E+07	6.1E+06	1.7E+07	65	35
60-70 cm	Organic	3.2E+07	1.8E+07	5.0E+07	64	36

Table SI 3.6 Supplemental 16S rRNA Amplicon Sequence Summary. Summary statistics for 16S rRNA amplicon sequencing reads used in downstream analysis (N = 51).

Sampling Location	Soil Depth (cm)	Sample Soil Type	Total Reads	QC Reads	Percentage of Total Reads Passed QC	Denoised Reads	Merged Reads	Percentage of Total Reads Passed Merge	Non-Chimeric Reads	Percentage of Total Reads Non-Chimeric	Rarified Reads	Percentage of Rarified Non-Chimeric Reads
Toolik MAT	0-10	Organic	145,893	135,011	92.5	131,009	112,610	77.2	99,213	68.0	50,487	50.9
Toolik MAT	10-20	Organic	143,621	132,327	92.1	130,652	118,987	82.9	113,108	78.8	50,487	44.6
Toolik MAT	20-30	Mineral	169,491	151,159	89.2	146,057	124,271	73.3	121,265	71.6	50,487	41.6
Toolik MAT	30-40	Mineral	144,516	126,819	87.8	122,281	101,393	70.2	98,581	68.2	50,487	51.2
Toolik MAT	40-50	Mineral	146,451	134,160	91.6	131,365	113,036	77.2	108,298	74.0	50,487	46.6
Toolik MAT	50-60	Mineral	150,291	136,413	90.8	134,033	119,080	79.2	116,510	77.5	50,487	43.3
Toolik MAT	60-70	Mineral	176,030	152,387	86.6	150,640	130,358	74.1	128,078	72.8	50,487	39.4
Toolik MAT	70-80	Mineral	140,707	127,591	90.7	125,232	113,744	80.8	112,623	80.0	50,487	44.8
Toolik MAT	80-90	Mineral	153,994	141,790	92.1	140,000	124,463	80.8	121,874	79.1	50,487	41.4
Toolik WS	0-10	Organic	152,304	138,741	91.1	133,977	118,540	77.8	114,110	74.9	50,487	44.2
Toolik WS	10-20	Organic	141,525	131,406	92.9	128,807	117,276	82.9	113,976	80.5	50,487	44.3
Toolik WS	20-30	Organic	179,751	165,089	91.8	160,086	143,047	79.6	138,967	77.3	50,487	36.3
Toolik WS	30-40	Organic	152,433	140,317	92.1	136,556	121,025	79.4	117,963	77.4	50,487	42.8
Toolik WS	40-50	Organic	128,652	119,347	92.8	118,859	109,161	84.9	108,166	84.1	50,487	46.7
Toolik WS	50-60	Organic	136,304	126,031	92.5	123,227	101,279	74.3	97,039	71.2	50,487	52.0
Toolik WS	60-70	**Organic**	**71,984**	**62,605**	**87.0**	**62,413**	**50,912**	**70.7**	**50,487**	**70.1**	**50,487**	**100**
Toolik WS	70-80	Organic	160,557	148,465	92.5	147,072	127,336	79.3	126,111	78.6	50,487	40.0
Toolik WS	80-90	Organic	184,135	171,370	93.1	169,908	150,769	81.9	148,565	80.7	50,487	34.0
Imnavait MAT	0-10	Organic	186,102	173,532	93.3	169,139	157,394	84.6	147,867	79.5	50,487	34.1
Imnavait MAT	10-20	Organic	183,512	170,117	92.7	165,179	143,596	78.3	134,175	73.1	50,487	37.6
Imnavait MAT	20-30	Mineral	198,388	179,830	90.7	175,505	158,690	80.0	149,953	75.6	50,487	33.7
Imnavait MAT	30-40	Mineral	166,394	149,995	90.1	147,659	133,360	80.2	130,345	78.3	50,487	38.7
Imnavait MAT	40-50	Mineral	205,995	190,971	92.7	188,847	170,584	82.8	167,215	81.2	50,487	30.2
Imnavait MAT	50-60	Mineral	194,935	180,092	92.4	178,448	155,989	80.0	154,251	79.1	50,487	32.7
Imnavait MAT	60-70	Mineral	213,609	188,730	88.4	187,380	165,323	77.4	164,634	77.1	50,487	30.7
Imnavait WS	0-10	Organic	172,255	157,020	91.2	150,094	132,458	76.9	124,259	72.1	50,487	40.6
Imnavait WS	10-20	Organic	159,528	147,334	92.4	146,228	136,053	85.3	132,874	83.3	50,487	38.0
Imnavait WS	20-30	Organic	205,779	190,252	92.5	185,419	163,696	79.6	158,643	77.1	50,487	31.8
Imnavait WS	30-40	Organic	132,079	121,675	92.1	118,549	104,426	79.1	102,155	77.3	50,487	49.4
Imnavait WS	40-50	Organic	159,637	148,434	93.0	144,638	127,701	80.0	122,224	76.6	50,487	41.3
Imnavait WS	50-60	Organic	129,215	118,911	92.0	115,954	101,657	78.7	98,961	76.6	50,487	51.0
Imnavait WS	60-70	Organic	161,786	141,231	87.3	138,077	114,718	70.9	112,325	69.4	50,487	44.9
Imnavait WS	70-80	Organic	147,401	135,626	92.0	133,684	116,765	79.2	115,817	78.6	50,487	43.6
Imnavait WS	80-90	Organic	156,850	144,366	92.0	142,755	115,801	73.8	113,187	72.2	50,487	44.6
Imnavait WS	90-100	Organic	139,103	128,207	92.2	125,823	112,836	81.1	112,077	80.6	50,487	45.0
Sagwon MAT	0-10	Organic	120,233	109,426	91.0	102,474	88,650	73.7	82,863	68.9	50,487	60.9
Sagwon MAT	10-20	Organic	130,657	119,780	91.7	113,138	96,670	74.0	94,001	71.9	50,487	53.7
Sagwon MAT	20-30	Organic	166,257	150,804	90.7	143,036	121,729	73.2	116,872	70.3	50,487	43.2
Sagwon MAT	30-40	Mineral	139,421	125,087	89.7	119,247	102,321	73.4	100,522	72.1	50,487	50.2
Sagwon MAT	40-50	Mineral	153,499	140,181	91.3	135,239	123,478	80.4	120,791	78.7	50,487	41.8
Sagwon MAT	50-60	Mineral	167,262	151,569	90.6	145,773	127,358	76.1	123,316	73.7	50,487	40.9
Sagwon MAT	60-70	Mineral	151,468	128,319	84.7	122,868	108,215	71.4	106,018	70.0	50,487	47.6
Sagwon MAT	70-80	Mineral	127,396	116,182	91.2	112,492	103,903	81.6	101,149	79.4	50,487	49.9
Sagwon MAT	80-90	Mineral	135,695	125,971	92.8	123,849	117,819	86.8	114,960	84.7	50,487	43.9
Sagwon WS	0-10	Organic	126,143	115,402	91.5	112,160	98,963	78.5	89,976	71.3	50,487	56.1
Sagwon WS	10-20	Organic	110,165	100,463	91.2	97,246	87,927	79.8	84,537	76.7	50,487	59.7
Sagwon WS	20-30	Organic	141,939	125,340	88.3	121,654	109,385	77.1	106,669	75.2	50,487	47.3
Sagwon WS	30-40	Organic	130,151	115,488	88.7	111,840	104,865	80.6	102,734	78.9	50,487	49.1
Sagwon WS	40-50	Organic	138,530	127,706	92.2	125,464	107,666	77.7	105,685	76.3	50,487	47.8
Sagwon WS	50-60	Organic	153,001	140,276	91.7	137,451	117,805	77.0	116,016	75.8	50,487	43.5
Sagwon WS	60-70	Organic	150,502	129,839	86.3	126,092	104,483	69.4	101,975	67.8	50,487	49.5

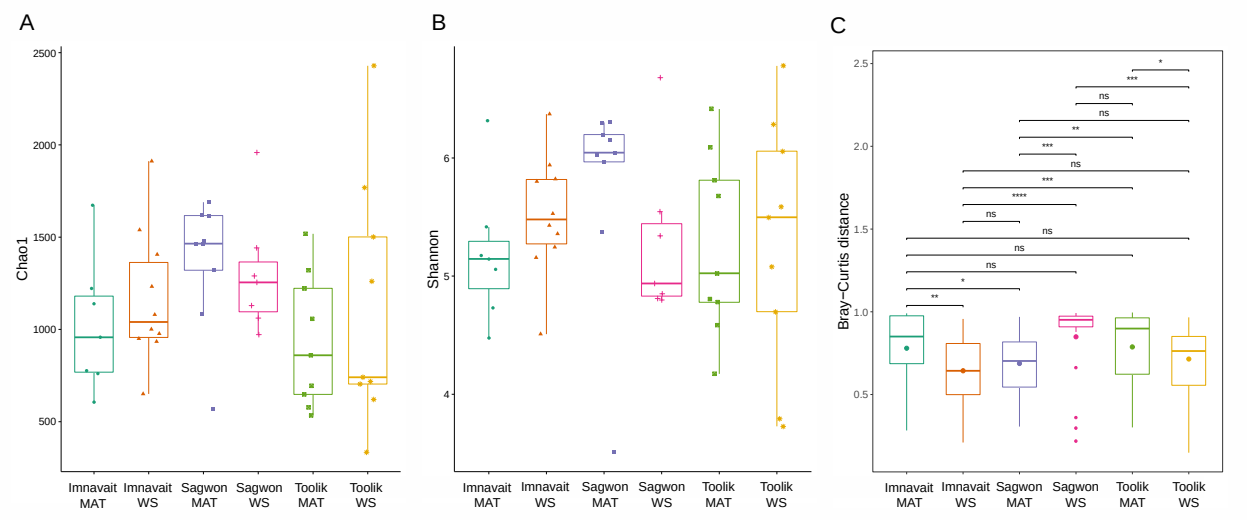

Figure SI 3.6 Supplemental Alpha Diversity. Boxplot for Chao1 (A) and Shannon (B) alpha diversity and Bray-Curtis (C) beta diversity based on the abundance of amplicon sequence variants (ASVs) at each sampling location. Asterisks indicate the significance of the differences in mean ASV abundance between sampling locations (ANOVA; *** $p < 0.001$; ** $p < 0.01$; * $p < 0.05$).

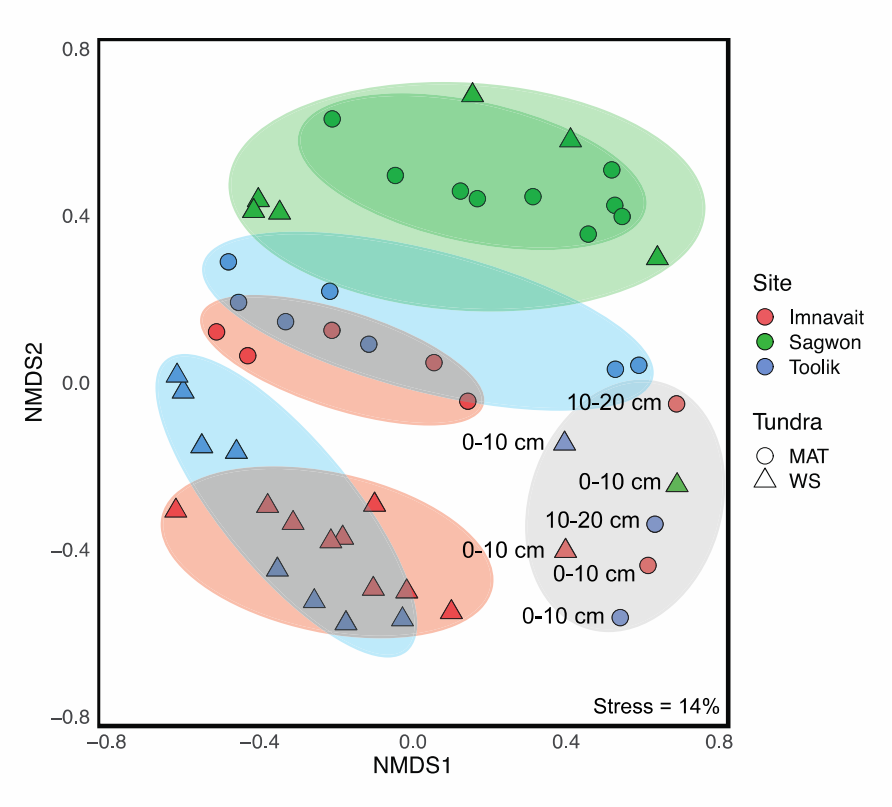

Figure SI 3.7 Supplemental OTU-Based NMDS Ordination. NMDS ordination based on the Bray-Curtis dissimilarity of operational taxonomic units (OTUs; clustered at 97% similarity) abundance within the soil microbiome reveals the same patterns of regional variation by site and between tundra types as ASV-based results shown in Figure 3.2C. The surface depth (0-10 cm) for most sampling locations ordinated separately from all other soil profile depths (gray ellipse). Each marker represents an individual depth sampled along the soil profile of a given site by tundra type in the NMDS plot.

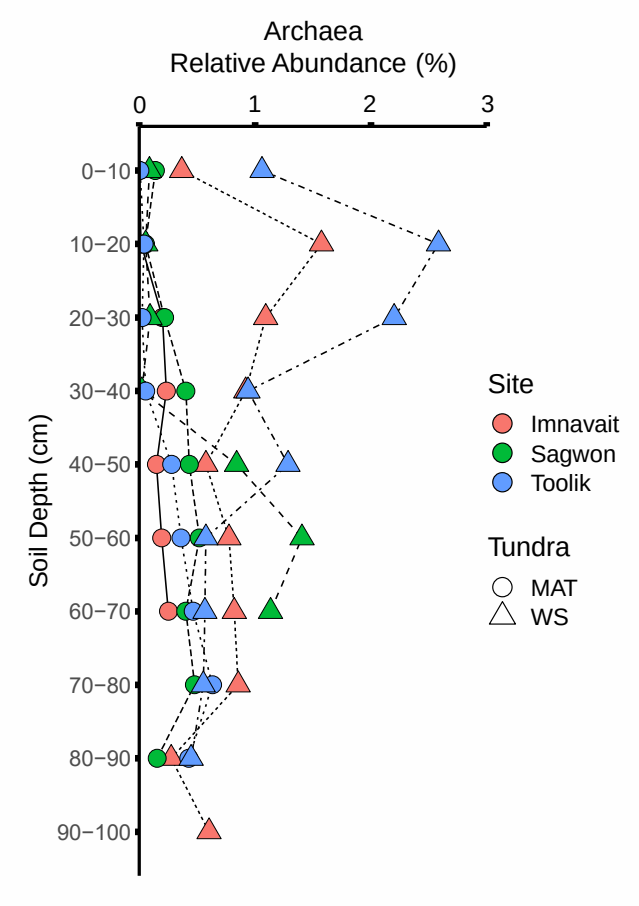

Figure SI 3.8 Supplemental Archaeal Abundance. Relative abundance of archaea by depth for each sampling location.

3.7 References

Apprill, A., McNally, S., Parsons, R., and Weber, L. (2015) Minor revision to V4 region SSU rRNA 806R gene primer greatly increases detection of SAR11 bacterioplankton. Aquatic Microbial Ecology 75(2): 129-137.

Barichivich, J., Briffa, K.R., Osborn, T.J., Melvin, T.M., and Caesar, J. (2012) Thermal growing season and timing of biospheric carbon uptake across the Northern Hemisphere Glob Biogeochem Cycles 26: GB4015.

Biasi, C., Meyer, H., Rusalimova, O., et al. (2008) Initial effects of experimental warming on carbon exchange rates, plant growth and microbial dynamics of a lichen-rich dwarf shrub tundra in Siberia. Plant Soil 307: 191–205.

Bolyen, E., Rideout, J.R., Dillon, M.R., et al. (2019) Reproducible, interactive, scalable and extensible microbiome data science using QIIME 2. Nature Biotechnology 37(8): 852-857.

Bottos, E.M., Kennedy, D.W., Romero, E.B., et al. (2018) Dispersal limitation and thermodynamic constraints govern spatial structure of permafrost microbial communities. FEMS Microbiology Ecology 94: fiy110.

Burkert, A., Douglas, T.A., Waldrop, M.P., and Mackelprang, R. (2019) Changes in the active, dead, and dormant microbial community structure across a Pleistocene permafrost chronosequence. Appl Environ Microbiol 85(7): e02646-18.

Callahan, B.J., McMurdie, P.J., Rosen, M.J., et al. (2016) DADA2: high-resolution sample inference from Illumina amplicon data. Nature Methods 13(7): 581-583.

Campbell, B.J., Polson, S.W., Hanson, T.E., Mack, M.C., and Schuur, E.A. (2010) The effect of nutrient deposition on bacterial communities in Arctic tundra soil. Environ Microbiol 12: 1842–1854.

Castro, H.F., Classen, A.T., Austin, E.E., et al. (2010) Soil microbial community responses to multiple experimental climate change drivers. Appl Environ Microbiol 76: 999–1007.

Chen, Y., Liu, F., Kang, L., et al. (2021) Large-scale evidence for microbial response and associated carbon release after permafrost thaw. Global Change Biology, 27(14), 3218-3229.

Chu, H., Fierer, N., Lauber, C.L., et al. (2010) Soil bacterial diversity in the Arctic is not fundamentally different from that found in other biomes. Environ Microbiol 12: 2998–3006.

Chu, H., Neufeld, J.D., Walker, K., and Grogan, P. (2011) The Influence of vegetation type on the dominant soil bacteria, archaea, and fungi in a Low Arctic Tundra Landscape. SSSA J 75(5): 1756-1765.

Conrad, R., Schutz, H., and Babbel, M. (1987) Temperature limitation on hydrogen turnover and methanogenesis in anoxic paddy soil. FEMS Microbiology Ecology 3: 281–289.

Coolen, M.J., and Orsi, W.D. (2015) The transcriptional response of microbial communities in thawing Alaskan permafrost soils. Frontiers in Microbiology 6: 197.

Deng, J., Gu, Y., Zhang, J., et al. (2015) Shifts of tundra bacterial and archaeal communities along a permafrost thaw gradient in Alaska. Mol Ecol 24: 222–234.

DeSantis, T.Z., Hugenholtz, P., Larsen, N., et al. (2006) Greengenes, a chimera-checked 16S rRNA gene database and workbench compatible with ARB. Appl Environ Microbiol 72(7): 5069-5072.

Deslippe, J.R., Hartmann, M., Simard, S.W., and Mohn, W.W. (2012) Long-term warming alters the composition of Arctic soil microbial communities, FEMS Microbiology Ecology 82(2): 303–315.

De Vos, P., Garrity, G.M., Jones, D., et al. (2009) Bergey's manual of systematic bacteriology, 2nd ed, vol 3. The Firmicutes. Springer, Dordrecht, Netherlands.

Emerson, D., Scott, J.J., Benes, J., and Bowden, W.B. (2015) Microbial iron oxidation in the Arctic tundra and its implications for biogeochemical cycling. Appl Environ Microbiol 81: 8066–8075.

Euskirchen, E.S., et al. (2006) Importance of recent shifts in soil thermal dynamics on growing season length, productivity, and carbon sequestration in terrestrial high-latitude ecosystems. Glob Change Biol 12: 731–50.

Frank-Fahle, B.A., Yergeau, E., Greer, C.W., Lantuit, H., and Wagner, D. (2014) Microbial functional potential and community composition in permafrost-affected soils of the NW Canadian Arctic. PLOS One 9: e84761.

Ganzert, L., Bajerski, F., and Wagner, D. (2014) Bacterial community composition and diversity of five different permafrost-affected soils of Northeast Greenland. FEMS Microbiol Ecol 89: 426–41.

Gittel, A., Bárta, J., Kohoutová, I., Mikutta, R., Owens, S., Gilbert, J., et al. (2014) Distinct microbial communities associated with buried soils in the Siberian tundra. ISME J 8: 841–853.

Hinzman, L.D., Bettez, N.D., Bolton, W.R., et al. (2005) Evidence and Implications of Recent Climate Change in Northern Alaska and Other Arctic Regions. Climatic Change 72: 251–298.

Hugelius, G., Strauss, J., Zubrzycki, S., et al. (2014) Estimated stocks of circumpolar permafrost carbon with quantified uncertainty ranges and identified data gaps. Biogeosciences 11: 6573–6593.

Hultman, J., Waldrop, M.P., Mackelprang, R., et al. (2015) Multi-omics of permafrost, active layer and thermokarst bog soil microbiomes. Nature 521(7551): 208-212.

Jansson, J.K. and Tas, N. (2014) The microbial ecology of permafrost. Nature Reviews Microbiology 12: 414-425.

Johnson, S.S., Hebsgaard, M.B., Christensen, T.R., et al. (2007) Ancient bacteria show evidence of DNA repair. Proc Natl Acad Sci USA 104: 14401–14405.

Jorgenson, M.T., Shur, Y.L., and Pullman, E.R. (2006) Abrupt increase in permafrost degradation in Arctic Alaska. Geophysical Research Letters 33(2): L02503.

Judd, K.E., and Kling, G.W. (2002) Production and export of dissolved C in arctic tundra mesocosms: The roles of vegetation and water flow. Biogeochemistry 60: 213–234.

Judd, K.E., Crump, B.C., and Kling, G.W. (2006) Environmental drivers control eco- system function in bacteria through changes in community composition. Ecology 87: 2068–2079.

Kim, H.M., Lee, M.J., Jung, J.Y., et al. (2016) Vertical distribution of bacterial community is associated with the degree of soil organic matter decomposition in the active layer of moist acidic tundra. Journal of Microbiology 54(11): 713-723.

Kolde, R., and Kolde, M.R. (2015) Pheatmap: Pretty Heatmaps.

Koyama, A., Wallenstein, M.D., Simpson, R.T., and Moore, J.C. (2014) Soil bacterial community composition altered by increased nutrient availability in Arctic tundra soils. Front Microbiol 5: 516.

Kraft, N.J., Adler, P.B., Godoy, O., et al. (2015) Community assembly, coexistence and the environmental filtering metaphor. Functional Ecology 29: 592–599.

Lamb, E.G., Han, S., Lanoil, B.D., et al. (2011) A high arctic soil ecosystem resists long-term environmental manipulations. Global Change Biology 17(10): 3187-3194.

Liang, R., et al. (2019) Predominance of anaerobic, spore-forming bacteria in metabolically active microbial communities from ancient Siberian permafrost. Appl Environ Microbiol 85: e00560-19.

Lipson, D.A., Haggerty, J.M., Srinivas, A., et al. (2013) Metagenomic insights into anaerobic metabolism along an arctic peat soil profile. PLOS ONE 8: e64659.

Liu, C., Cui, Y., Li, X., and Yao, M. (2021) microeco: an R package for data mining in microbial community ecology. FEMS Microbiology Ecology 97(2): fiaa255.

Mackelprang, R., Waldrop, M.P., DeAngelis, K.M., et al. (2011) Metagenomic analysis of a permafrost microbial community reveals a rapid response to thaw. Nature 480(7377): 368-371.

Mackelprang, R., Burkert, A., Haw, M., et al. (2017) Microbial survival strategies in ancient permafrost: insights from metagenomics. ISME J 11: 2305–2318.

Malard, L.A., and Pearce, D.A. (2018) Microbial diversity and biogeography in Arctic soils. Environmental Microbiology Reports 10(6): 611-625.

Malard L.A., Anwar, M.Z., Jacobsen, C.S., and Pearce, D.A. (2019) Biogeographical patterns in soil bacterial communities across the Arctic region, FEMS Microbiology Ecology 95(9): fiz128.

Martinez, M.A., Woodcroft, B.J., Ignacio Espinoza, J.C., et al. (2019) Discovery and ecogenomic context of a global Caldiserica-related phylum active in thawing permafrost, Candidatus Cryosericota phylum nov., Ca. Cryosericia class nov., Ca. Cryosericales ord. nov., Ca. Cryosericaceae fam. nov., comprising the four species Cryosericum septentrionale gen. nov. sp. nov., Ca. C. hinesii sp. nov., Ca. C. odellii sp. nov., Ca. C. terrychapinii sp. nov. Systematic and Applied Microbiology 42: 54-66.

Metje, M., and Frenzel, P. (2007) Methanogenesis and methanogenic pathways in a peat from subarctic permafrost. Environ Microbiol 9: 954–964.

Monteux, S., Weedon, J.T., Blume-Werry, G., et al. (2018) Long-term in situ permafrost thaw effects on bacterial communities and potential aerobic respiration. ISME J 12: 2129-2141.

Müller, O., Bang-Andreasen, T., White, R.A., et al. (2018) Disentangling the complexity of permafrost soil by using high resolution profiling of microbial community composition, key functions and respiration rates. Environ Microbiol 20: 4328–4342.

Neufeld, J.D., and Mohn, W.W. (2005) Unexpectedly high bacterial diversity in Arctic tundra relative to boreal forest soils, revealed by serial analysis of ribosomal sequence tags. Appl Environ Microbiol 71: 5710–5718.

Nielsen, U.N., and Ball, B.A. (2015) Impacts of altered precipitation regimes on soil communities and biogeochemistry in arid and semi-arid ecosystems. Glob Change Biol 21: 1407–1421.

Oksanen, J., Blanchet, F.G., Friendly, M., et al. (2019) Vegan: Community Ecology Package. R Package, Version 2.5–5.

Osterkamp, T.E., and Romanovsky, V.E. (1999) Evidence for warming and thawing of discontinuous permafrost in Alaska. Permafrost and Periglacial Processes 10(1): 17-37.

Parada, A.E., Needham, D.M., and Fuhrman, J.A. (2016) Every base matters: assessing small subunit rRNA primers for marine microbiomes with mock communities, time series and global field samples. Environmental Microbiology 18(5): 1403-1414.

Pedregosa, F., Varoquaux, G., Gramfort, A., et al. (2011) Scikit-learn: Machine learning in Python. Journal of Machine Learning Research 12: 2825-2830.

Ricketts, M.P., Matamala, R., Jastrow, J.D., et al. (2020) The effects of warming and soil chemistry on bacterial community structure in Arctic tundra soils. Soil Biology and Biochemistry 148: 107882.

Rinnan, R., Michelsen, A., Bååth, E., and Jonasson, S. (2007) Fifteen years of climate change manipulations alter soil microbial communities in a subarctic heath ecosystem. Global Change Biology 13(1): 28-39.

Romanowicz, K.J., Crump, B.C., and Kling, G.W. (2021) Rainfall alters permafrost soil redox conditions, but meta-omics show divergent microbial community responses by tundra type in the Arctic. Soil Systems 5: 1-17.

Saidi-Mehrabad, A., Neuberger, P., Hajihosseini, M., et al. (2020) Permafrost microbial community structure changes across the Pleistocene-Holocene boundary. Front Environ Sci 8(133): 1-11.

Schostag, M., Priemé, A., Jacquiod, S., et al. (2019) Bacterial and protozoan dynamics upon thawing and freezing of an active layer permafrost soil. ISME J 13(5): 1345-1359.

Schuur, E.A.G., Bockheim, J., Canadell, J.G., et al. (2008) Vulnerability of permafrost carbon to climate change: implications for the global carbon cycle. BioScience 58(8): 701-714.

Serreze, M.C., Walsh, J.E., Chapin, F.S., et al. (2000) Observational evidence of recent change in the northern high-latitude environment Climatic. Change 46: 159–207.

Siciliano, S.D., Palmer, A.S., Winsley, T., et al. (2014) Soil fertility is associated with fungal and bacterial richness, whereas pH is associated with community composition in polar soil microbial communities. Soil Biol Biochem 78: 10–20.

Singh, P., Singh, S.M., Singh, R.N., et al. (2017) Bacterial communities in ancient permafrost profiles of Svalbard, Arctic. Journal of Basic Microbiology 57: 1018-1036.

Tank, M., and Bryant, D.A. (2015) Nutrient requirements and growth physiology of the photoheterotrophic Acidobacterium, Chloracidobacterium thermophilum. Frontiers in Microbiology 6: 226.

Tarnocai, C. (1993) Sampling frozen soils. In: Carter, M.R. (ed) Soil Sampling and Methods of Analysis. Taylor & Francis, Boca Raton, 755–767.

Tarnocai, C., Canadell, J.G., Schuur, E.A.G., et al. (2009) Soil organic carbon pools in the northern circumpolar permafrost region. Global Biogeochemical Cycles 23(2): GB2023.

Taş, N., Prestat, E., Wang, S., et al. (2018) Landscape topography structures the soil microbiome in arctic polygonal tundra. Nature Communications 9(777): 1-13.

Team, R.C. (2018) R: A language and environment for statistical computing.

Tripathi, B.M., Kim, M., Kim, Y., et al. (2018) Variations in bacterial and archaeal communities along depth profiles of Alaskan soil cores. Scientific Reports 8(1): 1-11.

Tripathi, B.M., Kim, H.M., Jung, J.Y., et al. (2019) Distinct taxonomic and functional profiles of the microbiome associated with different soil horizons of a moist tussock tundra in Alaska. Frontiers in Microbiology 10(1442): 1-14.

Tveit, A.T., Urich, T., Frenzei, P., and Svenning, M.M. (2015) Metabolic and trophic interactions modulate methane production by arctic peat microbiota in response to warming. Proc Natl Acad Sci USA 112: E2507–E2516.

Varsadiya, M., Urich, T., Hugelius, G., and Barta, J. (2021) Microbiome structure and functional potential in permafrost soils of the Western Canadian Arctic. FEMS Micobiology Ecology 97(3): fiab008.

Waldrop, M.P., Wickland, K.P., White III, R., et al. (2010) Molecular investigations into a globally important carbon pool: Permafrost-protected carbon in Alaskan soils. Global Change Biology 16(9): 2543-2554.

Walker, M.A., Daniëls, F.J., and van der Maarel, E. (1994) Circumpolar arctic vegetation: Introduction and perspectives. Journal of Vegetation Science 5(6): 757-764.

Wallenstein, M.D., McMahon, S., and Schimel, J. (2007) Bacterial and fungal community structure in Arctic tundra tussock and shrub soils. FEMS Microbiology Ecology 59(2): 428–435.

Wang, N.F., Zhang, T., Yang, X., et al. (2016) Diversity and composition of bacterial community in soils and lake sediments from an arctic lake area. Frontiers in Microbiology 7: 1170.

Wilhelm, R.C., Niederberger, T.D., Greer, C., and Whyte, L.G. (2011) Microbial diversity of active layer and permafrost in an acidic wetland from the Canadian High Arctic. Can J Microbiol 57: 303–315.

Willerslev, E., Hansen, A.J., Rønn, R., et al. (2004) Long-term persistence of bacterial DNA. Current Biology 14: R9–R10.

Williams, P.J., and Smith, M.W. (1989) The Frozen Earth: Fundamentals of geocryology. Cambridge University Press.

Wunderlin, T., Junier, T., Roussel-Delif, L., Jeanneret, N., and Junier, P. (2014) Endospore-enriched sequencing approach reveals unprecedented diversity of Firmicutes in sediments. Environ Microbiol Rep 6: 631–639.

Yergeau, E., Hogues, H., Whyte, L.G., and Greer, C.W. (2010) The functional potential of high Arctic permafrost revealed by metagenomic sequencing, qPCR and microarray analyses. ISME J 4: 1206–1214.

Zak, D.R., and Kling, G.W. (2006) Microbial community composition and function across an arctic tundra landscape. Ecology 87(7): 1659-1670.

Chapter 4.

Fe-Mediated Microbial Growth during Extended Permafrost Thaw is Strongly Coupled with Gene Expression for Organic Carbon Degradation in Arctic Tundra [3]

4.1 Abstract

Recent thawing of permafrost soils in the Arctic tundra is predicted to increase microbial activity leading to faster degradation of previously-frozen organic carbon (OC) and the release of carbon dioxide (CO_2) and methane (CH_4) to the atmosphere. Yet it remains uncertain how the soil microbiome will respond to permafrost thaw or modulate the relative proportions of CO_2 and CH_4 produced by the degradation of OC in thawing permafrost soils. Here, I used high-throughput metagenomic and metatranscriptomic sequencing to determine the relative and absolute changes in microbiome composition, genomic potential, and gene expression during extended thaw incubations of tundra soil collected from a region of continuous permafrost in northern Alaska. Organic soils from the tundra active-layer (0-50 cm), transition-zone (50-70 cm), and permafrost (70+ cm) depths were incubated at 4°C for up to 30 days to mimic an extended summer thaw duration. Results suggest that after 30 days of thaw under anoxic conditions, the growth of Fe(III)-reducing bacteria increased more than four orders of magnitude in absolute abundance and accounted for ~80% of the relative abundance within the transition-zone and permafrost microbiomes. The genomic potential and gene expression for Fe(III) reduction increased concurrently with genes associated with benzoate degradation and pyruvate metabolism, where pyruvate is used to generate acetate that can be oxidized, along with benzoate, to CO_2 when coupled with Fe(III) reduction. These results indicate strong coupling between Fe(III) reduction and the degradation of OC following permafrost thaw. Thus, extended permafrost thaw events will likely promote greater growth and gene expression of Fe(III)-reducing taxa coupled with substantial oxidation of newly thawed OC to CO_2 in Fe-rich organic tundra soils across the Arctic.

[3] Prepared as: Karl J. Romanowicz, Byron C. Crump, George W. Kling. Fe-mediated microbial growth during extended permafrost thaw is strongly coupled with gene expression for organic carbon degradation in arctic tundra.

4.2 Introduction

Permafrost soils of the Arctic tundra contain an estimated 1,600 Pg of organic carbon (OC), accounting for ~60% of the global belowground OC pool, the majority of which is stored in a perennially frozen state (Tarnocai et al. 2009, Hugelius et al. 2014). However, recent warming in the Arctic has increased soil temperatures (Osterkamp & Romanovsky 1999) and thawed large areas of permafrost (Zhang et al. 2006). These warming-induced changes to permafrost will likely increase microbial activity following thaw, leading to more degradation of previously frozen OC and the release of carbon dioxide (CO_2) and methane (CH_4) to the atmosphere (Schuur et al. 2009, Xue et al. 2016, Turetsky et al. 2020). An increase in the release of CO_2 and CH_4 to the atmosphere from thawing permafrost soils could initiate a positive feedback loop on climate warming that would affect the entire global climate system (Stocker 2014, Schuur et al. 2015).

The fate of the OC pool in permafrost soils is critical to the global climate system, yet major uncertainties in our current understanding of permafrost thaw remain. These uncertainties include which microbes respond to permafrost thaw, how quickly they respond following thaw, and how their response modulates the relative proportions of CO_2 and CH_4 that will be produced by the decomposition of OC in thawing permafrost soils. Previous studies that document the response of the permafrost microbiome to short-term warming (i.e., days) in laboratory-based incubations have shown rapid, substantial shifts in composition, genomic potential, and gene expression within a few days of thaw (Mackelprang et al. 2011, Coolen & Orsi 2015, Hultman et al. 2015). These rapid changes in the microbiome have also been used to predict post-thaw biogeochemical rates of OC degradation (Mackelprang et al. 2011) and methanogenesis (Hultman et al. 2015). However, the results of short-term lab-based studies correspond weakly or not at all with *in situ* soil warming experiments in tundra ecosystems that show little or no change in the composition of the permafrost microbiome following years of passive surface warming that extends thaw depth and duration into the permafrost (Rinnan et al. 2007, Biasi et al. 2008, Lamb et al. 2011). Temperature is a key limiting factor for microbial metabolism (Davidson & Janssens 2006) and different outcomes between field and lab-based experiments may be due to different timescales over which soil temperature is manipulated and maintained. Differences in tundra type (i.e., dominant vegetation) and abiotic soil properties between field and lab-based experiments also likely impact the microbial response to short-term thaw duration and should be considered when comparing results across the Arctic landscape.

Characterizing short-term microbial responses to permafrost thaw is a necessary first step in understanding the biogeochemical shifts that may occur under a warming Arctic (Mackelprang et al. 2011, Coolen & Orsi 2015, Romanowicz et al. 2021), but it does little to help understand the successional trajectory of the permafrost microbiome following extended thaw duration (i.e., thaw duration exceeding 30 days annually). The fate of the OC pool in permafrost soils will largely be determined by the persistent changes to the soil microbiome following extended permafrost thaw (Ricketts et al. 2020). Warmer soil temperatures, earlier spring thaw, and later fall freeze-up have all contributed to an increase in annual thaw depth and an extended duration of annual thaw along tundra soil profiles (Serreze et al. 2000, Euskirchen et al. 2006, Barichivich et al. 2012). The duration of annual thaw is also strongly correlated with the composition of the permafrost microbiome and could be used to predict the microbial response to extended permafrost thaw (Romanowicz & Kling, *In Review*). For example, the composition and genomic potential of the microbiome in recently thawed permafrost soils (i.e., transition-zone depths) was found to be indistinguishable from the underlying perennially-frozen permafrost microbiome despite decades of intermittent thaw frequency (Romanowicz & Kling, *In Review*). This suggests that thaw duration rather than thaw frequency has a greater impact on the composition of the microbiome within tundra soils. Notably in that study, the transition-zone depths experienced less than half the number of thaw days (~22 days of thaw annually) compared to the overlying annually-thawed surface active layer (~51 days) (Romanowicz & Kling, *In Review*). These findings are more consistent with field-based warming experiments showing little to no change in the permafrost microbiome following years of moderate heating from the soil surface to mimic its natural extension into the permafrost (Rinnan et al. 2007, Biasi et al. 2008, Lamb et al. 2011). Thus, the microbial response to future permafrost thaw, including their genomic potential to degrade recently thawed OC stocks, will likely be influenced by intermediate stages of compositional and functional changes that shift the permafrost microbiome towards the current active-layer microbiome as thaw frequency and duration increase with depth along the soil profile.

The microbial response to permafrost thaw is also influenced by soil redox conditions (Lipson et al. 2012, Woodcroft et al. 2018, Miner et al. 2022), where persistent water saturation following permafrost thaw and flooding of the soil environment leads to oxygen (O_2) limitations and anoxic soil conditions (Smith et al. 2005). These anoxic conditions promote anaerobic and fermentative microbial processes responsible for the majority of OC degradation in thawing

permafrost soils (Sturtevant & Oechel 2013, Herndon et al. 2015, Yang et al. 2016, Romanowicz et al. 2021). Anaerobic degradation processes in thawing permafrost soils are tightly coupled to the cycling of elements including iron (Fe), which can serve as terminal electron acceptors in anaerobic respiration (Dettling et al. 2006, Lipson et al. 2010). Tundra soils are often rich in reactive Fe minerals that bind up to 20% of total OC in intact permafrost soils and protect it from degradation through Fe-OC associations (Mu et al. 2016, Patzner et al. 2020). However, by providing a terminal electron acceptor for anaerobic respiration following thaw, Fe(III) minerals also enhance the degradation of permafrost OC that can lead to substantial CO_2 formation, accounting for 40 to 60% of total ecosystem respiration in low-lying tundra regions (Lipson et al. 2013). Fe-mediated microbial growth can also suppress the production of CH_4 when Fe(III)-reducing bacteria outcompete methanogenic archaea for organic substrates (Lipson et al. 2012, Miller et al. 2015, Patzner et al. 2022a). To predict relative proportions of CO_2 and CH_4 released from thawing permafrost soils, it is necessary to identify how the pathways of OC degradation under anoxic conditions are affected by Fe-mediated processes that are prevalent in arctic tundra.

Here, we simulated thaw along the depth profile of an Fe-rich organic tundra soil using frozen soil samples from the active-layer, transition-zone, and permafrost depths that were gradually thawed to 4°C and incubated under anoxic conditions for 30 days. These incubation conditions reflect a representative thaw temperature and soil redox state maintained for longer than the minimum duration of annual thaw in the transition zone (~22 days) as measured from long-term thaw depth surveys at our field site. We determined the extent of initial differences in microbiome composition between each soil layer along the soil profile and identified the dominant microbial taxa and their genomic pathways of OC degradation during short-term (7-day) and extended (30-day) thaw duration by measuring relative and absolute changes in microbiome composition, genomic potential, and gene expression during the incubation experiment.

4.3 Methods

4.3.1 Study Site and Soil Core Collection

Soil core samples were collected on 19 July 2019 in wet sedge tundra at Imnavait Creek (68°36'35.36"N 149°18'29.80"W), located along the trans-Alaskan pipeline on the North Slope of the Brooks Range in northern Alaska, USA. A detailed description of the study site is given

elsewhere (Romanowicz et al. 2021, Romanowicz & Kling, *In Review*). Briefly, wet sedge tundra forms as a rich fen complex at the base of hillslopes and is dominated by *Carex aquatilis* and other sedges (Walker et al. 1994). Within the wet sedge tundra at Imnavait Creek, a single soil core (10 cm diameter × 1 m length) was collected using a SIPRE (Snow, Ice, and Permafrost Research Establishment; Carter & Gregorich 2007) corer with carbide bits (Jon's Machine Shop, Fairbanks, AK) from an inter-tussock location representative of the valley bottom (i.e., roughly equidistant between the bottom of the hillslope and the stream). The soil core was scraped horizontally, perpendicular to the depth axis, using aseptic techniques in the field to remove outer layers of soil and then separated into 30-cm increments, wrapped in aluminum foil, labeled by depth to reconstruct the soil profile in the lab, placed in a cooler with ice, and immediately frozen at -80°C upon return from the field.

4.3.2 Soil Incubation Design

Soil incubations in the laboratory were used to measure changes in microbiome composition, genomic potential, and gene expression in response to short-term and extended thaw duration using soil collected from multiple depths along the soil core. Soil samples (~50 g, wet mass) were taken from three distinct soil layers representing the active layer (AL, 0-50 cm), transition zone (TZ, 50-70 cm), and permafrost (PF, 70+ cm) following homogenization of each (frozen) soil layer and placed in 250 mL amber jars in triplicate (N = 9). Each incubation jar also contained 50 mL of deionized water and the soil samples were mixed with the deionized water to create soil slurries that were then incubated at 4°C in the dark for the duration of the experiment. The soil layer depths used (AL, TZ, PF) were determined from long-term thaw depth surveys described elsewhere (Kling et al. 2014, Romanowicz & Kling, *In Review*; Chapter 3). Soil subsamples (~2 g, wet mass) were collected frozen from each soil layer replicate prior to starting the incubation experiment to represent time point zero (T0). Incubation jars were then sealed with an airtight lid containing a septum and purged with N_2 to simulate natural anoxic conditions in the soils. Additional soil subsamples (~2 g, wet mass) were collected at 7-days (T7) and 30-days following thaw (T30) and immediately frozen at -80°C until extraction.

4.3.3 Nucleic Acid Extraction and Sequencing

Microbial RNA and DNA were extracted from soil subsamples collected at each incubation time point (N = 27, for RNA and DNA, respectively) using the RNeasy PowerSoil Total RNA Isolation kit (Qiagen) and RNeasy PowerSoil DNA Elution Accessory kit (Qiagen), respectively, following the manufacturer's protocol. Genomic DNA was amplified through polymerase chain reaction (PCR) using dual-barcoded 16S rRNA gene primers 515f-806r (Apprill et al. 2015, Parada et al. 2016) to profile the bacterial and archaeal communities. PCR amplicons (N = 27) were pooled into a single library and submitted to the University of Michigan Microbiome Core for high-throughput sequencing on the Illumina MiSeq platform. Metagenome reads were generated from genomic DNA (N = 27). Metatranscriptome reads were generated from total RNA extractions (N = 15; no RNA yield from time points T0 and T7 in the transition-zone and permafrost microbiomes). All reads were sequenced at the University of Michigan Advanced Genomics Core on the Illumina NextSeq platform using high-output 150 cycle paired-end reads.

4.3.4 16S rRNA Gene Analysis

Sequencing data from 16S amplicons were downloaded from Illumina BaseSpace and analyzed using QIIME2 (v. 2020.11) (Bolyen et al., 2019) on the Great Lakes High Performance Computing Cluster (University of Michigan, USA). Raw forward and reverse sequencing reads were quality filtered with DADA2 (Callahan et al. 2016). Taxonomy was assigned to amplicon sequence variants (ASVs) using scikit-learn naïve Bayes taxonomy classifier (Pedregosa et al. 2011) against the GreenGenes 99% database (v. 13.8) (DeSantis et al. 2006). ASVs were chosen over operational taxonomic units (OTUs) following recent benchmark studies (Callahan et al. 2017, Chiarello et al. 2022). See also the 16S sequencing reads summary (Table SI 4.3).

4.3.5 Metagenome Analysis

DNA sequences were trimmed and quality-filtered with the BBDuk algorithm from BBMap (Bushnell 2015) with dereplication. Quality-controlled metagenome reads from each sample were co-assembled using MEGAHIT (Li et al. 2015). The co-assembled contigs were indexed using Bowtie2 (Langmead & Salzberg 2012) and short reads from each sample were individually mapped to the indexed contigs using BBMap (Bushnell 2015). A contigs database was created from the co-assembly using Anvi'o (Eren et al. 2015) with the abundance information

for all contigs merged into an Anvi'o profile. Coding sequences (CDS) within the contigs database were predicted with PRODIGAL (Hyatt et al. 2010) while HMMER (Eddy 2011) was used to search for and tabulate the occurrence of single-copy housekeeping genes for bacteria and archaea from two collections (Campbell et al. 2013, Rinke et al. 2013). CDS were also annotated to the Kyoto Encyclopedia of Genes and Genomes database (KEGG) (Kanehisa et al. 2008) as well as taxonomically annotated using the online GhostKOALA program (Kanehisa et al. 2016) and imported into the contigs database. Counts per annotation were normalized to genes per million (GPM) (Wagner et al. 2012) to reduce biases associated with library size and CDS length. See the metagenome sequencing reads summary (Table SI 4.4).

4.3.6 Metatranscriptome Analysis

RNA sequences were trimmed and quality-filtered with the BBDuk algorithm from BBMap (Bushnell 2015) without dereplication to determine the abundance of transcribed genes. Quality-controlled metatranscriptome reads were mapped to KEGG-annotated coding sequences (CDS) indexed from the metagenome assembly using BBMap to generate pile-up files (average read depth per gene), while SAMtools was used to extract counts and CDS lengths from the BBMap output (Li et al. 2015). On average, 65% of the metatranscriptome CDS were expressed (> 1 count per read) with 40% of expressed CDS assigned KEGG functional annotations, of which 99% were also assigned taxonomic annotations. Counts per annotation were normalized to transcripts per million (TPM) (Wagner et al. 2012) to reduce biases associated with library size and CDS length. See the metatranscriptome sequencing reads summary (Table SI 4.5).

4.3.7 Internal Standards for Gene Copy Abundance

The addition of DNA from the internal standard *Thermus thermophilus*, a bacterial taxon unlikely to be found in soil, prior to the nucleic acid extraction step allows for the quantitative comparison of the absolute abundance of bacterial and archaeal 16S rRNA gene copies across samples. Here, we followed methods described in Smets et al. (2016) to spike 5.5 ng of *T. thermophilus* DNA into our soil samples prior to extraction and then calculated the absolute abundance of 16S rRNA gene copies in each soil sample from the number of 16S rRNA gene copies of the internal standard recovered in the sequencing data. Absolute abundance values of 16S rRNA gene copies were also calculated at the phylum-level down to the genus-level in some cases based on the relative abundance of each taxon compared to the relative abundance of the

internal standard recovered in each sample. Previous studies have demonstrated that adding a DNA internal standard to soil prior to DNA extraction is an effective method for comparing bacterial and archaeal 16S rRNA gene abundances across samples (Smets et al. 2016, Morton et al. 2019).

4.3.8 Statistical Analysis

All statistical analyses were conducted in R (v. 4.1.2) (R Core Team, 2018) and considered significant at $p < 0.05$. Multivariate statistical analysis of the 16S amplicon sequencing data was conducted using the "microeco" package (Liu et al. 2021) and the "vegan" package (Oksanen et al. 2007). Shannon-Wiener diversity index was calculated with raw taxonomic gene counts and assessed via two-way ANOVA with post hoc Tukey honestly significant different (HSD) tests to determine the effects of soil layer and incubation time point on taxonomic alpha diversity. Bray-Curtis dissimilarity was calculated for ASV abundance and analyzed via permutational multivariate analysis of variance (PERMANOVA) using the "adonis()" function in the "vegan" package to determine the effects of soil layer, incubation time, and their interactions on the composition of each soil layer microbiome during the incubation experiment. Differences in ASV abundance by soil layers between all incubation time points were visualized through unconstrained principal coordinate analysis (PCoA) ordination using the "ggplot2" package (Villanueva & Chen 2019). Pairwise comparisons among dominant microbial phyla within each soil layer were conducted between each incubation time point via two-way ANOVA with post hoc Tukey HSD tests to determine if the relative abundance of each phylum changed following thaw in the incubation experiment.

The genomic potential and functional gene expression within each soil-layer microbiome at each incubation time point were determined from the GPM-normalized metagenomes and TPM-normalized metatranscriptomes, respectively, based on the relative abundance of genes annotated to KEGG tiers II-IV. Pairwise comparisons among functional genes within each soil layer microbiome were conducted between each incubation time point relative to T0 via two-way ANOVA with post hoc Tukey HSD tests to determine if the relative abundance of functional genes changed following thaw. The Shannon-Wiener diversity index was calculated ("vegan" package) with raw functional gene counts and assessed via two-way ANOVA with post hoc Tukey HSD tests to determine the effect of soil layer on functional gene alpha diversity. Beta diversity

treatment effects were estimated using PERMANOVA based on Bray-Curtis dissimilarity distance between GPM- or TPM-normalized functional gene counts using the the "vegan" package.

Differential gene expression (DGE) analysis was applied to the TPM-normalized metatranscriptomes, where DGE between incubation time points within each soil layer microbiome was determined using the glmFit function within edgeR (Robinson & Oshlack 2010) based on KEGG ortholog (KO) values, after setting *calcnormfactors* to "none" to avoid default TMM normalization by edgeR. The generalized linear models were fit to a design matrix based on the experimental design to test for differential expression between incubation time points within each soil layer microbiome while adjusting for differences between incubation replicates at each incubation time point. This was considered an additive linear model with incubation replicates as the blocking factor. TPM-normalized KOs were considered differentially expressed if the false discovery rate (FDR) (Benjamini & Hochberg 1995) value of p was < 0.05.

The microbial pathways for iron (Fe) metabolism, Fe acquisition, and Fe cycling were quantified as additional proxies for Fe-mediated microbial growth after thaw. Established gene annotation pipelines such as GhostKOALA (Kanehisa et al. 2016), used in this study, generally do not incorporate hidden Markov models (HMMs) capable of annotating Fe-related genes and gene neighborhoods, especially genes involved in Fe oxidation and dissimilatory Fe reduction. We re-annotated the metagenome and metatranscriptome contig assemblies using FeGenie (Garber et al. 2020), which provides a comprehensive database of HMMs based on genes related to Fe metabolism, Fe acquisition, and Fe cycling in bacteria and archaea. Counts within each Fe gene category were summarized as their relative abundance against the sum of all identified Fe genes. Pairwise comparisons were conducted via two-way ANOVA with post hoc Tukey HSD tests to determine if Fe-related genomic potential (metagenome) and gene expression (metatranscriptome) changed following thaw in the incubation experiment.

4.4 Results

4.4.1 Taxonomic Diversity of the Soil Microbiome During Thaw

Soil microbiome analysis of 16S rRNA gene amplicons resolved into amplicon sequence variants (ASVs) showed statistical differences in taxonomic alpha diversity between distinct soil layers along the profile of our soil core and between incubation time points within each soil layer

using Shannon-Wiener (H') diversity metrics (ANOVA; Table SI 4.3). Specifically, there was significantly greater taxonomic alpha diversity (H') between the active-layer microbiome and the transition-zone and permafrost microbiomes at each incubation time point ($p < 0.001$ for all), but no difference between the specific pair of transition-zone and permafrost microbiomes by time point ($p > 0.05$ for all). Within the active-layer microbiome there was no significant difference in taxonomic alpha diversity (H') between incubation time points ($p > 0.05$ for all), but there was a significant decrease in H' when the initial (T0) and short-term thaw duration (T7) time points were compared to the extended thaw duration time point (T30) in the transition-zone and permafrost microbiomes ($p < 0.05$ for all; Table SI 4.3).

Beta diversity results based on Bray-Curtis dissimilarity of ASV abundance indicated significant differences in taxonomic composition between soil layers, incubation time points, and soil layer × incubation time point interactions (PERMANOVA; $p < 0.001$ for all). Differences in ASV abundance between soil layers and their incubation time points were visualized through PCoA ordination based on Bray-Curtis dissimilarity (Figure 4.1A). There were four notable trends from the PCoA ordination. First, the active-layer microbiome was significantly, compositionally distinct from the transition-zone and permafrost microbiomes in ordination space throughout the incubation experiment ($p < 0.001$ for all; Figure 4.1A), while the transition-zone and permafrost microbiomes were compositionally indistinguishable from each other based on their shared abundance of ASVs ($p > 0.05$ for all; Figure 4.1A). Second, there were no significant differences in the beta diversity of ASV abundance between incubation time points T0 and T7 in any soil layer, indicating that there was no significance change in ASV abundance following the 7-day short-term thaw duration (Figure 4.1A). Third, the active-layer microbiome significantly shifted in composition at time point T30 compared to T0 or T7, indicating that extended thaw duration was sufficient to shift the composition of the active-layer microbiome from its initial composition at T0 (Figure 4.1A). Fourth, the transition-zone and permafrost microbiomes both shifted significantly in composition by T30, but the magnitude of their shift in composition was much greater than observed in the active-layer microbiome, indicating these microbiomes deeper in the soil were more susceptible to whole-community compositional shifts following extended thaw (Figure 4.1A).

The Venn diagram indicates that the greatest relative abundance of ASVs was shared between all three soil layers (79%; Figure 4.1B), with an additional 16.3% of ASV abundance shared between at least two soil layers (Figure 4.1B). Notably, these ASVs represented 95.3% of the relative abundance of all ASVs shared between soil layers but consisted of only 1,582 ASVs out of 9,842 total ASVs (Figure 4.1B). The active-layer microbiome had the greatest abundance of unique ASVs by soil layer (3.2%) compared to the permafrost microbiome (1%) and the transition-zone microbiome (0.6%; Figure 4.1B). There was also a greater proportion of ASVs shared between the transition-zone and permafrost microbiomes (10.7%; Figure 4.1B) than shared between the active-layer and transition-zone microbiomes (3.7%; Figure 4.1B) or active-layer and permafrost microbiomes (1.9%; Figure 4.1B).

4.4.2 Taxonomic Abundance of the Soil Microbiome During Thaw

Using taxonomic annotations of the 16S rRNA ASVs, we found that the composition of the microbiomes in all soil layers and at all incubation time points was dominated by bacteria (>99% relative abundance), but there were significant differences in the relative abundance of dominant bacterial taxa among soil layers, incubation time points, and soil layer × incubation time point interactions (ANOVA; $p < 0.05$ for all). Note that all p values for the main effects of soil layer and incubation time point are biased when the interaction term of soil layer × incubation time point is statistically significant. Within the active-layer microbiome, there was a significant increase in the relative abundance of Betaproteobacteria (+26.6%; $p < 0.001$) and a concurrent decrease in the relative abundance of Gammaproteobacteria (-0.8%; $p = 0.04$), Chloroflexi (-2.9%; $p = 0.03$), Verrucomicrobia (-5.2%; $p = 0.003$), and other bacterial taxa (combined -5.0%; $p = 0.01$) after 30 days of thaw relative to initial composition at T0 (Figure 4.2A; Table SI 4.6). Within the transition-zone microbiome, there was a significant increase in the relative abundance of Betaproteobacteria (+71.9%; $p < 0.001$) and a concurrent decrease in nearly all other dominant taxa including Acidobacteria (-3.2%; $p < 0.001$), Actinobacteria (-29.2%; $p < 0.001$), Deltaproteobacteria (-4.0%; $p < 0.001$), Bacteroidetes (-4.0%; $p = 0.001$), Caldiserica (-27.6%; $p < 0.001$), Chloroflexi (-6.1%; $p < 0.001$), Verrucomicrobia (-1.1%; $p = 0.04$), other bacterial taxa (-8.2%; $p < 0.001$), and Archaea (-0.4%; $p < 0.001$) at T30 relative to T0 (Figure 4.2B; Table SI 4.6). Trends within the permafrost microbiome from T0 to T30 were similar to trends in the transition-zone microbiome with a significant increase in the relative abundance of

Betaproteobacteria (+80.0%; $p < 0.001$) and a concurrent decrease in other dominant taxa including Acidobacteria (-4.1%; $p < 0.001$), Actinobacteria (-31.2%; $p < 0.001$), Deltaproteobacteria (-6.1%; $p < 0.001$), Bacteroidetes (-5.3%; $p = 0.001$), Caldiserica (-18.1%; $p < 0.001$), Chlorobi (-0.4%; $p < 0.001$), Chloroflexi (-7.8%; $p < 0.001$), Verrucomicrobia (-3.6%; $p = 0.04$), other bacterial taxa (-9.0%; $p < 0.001$), and Archaea (-0.7%; $p < 0.001$) (Figure 4.2C; Table SI 4.6).

The significant increase in the relative abundance of Betaproteobacteria in the active-layer microbiome (+26.6%), transition-zone microbiome (+71.9%), and permafrost microbiome (+80.0%; Figure 4.2; Table SI 4.6) at T30 was mostly attributed to *Rhodoferax* spp. (+10.3% AL; +62.3% TZ; +62.7% PF; Table 4.1). The cultivated lineage most closely related to the abundant ASV annotated as *Rhodoferax* spp. was the Fe(III)-reducing bacterium *R. ferrireducens* (BLASTN: percent identity = 100%; e-value = $2e^{-127}$). *Gallionella* spp., a known ferrous iron (Fe(II))-oxidizing bacterium, also contributed to the significant increase in Betaproteobacteria abundance in all soil layers (+7.7% AL; +1.6% TZ; +3.1% PF; $p < 0.05$ for all; Table 4.1). Several additional Fe(III)-reducing bacteria accounted for the remaining increase in taxonomic relative abundance following extended thaw duration (T30) in the transition-zone and permafrost microbiomes including *Clostridium* spp. (Firmicutes; +5.9% TZ; +1.7% PF) and *Pseudomonas* spp. (Gammaproteobacteria; +9.9% TZ; +7.5% PF; Table 4.1). The Fe(III)-reducing *Geobacter* spp. (Deltaproteobacteria) remained at low relative abundance throughout the incubation experiment in all soil layers (< 2% AL; < 0.3% TZ; < 0.4% PF; Table 4.1). Overall, the increase of Fe-cycling taxa associated with Fe(III)-reduction and Fe(II)-oxidation accounted for 20% of the total relative abundance of the active-layer microbiome, 83% of the transition-zone microbiome, and 78% of the permafrost microbiome at the end of the incubation (T30; Table 4.1).

Using the internal standard *Thermus thermophilus*, the calculated absolute abundance of total 16S rRNA gene copies increased more than two-orders of magnitude by T30 compared to initial abundance at T0 within the transition-zone and permafrost microbiomes, while the active-layer microbiome only experienced proportional shifts in the absolute abundance of dominant microbial taxa rather than a significant increase in overall absolute abundance of 16S rRNA gene copies between incubation time points (Figure SI 4.7). There was no significant change in absolute 16S rRNA gene copy abundance between incubation time points T0 and T7 within any soil layer

microbiome, with the exception of Gammaproteobacteria decreasing at T7 compared to T0 in the active-layer microbiome (Log_{10} fold-change = -0.95; p = 0.05; Table SI 4.7).

Within the active-layer microbiome, there was a significant increase in the absolute abundance of 16S rRNA gene copies associated with Betaproteobacteria (Log_{10} fold-change = +1.34; p = 0.02) primarily offset by a significant decrease in the absolute abundance of 16S rRNA gene copies associated with Gammaproteobacteria (Log_{10} fold-change = -1.05; p = 0.04) at T30 compared to T0 (Table SI 4.7). Within the transition-zone microbiome, there was a significant increase in the absolute abundance of 16S rRNA gene copies associated with Alphaproteobacteria (Log_{10} fold-change = +1.63; p = 0.003), Betaproteobacteria (Log_{10} fold-change = +3.71; p < 0.001), and Firmicutes (Log_{10} fold-change = +1.50; p = 0.005) with no significant decrease in absolute 16S rRNA gene copy abundance for any taxa at T30 compared to T0 (Table SI 4.7). Results from the permafrost microbiome at T30 compared to T0 were similar to those in the transition-zone microbiome with a significant increase in the absolute abundance of 16S rRNA gene copies associated with Alphaproteobacteria (Log_{10} fold-change = +1.63; p = 0.03), Betaproteobacteria (Log_{10} fold-change = +4.13; p < 0.001), and Firmicutes (Log_{10} fold-change = +1.33; p = 0.002) and no significant decrease in absolute 16S rRNA gene copy abundance of any taxa (Table SI 4.7).

The absolute abundance of 16S rRNA gene copies associated with each Fe(III)-reducing and Fe(II)-oxidizing taxon also increased by several orders of magnitude following extended thaw duration (T30) compared to initial values at T0 within each soil layer microbiome (ANOVA; Figure 4.3; Figure 4.4; Table SI 4.8). Specifically, there was a significant increase in the absolute abundance of 16S rRNA gene copies associated with *Rhodoferax* spp. in the active-layer microbiome (Log_{10} fold-change = +1.96; p = 0.02), transition-zone microbiome (Log_{10} fold-change = +4.44; p < 0.001), and permafrost microbiome (Log_{10} fold-change = +4.61; p = 0.001) by T30 compared to T0 (Figure 4.3A; Table SI 4.8). This represents an increase of more than four orders of magnitude in the absolute abundance of *Rhodoferax* spp. gene copies in the transition-zone and permafrost microbiomes after 30 days of incubation (Figure 4.3A; Table SI 4.8). *Clostridium* spp. was the only other Fe(III)-reducing taxon to increase significantly by T30 compared to T0 in the transition-zone microbiome (Log_{10} fold-change = +1.85; p = 0.02) and permafrost microbiome (Log_{10} fold-change = +1.68; p = 0.002; Fig. 3B; Table SI 4.8). *Geobacter* spp. showed no significant increase in absolute abundance after 30 days in any soil layer

microbiome ($p > 0.05$ for all; Figure 4.3C; Table SI 4.8). While *Pseudomonas* spp. showed the greatest increase in absolute abundance in all soil-layer microbiomes by T30 compared to T0 (Log_{10} fold-change = +5.84 AL; +5.84 TZ; +4.77 PF), this increase in abundance was not considered significant due to substantial variations in absolute abundance between the incubation replicates within each soil layer ($p > 0.05$ for all; Figure 4.3D; Table SI 4.8). The absolute abundance of 16S rRNA gene copies associated with the Fe(II)-oxidizing *Gallionella* spp. increased significantly after 30 days of thaw in the active layer (Log_{10} fold-change = +1.57; $p = 0.03$), in the transition-zone microbiome (Log_{10} fold-change = +3.75; $p = 0.04$), and in the permafrost microbiome (Log_{10} fold-change = +4.04; $p = 0.02$; Figure 4.4; Table SI 4.8).

4.4.3 Genomic Potential and Gene Expression of the Soil Microbiome During Thaw

Metagenome analyses revealed that the genomic potential of the active-layer microbiome was significantly greater than the potential in the transition-zone or permafrost microbiomes at all incubation time points due to a greater diversity of functional genecalls (H'; ANOVA; $p < 0.001$ for all; Figure SI 4.8). There was also no significant change in genecall diversity within the active-layer microbiome during short-term (T7) or extended (T30) thaw duration compared to T0 ($p > 0.05$ for all; Figure SI 4.8). In contrast, the genomic potential of the transition-zone and permafrost microbiomes significantly decreased in genecall diversity from T0 to T30 ($p < 0.001$ TZ; $p < 0.01$ PF; Figure SI 4.8). These differences in genomic potential derived from the metagenome were consistent with differences in the diversity of expressed functional genecalls observed in the metatranscriptome (H'; ANOVA; $p < 0.01$ for all; Figure SI 4.8). Specifically, there was a greater diversity of functional genecalls expressed by the active-layer microbiome during short-term (T7) and extended (T30) thaw duration time points compared to the diversity of functional genecalls expressed by the transition-zone or permafrost microbiomes at any time point in the incubation ($p < 0.001$ for all; Figure SI 4.8).

The genomic potential of each soil layer microbiome was dominated by functional genes annotated to the KEGG tier II category "Metabolism", followed by genes annotated as "Genetic Information Processing", "Environmental Information Processing", and "Cellular Processes" (GPM; Table SI 4.9). Notably, we found that the relative abundance of genecalls annotated to all four KEGG categories was statistically similar between incubation time points T0 and T7 but differed significantly from time point T30 within each soil-layer microbiome (ANOVA; $p < 0.05$

for all; Table SI 4.9). At the KEGG tier III level (sub-categories within tier II), there was a significant difference in the relative abundance of only half of the functional gene categories in the active-layer microbiome (11 of 22 categories), but almost all of the functional gene categories in the transition-zone microbiome (20 of 22 categories) and permafrost microbiome (15 of 22 categories) differed significantly after 30 days compared to initial values at T0 (ANOVA; $p < 0.05$ for all; Figure 4.5; Table SI 4.10). Specifically, in the active-layer microbiome by T30 compared to T0 there was significantly greater abundance for functional genes associated with the metabolism of cofactors and vitamins, xenobiotics biodegradation and metabolism, signal transduction, and cell motility with a concurrent decrease in the relative abundance of functional genes associated with carbohydrate metabolism, metabolism of terpenoids and polyketides, nucleotide metabolism, folding, sorting, and degradation, replication and repair, transcription, and cell growth and death ($p < 0.05$ for all; Figure 4.5; Table SI 4.10). From T0 to T30 the transition-zone and permafrost microbiomes shared a similar change in the relative abundance of functional genes, including an increase in the relative abundance of functional genes associated with amino acid metabolism, energy metabolism, metabolism of cofactors and vitamins, xenobiotics biodegradation and metabolism, membrane transport, signal transduction, cell motility, and transport and catabolism with a concurrent decrease in the relative abundance of carbohydrate metabolism, metabolism of terpenoids and polyketides, nucleotide metabolism, folding, sorting, and degradation, replication and repair, transcription, and translation ($p < 0.05$ for all; Figure 4.5; Table SI 4.10). The transition-zone microbiome also experienced an increase from T0 to T30 in the relative abundance of functional genes associated with glycan biosynthesis and metabolism, lipid metabolism, and cell growth and depth as well as a concurrent decrease in signaling molecules and cellular community ($p < 0.05$ for all; Figure 4.5; Table SI 4.10).

The change in microbial gene expression in response to short-term and extended thaw duration using TPM-normalized metatranscriptomes annotated at KEGG tiers II-IV could only be determined within the active-layer microbiome. Furthermore, no comparisons can be made for differential gene expression (DGE) between incubation time points T0 or T7 within the transition-zone and permafrost microbiomes due to the lack of sufficient RNA yield for sequencing from the soil samples (see section *4.3.6 Metatranscriptome Assembly* for details). Our DGE analysis in the active-layer microbiome indicated that the greatest differential expression of KEGG orthologs (KOs) occurred between incubation time points T7 to T30 (8.5% of KOs) compared to time points

T0 to T7 (4.1% of KOs; FDR < 0.05 for all; Table SI 4.11). These DGE results represent a significant change in the expression of thousands of KOs within the active-layer microbiome and include many KOs associated with the significant KEGG tier II-IV pathways described above.

4.4.4 Fe-Mediated Genomic Potential and Gene Expression During Thaw

The genomic potential and gene expression for microbial pathways associated with Fe metabolism, Fe acquisition, and Fe cycling were quantified from the metagenome and metatranscriptome, respectively, using FeGenie (Garber et al. 2020). Counts within each Fe functional gene category were summarized as their relative abundance against the sum of all identified Fe functional genes (Figure 4.6; Table SI 4.12). The mean relative abundance of Fe metabolism genes associated with Fe regulation and Fe storage in the metagenome significantly decreased by T30 compared to T0 in all soil layer microbiomes (ANOVA; $p < 0.05$ for all; Figure 4.6A; Table SI 4.12). The mean relative abundance of Fe regulation and Fe storage genes expressed in the metatranscriptome significantly decreased in the active-layer microbiome by T7 and T30 compared to T0 (Fe regulation: -21.5% T7, -25.4% T30; Fe storage: -9.1% T7, -6.7% T30; $p < 0.05$ for all; Figure 4.6B; Table SI 4.12). The mean relative abundance of Fe acquisition genes associated with Fe transport in the metagenome significantly increased in the active-layer microbiome by T30 but did not change in the transition-zone microbiome or the permafrost microbiome ($p > 0.05$ for all; Figure 4.6A; Table SI 4.12). However, the mean relative abundance of Fe acquisition genes associated with siderophore transport did significantly increase by T30 compared to T0 within the active-layer microbiome (+7.5), transition-zone microbiome (+22.4%), and permafrost microbiome (+25.5%; $p < 0.001$ for all; Figure 4.6A; Table SI 4.12). Likewise, there was a significant increase in the mean relative abundance of expressed genes associated with siderophore transport in the active-layer microbiome by T7 (+25.8%) and T30 (+26.7%) compared to T0 ($p < 0.001$ for both; Figure 4.6B; Table SI 4.12). The mean relative abundance of Fe cycling genes associated with Fe oxidation and Fe reduction in the metagenome significantly increased in the transition-zone microbiome and the permafrost microbiome but not in the active-layer microbiome by T30 compared to T0 (Fe oxidation: +4.8% TZ, +4.3% PF; Fe reduction: +3.9% TZ, +2.6% PF; $p < 0.05$ for all; Figure 4.6A; Table SI 4.12).

4.4.5 Carbon Degradation Genomic Potential and Gene Expression During Thaw

The relative abundance of functional genes associated with the degradation of aromatic compounds, pyruvate metabolism, and methane metabolism was investigated in the metagenome. This includes the KEGG tier IV categories of aromatic compound degradation (KO path 01220), benzoate degradation (KO path 00362), aminobenzoate degradation (KO path 00627), fluorobenzoate degradation (KO path 00364), pyruvate metabolism (KO path 00620), and methane metabolism (KO path 00680; Table 2). There was a significant increase in the relative abundance of genecalls associated with the degradation of aromatic compounds, benzoate degradation, aminobenzoate degradation, fluorobenzoate degradation, and pyruvate metabolism in all soil layer microbiomes by T30 compared to T0 ($p < 0.05$ for all; Table 4.2), with the exception of fluorobenzoate degradation and pyruvate metabolism in the active-layer microbiome ($p > 0.05$ for both; Table 4.2). Notably, there was a significant decrease in methane metabolism in the transition-zone and permafrost microbiomes by T30 compared to T0 ($p < 0.05$ for all; Table 4.2). We also found a significant increase in the relative abundance of genecalls associated with flagellar assembly (Cellular Processes; KO path 02040) in all soil layer microbiomes by T30 compared to T0 ($p < 0.05$ for all; Table 4.2). Many of the KOs that were significantly differentially expressed by T30 in the active-layer metatranscriptome were also annotated as the degradation of aromatic compounds, benzoate degradation, pyruvate metabolism, methane metabolism, and flagellar assembly (DGE; FDR < 0.05 for all; Table SI 4.11).

4.5 Discussion

A laboratory incubation experiment simulated thaw for up to 30 days under representative field conditions (temperature of 4°C and anoxic) along the depth profile of an Fe-rich organic tundra. We found no measurable microbial response to short-term (7-day) thaw duration in any soil layer from the upper active layer into the deeper permafrost regardless of initial differences in microbiome composition and genomic potential between soil layers. However, we did find a substantial microbial response to extended (30-day) thaw duration in all soil layers that was driven primarily by the growth of bacterial taxa known to possess Fe cycling capabilities. The genomic potential and gene expression associated with Fe-cycling pathways and OC degradation increased concurrently within all soil layers during the incubation, indicating a strong coupling between Fe(III) reduction, Fe(II) oxidation, and OC degradation following thaw. These findings suggest

that microbial growth and gene expression during extended thaw was mediated primarily by the accessibility of reactive Fe under anoxic conditions in thawing permafrost soils. The substantial Fe-mediated growth of bacterial taxa during extended thaw will likely impact the microbial degradation of Fe-bound OC and CO_2 production as climate warms in the Arctic.

4.5.1 Soil Microbiome Composition Differs between Soil Layers

Previous research at the Imnavait Creek field site in northern Alaska showed that microbiome composition differed by depth along the soil profile in wet sedge tundra (Chapter 3; Romanowicz & Kling, *In Review*). Here, our taxonomic results between soil layers are generally consistent with that study and with numerous studies conducted in arctic tundra (Deng et al. 2015, Kim et al. 2016, Singh et al. 2017, Tripathi et al. 2018, Varsadiya et al. 2021). Notably, we found significant differences in dominant bacterial taxa between the active-layer microbiome and the underlying transition-zone and permafrost microbiomes in the initial (frozen) soils analyzed at T0 (Figure 4.1) that were mostly due to variations in the abundance of Acidobacteria, Actinobacteria, Alphaproteobacteria, Bacteroidetes, Caldiserica, Firmicutes, and Verrucomicrobia (Figure 4.2). The transition-zone and permafrost microbiomes, with greater relative abundance of Actinobacteria, Caldiserica, and Firmicutes, may represent a subset composition of relic taxa originally present when the permafrost formed (Willerslev et al. 2004, Kraft et al. 2015, Liang et al. 2019). For example, the high relative abundance of Actinobacteria in the transition-zone and permafrost microbiomes is likely due to their ability to form dormant and spore-like structures (Wunderlin et al. 2014) that can survive radiation, starvation, and extreme desiccation in the harsh permafrost environment (Johnson et al. 2007, De Vos et al. 2009). Likewise, Firmicutes are known to form endospores under the stressful conditions associated with permafrost, and they have been shown to persist at higher relative abundance than non-endospore forming taxa common in the active-layer microbiome (Burkert et al. 2019). The loss of non-endospore forming taxa in the transition-zone and permafrost microbiomes likely contributes to their significantly lower taxonomic alpha diversity compared to the active-layer microbiome (Table SI 4.3) and may differentially affect the microbial response to extended thaw duration between soil layers based on the recovery rate and growth of each taxon from its dormant state (see Lennon 2020 for discussion on increasing dormancy with soil depth).

4.5.2 Soil Microbiome Response to Short-Term Thaw Duration

Results clearly showed that the composition of the transition-zone and permafrost microbiomes differed from that in the seasonally thawed active layer at the beginning and end of the experiment (Figures 4.1 and 4.2). Yet, previous studies have documented that after only a short-term thaw duration of 2 days (at 5°C incubation), the composition of the permafrost microbiome and its functional genes can shift rapidly and start to resemble the composition found in the seasonally thawed active-layer of a black-spruce forest site in northern Alaska (Mackleprang et al. 2011). In a separate incubation study conducted on permafrost soils collected from moist acidic tussock tundra in the Imnavait Creek region, it was found that the transcriptional profiles of expressed functional genes rapidly shifted towards ribosomal protein production for microbial growth and enzymatic genes associated with OC degradation following a short-term thaw duration of 11 days (at 4°C incubation; Coolen & Orsi 2015). In both incubation studies, there was a significant and rapid shift in the composition of the permafrost microbiome towards the composition of the active-layer microbiome following short-term thaw duration regardless of initial differences in dominant vegetation and abiotic soil properties between sampling sites (Mackleprang et al. 2011, Coolen & Orsi 2015).

However, the results of these lab-based studies correspond weakly or not at all with multi-year *in situ* soil warming experiments in tundra soils that show little or no change in the composition of the permafrost microbiome following a moderate increase in soil temperatures (Rinnan et al. 2007, Biasi et al. 2008, Lamb et al. 2011). For example, Biasi et al. (2008) detected no significant change in soil microbiome composition following two years of experimental surface warming (+3.6°C annually relative to control plots) in a Siberian dwarf-shrub tundra. Rinnan et al. (2007) demonstrated that more than 10 years of experimental surface warming (+4°C annually) was necessary to develop a significant change in soil microbiome composition in a subarctic shrub-heath tundra. In contrast, in Lamb et al. (2011), results from 16 years of experimental surface warming (+2°C annually) in a High Arctic shrub-heath tundra showed a complete lack of directional shifts in the soil microbiome as a whole. In each of these studies, moderate heating at the soil surface (+2 to +4°C annually) to mimic the natural extension of summer thaw into the permafrost increased belowground nutrient availability that strongly affected the plant communities, but the soil microbiome did not respond to warming. This lack of response also

limited any potential change in greenhouse gas fluxes in response to the experimental treatment regardless of initial differences in dominant vegetation and abiotic soil properties between sampling sites (Rinnan et al. 2007, Biasi et al. 2008, Lamb et al. 2011).

Our laboratory-based incubation experiment showed no significant microbiome response to a short-term thaw duration of 7 days (at 4°C) in wet sedge tundra soil. The composition of the microbiome in all three soil layers remained unchanged after 7 days of thaw from their initial frozen composition, with the transition-zone and permafrost microbiomes distinct from the active-layer microbiome yet indistinguishable from each other (Figure 4.1A). There was also no significant change in normalized gene counts (mean GPM) associated with any KEGG tier II or III functional pathways annotated from the metagenome following short-term thaw duration, with the exception of an increase in carbohydrate metabolism and decrease in cell growth and death in the active-layer microbiome (Figure 4.5). Only a small proportion of functional genes in the active-layer microbiome was significantly differentially expressed in the metatranscriptome following short-term thaw (4.1%; Table SI 4.11). Most of these differentially expressed genes were associated with an increase in carbohydrate metabolism expressed from the same taxa present at the start of the incubation experiment as well as from genes associated with Fe-cycling taxa (e.g., ribosomal proteins, flagellar assembly) that preceded their substantial growth during extended thaw over 30 days (Figures 4.3 and 4.4). The lack of quantifiable RNA extracted from the initial (T0) and short-term (T7) thaw duration transition-zone and permafrost samples indicates that the microbiomes of these soil layers were incapable of responding rapidly, for at least 7 days. These short-term thaw duration results between all soil layers in wet sedge tundra are more consistent with field-based warming experiments showing little to no change in the soil microbiome following years of moderate heating (+2 to +4°C surface warming; Rinnan et al. 2007, Biasi et al. 2008, Lamb et al. 2011).

The overall lack of a rapid microbial response to short-term thaw along the soil profile of wet sedge tundra (presented here) as compared to the substantial short-term microbial changes observed in thawing black spruce forest and moist acidic tussock tundra soils (Mackelprang et al. 2011, Coolen & Orsi 2015, respectively) is likely influenced by differences in dominant vegetation and soil abiotic properties that influence the composition of the microbiome between sampling sites. For example, geographic distance between sites and variations in landscape topography control dominant plant species and their litter biochemistry that influences the composition of the

soil microbiome (Judd et al. 2006, Zak & Kling 2006, Malard et al. 2019). At the black spruce forest site in sub-arctic Alaska, the soil microbiome at permafrost depths was initially dominated by taxa belonging to Bacteroidetes, Firmicutes, and Proteobacteria, but quickly shifted in dominance towards Actinobacteria and Chloroflexi after 2 days of thaw (Mackelprang et al. 2011). Likewise, the soil microbiome at a moist acidic tussock tundra site was dominated by Bacteroidetes and Firmicutes, with active taxa transcribing genes for stress response, survival strategies, and maintenance processes (Coolen & Orsi 2015). In contrast, in this study the soil microbiome in wet sedge tundra was dominated by anaerobic and fermentative taxa belonging to Actinobacteria, Caldiserica, Deltaproteobacteria, and Firmicutes at the start of the incubation, where most of these taxa naturally dominate the microbiome under the anoxic redox conditions following thaw such that no shift in their abundance was observed after 7 days of thaw (Figure 4.2).

Additional differences in soil type (organic vs. mineral) can also influence the composition of the soil microbiome (Malard et al. 2019). Specifically, the black spruce forest and moist acidic tussock tundra sites have a surface organic soil horizon (~10-20 cm thick) underlain by a dense mineral soil horizon within the active layer that extends into the permafrost (Mackelprang et al. 2011, Coolen & Orsi 2015). In contrast, the wet sedge tundra site in the valley bottom has an organic soil horizon that extends for meters from the soil surface into the permafrost before encountering mineral soil. Previous research in moist acidic tussock tundra has shown distinct differences in microbiome composition between organic and mineral soil horizons even within the seasonally-thawed active layer depths (Koyama et al. 2014, Romanowicz & Kling, *In Review*). This suggests that the initial composition of the microbiome within the organic soil horizon of the wet sedge tundra site differs from the microbiome composition found at corresponding depths within the mineral soil horizon of the black spruce forest and moist acidic tussock tundra sites. Together, these differences in dominant vegetation and soil abiotic properties between sampling sites likely contribute to initial differences in microbiome composition that differentially affect each microbiome's ability to respond rapidly to short-term thaw duration. Here, our results suggest that short-term thaw duration is likely incapable of inducing a rapid shift in whole-community composition or genomic potential in any soil layer along the depth profile of organic wet sedge tundra, which is the dominant tundra type of arctic lowlands and coastal plains.

4.5.3 Soil Microbiome Response to Extended Thaw Duration

An extended thaw duration of 30 days (at 4°C incubation) was clearly sufficient to induce a microbiome-wide shift in composition and genomic potential, especially within the transition-zone and permafrost microbiomes of wet sedge tundra (Figures 4.1, 4.2, and 4.5). At all soil depths, Fe(III)-reducing bacterial taxa increased in relative and absolute abundance during extended thaw to become the most dominant taxa in each soil layer microbiome (Figures 4.2, 4.3; Table 4.1). *Rhodoferax* spp., most closely related to the Fe(III)-reducing bacterium *R. ferrireducens*, increased by ~62% in relative abundance in both the transition-zone and permafrost microbiomes compared to an almost undetectable abundance at the start of the incubation experiment (Table 4.1). This was equivalent to an increase of more than 4-orders of magnitude in the absolute abundance of *Rhodoferax* 16S gene copies in both soil layers after 30 days of thaw (Figure 4.3A). Emerson et al. (2015) previously found that *R. ferrireducens* was the most abundant OTU recovered (> 50% of total reads) from numerous microbial iron mats occurring in the Imnavait Creek region, suggesting the dominant role of this Fe(III)-reducing taxon in Fe-rich tundra surface soils; the results in the current study indicate that it also can dominate in deeper, Fe-rich soils. *R. ferrireducens* is a facultative Fe(III)-reducing anaerobe capable of dissimilatory Fe(III) reduction when coupled with OC degradation via acetate and benzoate oxidation to CO_2 (Finneran et al. 2003). As such, we found a concurrent increase in gene abundance associated with benzoate, aminobenzoate, and fluorobenzoate degradation as well as pyruvate metabolism after 30 days of thaw, especially within the transition-zone and permafrost microbiomes (Table 4.2). Pyruvate is used to generate acetate that can be oxidized, along with benzoate and its derivatives, to CO_2 when coupled with dissimilatory Fe(III) reduction by *R. ferrireducens* (Finneran et al. 2003). Together, these results indicate strong coupling between Fe(III) reduction and the degradation of OC by *Rhodoferax* spp. following extended permafrost thaw.

We also found that *Gallionella* spp., a microaerophilic Fe(II)-oxidizing autotroph, increased by ~8% in relative abundance in the active-layer microbiome and by ~2-3% in both the transition-zone and permafrost microbiomes (Table 4.1). This was also equivalent to an increase of nearly 4-orders of magnitude in the absolute abundance of *Gallionella* 16S gene copies in each soil layer after 30 days of thaw, with absolute growth rates similar to those observed for *Rhodoferax* spp. (Figure 4.4). *Gallionella* spp. is capable of oxidizing Fe(II) using CO_2 as an electron acceptor, where CO_2 is reduced back to acetate (Hallberg & Ferris 2004). These Fe-

cycling metabolic processes between *Rhodoferax* spp. and *Gallionella* spp. appear to be complementary to each other, where *Rhodoferax* oxidizes acetate and benzoate to CO_2 in order to facilitate Fe(III) reduction while *Gallionella* reduces CO_2 back to acetate when oxidizing Fe(II). Thus, the end products from these two species' energy metabolism are also each other's starting products that likely perpetuates their extreme Fe-mediated growth.

However, the Fe-cycling metabolic processes facilitating *Rhodoferax* and *Gallionella* growth assumes that the incubation conditions during the thaw experiment were sub-oxic rather than strictly anoxic. This is because the microaerophilic *Gallionella* spp. requires sub-oxic conditions to support its growth (0.1-1% O_2 concentration; Hanert 1981). Meanwhile, *R. ferrireducens* is one of only two known facultative Fe(III)-reducing anaerobes capable of reducing Fe(III) under sub-oxic conditions (Finneran et al. 2003). Further support for assuming sub-oxic rather than anoxic incubation conditions comes from the lack of growth of *Geobacter* spp. (Deltaproteobacteria) throughout the thaw duration experiment (< 2% relative abundance, Table 4.1). *Geobacter* is a strictly obligate Fe(III)-reducing anaerobe (Lovely & Chapelle 1995) and typically the dominant Fe(III)-reducer in the anoxic zone of Fe-cycling biofilms in tundra soils (Emerson et al. 2015). The lack of growth of *Geobacter* spp. coupled with the substantial growth of *Rhodoferax* spp. and *Gallionella* spp. strongly suggests that the incubation conditions were sub-oxic and not anoxic.

Anoxic (and sub-oxic) redox conditions commonly occur in thawing permafrost soils and promote anaerobic and fermentative microbial processes that are responsible for the majority of OC degradation in low-lying tundra (Smith et al. 2005, Sturtevant & Oechel 2013, Herndon et al. 2015). Tundra soils near Imnavait Creek are rich in reactive Fe minerals (Emerson et al. 2015) that provide a terminal electron acceptor for anaerobic respiration (Dettling et al. 2006, Lipson et al. 2010). The reductive dissolution of Fe(III) enhances the degradation of permafrost OC through substantial CO_2 formation following thaw, accounting for 40 to 60% of total ecosystem respiration in low-lying tundra regions (Lipson et al. 2013). Fe(III)-reducing bacteria can also suppress the production of CH_4 by outcompeting methanogenic archaea for substrates (Lipson et al. 2012, Miller et al. 2015). Our results suggest that the oxidation of acetate by *Rhodoferax* spp. when coupled with Fe(III) reduction will limit acetate availability for methanogenesis via the acetoclastic pathway, which is a major methanogenic pathway in organic tundra soils (Whiticar 1999). Dissimilatory Fe(III) reduction is more thermodynamically favorable than methanogenesis

under anoxic conditions (Lipson et al. 2013) and there will likely be more CO_2 production than CH_4 production in these Fe-rich permafrost soils following extended thaw duration. Consistent with this idea, there was a significant decrease in gene abundance annotated for methane metabolism, mostly associated with pathways of methanogenesis and not methanotrophic or methylotrophic pathways (Table 4.2). These results are also consistent with recent studies investigating *in situ* rates and pathways of Fe(III)-reduction in thawing permafrost hillslopes, where substantial growth of *Rhodoferax* spp. and other Fe(III)-reducing taxa promoted greater gene expression for dissimilatory Fe(III) reduction that suppressed acetoclastic methanogenesis (Patzner et al. 2022b).

4.6 Conclusion

Results from this study show that Fe cycling promotes substantial microbial growth in the absolute abundance (+2 to +4 orders of magnitude) of Fe(III)-reducing and Fe(II)-oxidizing bacteria in permafrost soils during an extended thaw duration of 30 days in wet sedge tundra. These shifts were dominated by the Betaproteobacteria Fe(III)-reducing bacterium *Rhodoferax* spp. and Fe(II)-oxidizing bacterium *Gallionella* spp., especially within the transition-zone and permafrost microbiomes. The active-layer microbiome experienced a similar shift in composition with an increase in Fe-cycling taxa, but the magnitude of this shift was much more limited (~20% increase in microbiome relative abundance) compared to the shifts in transition-zone and permafrost microbiomes (~83% and ~78% increase, respectively). Our results suggest that Fe(III) minerals provide a terminal electron acceptor for pathways of anaerobic respiration associated with the degradation of aromatic compounds such as acetate and benzoate, while suppressing CH_4 metabolism. Thus, the growth of Fe(III)-reducing bacteria is likely coupled with greater OC degradation and CO_2 production rather than acetoclastic methanogenesis under anoxic conditions during the initial 30 days of thaw in these soils. As such, we also found evidence for a concurrent increase in the genomic potential and gene expression of Fe(III)-reduction and the degradation of aromatic compounds during the incubation experiment in all soil layers, indicated strong coupling between Fe(III) reduction and OC degradation. As thaw duration increases at depth due to climate warming, it is likely that previously frozen Fe-rich permafrost soils will initially promote greater growth and gene expression from Fe(III)-reducing bacteria that could release Fe-bound OC to microbial degradation and eventual respiration as CO_2. The immediate implications of these

findings apply broadly across the Arctic because wet sedge tundra constitutes the major tundra type of low-lying regions along the foothills and coastal plains. However, the long-term implications of Fe-mediated microbial growth and OC degradation following years of extended thaw duration, especially within the transition-zone and permafrost soil depths, remain unknown.

4.7 Acknowledgement

I thank Rose Cory, Jason Dobkowski, Natasha Griffin, Ted Bambakidis, and colleagues of the NSF Arctic LTER and Toolik Lake Field Station for assistance. I acknowledge the University of Michigan Microbiome Core, the Advanced Genomics Core, and the Advanced Research Computing Technology Services. Support for this work came from NSF grants DEB-1637459, DEB-1754835, and OPP-1936769. Additional block grant funding was provided by the Department of Ecology and Evolutionary Biology, University of Michigan.

Table 4.1 Relative Abundance of Dominant Fe-Cycling Taxa. Relative abundance (mean ± SD) of dominant Fe(III)-reducing and Fe(II)-oxidizing bacterial taxa recovered from 16S rRNA amplicon sequence variants (ASVs). Percent change values denote the mean change in relative abundance for each Fe-related taxon compared to incubation time point T0 within each soil layer microbiome. Bold values indicate a significant difference ($p < 0.05$) in mean relative abundance for each Fe-related taxon compared to incubation time point T0 within each soil layer microbiome.

Soil Layer & Timepoint	Fe(III)-Reduction								Fe(II)-Oxidation	
	Rhodoferax spp.		*Clostridium* spp.		*Pseudomonas* spp.		*Geobacter* spp.		*Gallionella* spp.	
	Relative Abundance (%)	% Change from T0	Relative Abundance (%)	% Change from T0	Relative Abundance (%)	% Change from T0	Relative Abundance (%)	% Change from T0	Relative Abundance (%)	% Change from T0
Active Layer										
T0	0.2 ± 0.0	-	0.5 ± 0.0	-	< 0.1	-	0.4 ± 0.2	-	0.3 ± 0.2	-
T7	0.6 ± 0.3	0.4	1.1 ± 0.3	0.6	< 0.1	0.0	0.6 ± 0.2	0.2	0.3 ± 0.2	0.0
T30	**10.5 ± 0.9**	**10.3**	0.6 ± 0.3	0.1	< 0.1	0.0	1.8 ± 1.0	1.4	**8.0 ± 5.2**	**7.7**
Transition Zone										
T0	< 0.1	-	3.3 ± 0.7	-	< 0.1	-	0.2 ± 0.1	-	< 0.1	-
T7	< 0.1	0.0	3.0 ± 0.4	-0.3	< 0.1	0.0	0.3 ± 0.1	0.1	< 0.1	0.0
T30	**62.3 ± 13.7**	**62.3**	**9.2 ± 4.3**	**5.9**	9.9 ± 17.2	9.9	**< 0.1**	**-0.2**	**1.6 ± 0.8**	**1.6**
Permafrost										
T0	< 0.1	-	3.2 ± 0.6	-	< 0.1	-	0.3 ± 0.1	-	< 0.1	-
T7	< 0.1	0.0	3.1 ± 0.5	-0.1	< 0.1	0.0	0.4 ± 0.1	0.1	< 0.1	0.0
T30	**62.7 ± 9.1**	**62.7**	**4.9 ± 0.5**	**1.7**	7.5 ± 6.5	7.5	**< 0.1**	**-0.3**	**3.1 ± 1.7**	**3.1**

Table 4.2 KEGG Tier IV Pathways Related to Carbon Degradation. Normalized gene counts (GPM; mean ± SD) of KEGG Tier IV metabolism pathways related to the degradation of aromatic compounds, pyruvate metabolism, and methane metabolism, as well as cellular processes related to flagellar assembly derived from the metagenome. Bold values indicate a significant difference ($p < 0.05$) in mean counts for each KEGG pathway compared to incubation time point T0 within each soil layer microbiome.

Soil Layer & Time Point	Metabolism						Cellular Processes
	Aromatic Compound Degradation	Benzoate Degradation	Aminobenzoate Degradation	Fluorobenzoate Degradation	Pyruvate Metabolism	Methane Metabolism	Flagellar Assembly
Active Layer							
T0	5,144 ± 162	1,108 ± 44	388 ± 18	796 ± 37	4,576 ± 63	1,616 ± 150	2,535 ± 118
T7	5,008 ± 564	1,086 ± 204	346 ± 58	778 ± 24	4,737 ± 135	1,607 ± 35	2,413 ± 242
T30	**6,873 ± 778**	**1,869 ± 268**	**603 ± 108**	990 ± 130	4,781 ± 194	1,682 ± 202	**6,459 ± 447**
Transition Zone							
T0	3,066 ± 133	198 ± 36	46 ± 8	160 ± 21	4,405 ± 209	1,906 ± 277	289 ± 78
T7	2,957 ± 173	166 ± 28	37 ± 7	143 ± 14	4,309 ± 112	1,853 ± 515	236 ± 35
T30	**15,354 ± 526**	**4,253 ± 89**	**1,002 ± 130**	**1,437 ± 125**	**5,551 ± 192**	**752 ± 71**	**15,357 ± 947**
Permafrost							
T0	3,266 ± 73	199 ± 27	43 ± 3	144 ± 5	4,164 ± 140	2,097 ± 237	189 ± 50
T7	3,210 ± 65	261 ± 28	43 ± 10	177 ± 24	4,282 ± 76	2,643 ± 306	204 ± 34
T30	**14,224 ± 931**	**4,151 ± 150**	**961 ± 153**	**1,469 ± 59**	**5,555 ± 66**	**657 ± 84**	**16,865 ± 1,097**

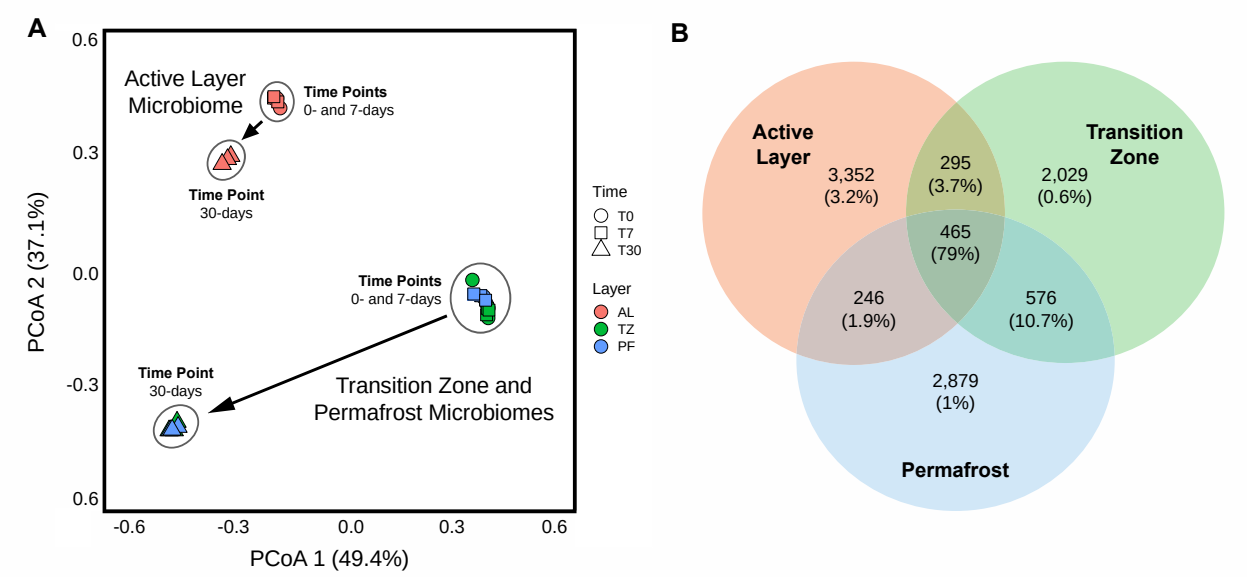

Figure 4.1 Beta Diversity of 16S rRNA ASVs within each Soil Layer Microbiome. Ordination (A) from principal coordinate analysis (PCoA) based on Bray-Curtis dissimilarity in the relative abundance of 16S rRNA amplicon sequence variants (ASVs) within each soil layer microbiome. Each point represents an individual sampling replicate from each soil layer collected at each incubation time point during the experiment (N = 27). Venn diagram (B) of unique and shared 16S rRNA amplicon sequence variants (ASVs) for each soil layer microbiome. The total ASVs of each soil layer and those ASVs shared between soil layers are shown as counts. The relative abundance that each ASV count represents is shown as a percentage in parentheses.

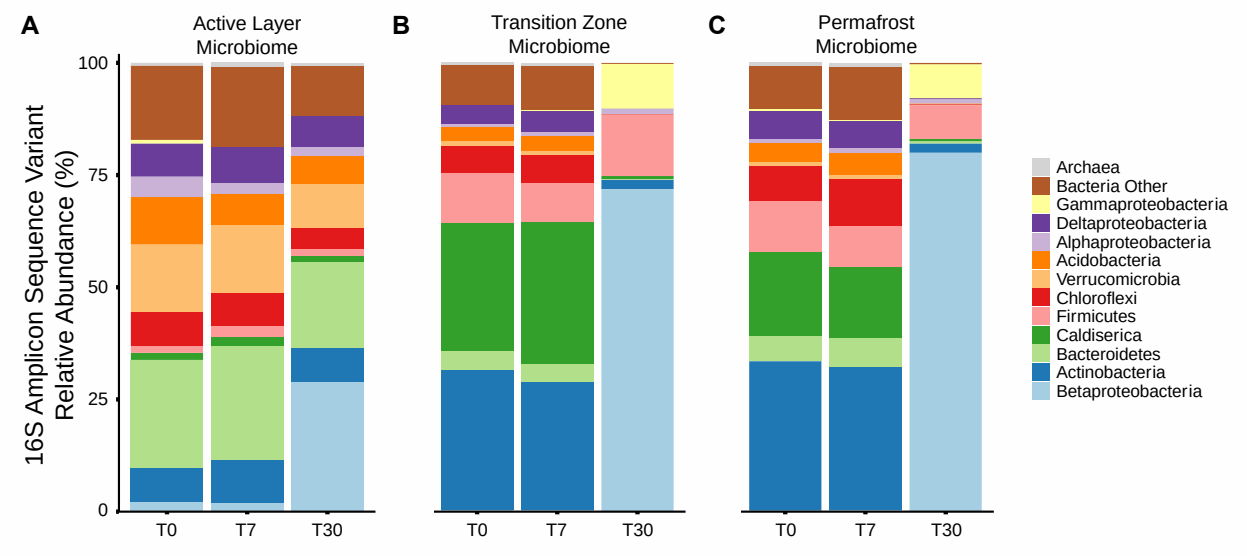

Figure 4.2 Relative Abundance of Dominant Bacteria and Archaea. Relative abundance (mean %) of dominant bacterial phyla and archaea within the (A) active-layer microbiome, (B) transition-zone microbiome, and (C) permafrost microbiome derived from the 16S rRNA amplicon sequence variants (ASVs). Proteobacteria are resolved to the class level.

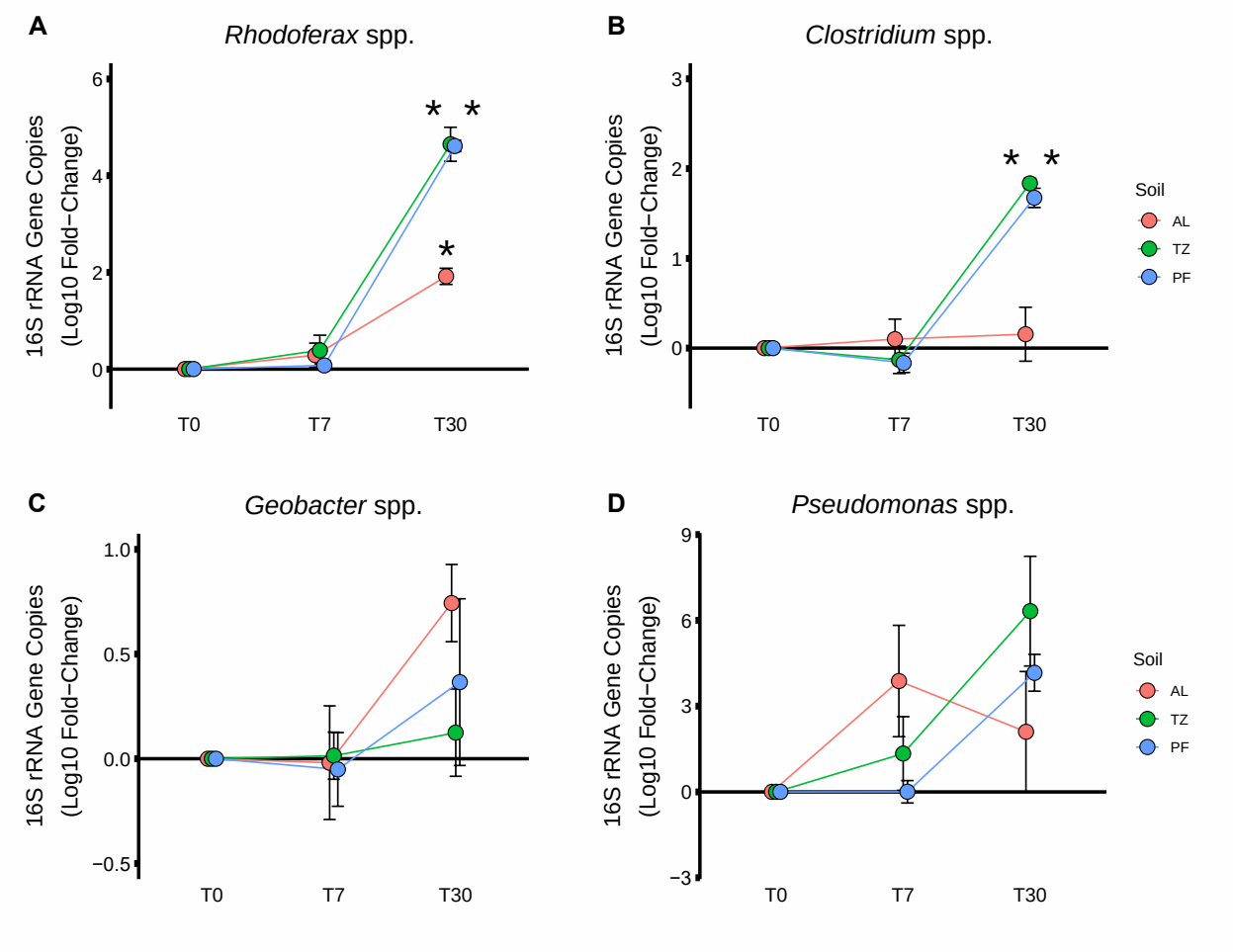

Figure 4.3 Change in Absolute Abundance of Dominant Fe(III)-Reducing Taxa. Log_{10} fold-change (mean ± SE) in absolute abundance of 16S rRNA gene copies for the dominant Fe(III)-reducing bacterial taxa (A) *Rhodoferax* spp., (B) *Clostridium* spp., (C) *Geobacter* spp., and (D) *Pseudomonas* spp. compared to incubation sampling time point T0 within each soil layer microbiome. An asterisk indicates a significant Log_{10} fold-change ($p < 0.05$) compared to incubation time point T0 within each soil layer microbiome.

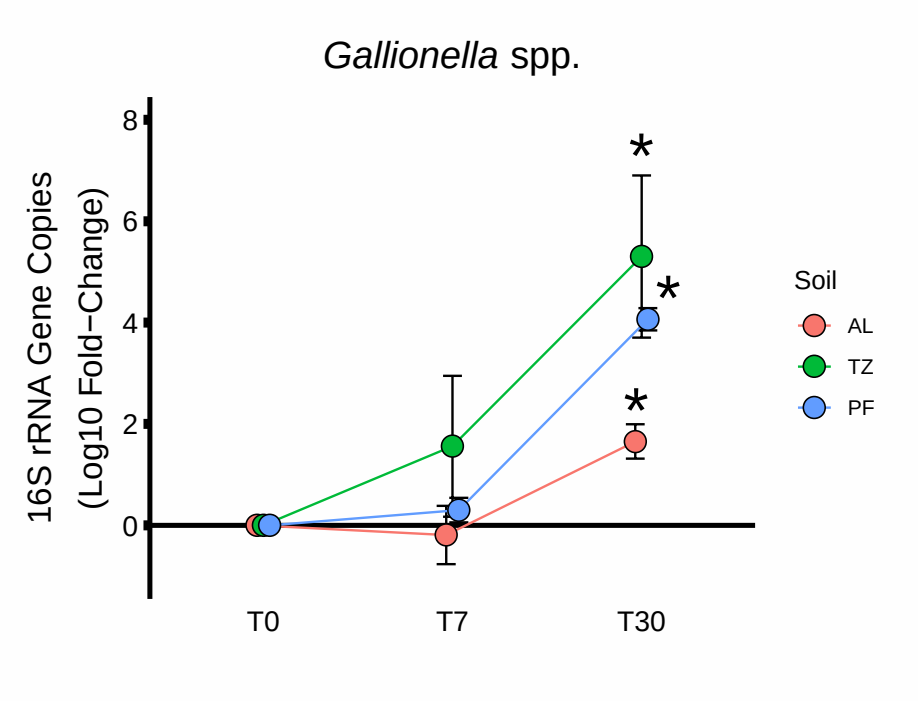

Figure 4.4 Change in Absolute Abundance of Dominant Fe(II)-Oxidizing Taxon. Log_{10} fold-change (mean ± SE) in absolute abundance of 16S rRNA gene copies for the Fe(II)-oxidizing *Gallionella* spp. compared to incubation time point T0 within each soil layer microbiome. An asterisk indicates a significant Log_{10} fold-change ($p < 0.05$) compared to incubation time point T0 within each soil layer microbiome.

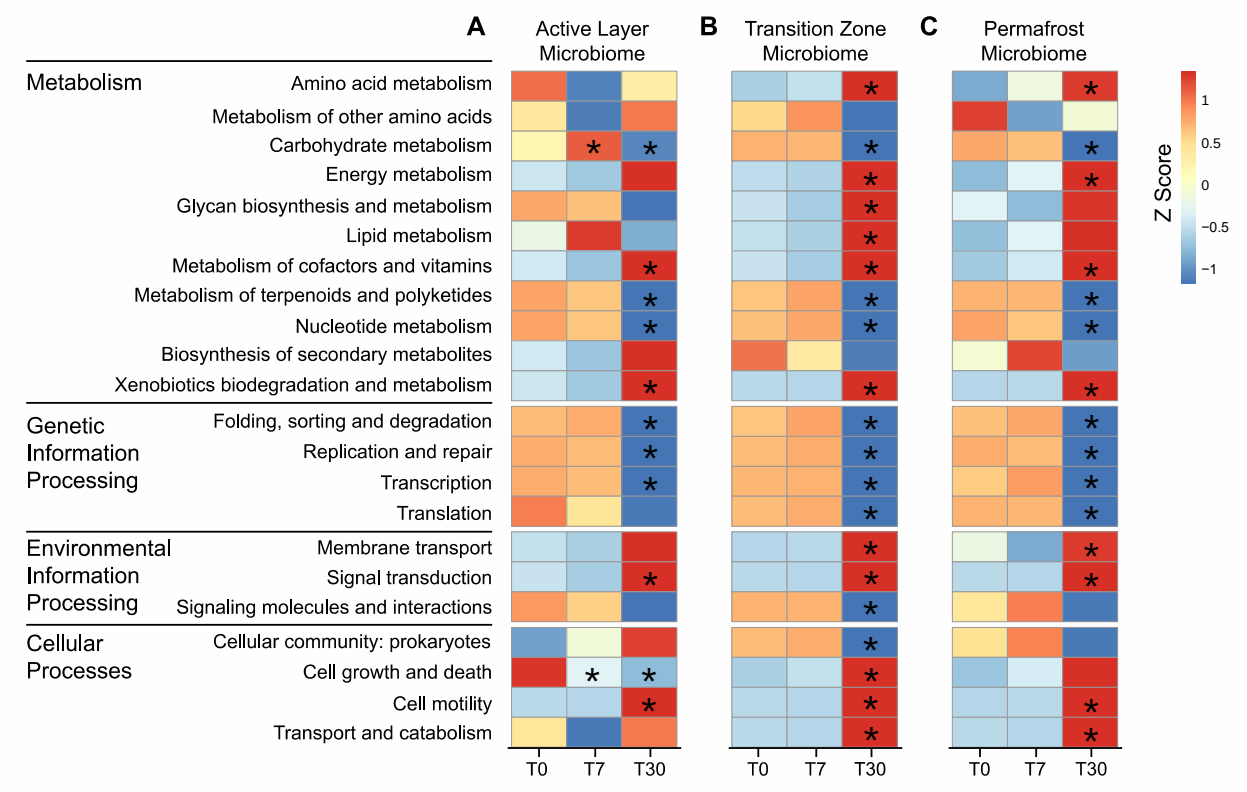

Figure 4.5 Genomic Potential within each Soil Layer Microbiome. Heatmap of genomic potential in the (A) active-layer microbiome, (B) transition-zone microbiome, and (C) permafrost microbiome based on Z-score transformations of the mean relative abundance of GPM-normalized metagenome genecalls belonging to KEGG tier III functional pathways for each incubation time point within each soil layer microbiome. An asterisk indicates a significant change ($p < 0.05$) in mean relative abundance of genecalls for each KEGG pathway compared to incubation time point T0 within each soil layer microbiome.

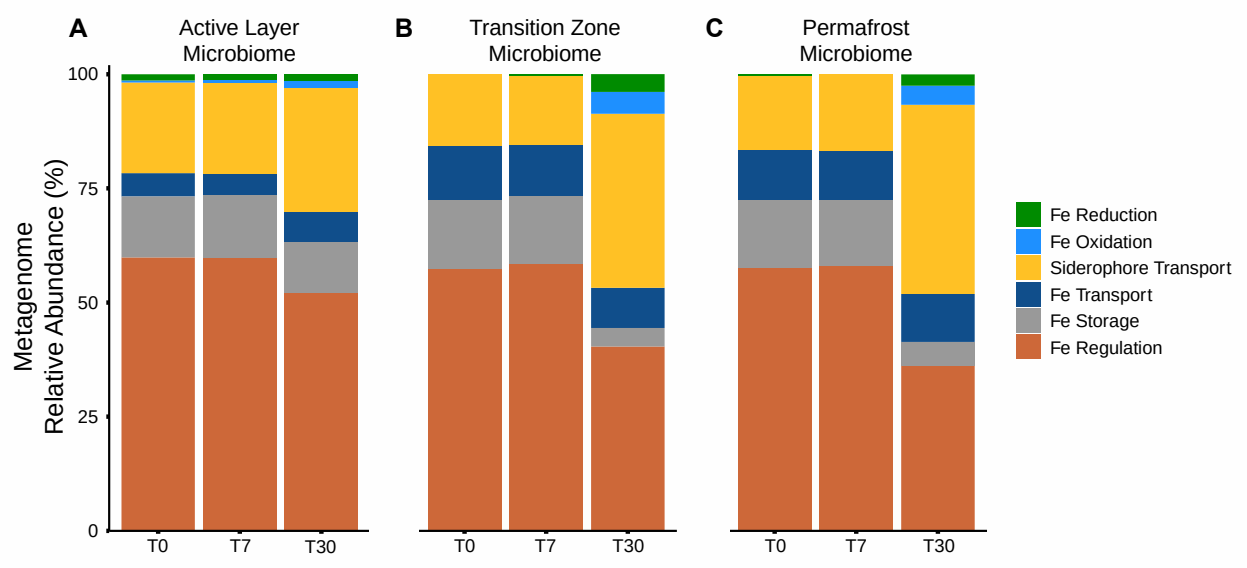

Figure 4.6 Fe-Mediated Functional Gene Potential. Relative abundance (mean %) of each iron (Fe)-related functional gene category derived from the FeGenie analysis in the (A) active-layer microbiome, (B) transition-zone microbiome, and (C) permafrost microbiome based on contig assemblies for each soil layer microbiome.

Table SI 4.3 Supplemental 16S rRNA Amplicon Sequence Summary. Summary of 16S rRNA amplicon (DNA) sequence reads with alpha diversity metrics. The sample with the lowest total reads is denoted in BOLD (PF.T30.2) and represents the read rarefication cutoff value used for the entire dataset.

Sample ID	Soil Layer	Time Point	Incubation Replicate	Total Reads	Rarified Reads	ASV Unique	ASV Diversity (H')
AL.T0.1	AL	T0	1	200,301	71,245	1,071	4.91
AL.T0.2	AL	T0	2	317,361	71,245	2,253	5.87
AL.T0.3	AL	T0	3	410,040	71,245	2,551	5.99
AL.T7.1	AL	T7	1	329,477	71,245	1,450	5.43
AL.T7.2	AL	T7	2	342,483	71,245	1,229	5.07
AL.T7.3	AL	T7	3	390,243	71,245	1,451	5.32
AL.T30.1	AL	T30	1	216,755	71,245	1,009	4.81
AL.T30.2	AL	T30	2	280,778	71,245	999	4.66
AL.T30.3	AL	T30	3	252,338	71,245	1,053	4.71
TZ.T0.1	TZ	T0	1	208,763	71,245	969	4.23
TZ.T0.2	TZ	T0	2	182,398	71,245	665	3.71
TZ.T0.3	TZ	T0	3	214,469	71,245	938	4.27
TZ.T7.1	TZ	T7	1	227,446	71,245	799	3.84
TZ.T7.2	TZ	T7	2	220,625	71,245	868	4.08
TZ.T7.3	TZ	T7	3	247,652	71,245	1,018	4.27
TZ.T30.1	TZ	T30	1	99,212	71,245	83	1.08
TZ.T30.2	TZ	T30	2	118,575	71,245	93	1.44
TZ.T30.3	TZ	T30	3	151,341	71,245	91	1.56
PF.T0.1	PF	T0	1	247,561	71,245	1,032	4.48
PF.T0.2	PF	T0	2	239,203	71,245	1,055	4.56
PF.T0.3	PF	T0	3	243,173	71,245	984	4.35
PF.T7.1	PF	T7	1	231,466	71,245	1,145	4.74
PF.T7.2	PF	T7	2	272,023	71,245	1,424	4.94
PF.T7.3	PF	T7	3	255,589	71,245	1,083	4.53
PF.T30.1	PF	T30	1	113,760	71,245	154	1.86
PF.T30.2	**PF**	**T30**	**2**	**71,245**	**71,245**	**103**	**1.45**
PF.T30.3	PF	T30	3	105,537	71,245	122	1.41

Table SI 4.4 Supplemental Metagenome Sequence Summary. Summary of metagenome (DNA) sequence reads with alpha diversity metrics.

Sample ID	Soil Layer	Time Point	Incubation Replicate	Mapped Reads	Proper Pairs (%)	Mean Coverage (%)	Gene Richness	Gene Abundance	Gene Diversity (H')
MG37	AL	T0	1	7,306,878	54.1	41.4	442,009	2,105,340	12.30
MG38	AL	T0	2	4,952,240	51.8	28.0	372,252	1,423,614	12.23
MG39	AL	T0	3	5,505,102	46.1	31.1	396,670	1,575,218	12.23
MG46	AL	T7	1	7,964,504	39.4	45.1	502,644	2,270,238	12.40
MG47	AL	T7	2	7,661,574	46.0	43.4	469,720	2,187,108	12.34
MG48	AL	T7	3	7,086,521	44.2	40.2	455,828	2,017,807	12.31
MG55	AL	T30	1	7,523,832	31.2	42.5	521,939	2,267,908	12.36
MG56	AL	T30	2	8,837,029	39.6	50.0	533,492	2,682,524	12.34
MG57	AL	T30	3	8,503,122	44.4	47.9	530,499	2,581,525	12.41
MG40	TZ	T0	1	6,652,912	52.3	37.5	245,198	2,146,489	10.52
MG41	TZ	T0	2	6,796,127	70.2	38.4	184,410	2,227,399	10.35
MG42	TZ	T0	3	7,032,841	58.8	39.5	219,975	2,285,000	10.58
MG49	TZ	T7	1	10,892,048	39.0	61.5	237,430	3,569,391	10.09
MG50	TZ	T7	2	6,731,231	48.0	37.9	218,567	2,166,288	10.60
MG51	TZ	T7	3	7,796,826	61.5	44.0	215,057	2,490,079	10.47
MG58	TZ	T30	1	9,614,409	33.4	54.5	153,088	3,455,362	9.27
MG59	TZ	T30	2	11,002,154	42.5	62.3	182,586	3,906,642	9.51
MG60	TZ	T30	3	9,780,558	44.9	55.4	176,793	3,510,015	9.93
MG43	PF	T0	1	6,815,432	53.7	38.3	212,433	2,201,935	10.65
MG44	PF	T0	2	6,378,144	50.6	35.9	206,848	2,085,707	10.56
MG45	PF	T0	3	8,018,779	49.9	45.2	223,769	2,636,855	10.50
MG52	PF	T7	1	8,347,188	33.9	47.0	249,708	2,652,600	10.74
MG53	PF	T7	2	8,664,363	54.1	48.7	265,488	2,729,196	10.96
MG54	PF	T7	3	8,161,837	41.9	45.9	235,465	2,590,998	10.68
MG61	PF	T30	1	10,025,330	41.0	56.7	205,693	3,552,264	10.05
MG62	PF	T30	2	10,390,831	40.7	58.8	192,847	3,798,916	9.77
MG63	PF	T30	3	10,113,057	35.1	57.3	180,851	3,604,546	9.70

Table SI 4.5 Supplemental Metatranscriptome Sequence Summary. Summary of metatranscriptome (RNA) sequence reads with alpha diversity metrics.

Sample ID	Soil Layer	Time Point	Incubation Replicate	Mapped Reads	Proper Pairs (%)	Mean Coverage (%)	Gene Richness	Gene Abundance	Gene Diversity (H')
MT37	AL	T0	1	4,106,195	79.0	22.6	41,508	160,490	9.71
MT38	AL	T0	2	2,875,661	77.7	15.7	23,735	72,934	9.02
MT39	AL	T0	3	3,507,491	78.5	19.4	33,095	107,302	9.44
MT46	AL	T7	1	4,762,487	77.8	26.2	97,985	451,835	10.43
MT47	AL	T7	2	5,034,168	79.9	27.8	94,411	526,284	10.47
MT48	AL	T7	3	4,869,394	78.4	26.6	107,157	518,955	10.70
MT55	AL	T30	1	5,919,513	77.1	32.9	128,787	727,474	10.54
MT56	AL	T30	2	4,161,462	78.0	23.1	85,364	484,184	10.52
MT57	AL	T30	3	5,562,272	76.8	30.6	116,281	575,702	10.72
MT58	TZ	T30	1	3,657,616	74.6	20.2	59,181	982,267	9.45
MT59	TZ	T30	2	3,878,612	74.5	21.1	68,933	1,046,071	9.60
MT60	TZ	T30	3	5,087,129	73.7	27.7	77,084	1,391,742	9.60
MT61	PF	T30	1	4,462,673	77.6	24.7	68,437	1,361,347	9.26
MT62	PF	T30	2	4,079,844	75.3	22.4	70,490	1,283,174	9.28
MT63	PF	T30	3	5,298,850	77.7	29.5	72,045	1,621,022	9.13

Table SI 4.6 Supplemental Relative Abundance of Dominant Microbial Taxa. Relative abundance (mean % ± SD) of dominant bacterial phyla and archaea derived from 16S rRNA amplicon sequence variants (ASVs). Proteobacteria are resolved to class. Percent change values denote the mean change in relative abundance for each taxon compared to incubation time point T0 within each soil layer microbiome. Bold values indicate a significant difference ($p < 0.05$) in mean relative abundance for each taxon compared to incubation time point T0 within each soil layer microbiome.

Soil Layer & Time Point	Acidobacteria		Actinobacteria		Alphaproteobacteria		Betaproteobacteria		Deltaproteobacteria		Gammaproteobacteria		Bacteroidetes	
	Rel. Abund. (%)	% Change from T0	Rel. Abund. (%)	% Change from T0	Rel. Abund. (%)	% Change from T0	Rel. Abund. (%)	% Change from T0	Rel. Abund. (%)	% Change from T0	Rel. Abund. (%)	% Change from T0	Rel. Abund. (%)	% Change from T0
Active Layer														
T0	10.6 ± 3.3	-	7.5 ± 1.0	-	4.6 ± 2.2	-	2.2 ± 1.2	-	7.4 ± 1.0	-	0.8 ± 0.6	-	24.1 ± 10.5	-
T7	7.0 ± 0.5	-3.6	9.7 ± 1.3	2.2	2.7 ± 0.2	-1.9	2.0 ± 0.5	-0.2	8.0 ± 0.5	0.6	0.1 ± 0.0	-0.7	25.3 ± 3.4	1.2
T30	6.4 ± 0.8	-4.2	7.6 ± 0.4	0.1	2.0 ± 0.3	-2.6	**28.8 ± 2.2**	**26.6**	6.9 ± 0.3	-0.5	**< 0.1**	**-0.8**	19.4 ± 3.3	-4.7
Transition Zone														
T0	3.3 ± 0.7	-	31.3 ± 5.1	-	0.7 ± 0.2	-	0.4 ± 0.2	-	4.1 ± 0.4	-	0.1 ± 0.0	-	4.2 ± 1.5	-
T7	3.5 ± 0.2	0.2	28.6 ± 3.3	-2.7	0.9 ± 0.1	0.2	0.4 ± 0.1	0.0	4.7 ± 0.9	0.6	0.1 ± 0.0	0.0	4.0 ± 0.6	-0.2
T30	**0.1 ± 0.0**	-3.2	**2.1 ± 0.8**	**-29.2**	1.2 ± 0.1	0.5	**71.9 ± 14.5**	**71.5**	**0.1 ± 0.0**	**-4.0**	9.9 ± 17.2	9.8	**0.2 ± 0.0**	**-4.0**
Permafrost														
T0	4.2 ± 0.1	-	33.3 ± 0.6	-	0.9 ± 0.1	-	0.2 ± 0.1	-	6.3 ± 1.0	-	0.4 ± 0.1	-	5.8 ± 0.1	-
T7	4.8 ± 0.2	0.6	31.8 ± 1.7	-1.5	1.3 ± 0.2	0.4	0.3 ± 0.1	0.1	5.8 ± 0.7	-0.5	0.4 ± 0.2	0.0	6.6 ± 0.4	0.8
T30	**0.1 ± 0.0**	**-4.1**	**2.1 ± 0.6**	**-31.2**	1.0 ± 1.3	0.1	**80.0 ± 8.0**	**79.8**	**0.2 ± 0.1**	**-6.1**	7.6 ± 6.6	7.2	**0.5 ± 0.2**	**-5.3**

Soil Layer & Time Point	Caldiserica		Chlorobi		Chloroflexi		Firmicutes		Verrucomicrobia		Bacteria Other		Archaea	
	Rel. Abund. (%)	% Change from T0	Rel. Abund. (%)	% Change from T0	Rel. Abund. (%)	% Change from T0	Rel. Abund. (%)	% Change from T0	Rel. Abund. (%)	% Change from T0	Rel. Abund. (%)	% Change from T0	Rel. Abund. (%)	% Change from T0
Active Layer														
T0	1.6 ± 0.5	-	4.4 ± 0.5	-	7.7 ± 1.1	-	1.4 ± 0.2	-	15.0 ± 0.9	-	12.1 ± 2.3	-	0.6 ± 0.1	-
T7	2.0 ± 0.3	0.4	5.6 ± 0.6	1.2	7.2 ± 0.5	-0.5	**2.4 ± 0.5**	**1.0**	15.1 ± 1.3	0.1	12 ± 1.5	-0.1	**0.9 ± 0.1**	**0.3**
T30	1.2 ± 0.4	-0.4	4.1 ± 0.5	-0.3	**4.8 ± 1.1**	**-2.9**	1.4 ± 0.4	0.0	**9.8 ± 1.3**	**-5.2**	**7.1 ± 0.8**	**-5.0**	0.5 ± 0.1	-0.1
Transition Zone														
T0	28.3 ± 4.9	-	0.5 ± 0.4	-	6.2 ± 1.7	-	11.1 ± 0.9	-	1.1 ± 0.8	-	8.4 ± 0.8	-	0.4 ± 0.1	-
T7	31.6 ± 5.9	3.3	0.3 ± 0.0	-0.2	6.4 ± 0.6	0.2	8.6 ± 0.6	-2.5	0.6 ± 0.2	-0.5	9.7 ± 2.7	1.3	0.6 ± 0.1	0.2
T30	**0.7 ± 0.2**	**-27.6**	< 0.1	-0.5	**0.1 ± 0.0**	**-6.1**	13.6 ± 4.4	2.5	**< 0.1**	**-1.1**	**0.2 ± 0.0**	**-8.2**	**< 0.1**	**-0.4**
Permafrost														
T0	18.6 ± 2.4	-	0.4 ± 0.0	-	8.1 ± 0.6	-	11.1 ± 0.6	-	0.9 ± 0.1	-	9.2 ± 0.1	-	0.7 ± 0.2	-
T7	15.9 ± 2.9	-2.7	0.6 ± 0.1	0.2	10.5 ± 2.2	2.4	9.4 ± 1.2	-1.7	0.8 ± 0.1	-0.1	11.2 ± 0.9	2.0	0.8 ± 0.1	0.1
T30	**0.5 ± 0.1**	**-18.1**	**< 0.1**	**-0.4**	**0.3 ± 0.0**	**-7.8**	**7.5 ± 0.4**	**-3.6**	**< 0.1**	**-0.9**	**0.2 ± 0.0**	**-9.0**	**< 0.1**	**-0.7**

Table SI 4.7 Supplemental Absolute Abundance of Dominant Microbial Taxa. Absolute abundance (mean 16S rRNA gene copies) for dominant bacterial phyla and archaea derived from 16S rRNA amplicon sequencing relative to *Thermus thermophilus* internal standard recovered from sequencing. Proteobacteria are resolved to class. Log fold-change (Log10) values denote the mean magnitude of change compared to incubation time point T0 within each soil layer microbiome. Bold values indicate a significant difference ($p < 0.05$) in mean 16S rRNA gene copies for each taxon compared to incubation time point T0 within each soil layer microbiome.

Soil Layer & Time Point	Acidobacteria		Actinobacteria		Alphaproteobacteria		Betaproteobacteria		Deltaproteobacteria		Gammaproteobacteria		Bacteroidetes	
	16S Gene Copy Abund.	LogFC from T0	16S Gene Copy Abund.	LogFC from T0	16S Gene Copy Abund.	LogFC from T0	16S Gene Copy Abund.	LogFC from T0	16S Gene Copy Abund.	LogFC from T0	16S Gene Copy Abund.	LogFC from T0	16S Gene Copy Abund.	LogFC from T0
Active Layer														
T0	1,290,876,036	-	935,455,160	-	544,816,376	-	258,090,069	-	918,643,240	-	91,049,482	-	3,223,765,902	-
T7	684,710,617	-0.28	913,541,709	-0.01	250,062,541	-0.34	199,143,708	-0.11	755,207,970	-0.09	**10,240,880**	**-0.95**	2,313,046,255	-0.14
T30	1,218,889,148	-0.02	1,467,908,994	0.20	372,332,369	-0.17	**5,644,080,017**	**1.34**	1,361,323,075	0.17	**8,057,382**	**-1.05**	3,935,827,443	0.09
Transition Zone														
T0	13,424,752	-	128,609,515	-	2,992,878	-	1,482,227	-	16,709,018	-	448,004	-	17,526,159	-
T7	13,086,031	-0.01	99,651,286	-0.11	3,111,926	0.02	1,217,674	-0.09	16,080,493	-0.02	364,096	-0.09	15,225,602	-0.06
T30	5,268,849	-0.41	228,534,354	0.25	**126,367,299**	**1.63**	**7,627,422,958**	**3.71**	11,412,933	-0.17	1,311,625,915	3.47	19,128,716	0.04
Permafrost														
T0	30,613,347	-	244,100,976	-	6,512,764	-	1,343,167	-	47,071,320	-	2,683,893	-	42,140,953	-
T7	24,769,600	-0.09	161,744,268	-0.18	6,641,625	0.01	1,543,251	0.06	30,281,642	-0.19	2,023,287	-0.12	34,231,439	-0.09
T30	26,685,412	-0.06	504,620,798	0.32	**277,377,167**	**1.63**	**18,063,502,416**	**4.13**	53,798,182	0.06	2,097,522,949	2.89	123,404,414	0.47

Soil Layer & Time Point	Caldiserica		Chlorobi		Chloroflexi		Firmicutes		Verrucomicrobia		Bacteria Other		Archaea	
	16S Gene Copy Abund.	LogFC from T0	16S Gene Copy Abund.	LogFC from T0	16S Gene Copy Abund.	LogFC from T0	16S Gene Copy Abund.	LogFC from T0	16S Gene Copy Abund.	LogFC from T0	16S Gene Copy Abund.	LogFC from T0	16S Gene Copy Abund.	LogFC from T0
Active Layer														
T0	204,927,622	-	567,895,422	-	954,628,484	-	181,854,297	-	1,911,661,630	-	1,184,054,893	-	75,846,668	-
T7	182,868,067	-0.05	556,500,312	-0.01	711,857,876	-0.13	236,578,761	0.11	1,481,097,761	-0.11	953,604,266	-0.09	91,495,740	0.08
T30	238,382,323	0.07	801,216,389	0.15	876,050,497	-0.04	303,677,086	0.22	1,879,736,917	-0.01	1,160,235,765	-0.01	108,418,410	0.16
Transition Zone														
T0	116,303,832	-	1,919,222	-	25,568,750	-	45,653,227	-	4,417,455	-	16,431,642	-	1,778,701	-
T7	122,426,285	0.02	982,426	-0.29	23,127,188	-0.04	32,065,745	-0.15	2,351,042	-0.27	14,790,745	-0.05	1,901,511	0.03
T30	71,323,253	-0.21	552,136	-0.54	10,248,571	-0.40	**1,432,071,546**	**1.50**	1,099,592	-0.60	6,548,777	-0.40	469,183	-0.58
Permafrost														
T0	134,447,823	-	2,758,346	-	58,860,684	-	81,911,744	-	6,295,235	-	44,432,944	-	5,108,168	-
T7	80,679,177	-0.22	2,863,939	0.02	53,950,486	-0.04	46,338,000	-0.25	4,204,487	-0.18	34,521,341	-0.11	4,255,172	-0.08
T30	113,470,195	-0.07	3,720,752	0.13	59,111,972	0.00	**1,755,495,580**	**1.33**	6,570,119	0.02	34,159,464	-0.11	4,326,127	-0.07

Table SI 4.8 Supplemental Absolute Abundance of Fe-Cycling Taxa. Absolute abundance (mean 16S rRNA gene copies) for Fe(III)-reducing and Fe(II)-oxidizing bacterial taxa derived from 16S rRNA amplicon sequencing relative to *Thermus thermophilus* internal standard recovered from sequencing. Log fold-change (Log10) values denote the mean magnitude of change compared to incubation time point T0 within each soil layer microbiome. Bold values indicate a significant difference ($p < 0.05$) in mean 16S rRNA gene copies for each Fe-related taxon compared to incubation time point T0 within each soil layer microbiome.

	Fe(III)-Reduction								Fe(II)-Oxidation	
Soil Layer	*Rhodoferax* spp.		*Clostridium* spp.		*Pseudomonas* spp.		*Geobacter* spp.		*Gallionella* spp.	
& Timepoint	16S Gene Copy Abund.	LogFC from T0	16S Gene Copy Abund.	LogFC from T0	16S Gene Copy Abund.	LogFC from T0	16S Gene Copy Abund.	LogFC from T0	16S Gene Copy Abund.	LogFC from T0
Active Layer										
T0	22,837,892	-	68,737,542	-	0 *	-	52,260,722	-	37,540,135	-
T7	62,104,789	0.43	105,843,251	0.19	568,399	5.75	61,478,635	0.07	27,690,330	-0.13
T30	**2,102,988,629**	**1.96**	133,124,156	0.29	687,327	5.84	393,303,095	0.88	**1,403,503,149**	**1.57**
Transition Zone										
T0	237,444	-	13,726,476	-	1,876	-	979,097	-	31,085	-
T7	374,663	0.20	10,571,308	-0.11	5,129	0.44	1,076,918	0.04	39,304	0.10
T30	**6,601,441,525**	**4.44**	**981,081,668**	**1.85**	1,311,625,915	5.84	822,827	-0.08	**176,474,905**	**3.75**
Permafrost										
T0	353,067	-	23,655,541	-	35,258	-	2,451,571	-	56,769	-
T7	402,647	0.06	16,201,874	-0.16	76,711	0.34	2,157,046	-0.06	106,251	0.27
T30	**14,286,228,746**	**4.61**	**1,136,268,778**	**1.68**	2,084,925,811	4.77	9,855,702	0.60	**625,513,764**	**4.04**

Table SI 4.9 Supplemental Summary of KEGG Tier II Genecalls for Metagenome. Values (mean ± SD) are normalized gene counts (GPM; metagenome) for each KEGG category. Bold values indicate a significant difference ($p < 0.05$) in mean counts compared to incubation time point T0 within each soil layer microbiome.

Soil Layer & Time Point	Metabolism	Genetic Processing	Environmental Processing	Cellular Processes
	GPM	GPM	GPM	GPM
Active Layer				
T0	684,143 ± 1,049	157,744 ± 567	125,350 ± 1,020	32,763 ± 442
T7	687,621 ± 2,982	155,867 ± 1,230	123,852 ± 3,571	32,659 ± 509
T30	**674,498 ± 2,291**	**146,021 ± 2314**	**141,084 ± 3,327**	**38,398 ± 469**
Transition Zone				
T0	658,697 ± 4,392	171,935 ± 1,687	134,546 ± 2306	34,821 ± 995
T7	656,810 ± 1,047	174,270 ± 1333	133,783 ± 1,171	35,137 ± 629
T30	**629,711 ± 975**	**119,326 ± 1,300**	**201,304 ± 1,748**	**49,658 ± 1,585**
Permafrost				
T0	671,359 ± 758	165,776 ± 709	129,772 ± 1,455	33,093 ± 1,077
T7	676,118 ± 2,748	165,736 ± 1,429	123,026 ± 207	35,121 ± 1,423
T30	**630,124 ± 1,845**	**118,325 ± 1,535**	**199,538 ± 1,227**	**52,014 ± 837**

Table SI 4.10 Supplemental Summary of KEGG Tier III Genecalls for Metagenome. Values (mean ± SD) are normalized gene counts (GPM; metagenome) for each KEGG category. Bold values indicate a significant difference ($p < 0.05$) in mean counts compared to incubation time point T0 within each soil layer microbiome.

KEGG Tier III Pathways	Active Layer Microbiome			Transition Zone Microbiome			Permafrost Microbiome		
	T0	T7	T30	T0	T7	T30	T0	T7	T30
Metabolism									
Amino acid metabolism	39,363 ± 109	38,995 ± 310	39,233 ± 255	32,928 ± 935	33,566 ± 268	**42,987 ± 611**	32,968 ± 1,070	36,566 ± 1,043	**43,635 ± 530**
Metabolism of other amino acids	19,662 ± 397	19,452 ± 277	19,749 ± 423	18,187 ± 493	18,329 ± 476	17,532 ± 772	18,324 ± 251	18,177 ± 703	18,233 ± 250
Carbohydrate metabolism	120,966 ± 517	**126,887 ± 161**	**113,063 ± 1,281**	137,201 ± 865	136,691 ± 607	**79,142 ± 2,597**	138,503 ± 1,716	133,880 ± 3,448	**76,779 ± 2,000**
Energy metabolism	60,838 ± 1,490	60,680 ± 160	62,067 ± 584	46,170 ± 1,641	45,396 ± 2,253	**62,947 ± 1,041**	50,376 ± 1,131	53,034 ± 780	**63,150 ± 554**
Glycan biosynthesis and metabolism	28,245 ± 126	28,187 ± 974	27,186 ± 746	22,496 ± 297	22,167 ± 580	**26,224 ± 225**	22,763 ± 422	21,788 ± 567	26,338 ± 312
Lipid metabolism	21,051 ± 127	21,166 ± 330	21,003 ± 206	17,884 ± 158	17,826 ± 182	**18,768 ± 151**	17,085 ± 112	17,437 ± 272	18,881 ± 260
Metabolism of cofactors and vitamins	71,967 ± 595	71,503 ± 518	**74,790 ± 343**	69,090 ± 1,289	68,142 ± 248	**78,246 ± 238**	72,305 ± 675	73,123 ± 479	**78,945 ± 721**
Metabolism of terpenoids and polyketides	19,971 ± 221	19,807 ± 432	**18,212 ± 411**	21,783 ± 779	22,506 ± 1,439	**13,835 ± 303**	19,067 ± 99	19,022 ± 566	**13,916 ± 208**
Nucleotide metabolism	77,470 ± 896	77,155 ± 172	**74,082 ± 512**	90,739 ± 1,662	92,130 ± 3,132	**68,424 ± 646**	87,406 ± 739	85,645 ± 1,242	**68,428 ± 395**
Biosynthesis of other secondary metabolites	2,462 ± 42	2,452 ± 25	2,527 ± 58	2,653 ± 90	2,613 ± 49	2,525 ± 19	2,760 ± 46	3,000 ± 38	2,592 ± 79
Xenobiotics biodegradation and metabolism	5,100 ± 70	4,907 ± 482	**6,728 ± 858**	873 ± 114	761 ± 100	**10,188 ± 223**	814 ± 70	999 ± 123	**10,254 ± 296**
Genetic Information Processing									
Folding, sorting and degradation	35,547 ± 368	35,610 ± 233	**33,709 ± 538**	34,968 ± 264	35,491 ± 257	**29,690 ± 172**	34,229 ± 350	34,569 ± 674	**29,517 ± 306**
Replication and repair	48,668 ± 507	48,557 ± 509	**45,869 ± 462**	48,360 ± 729	49,017 ± 1,478	**34,126 ± 927**	47,492 ± 355	47,086 ± 527	**34,196 ± 748**
Transcription	630 ± 59	625 ± 75	**520 ± 27**	766 ± 110	770 ± 253	**137 ± 52**	795 ± 102	880 ± 146	**174 ± 66**
Translation	72,899 ± 387	71,075 ± 519	65,923 ± 1,413	87,842 ± 1,031	88,993 ± 713	**55,374 ± 174**	83,261 ± 607	83,201 ± 878	**54,438 ± 585**
Environmental Information Processing									
Membrane transport	72,222 ± 1,751	71,842 ± 3869	77,874 ± 3,739	100,469 ± 2,953	100,504 ± 1,201	**106,885 ± 1,308**	94,763 ± 927	89,362 ± 196	**106,453 ± 1,068**
Signal transduction	52,879 ± 1,101	51,768 ± 330	**63,018 ± 1,316**	33,988 ± 668	33,190 ± 666	**94,403 ± 2,940**	34,931 ± 563	33,567 ± 358	**93,053 ± 1,068**
Signaling molecules and interaction	249 ± 34	241 ± 22	192 ± 13	89 ± 12	89 ± 12	**16 ± 5**	78 ± 5	96 ± 21	31 ± 7
Cellular Processes									
Cellular community - prokaryotes	16,292 ± 419	16,696 ± 388	17,371 ± 110	22,676 ± 742	23,027 ± 546	**14,859 ± 1,871**	21,984 ± 822	23,788 ± 1,205	16,137 ± 1,374
Cell growth and death	11,967 ± 85	**11,635 ± 89**	**11,542 ± 50**	11,430 ± 396	11,480 ± 57	**12,145 ± 49**	10,570 ± 210	10,761 ± 108	11,811 ± 230
Cell motility	3,604 ± 127	3,485 ± 233	**8,641 ± 468**	475 ± 103	406 ± 52	**20,299 ± 1,140**	332 ± 72	367 ± 86	**21,976 ± 1,311**
Transport and catabolism	771 ± 14	746 ± 63	781 ± 34	217 ± 30	200 ± 61	**2,351 ± 225**	178 ± 21	175 ± 41	**2,072 ± 88**

Table SI 4.11 Supplemental Summary of DGE from Metatranscriptome. Values represent counts of KEGG orthologs (KOs; i.e., genes) considered to be differentially expressed if the False Discovery Rate (FDR) was < 0.05. "Higher" or "Lower" differential expression is relative to the second variable in the comparison (e.g., "T0 to T7" summarizes higher or lower gene expression in T7 relative to T0).

DGE Analysis	Unique KEGG Orthologs (KOs)			Significantly Different
	Higher	Lower	Not Significant	
Active Layer				
T0 to T7	4,026	779	116,526	4.1%
T7 to T30	3,969	5,525	111,837	8.5%

Table SI 4.12 Supplemental FeGenie Summary. Relative abundance (mean % ± SD) of iron (Fe)-related gene categories derived from FeGenie analysis for the metagenome and metatranscriptome. Percent change values denote the mean change in relative abundance for each Fe-related gene category compared to incubation time point T0 within each soil layer microbiome. Bold values indicate a significant difference ($p < 0.05$) in mean relative abundance for each Fe-related gene category compared to incubation time point T0 within each soil layer microbiome. No statistical tests were applied to the transition-zone or permafrost microbiomes in the metatranscriptome.

Soil Layer & Timepoint	Fe Metabolism				Fe Acquisition				Fe Cycling			
	Fe Regulation		Fe Storage		Fe Transport		Siderophore Transport		Fe Oxidation		Fe Reduction	
	Rel. Abund. (%)	% Change from T0	Rel. Abund. (%)	% Change from T0	Rel. Abund. (%)	% Change from T0	Rel. Abund. (%)	% Change from T0	Rel. Abund. (%)	% Change from T0	Rel. Abund. (%)	% Change from T0
Metagenome												
Active Layer												
T0	59.9 ± 1.9	-	13.6 ± 1.2	-	4.8 ± 0.7	-	19.9 ± 0.2	-	0.5 ± 0.3	-	1.4 ± 0.2	-
T7	60.1 ± 2.1	0.2	13.7 ± 0.6	0.1	4.3 ± 0.1	-0.5	20.0 ± 1.1	0.1	0.8 ± 0.4	0.3	1.2 ± 0.2	-0.2
T30	**52.2 ± 1.6**	**-7.7**	**11.2 ± 0.4**	**-2.4**	**6.4 ± 0.8**	**1.6**	**27.4 ± 1.9**	**7.5**	1.5 ± 0.6	1.0	1.4 ± 0.1	0.0
Transition Zone												
T0	58.5 ± 2.5	-	15.3 ± 1.3	-	10.3 ± 1.1	-	15.8 ± 2.5	-	< 0.1	-	< 0.1	-
T7	59.4 ± 1.5	0.9	15.2 ± 1.8	-0.1	10.0 ± 1.7	-0.3	15.1 ± 1.3	-0.7	< 0.1	0.0	0.4 ± 0.3	0.4
T30	**40.4 ± 3.8**	**-18.1**	**4.1 ± 0.1**	**-11.2**	8.6 ± 1.8	-1.7	**38.2 ± 1**	**22.4**	**4.8 ± 1**	**4.8**	**3.9 ± 0.3**	**3.9**
Permafrost												
T0	59.1 ± 2.6	-	15.3 ± 1	-	8.8 ± 0.9	-	16.4 ± 2.8	-	< 0.1	-	< 0.1	-
T7	59.5 ± 2.9	0.4	14.5 ± 2.5	-0.8	8.8 ± 1	0.0	17.1 ± 0.7	0.7	< 0.1	0.0	0.4 ± 0.4	0.4
T30	**36.1 ± 5.2**	**-23.0**	**5 ± 0.5**	**-10.3**	10 ± 0.7	1.2	**41.9 ± 3.9**	**25.5**	**4.3 ± 1.3**	**4.3**	**2.6 ± 1.7**	**2.6**
Metatranscriptome												
Active Layer												
T0	71.7 ± 4.4	-	23.6 ± 2.2	-	< 0.1	-	3.6 ± 3.5	-	< 0.1	-	1.2 ± 2.0	-
T7	**50.2 ± 8.2**	**-21.5**	16.9 ± 4.0	-6.7	< 0.1	0.0	**29.4 ± 3.4**	**25.8**	2.9 ± 4.4	2.9	3.0 ± 3.0	1.8
T30	**46.3 ± 4.5**	**-25.4**	**14.5 ± 3.5**	**-9.1**	0.8 ± 0.7	0.8	**30.3 ± 2.8**	**26.7**	3.7 ± 1.0	3.7	1.8 ± 2.0	0.6
Transition Zone												
T30	31.3 ± 3.7	-	9.6 ± 1.3	-	6.9 ± 2.4	-	29.6 ± 5.8	-	9.6 ± 3.3	-	12.9 ± 0.2	-
Permafrost												
T30	30.8 ± 1.6	-	11.5 ± 4.9	-	6.5 ± 0.6	-	31.6 ± 1.0	-	9.9 ± 3.6	-	9.7 ± 1.4	-

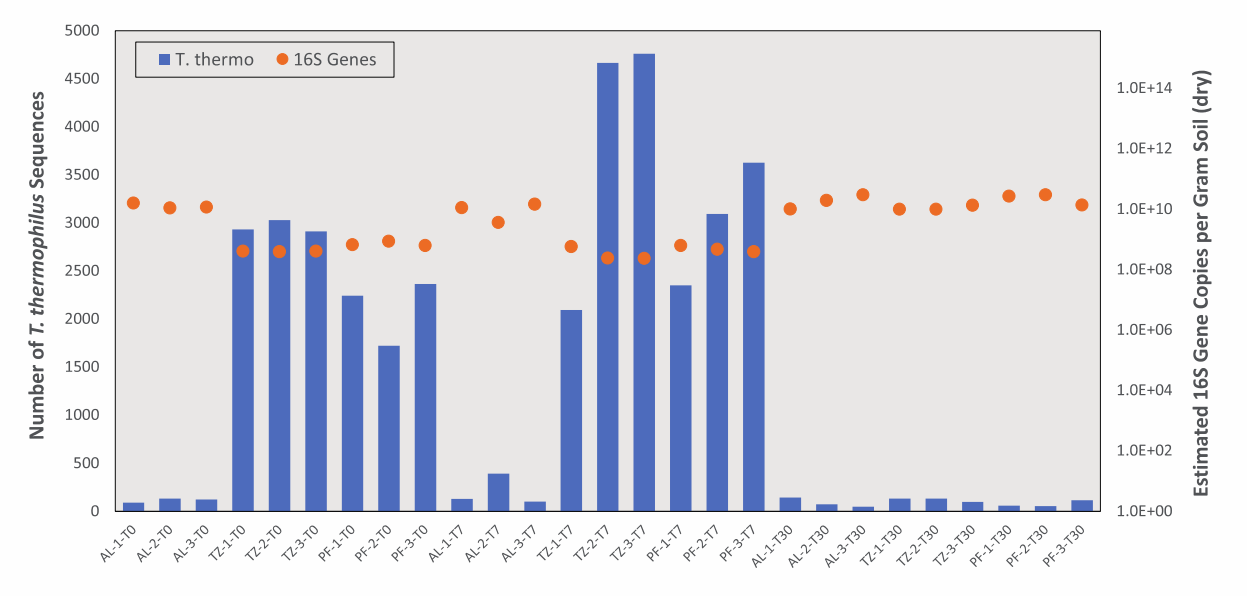

Figure SI 4.7 Supplemental 16S rRNA Gene Copies. Absolute abundance of 16S rRNA gene copies per gram of soil (orange dots; right-hand y-axis) for all microbial taxa within each soil layer microbiome scaled relative to *Thermus thermophilus* internal standard values (blue bars; left-hand y-axis) recovered from 16S rRNA amplicon sequencing.

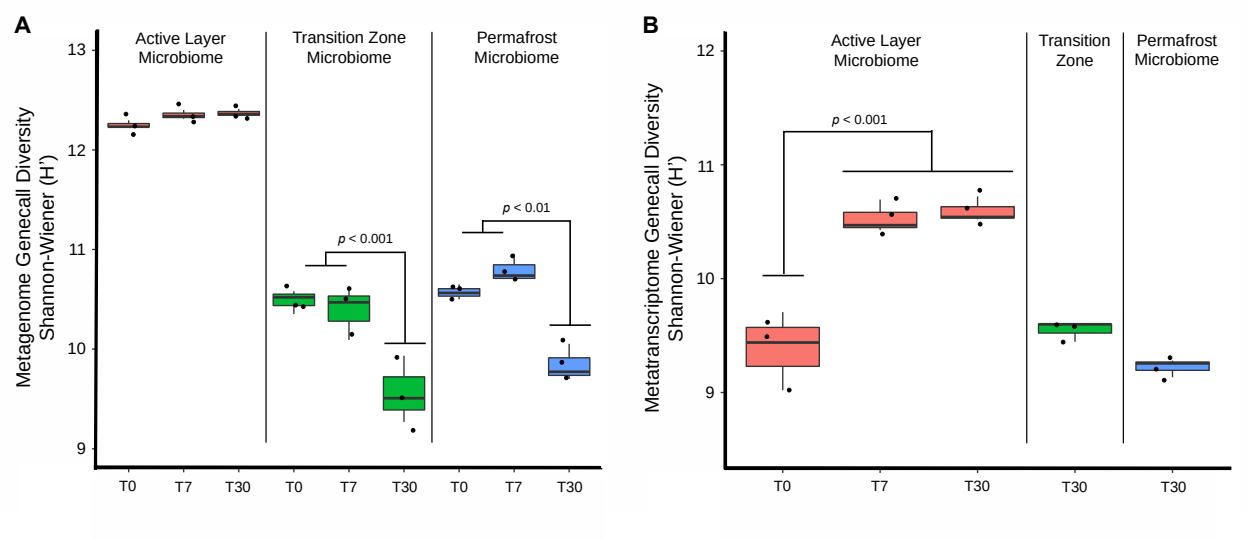

Figure SI 4.8 Supplemental Alpha Diversity Summary. Boxplot representing the (A) metagenome and (B) metatranscriptome alpha diversity (mean H' ± SD) of functional genecalls based on the Shannon-Wiener (H') metric. Significant differences were determined from ANOVA between incubation time points within each soil layer microbiome.

4.8 References

Apprill, A., McNally, S., Parsons, R. and Weber, L., 2015. Minor revision to V4 region SSU rRNA 806R gene primer greatly increases detection of SAR11 bacterioplankton. Aquatic Microbial Ecology, 75(2), 129-137.

Barichivich, J., Briffa, K.R., Osborn, T.J., Melvin, T.M. and Caesar, J., 2012. Thermal growing season and timing of biospheric carbon uptake across the Northern Hemisphere. Global Biogeochemical Cycles, 26(4).

Benjamini, Y. and Hochberg, Y., 1995. Controlling the false discovery rate: a practical and powerful approach to multiple testing. Journal of the Royal statistical society: series B (Methodological), 57(1), 289-300.

Biasi, C., Meyer, H., Rusalimova, O., et al. (2008) Initial effects of experimental warming on carbon exchange rates, plant growth and microbial dynamics of a lichen-rich dwarf shrub tundra in Siberia. Plant Soil 307: 191–205.

Bolyen, E., Rideout, J.R., Dillon, M.R., Bokulich, N.A., Abnet, C.C., Al-Ghalith, G.A., Alexander, H., Alm, E.J., Arumugam, M., Asnicar, F. and Bai, Y., 2019. Reproducible, interactive, scalable and extensible microbiome data science using QIIME 2. Nature biotechnology, 37(8), 852-857.

Burkert, A., Douglas, T.A., Waldrop, M.P. and Mackelprang, R., 2019. Changes in the active, dead, and dormant microbial community structure across a Pleistocene permafrost chronosequence. Applied and environmental Microbiology, 85(7), e02646-18.

Bushnell, B., 2015. BBMap short-read aligner, and other bioinformatics tools.

Callahan, B.J., McMurdie, P.J., Rosen, M.J., Han, A.W., Johnson, A.J.A. and Holmes, S.P., 2016. DADA2: High-resolution sample inference from Illumina amplicon data. Nature methods, 13(7), 581-583.

Callahan, B.J., McMurdie, P.J. and Holmes, S.P., 2017. Exact sequence variants should replace operational taxonomic units in marker-gene data analysis. The ISME journal, 11(12), 2639-2643.

Campbell, J.H., O'Donoghue, P., Campbell, A.G., Schwientek, P., Sczyrba, A., Woyke, T., Söll, D. and Podar, M., 2013. UGA is an additional glycine codon in uncultured SR1 bacteria from the human microbiota. Proceedings of the National Academy of Sciences, 110(14), 5540-5545.

Carter, M.R. and Gregorich, E.G., 2007. Soil sampling and methods of analysis. CRC press.

Chiarello, M., McCauley, M., Villéger, S. and Jackson, C.R., 2022. Ranking the biases: The choice of OTUs vs. ASVs in 16S rRNA amplicon data analysis has stronger effects on diversity measures than rarefaction and OTU identity threshold. PloS one, 17(2), e0264443.

Coolen, M.J. and Orsi, W.D., 2015. The transcriptional response of microbial communities in thawing Alaskan permafrost soils. Frontiers in microbiology, 6, 197.

Davidson, E.A. and Janssens, I.A., 2006. Temperature sensitivity of soil carbon decomposition and feedbacks to climate change. Nature, 440(7081), 165-173.

Deng, J., Gu, Y., Zhang, J., et al. (2015) Shifts of tundra bacterial and archaeal communities along a permafrost thaw gradient in Alaska. Mol Ecol 24: 222–234.

DeSantis, T.Z., Hugenholtz, P., Larsen, N., Rojas, M., Brodie, E.L., Keller, K., Huber, T., Dalevi, D., Hu, P. and Andersen, G.L., 2006. Greengenes, a chimera-checked 16S rRNA gene database and workbench compatible with ARB. Applied and environmental microbiology, 72(7), 5069-5072.

Dettling, M.D., Yavitt, J.B. and Zinder, S.H., 2006. Control of organic carbon mineralization by alternative electron acceptors in four peatlands, Central New York State, USA. Wetlands, 26(4), 917-927.

De Vos, P., Garrity, G.M., Jones, D., et al. (2009) Bergey's manual of systematic bacteriology, 2nd ed, vol 3. The Firmicutes. Springer, Dordrecht, Netherlands.

Eddy, S.R., 2011. Accelerated profile HMM searches. PLoS computational biology, 7(10), e1002195.

Emerson, D., Scott, J.J., Benes, J. and Bowden, W.B., 2015. Microbial iron oxidation in the arctic tundra and its implications for biogeochemical cycling. Applied and environmental microbiology, 81(23), 8066-8075.

Eren, A.M., Esen, Ö.C., Quince, C., Vineis, J.H., Morrison, H.G., Sogin, M.L. and Delmont, T.O., 2015. Anvi'o: an advanced analysis and visualization platform for 'omics data. PeerJ, 3, e1319.

Euskirchen, E.S., McGUIRE, A.D., Kicklighter, D.W., Zhuang, Q., Clein, J.S., Dargaville, R.J., Dye, D.G., Kimball, J.S., McDonald, K.C., Melillo, J.M. and Romanovsky, V.E., 2006. Importance of recent shifts in soil thermal dynamics on growing season length, productivity, and carbon sequestration in terrestrial high-latitude ecosystems. Global Change Biology, 12, 731-750.

Finneran, K.T., Johnsen, C.V. and Lovley, D.R., 2003. Rhodoferax ferrireducens sp. nov., a psychrotolerant, facultatively anaerobic bacterium that oxidizes acetate with the reduction of Fe (III). International Journal of Systematic and Evolutionary Microbiology, 53(3), 669-673.

Garber, A.I., Nealson, K.H., Okamoto, A., McAllister, S.M., Chan, C.S., Barco, R.A. and Merino, N., 2020. FeGenie: a comprehensive tool for the identification of iron genes and iron gene neighborhoods in genome and metagenome assemblies. Frontiers in microbiology, 37.

Hallberg, R. and Ferris, F.G., 2004. Biomineralization by Gallionella. Geomicrobiology Journal, 21(5), 325-330.

Hanert, H.H., 1981. The genus Gallionella. In The prokaryotes (509-515). Springer, Berlin.

Herndon, E.M., Mann, B.F., Roy Chowdhury, T., Yang, Z., Wullschleger, S.D., Graham, D., Liang, L. and Gu, B., 2015. Pathways of anaerobic organic matter decomposition in tundra soils from Barrow, Alaska. Journal of Geophysical Research: Biogeosciences, 120(11), 2345-2359.

Hugelius, G., Strauss, J., Zubrzycki, S., Harden, J.W., Schuur, E.A.G., Ping, C.L., Schirrmeister, L., Grosse, G., Michaelson, G.J., Koven, C.D. and O'Donnell, J.A., 2014. Estimated stocks of circumpolar permafrost carbon with quantified uncertainty ranges and identified data gaps. Biogeosciences, 11(23), 6573-6593.

Hultman, J., Waldrop, M.P., Mackelprang, R., David, M.M., McFarland, J., Blazewicz, S.J., Harden, J., Turetsky, M.R., Shah, M.B. and VerBerkmoes, N.C., 2015. Multi-omics of permafrost, active layer and thermokarst bog soil microbiomes. Nature, 521(7551), 208-212.

Hyatt, D., Chen, G.L., LoCascio, P.F., Land, M.L., Larimer, F.W. and Hauser, L.J., 2010. Prodigal: prokaryotic gene recognition and translation initiation site identification. BMC bioinformatics, 11(1), 1-11.

Johnson, S.S., Hebsgaard, M.B., Christensen, T.R., Mastepanov, M., Nielsen, R., Munch, K., Brand, T., Gilbert, M.T.P., Zuber, M.T., Bunce, M. and Rønn, R., 2007. Ancient bacteria show evidence of DNA repair. Proceedings of the National Academy of Sciences, 104(36), 14401-14405.

Judd, K.E., Crump, B.C. and Kling, G.W., 2006. Environmental drivers control ecosystem function in bacteria through changes in community composition. Ecology, 87(8), 2068-2079.

Kanehisa, M., Araki, M., Goto, S., Hattori, M., Hirakawa, M., Itoh, M., Katayama, T., Kawashima, S., Okuda, S., Tokimatsu, T. and Yamanishi, Y., 2007. KEGG for linking genomes to life and the environment. Nucleic Acids Research, 36, D480-D484.

Kanehisa, M., Sato, Y. and Morishima, K., 2016. BlastKOALA and GhostKOALA: KEGG tools for functional characterization of genome and metagenome sequences. Journal of molecular biology, 428(4), 726-731.

Kim, H.M., Lee, M.J., Jung, J.Y., et al. (2016) Vertical distribution of bacterial community is associated with the degree of soil organic matter decomposition in the active layer of moist acidic tundra. Journal of Microbiology 54(11): 713-723.

Kling, G.W., Adams, H.E., Bettez, N.D., Bowden, W.B., Crump, B.C., Giblin, A.E., Judd, K.E., Keller, K., Kipphut, G.W., Rastetter, E.R. and Shaver, G.R., 2014. Land–water interactions. Alaska's changing arctic: Ecological consequences for tundra, streams, and lakes, 143-172.

Koyama, A., Wallenstein, M.D., Simpson, R.T. and Moore, J.C., 2014. Soil bacterial community composition altered by increased nutrient availability in Arctic tundra soils. Frontiers in microbiology, 5, 516.

Kraft, N.J., Adler, P.B., Godoy, O., James, E.C., Fuller, S. and Levine, J.M., 2015. Community assembly, coexistence and the environmental filtering metaphor. Functional ecology, 29(5), 592-599.

Lamb, E.G., Han, S., Lanoil, B.D., Henry, G.H., Brummell, M.E., Banerjee, S. and Siciliano, S.D., 2011. A High Arctic soil ecosystem resists long-term environmental manipulations. Global Change Biology, 17(10), 3187-3194.

Langmead, B. and Salzberg, S.L., 2012. Fast gapped-read alignment with Bowtie 2. Nature methods, 9(4), 357-359.

Lennon, J.T., 2020. Microbial life deep underfoot. mBio, 11, e03201-19.

Liang, R., Lau, M., Vishnivetskaya, T., Lloyd, K.G., Wang, W., Wiggins, J., Miller, J., Pfiffner, S., Rivkina, E.M. and Onstott, T.C., 2019. Predominance of anaerobic, spore-forming bacteria in

metabolically active microbial communities from ancient Siberian permafrost. Applied and environmental Microbiology, 85(15), e00560-19.

Li, D., Liu, C.M., Luo, R., Sadakane, K. and Lam, T.W., 2015. MEGAHIT: an ultra-fast single-node solution for large and complex metagenomics assembly via succinct de Bruijn graph. Bioinformatics, 31(10), 1674-1676.

Lipson, D.A., Jha, M., Raab, T.K. and Oechel, W.C., 2010. Reduction of iron (III) and humic substances plays a major role in anaerobic respiration in an Arctic peat soil. Journal of Geophysical Research: Biogeosciences, 115(G4).

Lipson, D.A., Zona, D., Raab, T.K., Bozzolo, F., Mauritz, M. and Oechel, W.C., 2012. Water-table height and microtopography control biogeochemical cycling in an Arctic coastal tundra ecosystem. Biogeosciences, 9(1), 577-591.

Lipson, D.A., Raab, T.K., Goria, D. and Zlamal, J., 2013. The contribution of Fe (III) and humic acid reduction to ecosystem respiration in drained thaw lake basins of the Arctic Coastal Plain. Global Biogeochemical Cycles, 27(2), 399-409.

Liu, C., Cui, Y., Li, X. and Yao, M., 2021. microeco: an R package for data mining in microbial community ecology. FEMS microbiology ecology, 97(2), fiaa255.

Lovley, D.R. and Chapelle, F.H., 1995. Deep subsurface microbial processes. Reviews of Geophysics, 33(3), 365-381.

Mackelprang, R., Waldrop, M.P., DeAngelis, K.M., David, M.M., Chavarria, K.L., Blazewicz, S.J., Rubin, E.M. and Jansson, J.K., 2011. Metagenomic analysis of a permafrost microbial community reveals a rapid response to thaw. Nature, 480(7377), 368-371.

Malard, L.A., Anwar, M.Z., Jacobsen, C.S. and Pearce, D.A., 2019. Biogeographical patterns in soil bacterial communities across the Arctic region. FEMS microbiology ecology, 95(9), fiz128.

Miller, K.E., Lai, C.T., Friedman, E.S., Angenent, L.T. and Lipson, D.A., 2015. Methane suppression by iron and humic acids in soils of the Arctic Coastal Plain. Soil Biology and Biochemistry, 83, 176-183.

Miner, K.R., Turetsky, M.R., Malina, E., Bartsch, A., Tamminen, J., McGuire, A.D., Fix, A., Sweeney, C., Elder, C.D. and Miller, C.E., 2022. Permafrost carbon emissions in a changing Arctic. Nature Reviews Earth & Environment, 3(1), 55-67.

Morton, J.T., Marotz, C., Washburne, A., Silverman, J., Zaramela, L.S., Edlund, A., Zengler, K. and Knight, R., 2019. Establishing microbial composition measurement standards with reference frames. Nature communications, 10(1), 1-11.

Mu, C.C., Zhang, T.J., Zhao, Q., Guo, H., Zhong, W., Su, H. and Wu, Q.B., 2016. Soil organic carbon stabilization by iron in permafrost regions of the Qinghai-Tibet Plateau. Geophysical Research Letters, 43(19), 10-286.

Oksanen, J., Kindt, R., Legendre, P., O'Hara, B., Stevens, M.H.H., Oksanen, M.J. and Suggests, M.A.S.S., 2007. The vegan package. Community ecology package, 10(631-637), p.719.

Osterkamp, T.E. and Romanovsky, V.E., 1999. Evidence for warming and thawing of discontinuous permafrost in Alaska. Permafrost and periglacial Processes, 10(1), 17-37.

Parada, A.E., Needham, D.M. and Fuhrman, J.A., 2016. Every base matters: assessing small subunit rRNA primers for marine microbiomes with mock communities, time series and global field samples. Environmental microbiology, 18(5), 1403-1414.

Patzner, M.S., Mueller, C.W., Malusova, M., Baur, M., Nikeleit, V., Scholten, T., Hoeschen, C., Byrne, J.M., Borch, T., Kappler, A. and Bryce, C., 2020. Iron mineral dissolution releases iron and associated organic carbon during permafrost thaw. Nature communications, 11(1), 1-11.

Patzner, M.S., Kainz, N., Lundin, E., Barczok, M., Smith, C., Herndon, E., Kinsman-Costello, L., Fischer, S., Straub, D., Kleindienst, S. and Kappler, A., 2022a. Seasonal Fluctuations in Iron Cycling in Thawing Permafrost Peatlands. Environmental Science & Technology.

Patzner, M.S., Logan, M., McKenna, A.M., Young, R.B., Zhou, Z., Joss, H., Mueller, C.W., Hoeschen, C., Scholten, T., Straub, D. and Kleindienst, S., 2022b. Microbial iron cycling during palsa hillslope collapse promotes greenhouse gas emissions before complete permafrost thaw. Communications Earth & Environment, 3(1), 1-14.

Pedregosa, F., Varoquaux, G., Gramfort, A., Michel, V., Thirion, B., Grisel, O., Blondel, M., Prettenhofer, P., Weiss, R., Dubourg, V. and Vanderplas, J., 2011. Scikit-learn: Machine learning in Python. the Journal of machine Learning research, 12, 2825-2830.

R Core Team, 2018. R: A language and environment for statistical computing; 2018.

Ricketts, M.P., Matamala, R., Jastrow, J.D., Antonopoulos, D.A., Koval, J., Ping, C.L., Liang, C. and Gonzalez-Meler, M.A., 2020. The effects of warming and soil chemistry on bacterial community structure in Arctic tundra soils. Soil Biology and Biochemistry, 148, 107882.

Rinke, C., Schwientek, P., Sczyrba, A., Ivanova, N.N., Anderson, I.J., Cheng, J.F., Darling, A., Malfatti, S., Swan, B.K., Gies, E.A. and Dodsworth, J.A., 2013. Insights into the phylogeny and coding potential of microbial dark matter. Nature, 499(7459), 431-437.

Rinnan, R., Michelsen, A., Bååth, E., and Jonasson, S. (2007) Fifteen years of climate change manipulations alter soil microbial communities in a subarctic heath ecosystem. Global Change Biology 13(1): 28-39.

Robinson, M.D. and Oshlack, A., 2010. A scaling normalization method for differential expression analysis of RNA-seq data. Genome biology, 11(3), 1-9.

Romanowicz, K.J., Crump, B.C. and Kling, G.W., 2021. Rainfall Alters Permafrost Soil Redox Conditions, but Meta-Omics Show Divergent Microbial Community Responses by Tundra Type in the Arctic. Soil Systems, 5(1), 17.

Romanowicz, K.J., and Kling, G.W. In Review. Summer thaw duration is a strong predictor of the soil microbiome and its response to permafrost thaw in arctic tundra. Environmental Microbiology.

Schuur, E.A., Vogel, J.G., Crummer, K.G., Lee, H., Sickman, J.O. and Osterkamp, T.E., 2009. The effect of permafrost thaw on old carbon release and net carbon exchange from tundra. Nature, 459(7246), 556-559.

Schuur, E.A., McGuire, A.D., Schädel, C., Grosse, G., Harden, J.W., Hayes, D.J., Hugelius, G., Koven, C.D., Kuhry, P., Lawrence, D.M. and Natali, S.M., 2015. Climate change and the permafrost carbon feedback. Nature, 520(7546), 171-179.

Serreze, M.C., Walsh, J.E., Chapin, F.S., Osterkamp, T., Dyurgerov, M., Romanovsky, V., Oechel, W.C., Morison, J., Zhang, T. and Barry, R.G., 2000. Observational evidence of recent change in the northern high-latitude environment. Climatic change, 46(1), 159-207.

Singh, P., Singh, S.M., Singh, R.N., et al. (2017) Bacterial communities in ancient permafrost profiles of Svalbard, Arctic. Journal of Basic Microbiology 57: 1018-1036.

Smets, W., Leff, J.W., Bradford, M.A., McCulley, R.L., Lebeer, S. and Fierer, N., 2016. A method for simultaneous measurement of soil bacterial abundances and community composition via 16S rRNA gene sequencing. Soil Biology and Biochemistry, 96, 145-151.

Smith, L.C., Sheng, Y., MacDonald, G.M. and Hinzman, L.D., 2005. Disappearing arctic lakes. Science, 308(5727), 1429-1429.

Stocker, T. ed., 2014. Climate change 2013: the physical science basis: Working Group I contribution to the Fifth assessment report of the Intergovernmental Panel on Climate Change. Cambridge University Press.

Sturtevant, C.S. and Oechel, W.C., 2013. Spatial variation in landscape-level CO2 and CH4 fluxes from arctic coastal tundra: Influence from vegetation, wetness, and the thaw lake cycle. Global Change Biology, 19(9), 2853-2866.

Tarnocai, C., Canadell, J.G., Schuur, E.A., Kuhry, P., Mazhitova, G. and Zimov, S., 2009. Soil organic carbon pools in the northern circumpolar permafrost region. Global biogeochemical cycles, 23(2).

Tripathi, B.M., Kim, M., Kim, Y., et al. (2018) Variations in bacterial and archaeal communities along depth profiles of Alaskan soil cores. Scientific Reports 8(1): 1-11.

Turetsky, M.R., Abbott, B.W., Jones, M.C., Anthony, K.W., Olefeldt, D., Schuur, E.A., Grosse, G., Kuhry, P., Hugelius, G., Koven, C. and Lawrence, D.M., 2020. Carbon release through abrupt permafrost thaw. Nature Geoscience, 13(2), 138-143.

Varsadiya, M., Urich, T., Hugelius, G., and Barta, J. (2021) Microbiome structure and functional potential in permafrost soils of the Western Canadian Arctic. FEMS Microbiology Ecology 97(3): fiab008.

Villanueva, R.A.M. and Chen, Z.J., 2019. ggplot2: elegant graphics for data analysis.

Wagner, G.P., Kin, K. and Lynch, V.J., 2012. Measurement of mRNA abundance using RNA-seq data: RPKM measure is inconsistent among samples. Theory in biosciences, 131(4), 281-285.

Walker, M.A., Daniëls, F.J. and van der Maarel, E., 1994. Circumpolar arctic vegetation: Introduction and perspectives. Journal of vegetation science, 5(6), 757-764.

Whiticar, M.J., 1999. Carbon and hydrogen isotope systematics of bacterial formation and oxidation of methane. Chemical Geology, 161(1-3), 291-314.

Willerslev, E., Hansen, A.J., Rønn, R., Brand, T.B., Barnes, I., Wiuf, C., Gilichinsky, D., Mitchell, D. and Cooper, A., 2004. Long-term persistence of bacterial DNA. Current Biology, 14(1), R9-R10.

Woodcroft, B.J., Singleton, C.M., Boyd, J.A., Evans, P.N., Emerson, J.B., Zayed, A.A., Hoelzle, R.D., Lamberton, T.O., McCalley, C.K., Hodgkins, S.B. and Wilson, R.M., 2018. Genome-centric view of carbon processing in thawing permafrost. Nature, 560(7716), 49-54.

Wunderlin, T., Junier, T., Roussel-Delif, L., Jeanneret, N. and Junier, P., 2014. Endospore-enriched sequencing approach reveals unprecedented diversity of Firmicutes in sediments. Environmental Microbiology Reports, 6(6), 631-639.

Xue, K., M Yuan, M., J Shi, Z., Qin, Y., Deng, Y.E., Cheng, L., Wu, L., He, Z., Van Nostrand, J.D., Bracho, R. and Natali, S., 2016. Tundra soil carbon is vulnerable to rapid microbial decomposition under climate warming. Nature Climate Change, 6(6), 595-600.

Yang, Z., Wullschleger, S.D., Liang, L., Graham, D.E. and Gu, B., 2016. Effects of warming on the degradation and production of low-molecular-weight labile organic carbon in an Arctic tundra soil. Soil Biology and Biochemistry, 95, 202-211.

Zak, D.R. and Kling, G.W., 2006. Microbial community composition and function across an arctic tundra landscape. Ecology, 87(7), 1659-1670.

Zhang, Y., Chen, W. and Riseborough, D.W., 2006. Temporal and spatial changes of permafrost in Canada since the end of the Little Ice Age. Journal of Geophysical Research: Atmospheres, 111(D22).

Chapter 5.
Conclusions, Implications, and Future Directions

Arctic tundra and its permafrost soils contain more than half of all terrestrial belowground organic carbon (OC) in a perennially frozen state that is increasingly threatened by climate change. Recent warming in the Arctic has already increased soil temperatures and thawed large areas of permafrost that may trigger increased microbial activity, leading to faster degradation of previously-frozen OC and the release of CO_2 and CH_4 to the atmosphere. Yet it remains uncertain how the soil microbiome will respond to permafrost thaw or modulate the relative proportions of CO_2 and CH_4 produced by the decomposition of OC in thawing permafrost soils. In the previous chapters of this dissertation, I described a series of field observations, manipulations, and laboratory incubations to answer the following questions: (1) How does rainfall-induced soil oxidation alter anoxic redox conditions and the composition of the microbiome in thawing permafrost soils; (2) How does summer thaw duration correlate with the composition of the soil microbiome by depth; and (3) How does extended thaw duration shift the composition and genomic potential of soil microbiome within distinct soil layers along the soil profiles of Arctic tundra (see Figure 1.1). The following are conclusions based on these research questions.

5.1 The Soil Microbiome and its Response to Rainfall in Arctic Tundra

Rainfall differentially affects soil redox conditions between tundra soil types due to inherent differences in soil drainage rates and the residence time of rainwater within tussock tundra and wet sedge tundra. The results presented in Chapter 2 of this dissertation indicate that rainfall increased the dissolved O_2 concentration among tundra soils, but the extent of soil oxygenation was 2.5-fold greater in tussock tundra compared with wet sedge tundra (Table 2.2). Gene expression from active microbial taxa in the tussock tundra microbiome experienced a significant shift following rainfall from anaerobic metabolic pathways to aerobic pathways of Fe(II) oxidation and an increase in ribosome transcription that indicates microbial growth (Figure 2.4). This response in the tussock tundra microbiome is due in large part to slower drainage rates through the

dense mineral soil of the active layer that prolonged the residence time of the oxygenated rainwater. In contrast, dissolved O_2 from rainfall in the rapidly-draining organic wet-sedge tundra soil did not appear to accumulate long enough, or to a sufficient concentration, to induce a microbiome-wide shift from anaerobic to aerobic metabolism. Gene expression from active microbial taxa in the wet sedge tundra microbiome remained consistent for anaerobic metabolism, fermentation pathways, and Fe(III) reduction before and after rainfall, regardless of the increase in dissolved O_2 introduced by the rainfall event (Figure 2.5). These results imply that increasing rainfall intensity, frequency, and accumulation across the Arctic tundra may serve only in maintaining persistently saturated conditions in low-lying regions that could enhance CH_4 production due to the high diversity of methanogenic archaea inhabiting wet sedge tundra soils.

5.2 The Soil Microbiome and its Response to Thaw Duration by Depth in Arctic Tundra

Thaw duration is a strong environmental factor that operates over time and space to regulate the composition of the surface active-layer, transition-zone, and deeper permafrost microbiomes in arctic tundra soils. The results presented in Chapter 3 indicate that differences in thaw duration by soil depth also account for regional differences in dominant microbial taxa between sites and tundra types that could not be explained by differences in abiotic soil properties (Figure 3.3). Furthermore, long-term thaw surveys indicate that while thaw depth is increasing over time (last ~20-30 years), the transition-zone microbiome is still indistinguishable from the permafrost microbiome (Figure 3.4). This suggests that thaw duration in the transition zone is still too low to shift the transition-zone microbiome composition away from that in the permafrost and toward that in the active layer. As climate warming continues and thaw duration increases at depth, I predict that for any tundra soil the microbiome composition (and thus function) will shift from the relic permafrost taxa toward current active-layer taxa. The strong correlations between microbiome composition and thaw duration from my soil profile surveys (Figure 3.5) imply that monitoring thaw duration and microbiome composition at depth may help predict the microbial response to future permafrost thaw.

5.3 The Soil Microbiome and its Response to Extended Thaw Duration in Arctic Tundra

The implications from the soil profile surveys (Chapter 3) suggest that thaw duration rather than thaw frequency has a greater impact on the composition and genomic potential of the microbiome within tundra soils. Results from the laboratory incubation experiment (Chapter 4)

indicates that an extended thaw duration of 30 days under anoxic conditions is sufficient to induce a microbiome-wide shift in composition and genomic potential within the transition-zone and permafrost microbiomes of wet sedge tundra. Specifically, these results suggest that Fe cycling promotes substantial microbial growth dominated by Fe(III)-reducing bacteria in permafrost soils during extended thaw duration (Figure 4.3). Fe(III) minerals are known to stabilize OC and protect it from degradation by generating Fe-OC associations that are more persistent in tundra soils. However, our results suggest that Fe(III) minerals are also providing a terminal electron acceptor for pathways of anaerobic respiration associated with the degradation of aromatic compounds, while suppressing CH_4 metabolism. Thus, the growth of Fe(III)-reducing bacteria is likely coupled with greater OC degradation and CO_2 production through anaerobic respiration rather than methanogenesis under anoxic conditions during extended thaw duration. As such, I found that the genomic potential and gene expression for Fe(III) reduction and the degradation of aromatic carbon increased concurrently during the incubation experiment in all soil layers (Table 4.2), indicating strong coupling between Fe(III) reduction and OC degradation. Results from my incubation experiment imply that previously frozen Fe-rich permafrost soils will likely promote greater growth and gene expression from Fe(III)-reducing bacteria that could release substantial quantities of Fe-bound OC to microbial degradation along the soil profile of wet sedge tundra.

5.4 Summary and Future Directions

The work presented in this dissertation advances our understanding of the dynamics and functions of the soil microbiome in arctic tundra in response to permafrost thaw. Specifically, I show how the ongoing changes in rainfall, redox conditions, and thaw duration induced by climate warming influence the composition of the soil microbiome, its genomic potential, and its gene expression associated with OC degradation in thawing permafrost soils. However, the process of permafrost thaw is more than a simple transition from a frozen to a thawed state. Rather, thawing permafrost soils undergo repeated freeze-thaw cycles on an annual, seasonal, and even daily basis. Freeze-thaw cycles can influence abiotic soil properties and alter the biological activity of the soil microbiome with implications for OC degradation. Such effects of repeated freeze-thaw cycles also highlight the importance of determining how thaw duration between freeze-thaw events affects the composition and genomic potential of the soil microbiome in order to better predict the microbial response to future thaw events.

The next step in furthering our understanding of the microbial response to permafrost thaw is to investigate how daily or seasonal freeze-thaw cycles affect the dynamics and functions of the microbiome in tundra soils. We should begin by investigating how previous freeze-thaw histories within tussock tundra and wet sedge tundra soils influence the current composition of the soil microbiome and its genomic potential in tundra environments. These freeze-thaw histories are analogous to our calculations for intermittent thaw frequency by soil depth and can be determined from the long-term thaw depth measurements presented in Chapter 3. For example, the active-layer soil depths have experienced freeze-thaw on an annual basis while the transition-zone depths experienced intermittent freeze-thaw over the past few decades (Table 3.1). An additional approach would also be to investigate how the microbiome within distinct soil layers along the soil profile of each tundra type responds to experimental freeze-thaw cycles on daily and seasonal time scales. Similar to the incubation experiment in Chapter 4, a laboratory-based experiment could be established to test the combined effects of extended thaw duration and repeated freeze-thaw cycles on the composition and genomic potential of the soil microbiome, with freeze periods lasting days to weeks between thaw events. Variations in the microbial response to freeze-thaw cycles between tundra types or between soil layers could play a crucial role in predicting the rates of OC degradation and GHG emissions from thawing permafrost soils across the Arctic tundra.

Appendices

APPENDIX A.

CHAPTER 2 SUPPLEMENTAL METHODS

A1. Mesocosm Design. Intact soil-plant cores (diameter 28 cm; length 31 ± 4 cm) were collected in triplicate from two dominant tundra types, tussock tundra and wet sedge tundra, from a sampling location that spanned several hundred meters from the top of the hillslope (tussock tundra) to the base of the hill (wet sedge tundra) in the Toolik region. Soil-plant cores were transferred to 20 L plastic buckets to establish the soil mesocosm experiment as previously described (Trusiak et al. 2019). In brief, soil mesocosms were housed in large plastic coolers (46 cm x 46 cm x 84 cm), with each cooler containing three mesocosms surrounded by an ice-filled water bath to keep the temperatures relatively constant and within the range of soils in the summer at the field site. Soil mesocosms were open to the atmosphere at the top and sealed at the bottom. The mesocosms were acclimated under static waterlogged conditions in the water bath for 4-7 days to generate reducing conditions observed in the field. DI water (1-2 L) was added to the soil mesocosms during the acclimation period to account for evapotranspiration and keep the water table constant in the mesocosms. After the acclimation period, each set of triplicate mesocosms from each tundra type were flushed with 20 L of DI water over one to four hours, called the "flushing period" (Figure SI 2.7). During the flushing period, mesocosms were drained from the bottom and DI water was added to the top to keep the water level constant until all flushes had been completed. After the flushing period, the mesocosms were allowed to re-acclimate to pre-rainfall soil redox conditions under static waterlogged conditions.

A2. Soil Properties. Soil pH was measured using a WTW SenTix pH 3210 meter and probe (range: -2 to +20 pH; resolution: 0.001 pH; Xylem Analytics, Weilheim, Germany). Conductivity was measured with a WTW Cond 3210 meter and probe (range: 0 to 1,000 mS; resolution: 0.001

mS; Xylem Analytics). Temperature was measured using a Fisherbrand Traceable digital thermometer with stainless-steel stem (range: -50 to +250°C; resolution: ± 1°C; Fisher Scientific). Dissolved soil O_2 was measured with a ProODO optical dissolved oxygen meter and probe (range: 0 to 50 mg O_2 L^{-1}; resolution: 0.01 mg O_2 L^{-1}; YSI, Yellow Springs, OH). Soil moisture was measured using a HydroSense II soil moisture sensor paired with the CS658 soil-water probe (range: 0 to 50% VWC; resolution: < 0.05% VWC; Campbell Scientific, Logan, UT). Bulk density of the soil was determined as the mass of dry soil (g) in an entire core divided by the soil volume (cm^3; dimensions of the soil contained in the core). Porosity of the soil was calculated from the volume of soil core occupied by water. Organic carbon content (%) was determined from combusting a subsample of dried soil for 6 hours at 550°C, assuming the mass of organic matter lost during ignition was 50% carbon.

A3. Modeling Soil O_2 Accumulation Rates. For our mass balance model (Figure SI 2.8), we used soil measurements from the abiotic response cores (ARC) (Trusiak et al. 2019) that include the initial soil O_2 concentration (mg O_2 L^{-1}) measured prior to the DI water flush, the final soil O_2 concentration (mg O_2 L^{-1}) measured at the end of the DI water flush, the length of each soil core (cm), the volume of DI water flushed through each soil core (L), and the duration of the DI water flush (hours), to estimate representative rates of soil O_2 accumulation (mg O_2 L^{-2} cm^{-1} hr^{-1}) for tussock tundra and wet sedge tundra soils (Eq. S1).

$$\textit{ARC Accumulation Rate} = \frac{\text{Final } [O_2]}{\text{Initial } [O_2]} \div \text{Core Length} \div \text{Vol. Flushed} \div \text{Flush Duration} \qquad \text{(S1)}$$

The representative ARC soil O_2 accumulation rates (mg O_2 L^{-2} cm^{-1} hr^{-1}; Eq. S1) were then corrected using the length of each soil core (cm) and the volume of DI water flushed through each soil core (L) in the biotic response cores (BRC) to estimate the rates of soil O_2 accumulation during the DI water flush (mg O_2 L^{-1} hr^{-1}) specific for BRC tundra mesocosms (F_{rain}; Eq. S2).

$$\textit{BRC Accumulation Rate} = \text{S1} \times \text{BRC Core Length} \times \text{BRC Vol. Flushed} \qquad \text{(S2)}$$

These BRC rates of soil O_2 accumulation (mg O_2 L^{-1} hr^{-1}; F_{rain}; Eq. S2) during the DI water flush were further corrected to the 15-cm sampling depth rather than through the entire length of each soil core to reflect soil O_2 concentrations at the sampling depth for microbial activity.

A4. Modeling Soil O_2 Consumption Rates. The average soil O_2 consumption rates (mg O_2 L^{-1} hr^{-1}) for tussock tundra and wet sedge tundra were calculated as the difference in the O_2 concentration at the end of the first flush (mg O_2 L^{-1}) and the O_2 concentration prior to the start of the second flush (i.e., end of re-acclimation period; mg O_2 L^{-1}) in the abiotic response cores (ARC) divided by the number of days of the re-acclimation period, then divided by 24 hours (S_{all}; Eq. S3). The soil O_2 consumption rates represent minimum estimates of O_2 consumption because they do not account for O_2 consumed during the very slow diffusion of O_2 into the surface stagnant boundary layer of the soil cores.

$$\textit{ARC Consumption Rate} = \frac{\text{Soil [O2] End of Flush 1} - \text{Soil [O2] Prior to Flush 2}}{\text{Days of Re-Acclimation Period}} \div 24 \text{ hours} \quad \text{(S3)}$$

A5. Modeling Soil O_2 Concentrations after Simulated Rainfall. The final concentration of dissolved O_2 (mg O_2 L^{-1}) at 15-cm depth at the end of the DI water flush in the biotic response cores (BRC) was estimated from the initial soil O_2 concentration (mg O_2 L^{-1}; M_t) measured at the 10-20 cm depth within each BRC tundra mesocosm prior to the DI water flush, the BRC soil O_2 accumulation rate (mg O_2 L^{-1} hr^{-1}; F_{rain}; corrected to 15-cm depth) during the DI water flush, and the duration of the DI water flush (hr) (M_f; Eq. S4).

$$\textit{Final BRC Soil } [O_2] \textit{ End of Flush} = \text{Initial BRC Soil } [O_2] + (S2 \times \text{BRC Flush Duration}) \quad \text{(S4)}$$

The final soil O_2 concentration at 15-cm depth at the 4-hour post-rainfall (T4) sampling time point was estimated from the final BRC soil O_2 concentration at the end of the DI water flush (M_f; Eq. S4) and the BRC soil O_2 consumption rate (mg O_2 L^{-1} hr^{-1}; S_{all}; Eq. S3), multiplied by 4 hours (M_{f+4}; Eq. S5).

$$\textit{Final BRC Soil } [O_2] \textit{ at T4} = S4 - \{S4 \times (S3 \times 4 \text{ hours})\} \quad \text{(S5)}$$

Likewise, the final soil O_2 concentration at 15-cm depth at the 24-hour post-rainfall (T24) sampling time point was estimated from the final BRC soil O_2 concentration at the end of the DI water flush (M_f; Eq. S4) and the BRC soil O_2 consumption rate (mg O_2 L^{-1} hr^{-1}; S_{all}; Eq. S3), multiplied by 24 hours (M_{f+24}; Eq. S6).

$$\textit{Final BRC Soil } [O_2] \textit{ at T24} = S4 - \{S4 \times (S3 \times 24 \text{ hours})\} \quad \text{(S6)}$$

A6. 16S rRNA Gene Amplification. The V4 region of the 16S rRNA gene was amplified from genomic DNA using the archaeal/bacterial primers, 515F (5'-GTGYCAGCMGCCGCGGTAA-3') and 806R (5'- GGACTACNVGGGTWTCTAAT-3') following the Earth Microbiome Project protocol. PCR reactions were conducted in duplicate for each sample with Platinum Hot Start PCR Master Mix (Thermo Fisher, Waltham, MA) in a 25 μL reaction volume under the following conditions: 94°C for 3 min; 35 cycles of 94°C for 45 sec, 50°C for 60 sec, 72°C for 90 sec; 72°C for 10 min. Duplicate amplifications were pooled, quantified with Qubit 4.0 fluorometry (Invitrogen, Carlsbad, CA), combined in equimolar concentrations, and cleaned using the MinElute PCR Purification Kit (Qiagen). The pooled amplicon library was submitted to the Microbiome Core at the University of Michigan for 2 x 150 bp paired-end sequencing on the Illumina MiSeq platform and used for downstream community profiling analysis.

A7. Metagenome and Metatranscriptome Sequencing. Co-extracted genomic DNA was purified with DNeasy PowerClean Pro Cleanup kit (Qiagen) following the manufacturer protocol and the quality and quantity were checked by gel electrophoresis and Qubit 4.0 fluorometry (Invitrogen) Whole libraries for metagenomes (N=15; 3 samples failed QC) were prepared using the Nextera XT kit (Illumina) and submitted to the Advanced Genomics Core at the University of Michigan for paired-end 150 bp sequencing on the Illumina HiSeq 4000 platform and used for downstream metagenomic analysis. Metatranscriptome sequences were generated from total RNA extractions with DNA contaminants removed via treatment with DNase I (Thermo Fisher) for 15 min at room temperature according to the manufacturer protocol. RNA samples were submitted to the Advanced Genomics Core at the University of Michigan for mRNA ribo-reduced library preparation using the Ribo-Zero Gold rRNA Removal kit (Epicentre, Madison, WI) and cDNA library generation with Truseq Stranded RNA LT kit (Illumina, San Diego, CA) and sequenced via paired-end 150 bp sequencing on the Illumina HiSeq 4000 platform and used for downstream metatranscriptomic analysis.

A8. References

Trusiak, A., Treibergs, L.A., Kling, G.W. and Cory, R.M., 2018. The controls of iron and oxygen on hydroxyl radical (• OH) production in soils. Soil Systems, 3(1).

APPENDIX B.

CHAPTER 3 SUPPLEMENTAL METHODS

B1. Tundra Types. This study investigates soil microbiomes within two tundra types: moist acidic tussock (MAT) tundra and wet sedge (WS) tundra. MAT tundra is dominated by *Eriophorum vaginatum* (tussock-forming sedge) and co-dominated by other graminoids, evergreen and deciduous shrubs, and bryophytes (Walker et al. 1994). WS tundra is dominated by sedges (*Carex aquatilis, C. chordorrhize, C. rotundata*) (Walker et al. 1994). MAT tundra typically forms on ice-rich sediments with a shallow active layer and low soil pH (3.8-5.5 in the Toolik Lake area), whereas WS tundra forms as a rich fen complex with greater active layer thaw depth than upslope MAT tundra (Walker et al. 1994).

B2. DNA Extraction and Sequencing. Genomic DNA was extracted in triplicate (0.3-0.4 g soil per replicate) from each 10-cm soil profile increment using the DNeasy PowerSoil DNA Isolation Kit (Qiagen, Germany). A DNeasy PowerClean Pro Cleanup Kit (Qiagen) was used to remove PCR inhibitors from the extracted DNA. DNA was then quantified using the Quant-iT dsDNA High Sensitivity Assay Kit and Qubit 4.0 fluorometer (Invitrogen, USA). DNA was amplified through polymerase chain reaction (PCR) using dual-barcoded primers 515f-806r of the V4 region of the 16S rRNA gene to profile the bacterial and archaeal communities (Apprill et al. 2015, Parada et al. 2016). Each 16S rRNA reaction contained 10 μL Platinum Hot Start PCR Master Mix (2x) (Thermo Fisher Scientific), 13 μL PCR-grade water, 0.5 μL forward primer (10 μM), 0.5 μL reverse primer (10 μM), and 1 μL template DNA. Amplifications were performed using a Mastercycler ProS thermocycler (Eppendorf, USA). The PCR conditions were: enzyme activation at 94°C for 3 min, followed by 35 cycles of denaturation at 94°C for 45 s, annealing at 50°C for 60 s, and extension at 72°C for 90 s, followed by final extension at 72°C for 10 min. Dual-barcoded PCR amplicons were pooled into a single library in equal molar concentration (50 ng/amplicon)

and submitted to the University of Michigan Microbiome Core for 2×150 bp paired-end high-throughput sequencing on the Illumina MiSeq platform.

B3. Bioinformatics. Amplicon sequence variants (ASVs) were filtered to remove chloroplast, mitochondria, and ASVs not assigned to bacteria or archaea classification. To assess community composition along the depth profile, samples were rarefied to 50,487 sequences per sample (average 116,360 QC sequences per sample prior to rarefying), with rarefaction plots asymptotic at ~20,000 sequences for all samples. QIIME2 artifacts were exported to R (v. 4.1.2) (R Core Team 2018) using the "qiime2R' package (Bisanz 2018) to conduct statistical analyses.

B4. Soil Physicochemical Measurements. Soil physicochemical properties were measured from each 10-cm soil profile increment. Soil pH and electrical conductivity ($\mu S\ cm^{-1}$) were measured in a soil:water suspension (1:5 ratio, w/v) using a WTW SenTix pH 3210 meter and probe (resolution: 0.001 pH; Xylem Analytics, Germany) and a WTW Cond 3210 meter and probe (resolution: 0.001 mS/cm; Xylem Analytics), respectively. Soil water content (%) was measured by weighing each sample before and after drying at 105°C for 12 h. Soil organic carbon content (%) was determined from loss on ignition (LOI) analysis by combusting a dried subsample at 550°C for 8 h, assuming the mass of organic matter lost during ignition was ~36% carbon for organic soils and ~7% carbon for mineral soils (G. Kling, unpublished).

B5. Caldiserica Annotations. The soil microbiomes in this study contain taxonomic annotations attributed to the phylum Caldiserica (family WCHB1-03; Fig. 3; Table SI 3.4). Caldiserica is also reported in numerous arctic studies (Monteux et al. 2018, Tas et al. 2018, Tripathi et al. 2018, 2019, Varsadiya et al. 2021). However, this taxonomic annotation in tundra soils is likely misleading due to recent taxonomic revisions. Caldiserica is a known hot spring sulfur-reducing chemoheterotroph within the 16S rRNA gene lineage 'OP5' and named for the sole isolate *Caldisericum exile* (Hugenholtz et al. 1998). In Martinez et al. (2019), seven Caldiserica metagenome-assembled genomes (MAGs) were characterized from a thawing permafrost site in arctic Sweden and proposed to form a divergent clade from *C. exile* at the phylum level. These permafrost Caldiserica, now proposed as *Candidatus* Cryosericota phylum, were characterized as carbohydrate and amino acid fermenters capable of using labile plant compounds and peptides while also encoded with adaptations to low temperatures (Martinez et al. 2019). Future studies

should recognize this discrepancy in taxonomic annotations based on currently available 16S rRNA gene databases.

B6. Bacterial Cell Viability Assays. Bacterial cells were separated from the soil matrix of select 10-cm soil profile increment using Nycodenz density cushion centrifugation following methods from Burkert et al. (2019). Three 10-cm soil increment depths were selected from each soil profile to represent a surface active layer depth (~10-20 cm), a transition zone depth (~40-50 cm), and a permafrost depth (~70-80 cm). To separate cells from soil debris, 5 g of soil was disrupted in 5 mL of a mild detergent consisting of 0.5% Tween 80 (Thermo Fisher Scientific) and 50 mM sodium pyrophosphate buffer (Alfa Aesar, USA) and vortexed for 15 min. Vortexed samples were centrifuged at 750 x g for 7 minutes at 4°C to remove large particles and debris. The supernatant (600 μL) was extracted and layered over 600 μL of 1.3 g/L Nycodenz (Cosmo Bio, USA) solution in a 2-mL tube. Tubes were centrifuged at 14,000 x g for 30 min at 4°C. The upper and middle phases (600 μL) containing bacterial cells were transferred into a sterile 2-mL tube and centrifuged at 10,000 x g for 15 min at 4°C. The supernatant was discarded, and the pellet was resuspended in 1 mL of 0.85% NaCl solution. The viability assay was performed with a Live/Dead BacLight Bacterial Viability Kit (Invitrogen) per manufacturer instructions. The stained cell suspensions were filtered onto a 25-mm-diameter 0.2-μm-pore-size black polycarbonate membrane and placed on a slide with sterile forceps. Images were captured at 60x total magnification (Nikon Eclipe T*i* confocal microscope). Viable cells (green fluorescence) and dead cells (red fluorescence) were counted using Imaris post-processing software (Oxford Instruments Group); and a consistent field of view (~62×212 μm area) was counted for live- and dead-stained cells. The average number of cells per field of view was multiplied by area of the filter, and the dilution factor was then corrected for dry weight to calculate the average number of cells per gram of soil dry weight (g dw^{-1}).

B7. Thaw Depth Measurements. Annual thaw depth measurements began in 1990 at a small watershed just south of Toolik Lake, and in 2002 in the Imnavait Creek basin. Thaw depth at each of 96 sites at Toolik and 75 sites at Imnavait was measured each year on 2 July and 11 August (plus or minus 1 day). UTM stakes every 100 m define the grids, and measurements were made every 25 m in between the UTM stakes. Survey grids at both sites cover a gently sloping hill of MAT tundra dominated by *E. vaginatum*, and at Imnavait the grid extends into WS tundra in the valley bottom and in the riparian zone of the creek. Within a 100 cm radius of each grid point,

a ruled stainless-steel rod was inserted in inter-tussock microhabitat (the space between tussocks) until the frozen layer was reached, and the distance was measured to the top of the upper soil organic mat (beneath the uppermost moss layer if present). Two measurements were made at each point from 1990-1999, and three measurements were made at each point from 2000 on. The measurements for all sites on the grid were averaged to arrive at a single number (plus a standard error) for each date in each year.

B8. Thaw Frequency and Thaw Duration Measurements. Thaw frequency over time was characterized by calculating the probability of thaw for each 10-cm depth increment of the soil profile. This represents the probability that in any given year the surface thaw would reach that depth. Probabilities were calculated for July and August sampling dates as measured from thaw depth surveys at Toolik MAT (1990-2018), Imnavait MAT (2003-2018), and Imnavait WS (2003-2018) tundra sites. Average thaw duration (i.e., the minimum number of days the soil at a given depth was thawed) was calculated from thaw depth measurements taken at seven time points from 2 June to 20 August in 2018 at Toolik and 21 June to 21 August in 2018 at Imnavait. These are "minimum" estimates of thaw duration because any particular depth may have thawed just after one survey but not been detected until the next survey.

B9. References

Apprill, A., McNally, S., Parsons, R. and Weber, L., 2015. Minor revision to V4 region SSU rRNA 806R gene primer greatly increases detection of SAR11 bacterioplankton. Aquatic Microbial Ecology, 75(2), 129-137.

Bisanz, J.E., 2018. qiime2R: Importing QIIME2 artifacts and associated data into R sessions. Version 0.99, 13.

Burkert, A., Douglas, T.A., Waldrop, M.P. and Mackelprang, R., 2019. Changes in the active, dead, and dormant microbial community structure across a Pleistocene permafrost chronosequence. Applied and environmental Microbiology, 85(7), e02646-18.

Hugenholtz, P., Pitulle, C., Hershberger, K.L. and Pace, N.R., 1998. Novel division level bacterial diversity in a Yellowstone hot spring. Journal of bacteriology, 180(2), 366-376.

Martinez, M.A., Woodcroft, B.J., Espinoza, J.C.I., Zayed, A.A., Singleton, C.M., Boyd, J.A., Li, Y.F., Purvine, S., Maughan, H., Hodgkins, S.B. and Anderson, D., 2019. Discovery and ecogenomic context of a global Caldiserica-related phylum active in thawing permafrost, Candidatus Cryosericota phylum nov., Ca. Cryosericia class nov., Ca. Cryosericales ord. nov., Ca. Cryosericaceae fam. nov., comprising the four species Cryosericum septentrionale gen. nov. sp.

nov., Ca. C. hinesii sp. nov., Ca. C. odellii sp. nov., Ca. C. terrychapinii sp. nov. Systematic and applied microbiology, 42(1), 54-66.

Monteux, S., Weedon, J.T., Blume-Werry, G., Gavazov, K., Jassey, V.E., Johansson, M., Keuper, F., Olid, C. and Dorrepaal, E., 2018. Long-term in situ permafrost thaw effects on bacterial communities and potential aerobic respiration. The ISME journal, 12(9), 2129-2141.

Parada, A.E., Needham, D.M. and Fuhrman, J.A., 2016. Every base matters: assessing small subunit rRNA primers for marine microbiomes with mock communities, time series and global field samples. Environmental microbiology, 18(5), 1403-1414.

Taş, N., Prestat, E., Wang, S., Wu, Y., Ulrich, C., Kneafsey, T., Tringe, S.G., Torn, M.S., Hubbard, S.S. and Jansson, J.K., 2018. Landscape topography structures the soil microbiome in arctic polygonal tundra. Nature communications, 9(1), 1-13.

Team, R.C., 2018. R: A language and environment for statistical computing. Version 4.1.2.

Tripathi, B.M., Kim, M., Kim, Y., Byun, E., Yang, J.W., Ahn, J. and Lee, Y.K., 2018. Variations in bacterial and archaeal communities along depth profiles of Alaskan soil cores. Scientific reports, 8(1), 1-11.

Tripathi, B.M., Kim, H.M., Jung, J.Y., Nam, S., Ju, H.T., Kim, M. and Lee, Y.K., 2019. Distinct taxonomic and functional profiles of the microbiome associated with different soil horizons of a moist tussock tundra in Alaska. Frontiers in microbiology, p.1442.

Varsadiya, M., Urich, T., Hugelius, G. and Bárta, J., 2021. Microbiome structure and functional potential in permafrost soils of the Western Canadian Arctic. FEMS microbiology ecology, 97(3), fiab008.

Walker, M.A., Daniëls, F.J. and van der Maarel, E., 1994. Circumpolar arctic vegetation: Introduction and perspectives. Journal of vegetation science, 5(6), 757-764.